



HAL
open science

Gold(I) Catalysis Under Visible Light

Zhonghua Xia

► **To cite this version:**

Zhonghua Xia. Gold(I) Catalysis Under Visible Light. Organic chemistry. Sorbonne Université, 2018. English. NNT : 2018SORUS606 . tel-02954132

HAL Id: tel-02954132

<https://theses.hal.science/tel-02954132>

Submitted on 30 Sep 2020

HAL is a multi-disciplinary open access archive for the deposit and dissemination of scientific research documents, whether they are published or not. The documents may come from teaching and research institutions in France or abroad, or from public or private research centers.

L'archive ouverte pluridisciplinaire **HAL**, est destinée au dépôt et à la diffusion de documents scientifiques de niveau recherche, publiés ou non, émanant des établissements d'enseignement et de recherche français ou étrangers, des laboratoires publics ou privés.

Sorbonne Université

Ecole Doctorale de Chimie Moléculaire de Paris Centre

Institut Parisien de Chimie Moléculaire / Equipe Méthodes et Applications en Chimie Organique

Gold(I) Catalysis Under Visible Light

Par Zhonghua XIA

Thèse de doctorat de Chimie Organique

Dirigée par Prof. Louis FENSTERBANK, Dr. Virginie MOURIES-MANSUY
et Dr. Cyril OLLIVIER

Présentée et soutenue publiquement le 19 octobre 2018

Devant un jury composé de :

M. Igor ALABUGIN	Professeur, Florida State University, USA	Rapporteur
M. Abderrahmane AMGOUNE	Professeur, Université Claude Bernard Lyon 1	Rapporteur
M. Philippe BELMONT	Professeur, Université Paris Descartes	Examineur
M. Matthieu SOLLOGOUB	Professeur, Sorbonne Université	Examineur
M. Louis FENSTERBANK	Professeur, Sorbonne Université	Directeur de thèse
Mme Virginie MOURIÈS-MANSUY	Maître de conférence-HDR, Sorbonne Université	Directeur de thèse

Sorbonne Université

Ecole Doctorale de Chimie Moléculaire de Paris Centre

Institut Parisien de Chimie Moléculaire / Equipe Méthodes et Applications en Chimie Organique

Gold(I) Catalysis Under Visible Light

Par Zhonghua XIA

Thèse de doctorat de Chimie Organique

Dirigée par Prof. Louis FENSTERBANK, Dr. Virginie MOURIES-MANSUY
et Dr. Cyril OLLIVIER

Présentée et soutenue publiquement le 19 octobre 2018

Devant un jury composé de :

M. Igor ALABUGIN	Professeur, Florida State University, USA	Rapporteur
M. Abderrahmane AMGOUNE	Professeur, Université Claude Bernard Lyon 1	Rapporteur
M. Philippe BELMONT	Professeur, Université Paris Descartes	Examinateur
M. Matthieu SOLLOGOUB	Professeur, Sorbonne Université	Examinateur
M. Louis FENSTERBANK	Professeur, Sorbonne Université	Directeur de thèse
Mme Virginie MOURIÈS-MANSUY	Maître de conférence-HDR, Sorbonne Université	Directeur de thèse

Si vous avez la chance d'avoir vécu jeune homme à Paris, où que vous alliez pour le reste de votre vie, cela ne vous quitte pas, car Paris est une fête. — Ernest Hemingway

If you are lucky enough to have lived in Paris as a young man, then wherever you go for the rest of your life, it stays with you, for Paris is a moveable feast. — Ernest Hemingway

假如你有幸年轻时在巴黎生活过，那么你此后一生中不论去到哪里，她都与你同在，因为巴黎是一席流动的盛宴。 — 欧内斯特·海明威

To me,

Follow your heart.

Acknowledgments

This work was carried out from October 2015 to October 2018 under the guidance of Prof. Louis Fensterbank, Dr. Virginie Mouriès-Mansuy and Dr. Cyril Ollivier in the laboratory “Méthodes et Applications en Chimie Organique (MACO)” at Institut Parisien de Chimie Moléculaire (IPCM), Sorbonne Université and involved many people to whom I would like to express my deep gratitude.

First of all, I warmly thank the members of the jury for accepting to be the reviewers of this thesis: Prof. Igor Alabugin from Florida State University, Tallahassee, USA, Prof. Abderrahmane Amgoune from Université Claude Bernard - Lyon 1, Prof. Philippe Belmont from Université Paris Descartes, Prof. Matthieu Sollogoub from Sorbonne Université. Your invaluable comments and suggestions would help me improve the quality of this thesis.

I want to express many thanks to my supervisor, Prof. Louis Fensterbank, who gives me an opportunity to pursue my Ph.D. study in MACO group and for his kind attention and excellent guidance throughout the past three years of my study and research. On the way to pursue science, we have many discussions, sometimes different opinions, it promotes us thinking a question more comprehensive and deeper, and I think that is research and chemistry. He has a wide knowledge, works efficient and hard. This three-year study life was accompanied by his candid discussion, pertinent criticism, constant encouragement, and unexpected humor. He taught me many things, like how to do research and to be a chemist, balance thinking and doing, working and playing. Moreover, we are 2018 Paris Marathon finishers in MACO group, I will be always proud of it.

I am truly grateful to Dr. Virginie Mouriès-Mansuy, my co-advisor, and the gold chemist, for her guidance and supports in my experiments. She is always ready for providing help and solving problems very quickly, I have to work very efficiently to follow her step. I would thank her patience teaching for experimental techniques and correction for the French summary of my thesis. I really appreciate her humor and cheer me up, especially when my reaction did not work very well, her encouragement motivates me a lot to achieve the goal.

I want to thanks Dr. Cyril Ollivier, my co-advisor, also the chef of photocatalysis and seminar. He has a wide knowledge of radical chemistry and photocatalysis, which provides me with very useful guidance and advice. I appreciate a lot the mechanism discussion with him, he always provides professional opinions about my questions. Also, his mildness and optimism always bring my peace and full of energy.

My appreciation is also given to people who participate in my projects. I want to thank Dr. Vincent Corcé, who participated in my second project and helped me to do the fluorescence quenching experiments and cyclic voltammetry experiments. Thanks for his work on my project and correction of the supporting information. Dr. Yves Gimbert and Dr. Héloïse Dossmann carried out the computational studies, it's significant for the mechanism explanation, and Jérémy Forté is acknowledged for the XRD analyses. I am grateful to Omar Khaled for HRMS and Cédric Przybylski for the MS analyses.

I also want to thank Dr. Bastien Nay and Frederic De Montigny, who are my committees in "comité de suivi", for their suggestions to my research.

And Natalia Del Rio, the nice and optimistic Spanish girl, who worked neighbor to my bench for one year, I appreciate our talk about chemistry and weekend. She has skilled experiment techniques and wide chemistry knowledge, gave me much useful advice.

Thanks to Alejandro, my Mexico friend who worked with me in the same office in my first year. Thanks for his advice in my chemistry and help me adopt the new life in a new group.

Many thanks to Avassaya Vanitcha, the nice and friendly Thailand girl, for her help in my first experiment, it's essential for me to adopt a new lab. Thanks!

I would like to say thanks to the MACO team. Dr. Corinne Aubert, who is the former director of IPCM, the Dean of the Faculty of Science and Engineering now, for her kindness; Dr. Gilles Lemièrre, who worked with me in the same lab, I appreciate his help and joke in the lab; Dr. Marc Petit for his security work in the Lab; Dr. Marion B. for her kindness; Dr. Marine for her cheering up; Dr. Muriel for her kindness and organization of group party.

I also say merci to all my current and former colleagues in the MACO team. Thanks to Anthony, the friendly and strong guy, I feel very lucky we are same year Ph.D. students, every time talking with him makes me peaceful and pleasant, his hardworking and optimistic always motivate me. Yes, I like beer too. Thanks to Laura H., the nice girl who can speak very fluent English. Thanks for her help when I have French language questions. Thanks to Christophe, the cool and responsible guy, I still remembered how he taught me to synthesize the Iridium photocatalyst, I followed his procedure and tips, and success for one time. Great! Valérie (Vava) for her kindness and friendliness, who can speak many languages, French, English, Spanish, Chinese, Japanese, and maybe more... She can speak many Chinese words now, even sing a song, Tian Mimi. Caleb for his friendliness and funny. Laura F. for her kindness and organization of group drinking, the after-work party in Champs-Élysées is impressing me even now; Jérémy for his kindness and fantastic humor; Maud for her funny and organization of group lunch. Thanks Nicola, the young America high school student, who can speak fluent

Chinese, also like Chinese food and culture very much. Amazing! Thanks to Francesco, the nice Italy practice student, I hope he can be a good chemist in the future. And thanks Julien, Simon, Ludwig, Fabrizio, Cédric, Etienne, Thibaut, Frédéric ...

I would like to thank Prof. Yongmin Zhang, for his kind concern to my study and life in the last three years. It's always very pleasant to talk to him, every time our talk makes me think more clearly about my situation and future. Thanks to my Chinese friends, Xiaolei, Yang, Jingwen and Teng, we can talk about everything in our lunchtime, we share happiness and sadness, I fell so luckily I have your friends! Also, I want to thanks to my junior Chinese colleagues, Yufeng, Ye, Fen, and Hengrui, they bring me happiness and company, it is invaluable!

Finally, I want to thanks my family, their love and support always make me happy and successful in my life.

I love Paris!

Zhonghua Xia
Sept 17, 2018, Paris

Contents

Acknowledgments	1
Contents	5
Abbreviations	7
Résumé	9
Introduction	27
Chapter 1 Background	29
1 Gold Catalysis	31
1.1 History of Gold Catalysis	31
1.2 Important Gold Intermediates: Vinylgold(I) and Gold(I) Acetylide.....	33
1.3 Au(I)/Au(III) Chemistry.....	36
2 Gold Catalysis Under Visible Light	40
2.1 Photocatalysis and Dual Catalysis.....	40
2.2 Dual Gold/Photoredox Catalysis	43
3 Iodoalkynes	52
3.1 Alkynyl Radicals	52
3.2 Halogen Bonding of (Iodoethynyl)benzene	53
Chapter 2 Dual Photoredox/Gold Catalysis	59
1 Background: Aryl Diazonium Salts	61
1.1 Two Types of Classic Name Reactions Involving Aryl Diazonium Salts	61
1.2 Reductive Potential of Aryl Diazonium Salts	63
1.3 Homolytic Dediazonation of Diazonium Salt.....	64
2 Project Aims and Introduction	69
3 Results and Discussion.....	73
3.1 Optimization Studies	73
3.2 Scope and Limitations	74
3.3 Proposed Mechanism	80
3.4 Conclusion.....	81
4 Experimental Section	82
4.1 General Experimental Details	82
4.2 General Procedure	83

4.3 Compound Characterizations	85
Chapter 3 Photosensitized Gold Catalysis	97
1 Background on Energy Transfer Process on Photocatalytic System	99
2 Project Aims and Introduction	105
3 Results and Discussion.....	108
3.1 Optimization Studies	108
3.2 Scopes and Limitations	115
3.3 Post-functionalization.....	118
4 Mechanism Investigation	119
4.1 Photoredox Catalysis.....	119
Conclusion of part 1: the photoredox catalysis is not possible to explain the mechanism, and it is difficult to prove the existence of halogen bonding in our reaction.	124
4.2 Oxidative Addition Involve Gold(III) Acetylide	124
4.3 Photosensitized Gold Catalysis	130
4.4 Proposed Mechanism and Conclusion	145
5 Experimental Section	146
5.1 General Informations.....	146
5.2 Substrate Synthesis.....	147
5.3 General Procedure for the Alkylative Cyclization	150
5.4 Investigation of Mechanism	151
5.5 Compound Characterizations	158
5.6 Crystallographic Data.....	176
5.7 Theoretical Studies.....	178
5.8 NMR Spectral Data	189
General Conclusion	193

Abbreviations

°C	degree Celsius
Ac	acetyl
aq.	aqueous
Ar	aryl
Bn	benzyl
cat.	catalyst
Cy	cyclohexyl
DFT	density functional theory
eq./equiv.	equivalent
ESI	electrospray ionization
Et	ethyl
HOMO	highest occupied molecular orbital
HRMS	high performance liquid chromatography
<i>i</i> -Pr	<i>iso</i> -propyl
IR	infrared
Ir	Iridium
<i>J</i>	coupling constant
L	ligand
LUMO	lowest occupied molecular orbital
<i>m</i>	<i>meta</i>
M	molar (mol/L)
m.p.	melting point
Me	methyl
MHz	Mega Hertz
mw	molecular weight
NIS	N-Iodosuccinimide
NMR	nuclear magnetic resonance
Nu	nucleophile
<i>o</i>	<i>ortho</i>
<i>p</i>	<i>para</i>

Ph	phenyl
phen	1,10-phenanthroline
rt	room temperature
SET	single electron transfer
TLC	thin layer chromatography

Résumé

Ce document de thèse comprend trois chapitres.

Le chapitre 1 est un bilan sur la catalyse à l'or, la catalyse à l'or sous lumière visible et la réactivité des iodoalcynes. Pendant des siècles, l'or a été considéré comme un métal inerte précieux et purement décoratif. Il est considéré comme le métal le plus précieux depuis des millénaires et constitue la base de la plupart des systèmes monétaires dans le monde. Au cours des deux dernières décennies, la catalyse homogène de l'or est devenue une méthodologie remarquable et utile pour la synthèse de molécules organiques complexes.¹ Récemment, les groupes de Glorius, Toste et de nombreux autres groupes ont reporté une catalyse dual complexe d'or(I)/photoredox entre des alcynes et des sels d'aryldiazonium.² Il nous est apparu important de trouver de nouveaux partenaires pour ces transformations. Nous nous sommes tournés vers les iodoalcynes qui ont un potentiel réducteur élevé par rapport aux sels d'aryldiazonium, mais ce sont des donneurs de liaison halogène. La liaison halogène est une interaction non covalente attrayante qui peut favoriser une réaction radicale avec les composés d'iodure soumis sous irradiation par la lumière visible.

Le chapitre 2 traitera d'un nouveau procédé de catalyse photorédox/or(I) par cyclisation arylative des o-alkynylphénols avec des sels d'aryldiazonium. Cette réaction se produit en douceur à température ambiante en l'absence de base et/ou d'additifs et offre une approche efficace pour la synthèse d'hétérocycles. La transformation est générale et ses limites feront l'objet d'une discussion. La réaction passe par la formation d'un intermédiaire vinyl-or(III) qui est obtenu par addition du radical aryl sur le complexe d'or(I) donnant un complexe d'or(II) qui est oxydé par action du catalyseur photoredox. Une étape d'élimination réductrice permet la formation des benzofuranes attendus.

Le chapitre 3 décrit une nouvelle méthode de synthèse de dérivés alcynyl-benzofurane obtenus à partir d' o-alkynylphénols et d'iodoalcyne en présence d'un système catalytique de

¹ Dorel, R.; Echavarren, A. M. *Chem. Rev.* **2015**, *115*, 9028.

² (a) Sahoo, B.; Hopkinson, M. N.; Glorius, F. *J. Am. Chem. Soc.* **2013**, *135*, 5505. (b) Hopkinson, M. N.; Sahoo, B.; Glorius, F. *Adv. Synth. Catal.* **2014**, *356*, 2794. (c) Tlahuext-Aca, A.; Hopkinson, M. N.; Sahoo, B.; Glorius, F. *Chem. Sci.* **2016**, *7*, 89. (d) Shu, X.-z.; Zhang, M.; Frei, H.; Toste, F. D. *J. Am. Chem. Soc.* **2014**, *136*, 5844. (e) He, Y.; Wu, H.; Toste, F. D. *Chem. Sci.* **2015**, *7*, 1194. (f) Kim, S.; Rojas-Martin, J.; Toste, F. D. *Chem. Sci.* **2016**, *7*, 85. (g) Huang, L.; Rudolph, M.; Rominger, F.; Hashmi, A. S. K. *Angew. Chem. Int. Ed.* **2016**, *55*, 4808.

Au(I) et Ir(III) la réaction étant conduite sous LED bleu. Cette transformation implique l'addition oxydante de l'iodoalkyne sur l'intermédiaire vinyl'd'or(I) par transfert d'énergie photo-induit. Sous irradiation à la lumière visible, l'état d'excitation triplet de l'intermédiaire vinylgold(I) et du partenaire iodure d'alcynyle est impliquée dans une séquence d'isomérisation -trans/cis par addition oxydative, donnant des produits de couplage Csp²-Csp après l'étape d'élimination réductrice. Les études mécanistiques et de modélisation moléculaire ont démontré qu'il s'agissait d'un phénomène de transfert d'énergie plutôt qu'un processus photoredox. Ce double procédé or/photo catalytique offre un nouveau mode d'activation dans la catalyse homogène de l'or. Ainsi, une nouvelle méthode de synthèse de dérivés d'alcynyl benzofurane a été mise au point à partir d'o-alkynylphénols et d'iodoalkynes en présence d'un mélange catalytique d'Au(I) et d'Ir(III) sous rayonnement LED bleu.

Chapitre 1 introduction

1 Catalyse à l'or

Au cours des deux dernières décennies, la catalyse homogène à l'or a été très fortement développée pour la synthèse de molécules organiques complexes. La majorité des cas s'appuient sur la π -activation des doubles liaisons et des triples liaisons par les complexes d'or(I) ou d'or(III) suivi de l'addition d'un nucléophile de façon intra ou intermoléculaire (schéma R1). Une étape finale de protodéauration en milieu acide permet la formation du produit souhaité. Durant le processus le catalyseur d'or reste au même degré d'oxydation (Schéma R1).

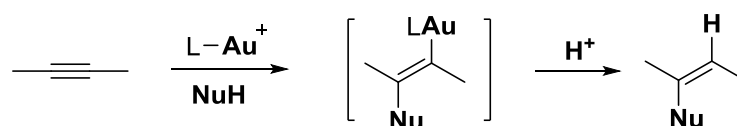


Schéma R1. Gold-catalyzed nucleophilic addition to alkynes.

La catalyse photoredox impliquant des complexes d'or a reçu beaucoup moins d'attention que la catalyse électrophile décrite précédemment. Avec un potentiel redox significativement élevé du couple Au(I)/Au(III) ($E_0 = 1,41$ V, supérieur à celui du couple Pd⁰/Pd^{II} $E_0 = 0,92$ V), des oxydants forts sont nécessaires pour permettre l'oxydation des espèces Au(I).

2 Gold catalysis under visible light

La combinaison de l'activation photoredox avec un second procédé catalytique impliqué dans les systèmes catalytiques duals est une application particulièrement intéressante. Ces dernières années, la catalyse à l'or sous l'action de la lumière visible a reçu une grande attention. La figure R1 montre le nombre explosif d'articles publiés dans ce domaine.³

³ MacMillan, W. C. et al. Photoredox catalysis in organic chemistry, *J. Org. Chem.*, **2016**, 81, 6898–6926.

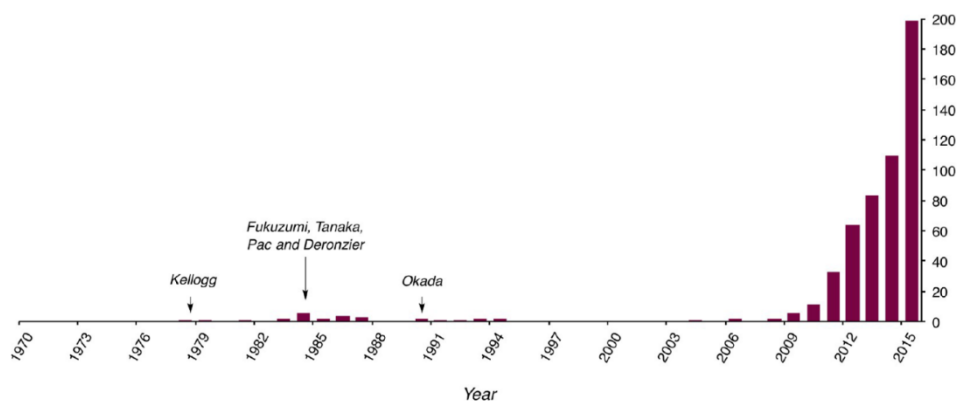


Figure R1. Articles publiés dans le domaine de la catalyse photorédox.

Afin d'élargir le champ d'application de l'hydrofonctionnalisation classique, diverses réactions catalysées par des complexes d'or impliquant la lumière visible ont été développées afin de contrer le problème du potentiel élevé du couple redox Au(I)/Au(III). Les premiers travaux marquants ont été reportés par les groupes de Glorius et Toste : une catalyse dual photoredox/or pour la fonctionnalisation d'alcynes. (Scheme R2).

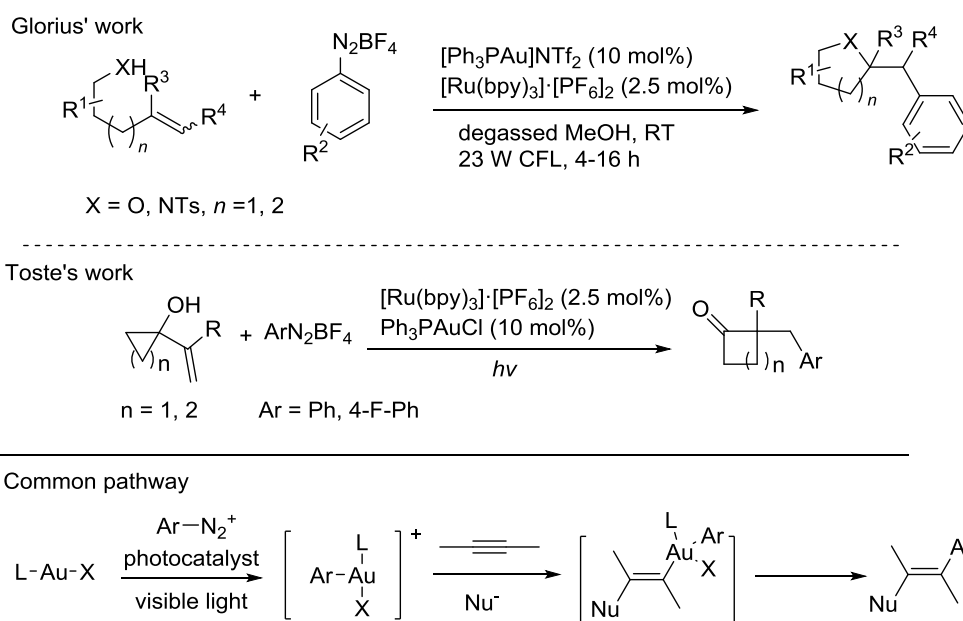


Schéma R2. Dual Au and photoredox catalytic difunctionalization of alkynes.

L'étape clé dans ces processus est l'oxydation des complexes d'Au(I) par le radical aryle généré au cours du processus ce qui permet la formation de l'intermédiaire Au(II) qui par SET permet la génération du complexes arylAu(III) qui après élimination réductrice donne les produits souhaités. La stratégie de cette catalyse dual photoredox utilisant des complexes d'or a été largement utilisée par plusieurs groupes de recherche dans une grande gamme de

réactions de couplage de radicaux aryle impliquant l'addition nucléophile aux systèmes π et aussi la fonctionnalisation de liaisons P-H et C(sp)-H ont été développées (schéma R3).⁴

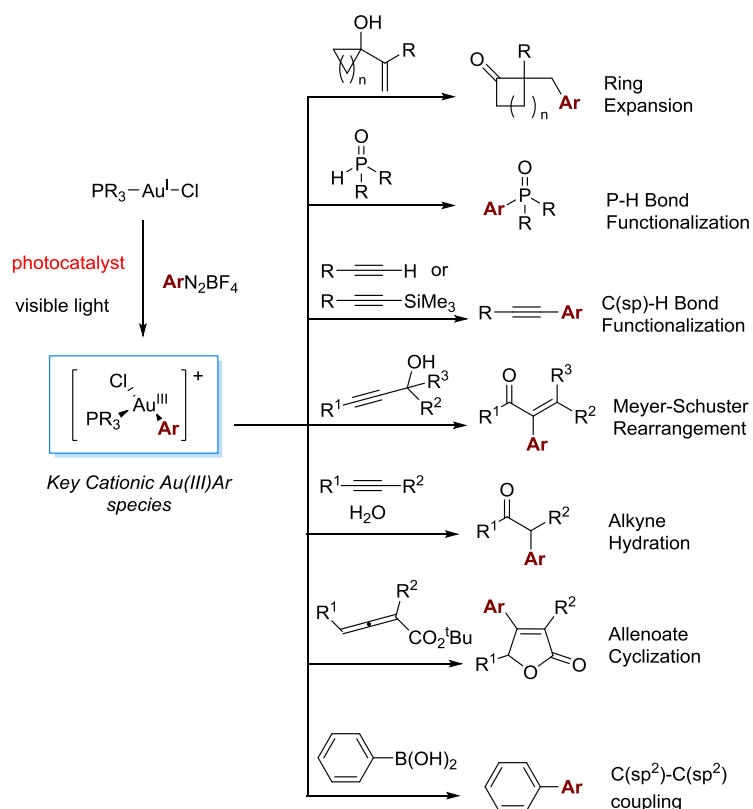


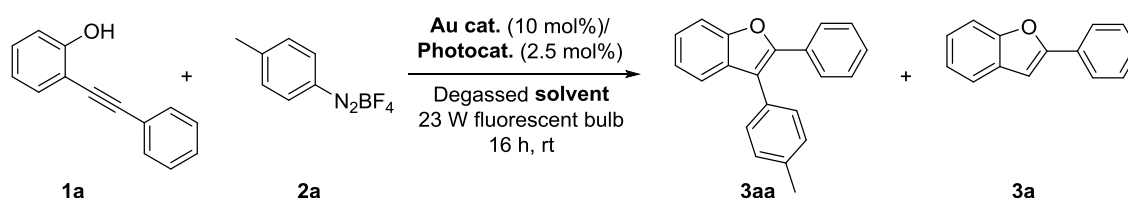
Schéma R3. Further expansion of the concept to various functionalization processes: P-H bond functionalization, C(sp)-H bond functionalization, Meyer-Schuster rearrangement, alkyne hydration, allenoate cyclization, C(sp²)-C(sp²) coupling.

⁴ Frank Glorius et., *Acc. Chem. Res.* **2016**, *49*, 2261–2272

Chapitre 2 catalyse dual photoredox/catalyse à l'or

Nous avons mis au point les conditions de réaction entre le 2-(phenylethynyl)phenol **1a** et le sel de *p*-tolylidiazonium **2a** comme substrats modèles (Table R1). En présence de Ph₃PAuCl et de Ru(bpy)₃(PF₆)₂, par irradiation par de la lumière visible, le tout dans du méthanol dégazé, nous avons obtenu le benzofurane attendu avec un rendement optimisé de 73%. En l'absence de photocatalyseur et de lumière visible le rendement en benzofurane chute, moins de 5%. Ces deux éléments sont donc indispensables pour la réaction (Table R1).

Table R1. Optimization of the Reaction Conditions.^a



Entry	Au cat.	Photocat.	Solvent	Yield of 3aa ^b (%)
1	Ph ₃ PAuNTf ₂	Ru(bpy) ₃ (PF ₆) ₂	MeOH	> 5; (3a , 60)
2	Au(NHC)Cl	Ru(bpy) ₃ (PF ₆) ₂	MeOH	9; (3a , 35)
3	Ph ₃ PAuCl ^d	Ru(bpy) ₃ (PF ₆) ₂	MeOH	45; (3a , 40)
4	Ph₃PAuCl	Ru(bpy)₃(PF₆)₂	MeOH	75 (73)^c
5 ^e	Ph ₃ PAuCl	none	MeOH	> 5; (3a , 30)
6 ^e	Ph ₃ PAuCl	Ru(bpy) ₃ (PF ₆) ₂	MeOH	> 5; (3a , 20)

^a General conditions: **1a** (0.2 mmol), [Au] catalyst (10 mol%), photocatalyst (2.5 mol%), **2a** (0.8 mmol), degassed solvent (2 mL), rt, 16 h, 23 W fluorescent light bulb. ^b Determined by ¹H NMR using butadiene sulfone as an internal standard. ^c Isolated yield. ^d 5 mol% used. ^e Reaction performed in the dark.

Avec ces conditions de réaction optimisées en main, nous avons regardé l'influence du sel de diazonium sur la réaction. Dans ce cas nous avons pris le 2-(phenylethynyl)phenol **1a** comme substrat modèle (table R2). Quand le sel de *para*-nitro aryldiazonium est utilisé comme agent d'arylation, le benzofurane **3ab** a été obtenu avec un excellent rendement de 86%. Quand le sel de diazonium est substitué en para par des groupements electroattracteur CF₃ (**2c**), CN (**2d**), et Br (**2e**) les rendements en benzofuranes sont bons. Lorsque le sel de diazonium n'est pas substitué un rendement de 65 % en produit **3af** est obtenu. La présence

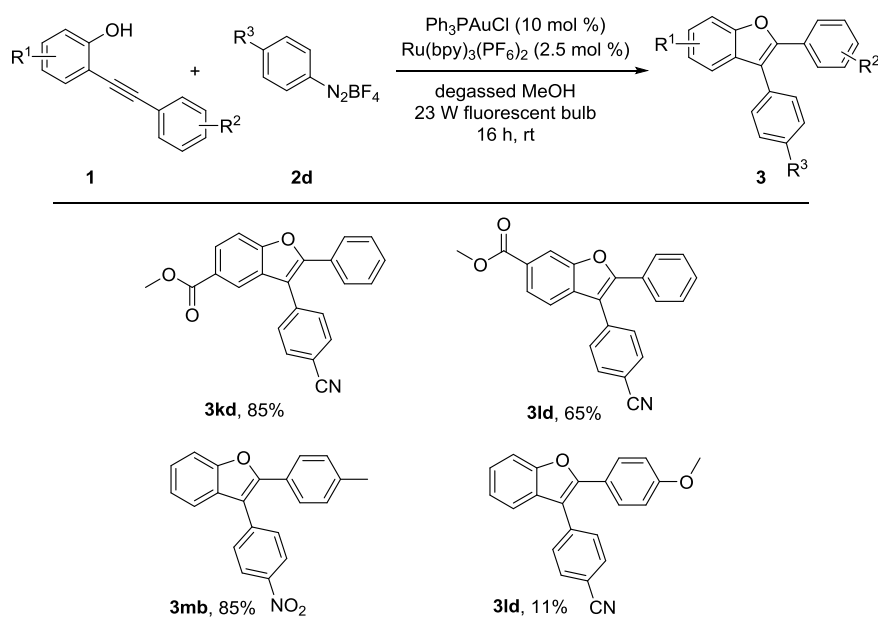
d'un groupement MeO fait chuter le rendement à 23% tandis que la présence d'un groupement ester en position méta a peu d'influence sur le rendement. Lorsque la position ortho est substituée par un CN un rendement faible en **3ai** est obtenu certainement du à un problème d'encombrement stérique.

Table R2. Scope of Aryl Diazonium Salts^a

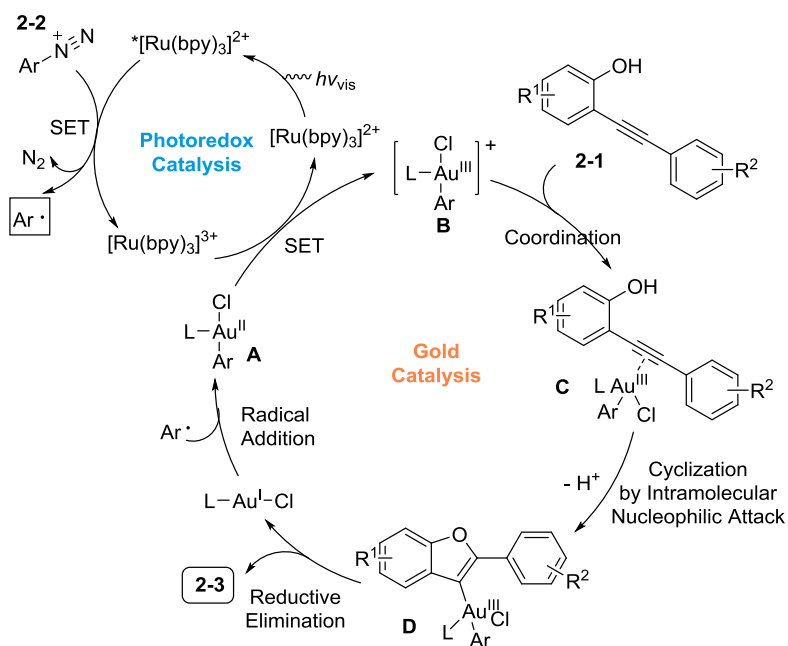
entry	2	3, yield(%)		entry	2	3, yield(%)
1		3aa , 73%		6		3af , 65%
2		3ab , 86%		7		3ag , 23%
3		3ac , 76%		8		3ah , 62%
4		3ad , 81%		9		3ai , 37%
5		3ae , 61%				

Reaction conditions: **1a** (0.2 mmol) and **2** (4 equiv), Ph₃PAuCl (10 mol %), Ru(bpy)₃(PF₆)₂ (2.5 mol %), degassed methanol (2 mL) under Ar, rt, 16 h , 23 W fluorescent light bulb; isolated yields of **3**.

Nous avons ensuite étudié l'effet des substituants sur les différents noyaux aromatiques (Table R3). Les rendements en benzofuranes sont bons sauf, une fois encore, lorsqu'il y a un groupement méthoxy en position para du sel de diazonium.

Table R3. Substitution effect of both aromatic rings^a

Reaction conditions: **1a** (0.2 mmol) and **2** (4 equiv), Ph_3PAuCl (10 mol %), $\text{Ru}(\text{bpy})_3(\text{PF}_6)_2$ (2.5 mol %), degassed methanol (2 mL) under Ar, rt, 16 h, 23 W fluorescent light bulb; isolated yields of **3**.

**Scheme R4.** Proposed Reaction Mechanisms.

Le mécanisme proposé est le suivant (Schéma R4). Sous l'action de la lumière visible le photocatalyseur de ruthénium est excité permettant par SET la formation du radical aryl par réduction. Celui-ci s'additionne sur le complexe d'or(I) pour générer l'espèce or(II) qui de nouveau par SET du photocatalyseur de ruthénium engendre le catalyseur d'or(III) cationique qui est capable d'activer la triple liaison et de déclencher ainsi l'étape de cyclisation par

addition nucléophile du phénol. Une étape finale d'élimination réductrice donne le benzofurane attendu **3**.

Chapitre 3 Catalyse d'or photosensibilisée

Nous nous sommes demandé si il était possible d'étendre cette réaction dual photoredox/catalyse à l'or avec d'autres partenaires que les sels de diazonium qui sont très souvent utilisés. Pour cela nous nous sommes intéressés à la réactivité des alcynes iodés aryliques.⁵

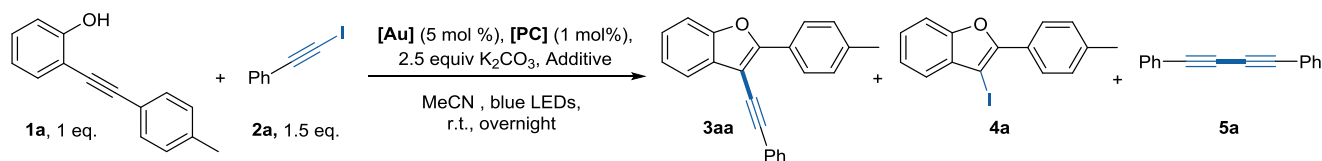
Ainsi, nous avons envisagé d'utiliser comme deuxième partenaire avec les *o*-alkynylphenols des alcynes iodés aryliques à la place des sels de diazoniums.⁶ Ce travail permettrait la formation tout à fait novatrice de liaison Csp²-Csp par catalyse photoredox.

Dans un premier un travail de screening a été entrepris avec le iodoalcynophenyl comme substrat modèle et le 2-(phenylethynyl)phenol afin trouver les meilleures conditions réactionnelles. Les conditions utilisées avec les sels de diazonium ont permis d'obtenir le produit attendu avec un faible rendement de 15% avec la formation du composé iodé **4a** à hauteur de 21%.

Changer le photocatalyseur par *fac*-Ir(ppy)₃ n'a fait que diminuer le rendement en produit **3aa**. L'utilisation d'un complexe d'or(I) plus électrophile comme (*p*-CF₃Ph)₃AuCl (**Au-CF₃**) et du photocatalyseur d'iridium Ir[dF(CF₃)ppy]₂(dtbbpy)PF₆ a permis d'obtenir le produit **3aa** avec un meilleur rendement de 56%. Enfin les meilleures conditions ont été obtenues en utilisant la phénantroline comme additif (Table R4).

⁵ For a dual catalysis example on a different system (aryldiazonium – TMS-alkyne), see: Kim, S., Rojas-Martin, J. & Toste, F. D. Visible light-mediated gold-catalysed carbon(sp²)–carbon(sp) cross-coupling. *Chem. Sci.* **7**, 85–88 (2016).

⁶ Xia, Z., Khaled, O., Mouriès-Mansuy, V., Ollivier, C. & Fensterbank, L. Dual Photoredox/Gold Catalysis Arylative Cyclization of *o*-Alkynylphenols with Aryldiazonium Salts: A Flexible Synthesis of Benzofurans. *J. Org. Chem.* **81**, 7182–7190 (2016).

Table R4. Defining the key parameters of the alkynative cyclization^a

[Au]: gold catalyst; [PC]: photocatalyst

Entry	[Au]	[PC]	Additive, 10 mol%	3aa yield (%) ^c	4a yield (%)
1 ^b	PPh ₃ AuCl	Ru(bpy) ₃ (PF ₆) ₂	-	15	21
2 ^b	PPh ₃ AuCl	fac-Ir(ppy) ₃	-	8	22
3 ^b	PPh ₃ AuCl	[Ir-F]	-	26	33
4	[Au-CF ₃]	[Ir-F]	-	56	22
5	[Au-CF ₃]	[Ir-F]	phen.	72 (71)	15
6	[Au-CF ₃]	[Ir-F]	phen. (1 equiv)	25	25
7	[Au-CF ₃]	[Ir-F]	quinuclidine	65	19
8	[Au-CF ₃]	-	phen.	26	29
9	[Au-CF ₃]	-	-	11	29
10	-	[Ir-F]	phen.	-	8
11 ^d	[Au-CF ₃]	[Ir-F]	phen.	-	27
12 ^e	[Au-CF ₃]	[Ir-F]	phen.	-	16

^a [Au-CF₃] = (*p*-CF₃Ph)₃PAuCl; [Ir-F] = Ir[dF(CF₃)ppy]₂(dtbbpy)PF₆; phen. = 1,10-phenanthroline. ^b Only 1 equiv of K₂CO₃ was used. ^c Yields are determined by ¹H NMR using 1,3,5-trimethoxybenzene as internal standard, yield in parentheses is isolated yield. ^d No K₂CO₃. ^e No light.

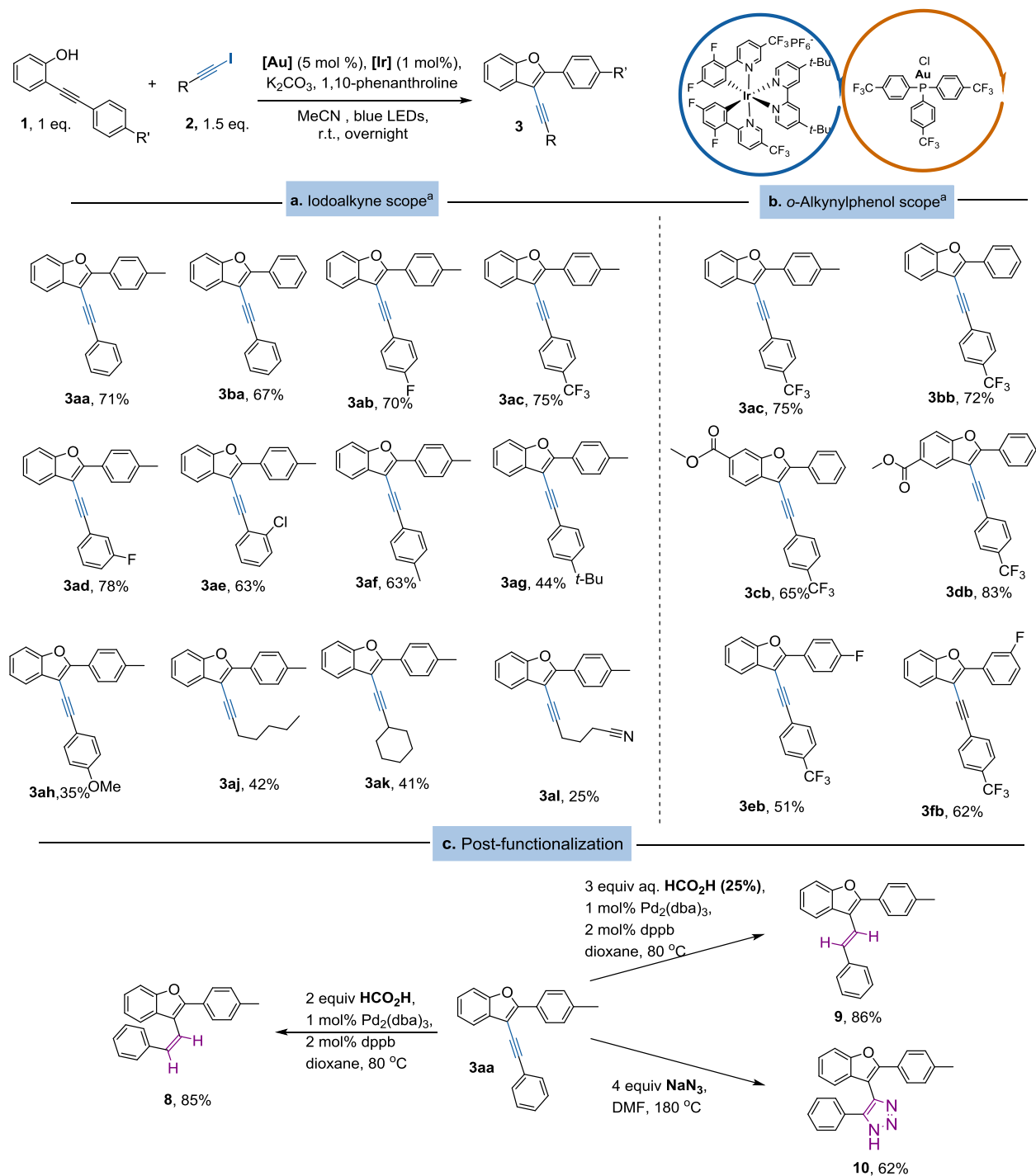
Etude de la réaction.

Ayant ces conditions optimisées en main nous avons fait varier la nature du phenol et de l'alcyne iodé (Figure R2a). Dans un premier temps nous avons fait varier la nature de l'iodoalcyne. Lorsque que l'iodoalcyne aryle porte un groupement electroattracteur en position para (CF₃, F) les benzofuranes attendus **3ab** et **3ac** ont été obtenus avec de bons rendements. Un groupe fluoro en méta ou un groupe chloro en position meta permet aussi d'obtenir **3ad** et **3ae** avec des bons rendements de 78 et 63% respectivement. La présence de groupement électro donneur (Me, *t*Bu, OMe) en para ou encore lorsque que le noyau phényl de l'iodoalcyne aryle n'est pas substitué permet la formation des benzofurane avec une

chute du rendement (**3af**, **3ag**, **3ba** et **3ah**). Aucune réaction n'est obtenue avec un iodolacyne portant un groupement nitro en position *para* du phenyl. Seul le produit de protodeauration **7** est obtenu. Pour finir, lorsque que le groupement phényl des iodoalcyne arylique porte des groupements *n*-pentyl, cyclohexyl, et 3-nitrile butyl Les rendements en benzofunrane sont plus faibles (**3aj-3al**, 25 et 42%).

Dans un deuxième temps nous avons regardé l'influence de la substitution des noyaux aromatiques du composé phénolique **1** en utilisant le 1-(iodoethynyl)-4-(trifluoromethyl)benzene **2c** comme alcyne model (Figure R2b). Aucun substituant, ou bien la présence des groupements CH₃ et F en *para* ou *mé*ta donne les benzofuranes **3bb**, **3ac**, **3eb** et **3fb** avec de bons rendements. La présence du groupement ester en *para* ou *mé*ta du phénol n'affecte pas le rendement. **3cb** et **3db** sont obtenus avec des rendements de 83 et 65% respectivement.

Nous avons pu post-fonctionnaliser le benzofurane **3** en effectuant des réactions d'hydrogénation *cis* et *trans* par action de palladium(0) et d'acide formique en modifiant les conditions expérimentales. Nous avons aussi pu obtenir le triazole **11** suivant une réaction de Huisgen par action de l'azoture de sodium dans le DMF à 180°C (Figure R2c).



^a 5 mol % [AuCF₃], 1 mol % [Ir-F], K₂CO₃ (2.5 eq.), 1,10-phenanthroline (10 mol%) MeCN, blue LEDs, r.t.; overnight

Figure R2. **a** Iodoalkynes **2** scope. **b** *O*-alkynylphenols **1** scope. **c** Post-functionalization of benzofuran **3aa**.

Etude mécanistique

Nous avons ensuite entrepris une étude mécanistique pour cette réaction de couplage.

L'utilisation de l'alcyne iodé **2b** portant un atome de fluore a permis de montrer que le passage par un intermédiaire radicalaire alcyne n'était pas possible comme cela a été proposé dans la première partie de cette thèse. En effet le potentiel redox du 1-fluoro-4-(iodoethynyl)benzene ($E_{1/2}(\mathbf{2b}) = -1.47 \text{ V vs SCE}$) est plus important que celui du photocatalyseur **[Ir-F]** catalyst ($E^*_{1/2} = -0.89 \text{ V vs SCE}$). Nous envisageons donc que la formation de l'intermédiaire Au(III) de type **B** (Schéma R4) se fait suivant une autre voie.

En nous basant sur des résultats de la littérature,⁷ un intermédiaire vinyl-Au(III) de type **D** (Schéma R4) peut être impliqué dans une étape d'élimination réductrice pour donner les benzofuranes formés. Pour cela nous avons synthétisé le vinylor(I) **6** avec un rendement de 82% (Scheme R5a).⁸ Sa structure a été confirmée par diffraction des rayons-X (CCDC 1850902, Scheme R5b). Lorsque le composé **6** est mis à réagir avec 1 équivalent d'alcyne iodé **2b** sous irradiation blue LEDs, un conversion faible de inférieure à 10% a été observée après 2h à température ambiante. Lorsque l'irradiation a été prolongée une nuit le produit **3ab** a été obtenu avec un rendement de 33% avec 20% de **4a** et 35% de produit issu de la protodeauration (**7**). (Scheme R5c). Cependant, l'addition de 10 mol% de **[Ir-F]** a permis de former **3ab** avec un excellent rendement de 95% (Scheme R5d).

⁷ Twilton, J., Le, C., Zhang, P., Evans R. W. & MacMillan, D. W. C. The merger of transition metal and photocatalysis. *Nat. Rev. Chem.* **1**, 0052 (2017).

⁸ Hashmi, A. S. K., Ramamurthi, T. D. & Rominger, F. On the Trapping of Vinylgold Intermediates *Adv. Synth. Catal.* **352**, 971–975 (2010).

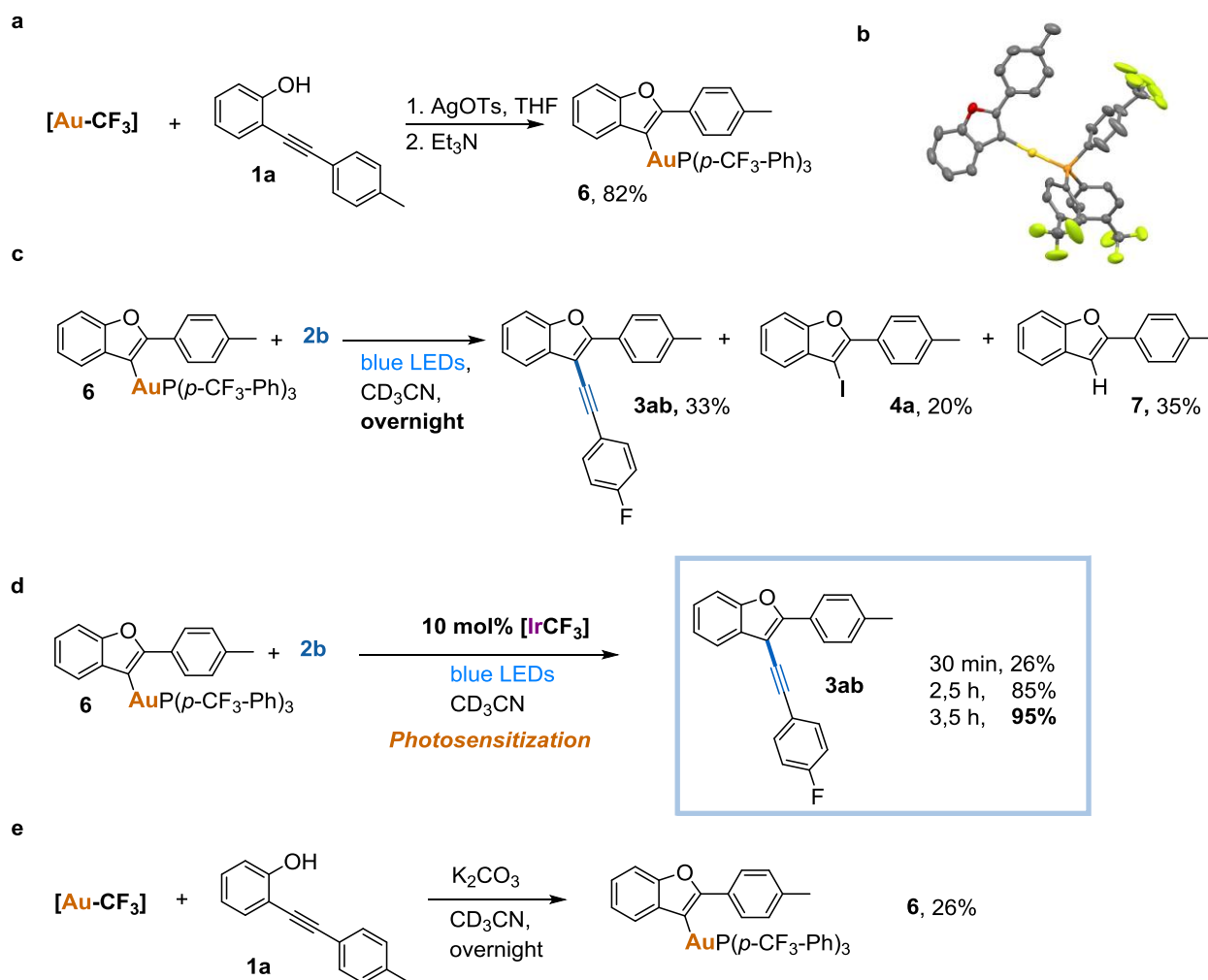


Schéma R5. A vinylgold(I) as plausible intermediate. **a** Preparation of vinylgold(I) **6**. **b** XRD structure of complex **6**. **c** Alkylation from **2b** and **6** under blue LEDs irradiation. **d** Alkylation from **2b** and **6** under blue LEDs irradiation in the presence of iridium photocatalyst. **e** Formation of vinylgold(I) **6** in the reaction conditions.

Etudes théoriques. Nous appuyant sur les résultats de De McCusker et MacMillan⁹ nous avons envisagé un transfert d'énergie du photocatalyseur vers le vinylor(I) avec l'implication d'un état excité pour **6** ($^3[\text{Ir-F}]$ ($^3\text{T}_1$)) (Figure R4).¹⁰

⁹ Welin, E. R., Le, C., Arias-Rotondo, D. M., McCusker, J. K. & MacMillan, D. W. C. Photosensitized energy transfer-mediated organometallic catalysis through electronically excited nickel(II). *Science* **355**, 380–385 (2017).

¹⁰ For an energy transfer with $[\text{Ir-F}]$, see: Lu, Z. & Yoon, T. P. Visible light photocatalysis of [2+2] styrene cycloadditions by energy transfer. *Angew. Chem. Int. Ed.* **51**, 10329–10332 (2012).

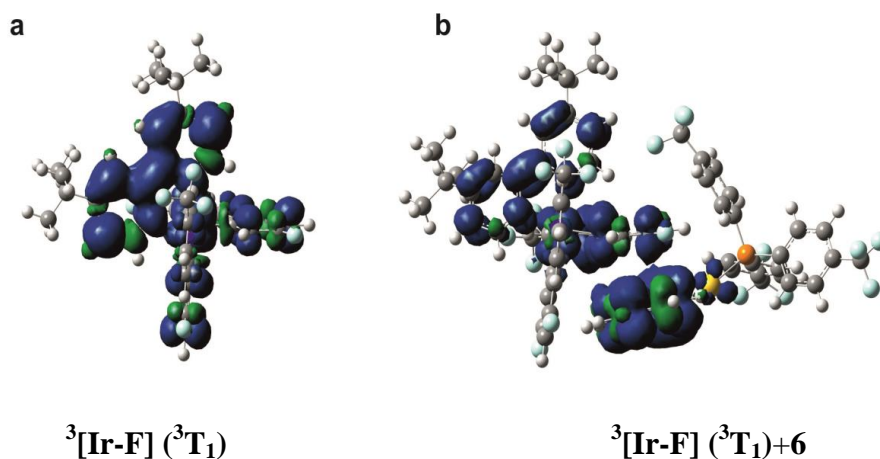


Figure R4. Spin density isosurface (isovalue 0.0006 a.u.). **a** Isolated ${}^3[\text{Ir-F}]$ complex. **b** $[\text{Ir-F}]^* ({}^3\text{T}_1)$ in the vicinity of **6**.

Ceci a été appuyé par des calculs théoriques (Figure R5).

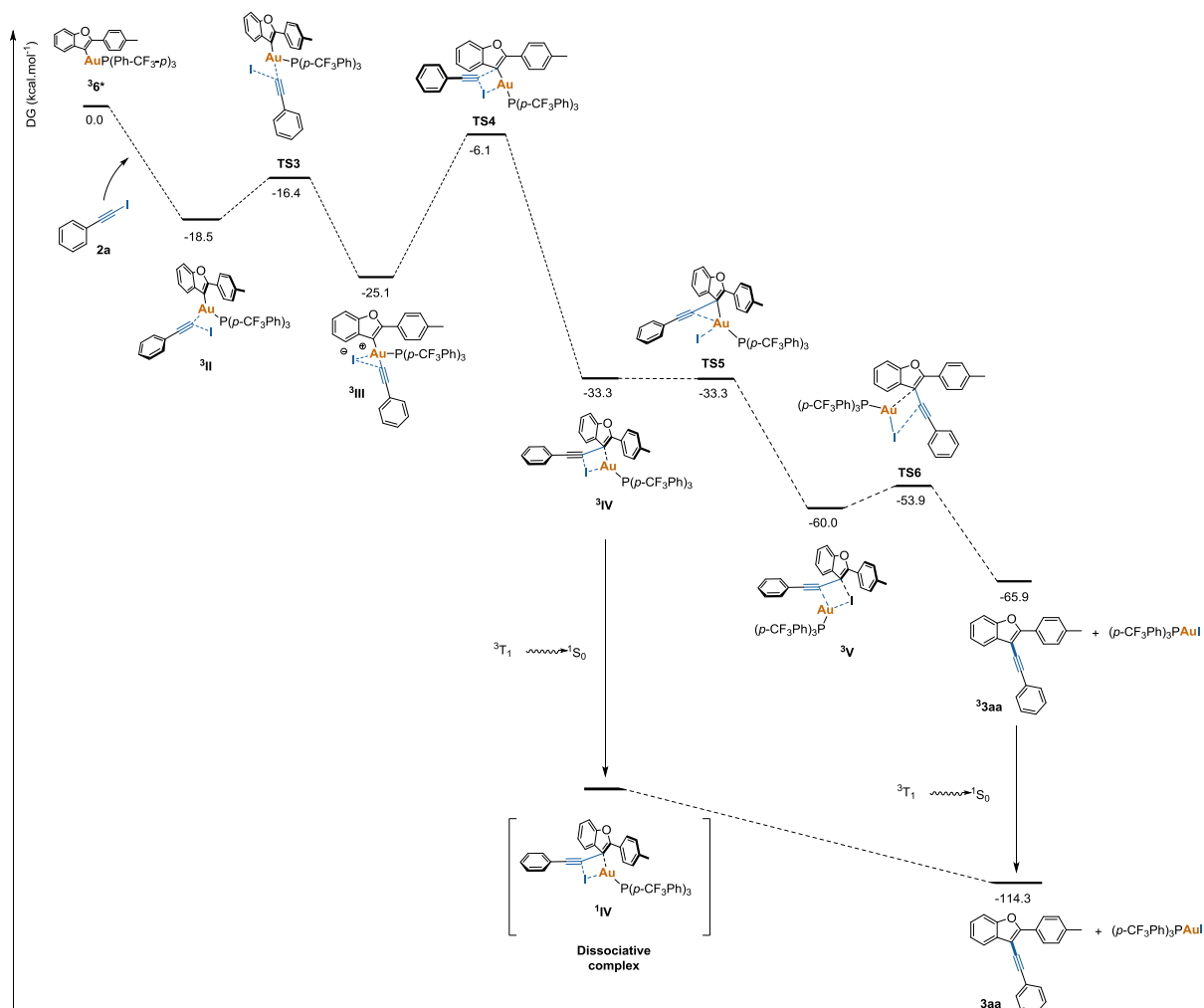


Figure R5. Potential energy surface of the reaction of ${}^3\mathbf{6}$ with $\mathbf{2a}$. Gibbs free energies (CH_3CN) are given relatively to the starting products and are in kcal/mol.

L'état excité $^3\mathbf{6}$ peut transférer son énergie à $\mathbf{2a}$. L'étude de la densité de spin autour de la liaison Au-C (portant l'iode) confirme que le transfert d'énergie a bien lieu à une distance relativement longue (3,6 Å). En suivant le chemin réactionnel explicité figure R5 le produit $\mathbf{3aa}$ est bien obtenu. Nous proposons donc le mécanisme réactionnel suivant (Figure R6). Une activation électrophile de la triple liaison donne le complexe vinylor(I). Ce dernier par transfert d'énergie du photocatalyseur d'iridium passe à l'état excité qui permet d'activer l'alcyne iodé qui après élimination réductrice donne le benzofurane attendu.

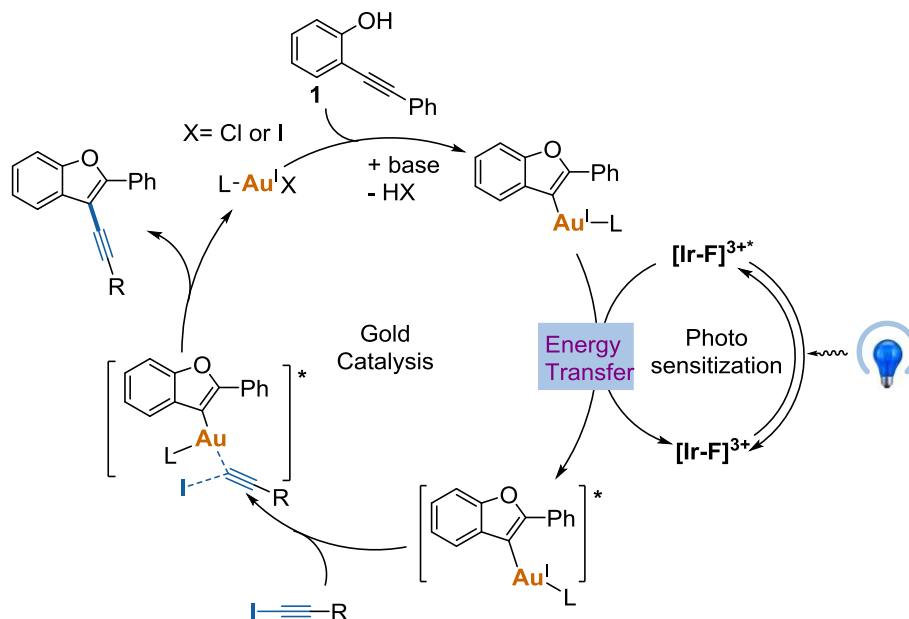


Figure R6. Mechanism proposal.

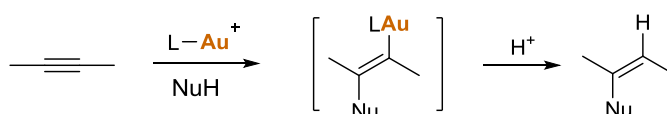
Conclusions

Au cours de ce travail nous avons mis au point une méthode efficace et générale de synthèse de benzofuranes par catalyse redox dual entre un sel de diazonium aryle et un *o*-alkynylphénols en présence d'un complexe d'or(I) et d'un photocatalyseur au ruthénium. Lorsque nous avons changé le partenaire de couplage et que nous avons fait réagir des iodoalcynes aryles nous avons bien obtenu les benzofuranes attendus. Nous avons mis en évidence par une étude mécanistique aussi bien en effectuant des réactions diagnostiques que des calculs théoriques que le système passait par un transfert d'énergie du photocatalyseur d'iridium sur le vinylor(I) formé par activation électrophile. Ce mécanisme jamais décrit dans la catalyse photoredox utilisant des complexes d'or(I) ouvre la voie à de nouvelles réactivités dans ce domaine.

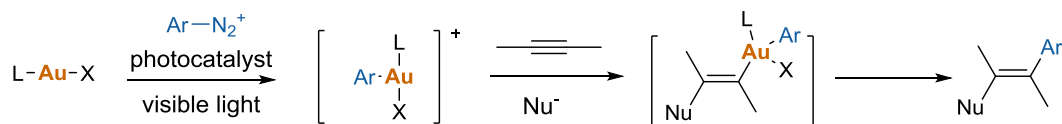
Introduction

Homogeneous gold catalysis has received great attention over the last decade.¹¹ The selective electrophilic activation of the carbon–carbon multiple bond by a gold complex generally constitutes the preliminary triggering event of the catalytic cycle.¹² In the vast majority of cases, the organogold species generated upon nucleophilic attack undergoes protodemetalation leading to hydrofunctionalized products (Figure Ia).

a) Gold-catalyzed nucleophilic addition to alkynes



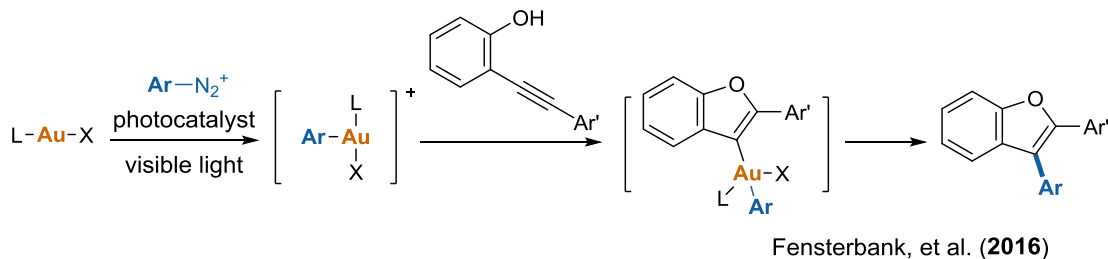
b) Dual Au and photoredox catalytic difunctionalization of alkynes



Glorius (2013), Toste (2014), Hashmi (2016)

c) Our work: gold(I) catalysis under visible light

i) first work: dual photoredox gold catalysis



ii) second work: photosensitized gold catalysis

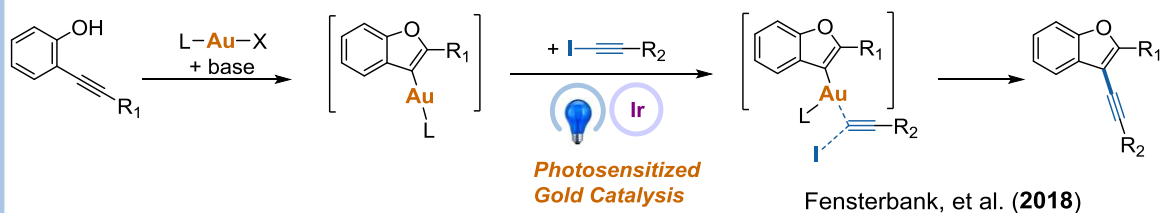


Figure I. Gold-catalyzed additions to alkynes.

¹¹ Dorel, R.; Echavarren, A. M. *Chem. Rev.* **2015**, *115*, 9028.

¹² Hashmi, A. S. K. *Chem. Rev.* **2007**, *107*, 3180.

Recently, the groups of Glorius, Toste and Hashmi reported a dual gold and photoredox catalytic difunctionalization of alkynes.¹³ In these transformations, aryldiazonium salts deliver aryl radicals under visible light irradiation. These radicals add to the gold catalyst, coordinated to alkynes and give the arylated compound rather than the hydrofunctionalized products (Figure Ib).

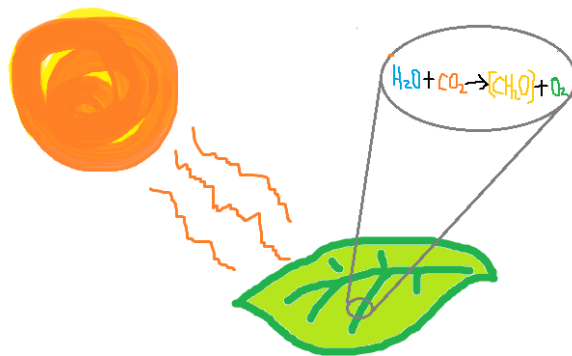
In 2016, we reported a dual photoredox/gold catalysis arylative cyclization of *ortho*-alkynylphenols with aryl diazonium salts: a flexible synthesis of benzofurans (Figure Ic-i).¹⁴ The reaction is proposed to proceed through a photoredox-promoted generation of a vinylgold(III) intermediate, formed by addition of the aryl radical to the gold catalyst and modulation of the oxidation state by the photocatalyst, following undergo reductive elimination to provide the heterocyclic coupling adduct. In 2018, we developed a new method for the synthesis of valuable alkynyl benzofuran derivatives devised from *o*-alkynylphenols and iodoalkynes in the presence of a catalytic mixture of Au(I) and Ir(III) under blue LED irradiation (Figure Ic-ii).¹⁵ This transformation involves a photosensitized oxidative addition of the iodoalkyne to the vinylgold(I) intermediate.

¹³ (a) Sahoo, B.; Hopkinson, M. N.; Glorius, F. *J. Am. Chem. Soc.* **2013**, *135*, 5505. (b) Hopkinson, M. N.; Sahoo, B.; Glorius, F. *Adv. Synth. Catal.* **2014**, *356*, 2794. (c) Tlahuext-Aca, A.; Hopkinson, M. N.; Sahoo, B.; Glorius, F. *Chem. Sci.* **2016**, *7*, 89. (d) Shu, X.-z.; Zhang, M.; Frei, H.; Toste, F. D. *J. Am. Chem. Soc.* **2014**, *136*, 5844. (e) He, Y.; Wu, H.; Toste, F. D. *Chem. Sci.* **2015**, *7*, 1194. (f) Kim, S.; Rojas-Martin, J.; Toste, F. D. *Chem. Sci.* **2016**, *7*, 85. (g) Huang, L.; Rudolph, M.; Rominger, F.; Hashmi, A. S. K. *Angew. Chem. Int. Ed.* **2016**, *55*, 4808.

¹⁴ Xia, Z.; Khaled, O.; Mouries-Mansuy, V.; Ollivier, C.; Fensterbank, L. Dual Photoredox/Gold Catalysis Arylative Cyclization of *o*-Alkynylphenols with Aryldiazonium Salts: A Flexible Synthesis of Benzofurans. *J. Org. Chem.* **2016**, *81*, 7182.

¹⁵ Has been submitted.

Chapter 1 Background



Photosynthesis, the Sun, 400 million years ago

1 Gold Catalysis

1.1 History of Gold Catalysis

For centuries, gold has been considered a precious, purely decorative inert metal. The symbol of gold is Au (from Latin: *aurum*), and the atomic number is 79. The pure form of gold is a bright, slightly reddish yellow, dense, soft, malleable, and ductile metal. Gold has accompanied humanity from very early days. It has been considered the most valuable metal since ancient times and forms the basis of most monetary systems in the world. Gold is in its elemental form naturally, and due to its low reactivity can be mined directly from the earth, which leads to prospecting and the "gold rush" in the second half of 19th century (Figure 1-1). It has always been valuable, which reflects the Greek myth of King Midas well. Today, Mayan art or Egyptian funerary masks are as beautiful as their first plaster and emphasize the resilience and inertia of metallic gold.¹⁶

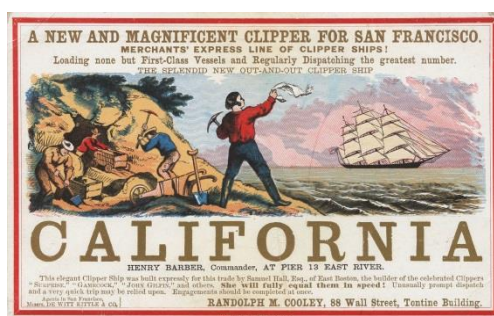


Figure 1-1. Gold rush in California, 1848–1855; Source: Website.

Alchemy is the philosophy and ancestor of a chemical philosophy in the Middle Ages, it is the embryo of contemporary chemistry. Its goal is to convert some basic metals into gold through chemical methods, to create panacea and to prepare elixir of life. The current science shows that this method does not work. But until the 19th century, alchemy had not been denied by scientific evidence. Some famous scientists, including Isaac Newton, have tried alchemy. The emergence of modern chemistry made people doubt the possibility of alchemy. Alchemy spanned at least 2,500 years under a complex network that existed in Mesopotamia, Ancient Egypt, Persia, India, China, Japan, North Korea, Ancient Greece, and Rome, as well as Muslim civilization, and then existed in Europe until the 19th century. Although it is

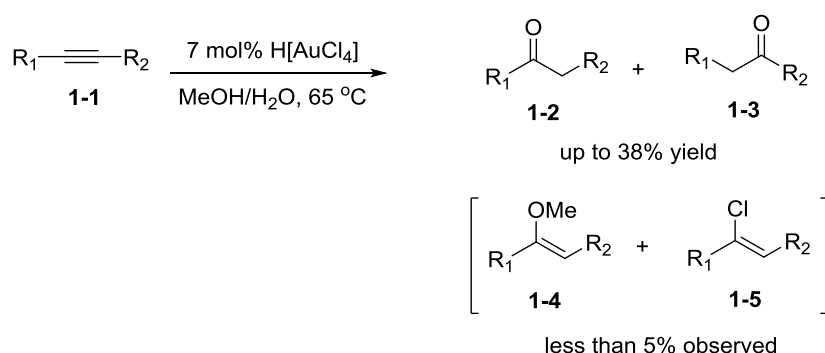
¹⁶ Hashmi, A. S. K. *Chem. Rev.* **2007**, *107*, 3180.

impossible to succeed, it has accumulated a lot of knowledge for the development and emergence of chemistry.

Chemically, gold is a transition metal and a group 11 element. It is one of the least reactive chemical elements and is solid under standard conditions. Gold often occurs in free elemental (native) form, as nuggets or grains, in rocks, in veins, and in alluvial deposits. Gold is resistant to most acids, though it does dissolve in aqua regia, a mixture of nitric acid and hydrochloric acid, which forms a soluble tetrachloroaurate anion. Gold is insoluble in nitric acid, which dissolves silver and base metals, a property that has long been used to refine gold and to confirm the presence of gold in metallic objects, giving rise to the term acid test. Gold also dissolves in alkaline solutions of cyanide, which are used in mining and electroplating.

However, gold was ignored in favor of other transition metals in the last century until chemists really began exploring homogeneous catalysis. The low catalytic activity may be erroneously deduced from the inertness of elemental gold, which is only soluble in aqua regia or oxidants such as air with the assistance by strong ligands such as cyanide.

The first reaction, which was catalyzed by homogeneous gold, was described in 1976, when Thomas,¹⁷ who worked with stoichiometric tetrachloroauric acid and alkynes in aqueous methanol, found as main products ketones **1-2** and **1-3** formed by a Markovnikov addition (Scheme 1-1). The observed by-products, less than 5% of the corresponding methyl-vinyl ethers (**1-4**) and vinyl chlorides (**1-5**), give a glimpse of the future, in which gold is often used today for direct nucleophilic additions. In this key paper for the field, types of products that later became very important in gold catalysis are reported.



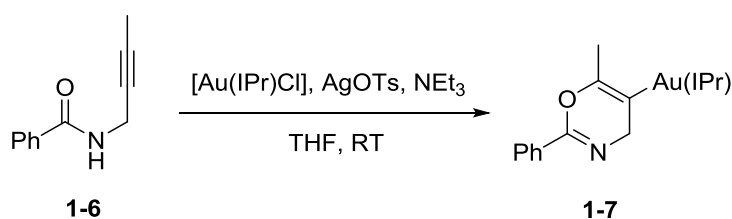
Scheme 1-1. Thomas gold(III)-catalyzed reaction.

¹⁷ Norman, R. O. C.; Parr, W. J. E.; Thomas, C. B. *J. Chem. Soc. Perkin. Trans. 1*, **1976**, 1983.

Now, gold(I) complexes are used as a very effective catalysts for electrophilic activation of alkynes under homogeneous conditions, and a wide range of versatile synthetic tools have been developed for the construction of carbon-carbon or carbon-heteroatom bonds.

1.2 Important Gold Intermediates: Vinylgold(I) and Gold(I) Acetylide

Gold-catalyzed organic reactions represent a truly fruitful area of research in organic chemistry. The tendency of gold to act as a Lewis acid that can activate for C-C multiple bonds has made the gold-catalyzed organic transformations of utmost importance. It is commonly accepted that cationic gold(I) complexes activate the C-C multiple bonds to form organogold species that will undergo nucleophilic attack to afford various products. For a clear understanding of the mechanism involved in these cationic gold (I) complexes, the capture of such intermediates has become very important. Fortunately, Hashmi et al. succeeded in the isolation of a vinylgold(I) intermediate complex (**1-7**)¹⁸ resulting from a 6-*endo-dig* cyclization of N-propargyl carboxamides (**1-6**)¹⁹ (Scheme 1-2).



Scheme 1-2. Gold-catalyzed cyclization of 2-alkynylphenol.

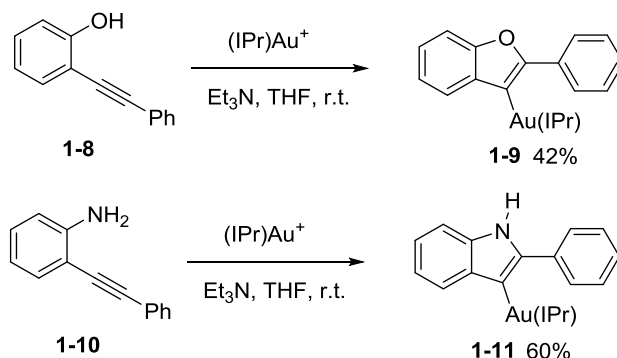
In 2010, Hashmi²⁰ reported a gold-catalyzed cyclization of 2-alkynylphenol (**1-8**) leading to furans (Scheme 1-3). In the presence of cationic gold complexes and triethylamine, the vinylgold(I) can be formed from 2-alkynylphenol (**1-8**) and 2-alkylaniline (**1-10**),

¹⁸ (a) Weyrauch, J. P.; Hashmi, A. S. K.; Schuster, A.; Hengst, T.; Schetter, S.; Littmann, A.; Rudolph, M.; Hamzic, M.; Visus, J.; Rominger, F.; Frey, W.; Bats, J. W. *Chem. Eur. J.* **2010**, *16*, 956. (b) Hashmi, A. S. K.; Rudolph, M.; Schymura, S.; Visus, J.; Frey, W. *Eur. J. Org. Chem.* **2006**, 4905. (c) Hashmi, A. S. K.; Weyrauch, J. P.; Frey, W.; Bats, J. W. *Org. Lett.* **2004**, *6*, 4391. For other studies on gold-catalyzed oxazole synthesis from propargyl carboxamide, see: (d) Milton, M. D.; Inada, Y.; Nishibayashi, Y.; Uemura, S. *Chem. Commun.* **2004**, *0*, 2712.

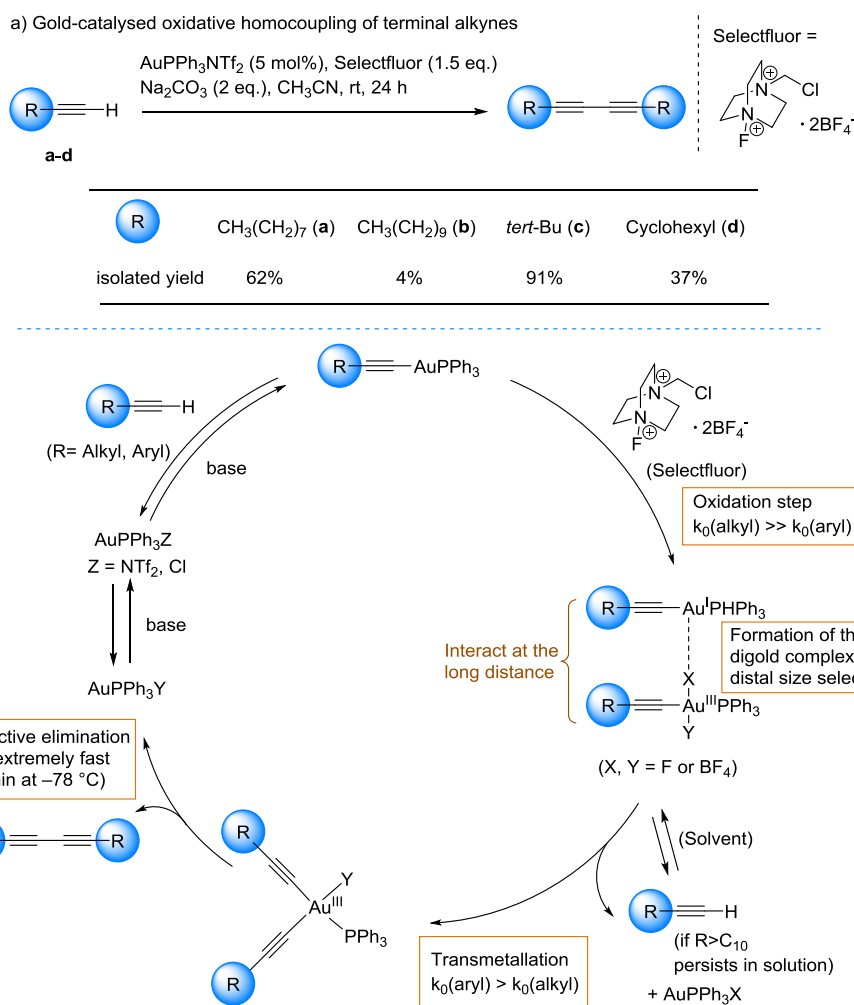
¹⁹ (a) Hashmi, A. S. K.; Ramamurthi, T. D.; Rominger, F. *Adv. Synth. Catal.* **2010**, *352*, 971. (b) Hashmi, A. S. K.; Ramamurthi, T. D.; Rominger, F. *J. Organomet. Chem.* **2009**, *694*, 592. (c) Hashmi, A. S. K. *Gold Bull.* **2009**, *42*, 275. (d) Hashmi, A. S. K.; Schuster, A. M.; Rominger, F. *Angew. Chem., Int. Ed.* **2009**, *48*, 8247. For previously reported vinylgold(I) complexes, see: (e) Weber, D.; Tarselli, M. A.; Gagné, M. R. *Angew. Chem., Int. Ed.* **2009**, *48*, 5733. (f) Liu, L.-P.; Xu, B.; Mashuta, M. S.; Hammond, G. B. *J. Am. Chem. Soc.* **2008**, *130*, 17642. (g) Mohr, F.; Falvello, L. R.; Laguna, M. *Eur. J. Inorg. Chem.* **2006**, 833.

²⁰ Hashmi, A. S. K.; Ramamurthi, T. D.; Rominger, F. *Adv. Synth. Catal.* **2010**, *352*, 971.

respectively. These two heteroarene gold(I) compounds were successfully isolated and characterized by NMR and X-ray diffraction analysis. These reaction conditions can broaden the scope of isolation of organometallic intermediates in gold-catalysed nucleophilic additions to alkynes.



Scheme 1-3. Aurated heteroarenes as alkyne-derived “vinylgold” intermediates.



Scheme 1-4. distal size selectivity with a digold catalyst.

In 2015, Antonio Leyva-Perez and Avelino Corma²¹ reported the homocoupling of terminal alkynes under gold-catalysed conditions (Scheme 1-4). This is a distal size selectivity of alkynes with gold catalysts, the initial rate of 1-decyne **a** is 3.5 times higher than 1-dodecyne **b**, and 1-decyne **a** smoothly converts to the homocoupling product (Scheme 1-4a). They proposed a mechanism involves the gold-catalysed homocoupling of alkynes with distal size selectivity. The formation of a Au(I)/Au(III) digold intermediate is responsible for the distal steric differentiation. The catalytic sequences include oxidation of gold(I) to gold (III), formation of the digold complex, transmetalation of the alkyne and reductive elimination (Scheme 1-4b). They proved that gold(I) acetylides could be oxidized by Selectfluor, forming the homocoupling product. The active acetylide gold species can decompose to O=PPh₃, the free terminal alkyne and gold mirror.

In 2010, Gouverneur²² reported a gold(I)-catalyzed cyclization-oxidative cross-coupling cascade of allenates and terminal alkynes, a various of β -alkynyl- γ -butenolides could be prepared (Scheme 1-5).

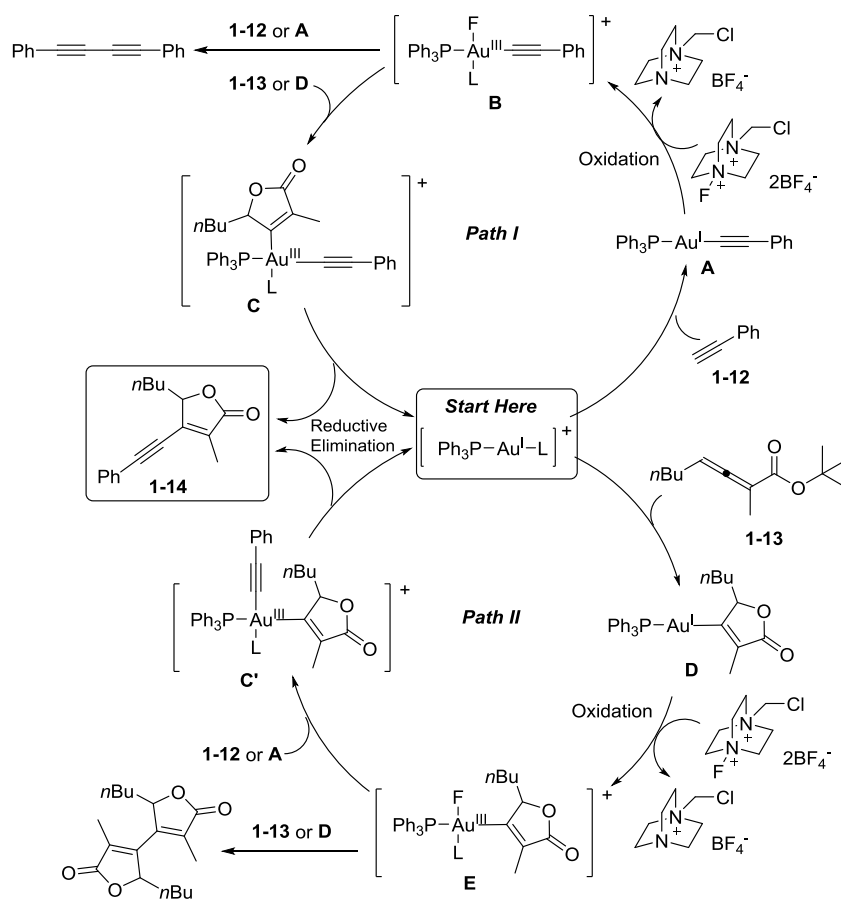
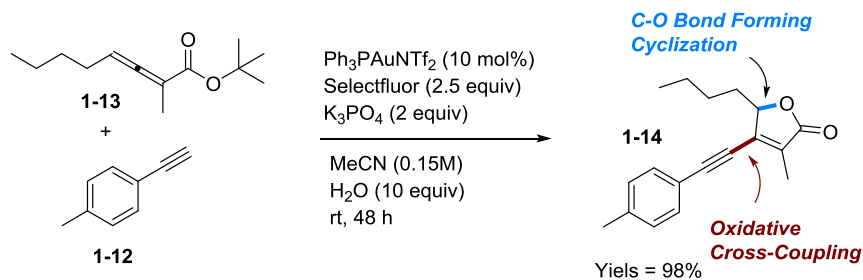
Two plausible pathways involving a Au(I)/Au(III) redox cycle are proposed. In the presence of base, the alkynylgold(I) intermediate **A** could be formed by initial deprotonation of the alkyne and subsequent coordination to the cationic gold(I) catalyst. The Selectfluor could oxidize the gold center to afford the square planar gold(III) cationic intermediate **B**. Toste et al.²³ showed the gold(III) complex **C** could result from coordination of this species **B** to the allene followed by nucleophilic attack of the pendant tert-butyl ester. After reductive elimination, this species delivers the cross-coupled product and regenerates the gold(I) catalyst (Scheme 1-5, path I).²⁴ Alternatively, vinylgold(I) species **D** would be formed by the allenolate cyclization between the cationic gold(I) catalyst and allene, and it could occur prior to the alkyne coordination step. In this pathway, oxidation of the organogold(I) intermediate **D** by Selectfluor would lead to the gold(III) complex **E**. After alkynylation, intermediate **C'** would undergo reductive elimination to afford the product and regenerate the catalyst (Scheme 1-5, path II).

²¹ Leyva-Pérez, A.; Doménech-Carbó, A.; Corma, A. *Nat. Commun.* **2015**, 6703.

²² For a seminal gold catalyzed alkynylation of a vinylgold intermediate relying on an external stoichiometric oxidant, see: Hopkinson, M. N.; Ross, J. E.; Giuffredi, G. T.; Gee, A. D.; Gouverneur, V. *Org. Lett.* **2010**, 12, 4904.

²³ Mankad, N. P.; Toste, F. D. *J. Am. Chem. Soc.* **2010**, 132, 12859.

²⁴ de Haro, T.; Nevado, C. *J. Am. Chem. Soc.* **2010**, 132, 1512.



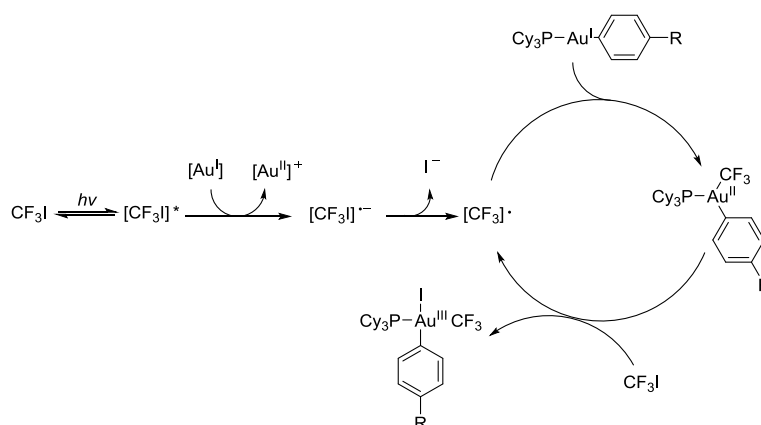
Scheme 1-5. Gold(I)-catalyzed cascade cyclization-oxidative cross-coupling and plausible reaction mechanism.

1.3 Au(I)/Au(III) Chemistry

Gold redox catalysis has received far less attention compared to the well-established foundation of carbophilic Au(I) Lewis acid catalysis. With a significantly high redox potential of the Au(I)/Au(III) couple ($E_0 = 1.41$ V, higher than that of the Pd⁰/Pd^{II} couple $E_0 = 0.92$ V), strong oxidants are required to allow the oxidation of Au(I) species, which limits the functional group compatibility of gold redox catalysis.

However, recent fundamental organometallic investigations have shown that the gold(I) complexes which contain particular electronic and structural features can undergo oxidative addition of C(sp³)-X bonds, C(sp²)-X bonds, as well as apolar σ -bonds (Si-Si, Sn-Sn, and even C-C).²⁵

In 2014, Toste showed that two-coordinate phosphine gold(I) aryl complexes reacted with CF₃I under near-ultraviolet irradiation.²⁶ The resulting gold(III) complexes are quite stable and were characterized by X-ray diffraction studies. Mechanistic investigation suggested that a photoinitiated radical chain reaction was involved (Scheme 1-6). Firstly, the gold(I) aryl complex reduced the photoexcited CF₃I to radical anion [CF₃I]^{•-}, which would split into iodide and [CF₃][•]. A tricoordinate gold(II) complex was formed through radical addition of [CF₃][•] to [(Cy₃P)Au(Ar)], which was followed by the oxidation by CF₃I to yield the trifluoromethyl aryl gold(III) complex.



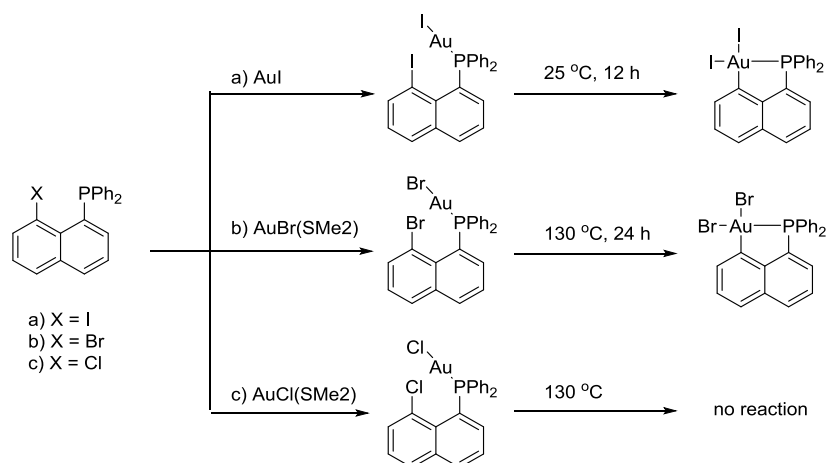
Scheme 1-6. Radical chain mechanism proposed for the formal oxidative addition of CF₃I to two-coordinate phosphine gold(I) aryl complexes (R=H, F, Me, OMe).

In the same year, Amgoune, Bourissou, and co-workers reported a (P,C) cyclometalated gold(III) complexes through activation of aryl halides at gold(I).²⁷ The 8-halonaphthyl phosphines ligands which position the C(sp²)-X bond in close proximity to the gold center upon coordination of the phosphine (Scheme 1-7). It readily occurs at room temperature for the intramolecular oxidative addition of the C(sp²)-I bond to give a stable P,C-cyclometallated gold(III) diiodo complex.

²⁵ Joost, M.; Amgoune, A.; Bourissou, D. *Angew. Chem. Int. Ed.*, **2015**, *54*, 15022.

²⁶ Winston, M. S.; Wolf, W. J.; Toste, F. D. *J. Am. Chem. Soc.*, **2014**, *136*, 7777.

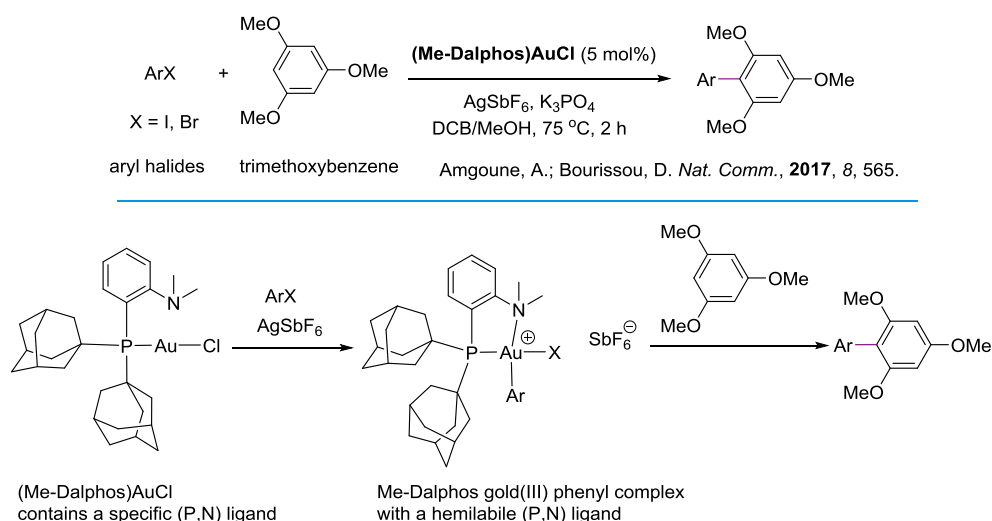
²⁷ Guenther, J.; Mallet-Ladeira, S.; Estevez, L.; Miqueu, K.; Amgoune, A.; Bourissou, D. *J. Am. Chem. Soc.*, **2014**, *136*, 1778.



Scheme 1-7. Coordination of 8-halo-naphthyl-phosphines to gold(I) followed by intramolecular C(sp²)-I and C(sp²)-Br oxidative addition.

This intramolecular unimolecular process was shown to follow first-order kinetics. For the oxidative addition of PhI to two-coordinate gold(I) complexes, the activation barrier is 10–15 kcal mol⁻¹ lower than that predicted for related intermolecular reactions. However, it requires heating at 130 °C for the activation of the corresponding C(sp²)-Br bond, and oxidative addition of the C(sp²)-Cl bond was not observed even at higher temperatures.

In 2017, Amgoune and Bourissou²⁸ reported cross couplings reactions through an Au(I)/Au(III) catalytic cycle which was promoted by bidentate ligands on gold (I) with specific characteristics (Scheme 1-8).

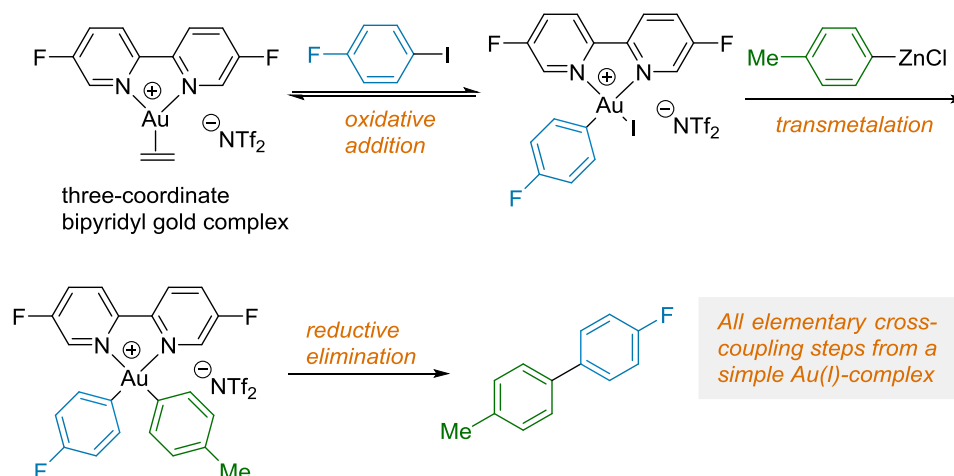


Scheme 1-8. Gold-catalyzed arylation of 1,3,5-trimethoxybenzene with aryl halides.

²⁸ Zeineddine, A.; Estévez, L.; Mallet-Ladeira, S.; Miqueu, K.; Amgoune, A.; Bourissou, D. *Nat. Comm.*, **2017**, *8*, 565.

This Au(I)/Au(III) catalytic cycle involves a catalytic sequence of Csp^2-X oxidative addition, Csp^2-H auration and reductive elimination, allowing a gold-catalyzed direct arylation of arenes with aryl halides. The (Me-Dalphos)AuCl contains an ancillary (P,N) ligand, which allows the oxidative addition of aryl halides to proceed.

In 2018, McGrady, Bower and Russell reported an available bipyridyl ligands facilitate oxidative addition of aryl iodides to Au(I) center, which undergo aryl-zinc transmetalation and reductive elimination to produce biaryl products (Scheme 1-9).²⁹



Scheme 1-9. Au-mediated Negishi cross-coupling.

The three-coordinate bipyridyl complexes of gold, $[(\kappa^2\text{-bipy})\text{Au}-(\eta^2\text{-C}_2\text{H}_4)][\text{NTf}_2]$, can be accessed readily by addition of 2,2'-bipyridine, or its derivatives, with the homoleptic gold ethylene complex prepared *in situ*. The three-coordinate bipyridyl gold complex undergoes sequential aryl-iodide oxidative addition, aryl-zinc transmetalation, and C–C reductive elimination to provide the first example of a Au-mediated Negishi cross-coupling. Relying on the simple bipyridyl ligand framework, this chemistry enhances backdonation from Au to facilitate the key Ar–I oxidative addition step.

²⁹ Harper, M. J.; Arthur, C. J.; Crosby, J.; Emmett, E. J.; Falconer, R. L.; Fensham-Smith, A. J.; Gates, P. J.; Leman, T.; McGrady, J. E.; Bower, J. F.; Russell, C. A. *J. Am. Chem. Soc.* **2018**, *140*, 4440.

2 Gold Catalysis Under Visible Light

2.1 Photocatalysis and Dual Catalysis

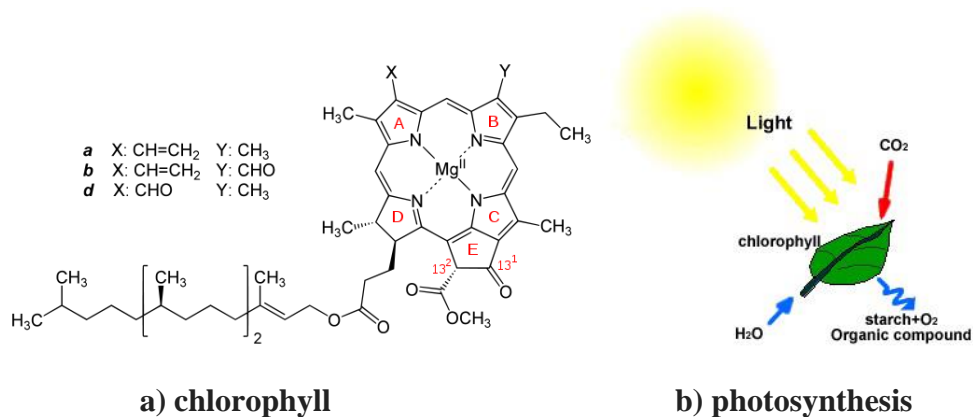


Figure 1-2. Structure of chlorophyll and process of photosynthesis.

What is photocatalysis? Generally speaking, photocatalysis is a reaction which uses light to activate a substance which modifies the rate of a chemical reaction without being involved itself. And the photocatalyst is the substance which can modify the rate of a chemical reaction using light irradiation. The most important photocatalyst in our earth may be the chlorophyll of plants. The left picture shows the structure of chlorophyll (Figure 1-2). At the center of the chlorin ring is a magnesium ion. And the right picture shows the process of photosynthesis (Figure 1-2): chlorophyll captures sunlight to turn water and carbon dioxide into oxygen and glucose. Concerning man-made photocatalysts that generate reactive radical species under light irradiation, then these free radicals can undergo secondary reactions.

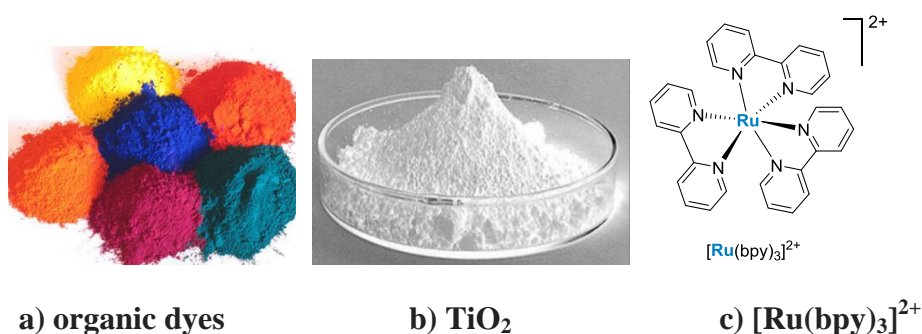
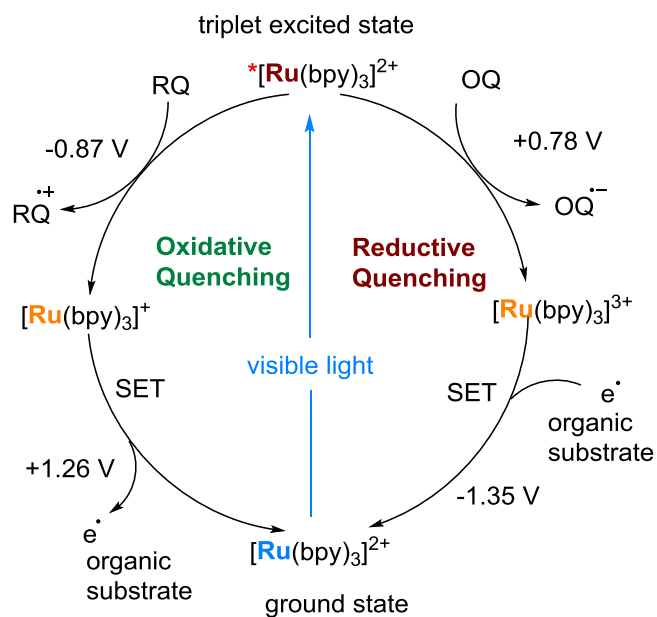


Figure 1-3. Man-made photocatalyst.

Alongside organic dyes and inorganic semiconductors (like titanium dioxide, TiO₂), the most widely-used photocatalysts are bipyridyl transition-metal complexes, like ruthenium-

tris(2,2'-bipyridyl) dichloride $[\text{Ru}(\text{bpy})_3]\text{Cl}_2$ and iridium catalyst $[\text{Ir}\{\text{dF}(\text{CF}_3)\text{ppy}\}_2(\text{dtbpy})]\text{PF}_6$ (Figure 1-3).



Scheme 1-10. Simplified photo absorption scheme.

Under visible light irradiation, the ground state Ru catalyst will transfer to triplet excited state (Scheme 1-10). The triplet excited state of Ru catalyst is both a strong oxidant and reductant. Single electron transfer (SET) can then occur, either from an organic substrate to the excited photocatalyst (termed “reductive quenching, RQ”) or from the photocatalyst to the substrate (termed “oxidative quenching, OQ”). The overall result of this process is the generation of radical-anions or radical-cations.³⁰

The Figure 1-4 shows the explosive number of papers published in the field of organic photoredox catalysis. It begins around 2009, when less than 10 papers was published, but there is about 200 photoredox papers published in 2015.³¹

³⁰ Stephenson, C. R. J. et al. *J. Org. Chem.* **2012**, *77*, 1617.

³¹ MacMillan, W. C. et al. *J. Org. Chem.*, **2016**, *81*, 6898.

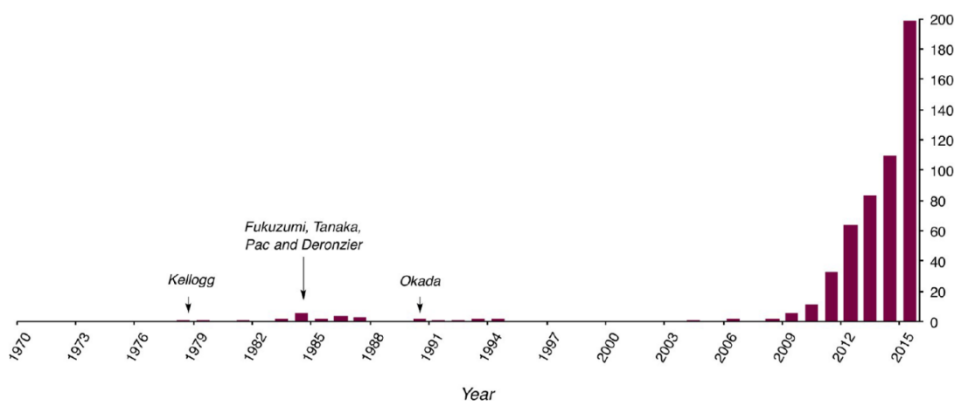
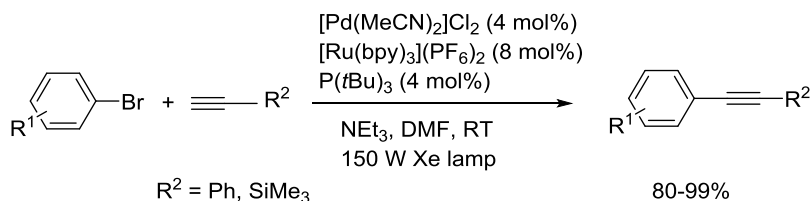


Figure 1-4. Papers published per year in the field of organic photoredox catalysis.

The first example of dual palladium/photoredox catalytic system was reported by Osawa in 2007 (Scheme 1-11).³² Here, the efficiency of the copper-free Sonogashira coupling was shown to significantly increase in the presence of $[\text{Ru}(\text{bpy})_3](\text{PF}_6)_2$ and visible light. The role of the photocatalyst was not elucidated and, consequently, the significance of combining photoredox and transition metal catalysis was not fully appreciated until the seminal report of Sanford and co-workers four years later.

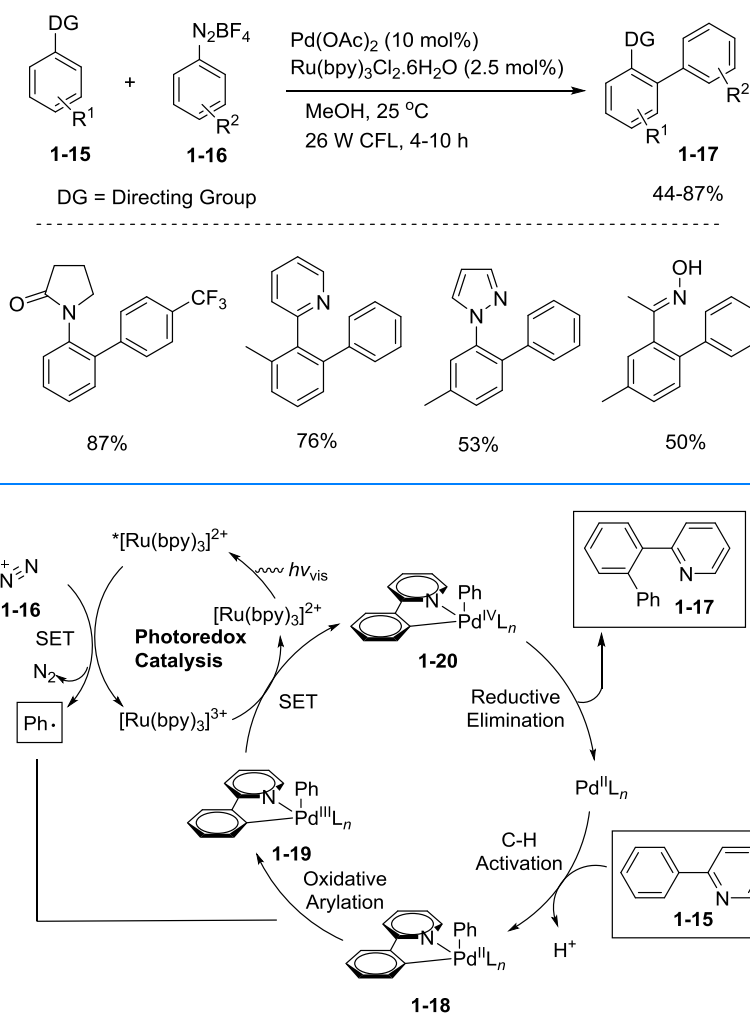


Scheme 1-11. Photoredox-promoted Sonogashira coupling.

In 2011, Sanford and co-workers³³ reported a dual photoredox/palladium catalysis involving direct arylation of unactivated arenes **1-15** by means of C-H bond activation (Scheme 1-12). The photocatalyst in this transformation is implicated in two key steps: (a) reduction of the aryldiazonium salt to generate an aryl radical and (b) oxidation of the Pd(III)-aryl species **1-19** via a SET event. In contrast to other synthetic routes to aryl coupling partner which required very high reaction temperatures, this process occurs at room temperature and thus highlights the capacity of photoredox catalysis to generate reactive species under remarkably mild conditions.

³² Osawa, M.; Nagai, H.; Akita, M. *Dalton Trans.* **2007**, 827.

³³ Kalyani, D.; McMurtrey, K. B.; Neufeldt, S. R.; Sanford, M. S. *J. Am. Chem. Soc.*, **2011**, *133*, 18566.



Scheme 1-12. Room-temperature arylation of unactivated arenes with aryldiazonium salts and proposed mechanism.

2.2 Dual Gold/Photoredox Catalysis

In recent years, gold catalysis under visible light has received great attention. In order to expand the scope of conventional hydrofunctionalization, various gold catalytic reactions involving visible light have been developed to overcome the high potential of the Au(I)/Au(III) redox couple. The first milestone works were reported by the groups of Glorius and Toste: a dual gold and photoredox catalytic difunctionalization of alkynes. Utilizing the methodology of dual gold/photoredox catalysis, a number of new difunctionalization reactions of π -systems developed by them and several other groups were reported later. In

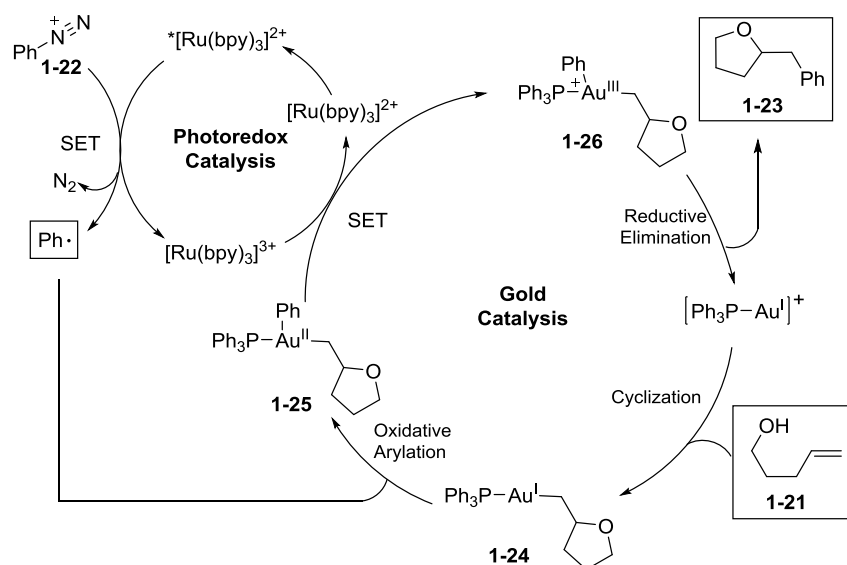
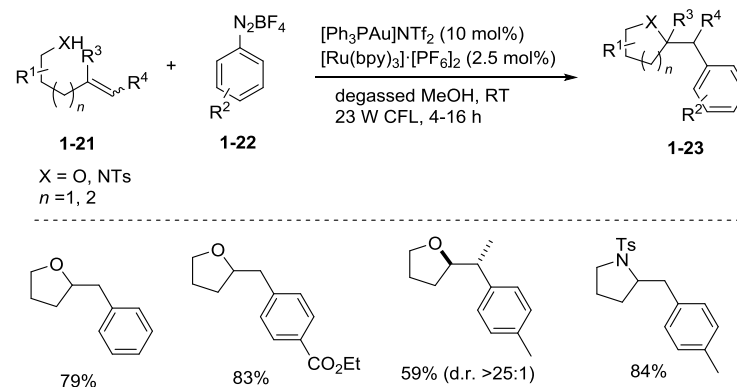
addition to photoredox, photosensitizer-free, and photoinduced energy transfer processes have been reported.

Recently, Glorius, Toste, and others, greatly extended the scope of gold redox catalysis by avoiding the use of a strong oxidant. In these studies, it is demonstrated that aryl radicals, *in situ* generated from aryl diazonium salts, could serve as effective oxidants to promote gold oxidation and lead to a cationic Au(III)/aryl species under photoactivation conditions (with or without photosensitizer).

The first example of combining gold catalysis with photoredox catalysis was established by Glorius and co-workers³⁴ in 2013 (Scheme 1-12). Utilizing the gold and photoredox dual-catalytic system, the intramolecular oxy- and aminoarylation of alkenes with aryldiazonium salts has been developed. In the presence of [Ru(bpy)₃][PF₆]₂ (2.5 mol%) and the gold(I) source [Ph₃PAu]NTf₂ (10 mol%), alkenyl alcohols or amines **1-21** reacted with aryldiazonium salts **1-22** and delivered the corresponding arylated heterocyclic compounds **1-23** (Scheme 1-12). This transformation can generate arylated heterocyclic compounds at room temperature under irradiation from a simple household light bulb. It demonstrates this dual-catalytic system can expand the scope of the nucleophilic addition reactions to carbon–carbon multiple bonds.

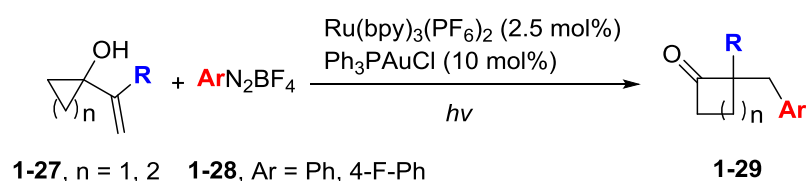
A mechanism involving a photoredox-induced homogeneous Au(I)/Au(III) redox cycle was proposed in Scheme 1-13. The first step is coordination of the cationic gold(I) catalyst to the alkene followed by intramolecular nucleophilic attack affording the alkylgold(I) complex **1-24**. Upon irradiation with visible light, the reaction of ArN₂BF₄ with photoexcited Ru(bpy)₃^{2+*} generates Ru(bpy)₃³⁺ and an aryl radical which oxidized the alkylgold(I) complex **1-24** to generate gold(II) species **1-25**. Single electron transfer to [Ru(bpy)₃]³⁺ would then regenerate the photoredox catalyst and afford the gold(III) complex **1-26** amenable to product-forming reductive elimination.

³⁴ Sahoo, B.; Hopkinson, M. N.; Glorius, F. *J. Am. Chem. Soc.*, **2013**, *135*, 5505.

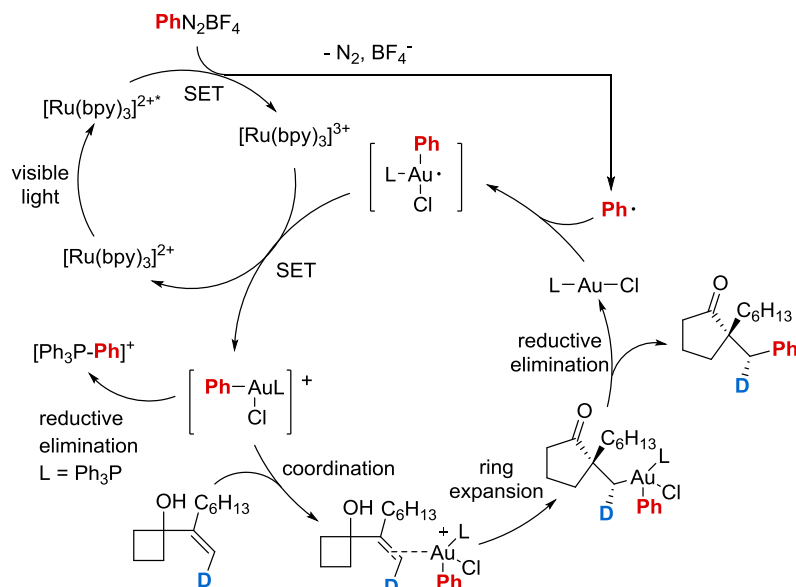


Scheme 1-13. Oxy- and aminoarylation of alkenes co-catalyzed by gold and proposed mechanism.

In 2014, Toste³⁵ demonstrated that light-mediated generation of aryl radicals from aryldiazonium salts could also be harnessed in dual photoredox Au-catalyzed protocols to accomplish arylation ring expansion, utilizing cyclopropanols and cyclobutanols **1-27** for the synthesis of cyclobutanones or cyclopentanones **1-29** (Scheme 1-14). The mechanistic studies showed that formal oxidative addition of gold(I) to aryldiazonium salts to form gold(III)–Ar species precedes the reaction with the alkene.

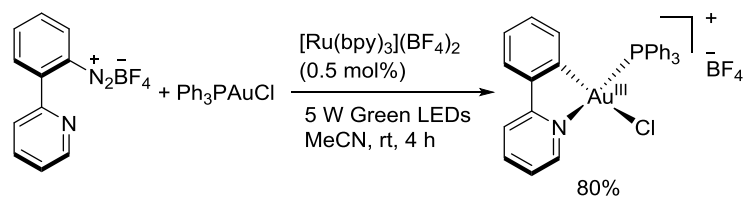


³⁵ Shu, X.-Z.; Zhang, M.; He, Y.; Frei, H.; Toste, F. D. *J. Am. Chem. Soc.* **2014**, *136*, 5844.



Scheme 1-14. Dual photoredox Au-catalyzed arylation ring expansion and proposed mechanism.

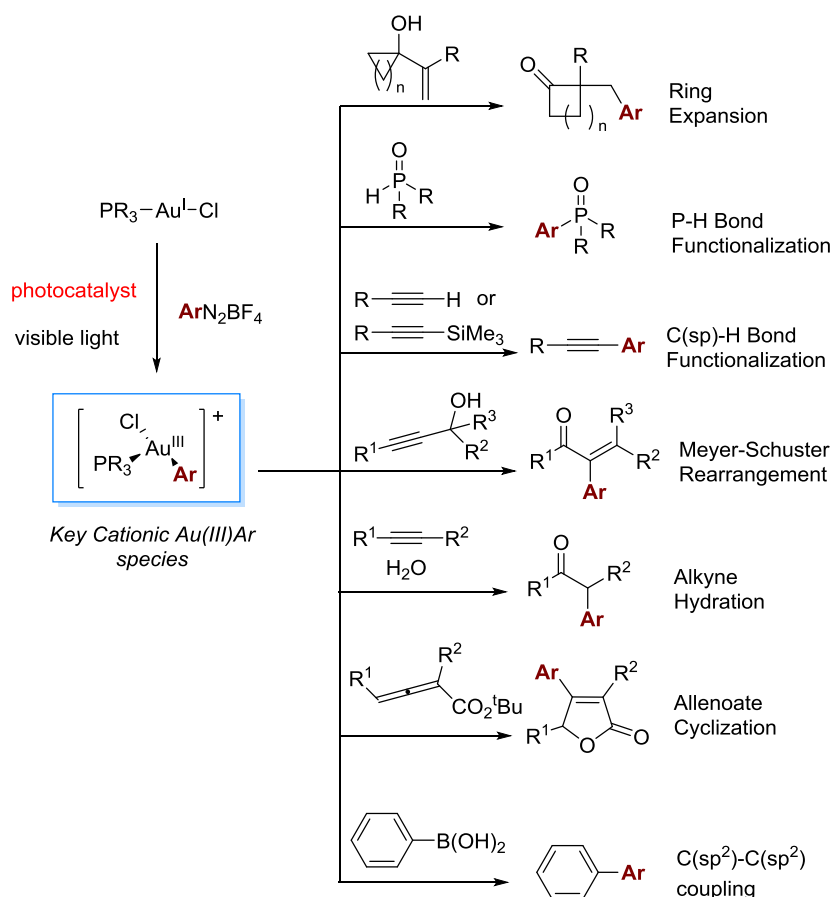
In this dual photoredox Au-catalyzed protocols, the aryl radicals generated from the aryldiazonium salts facilitate the challenging oxidation of gold(I) to gold(III). The oxidation of gold(I) was supported by mechanistic studies from the groups of Frei and Toste,³⁵ and Shin³⁶ used time-resolved FT-IR spectroscopic and XPS measurements, respectively. Moreover, the Glorius group³⁷ prepared and isolated arylgold(III) complexes directly from the stoichiometric reaction of PPh_3AuCl with the 2-pyridyl-substituted aryldiazonium salt, to confirm the key aryl radical-induced oxidation step (Scheme 1-15).



Scheme 1-15. Photoredox promoted oxidative addition to triphenylphosphinegold(I)chloride.

³⁶ Patil, D. V.; Yun, H.; Shin, S. *Adv. Synth. Catal.* **2015**, 357, 2622.

³⁷ Tlahuext-Aca, A.; Hopkinson, M. N.; Daniliuc, C. G.; Glorius, F. *Chem. - Eur. J.* **2016**, 22, 11587.



Scheme 1-16. Further expansion of the concept to various functionalization processes: P-H bond functionalization, C(sp)-H bond functionalization, Meyer-Schuster rearrangement, alkyne hydration, allenolate cyclization, C(sp²)-C(sp²) coupling.

The strategy of this dual gold redox catalysis was quickly utilized by several research groups and a range of aryl radical coupling reactions involving nucleophilic addition to π -systems and even P-H and C(sp)-H functionalization have been developed (Scheme 1-16). The key to success in these systems is the capacity of aryl radicals to oxidize gold(I) species first to a transient gold(II) species and then, upon SET oxidation, to arylgold(III) complexes which can undergo reductive elimination to give the product. The success of this dual photoredox Au-catalyzed protocols encouraged more research groups to expand the scope of unsaturated alkenes or alkynes, new transformations continue to be reported at a fast rate, like ring expansion,³⁵ P-H bond functionalization,³⁸ C(sp)-H bond functionalization,³⁹ Meyer-

³⁸ He, Y.; Wu, H.; Toste, F. D. *Chem. Sci.* **2015**, *6*, 1194.

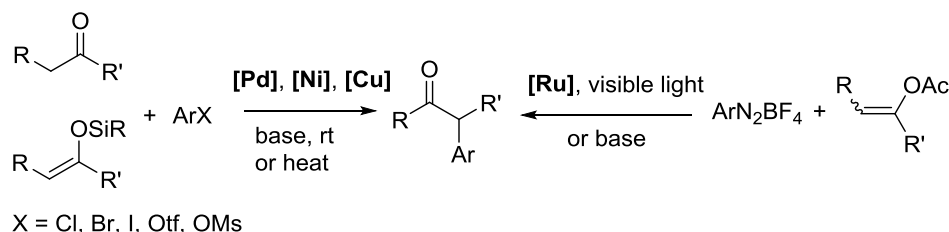
³⁹ (a) Tlahuext-Aca, A.; Hopkinson, M. N.; Sahoo, B.; Glorius, F. *Chem. Sci.* **2016**, *7*, 89. (b) Kim, S.; Rojas-Martin, J.; Toste, F. D. *Chem. Sci.* **2016**, *7*, 85.

Schuster rearrangement,⁴⁰ alkyne hydration,⁴¹ allenolate cyclization,⁴² C(sp²)-C(sp²) coupling.⁴³

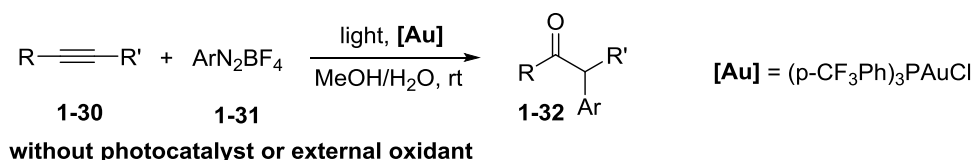
The high selectivity for cross-coupling over homodimerization and the ability to suppress background hydrofunctionalization make these transformations very attractive, and investigations focused on identification of new reaction classes with other organic radicals than aryl derivatives, or new mechanism pathways would help to greatly expand the scope of this concept and allow new gold-catalyzed transformations.

In 2015, Hashmi⁴⁴ reported a photosensitizer-free light-assisted gold-catalyzed 1,2-difunctionalization of alkynes (Scheme 1-17). Under visible-light irradiation, the gold-catalyzed intermolecular difunctionalization of alkynes **1-30** with aryl diazonium salts **1-31** affords a variety of α -aryl ketones **1-32**, and don't need external oxidants or photosensitizers.

1) Previous work: transition-metal catalysis and visible-light photoredox catalysis



2) Hashmi's work: visible-light-mediated gold redox catalysis



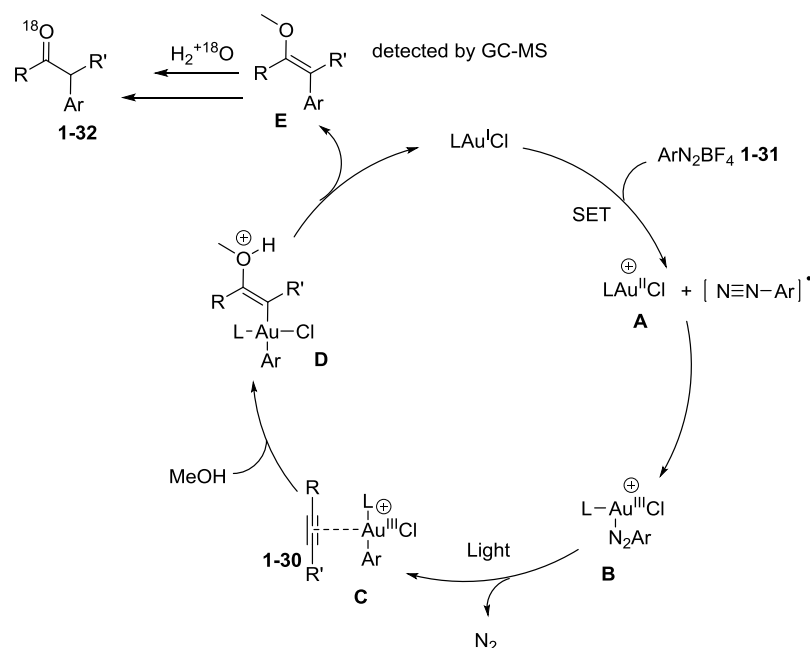
⁴⁰ (a) Tlahuext-Aca, A.; Hopkinson, M. N.; Garza-Sanchez, R. A.; Glorius, F. *Chem. - Eur. J.* **2016**, *22*, 5909. (b) Um, J.; Yun, H.; Shin, S. *Org. Lett.* **2016**, *18*, 484. (c) Alcaide, B.; Almendros, P.; Busto, E.; Luna, A. *Adv. Synth. Catal.* **2016**, *358*, 1526.

⁴¹ Tlahuext-Aca, A.; Hopkinson, M. N.; Garza-Sanchez, R. A.; Glorius, F. *Chem. - Eur. J.* **2016**, *22*, 5909.

⁴² Patil, D. V.; Yun, H.; Shin, S. *Adv. Synth. Catal.* **2015**, *357*, 2622.

⁴³ (a) Cornilleau, T.; Hermange, P.; Fouquet, E. *Chem. Commun.* **2016**, *52*, 10040. (b) Gauchot, V.; Lee, A.-L. *Chem. Commun.* **2016**, *52*, 10163.

⁴⁴ Huang, L.; Rudolph, M.; Rominger, F.; Hashmi, A. S. K. *Angew. Chem. Int. Ed.* **2016**, *55*, 4808.



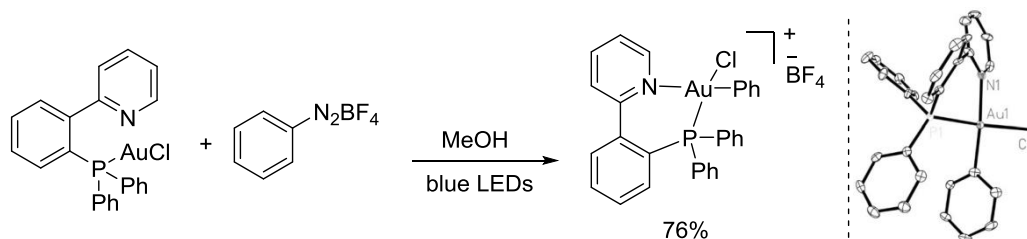
Scheme 1-17. photosensitizer-free light-assisted gold-catalyzed 1,2-difunctionalization of alkynes and proposed mechanism.

Variations of the ligand at the gold center revealed that electron-poor ligands provided better results. The yield of **1-31** improved to 87% with (4-CF₃C₆H₄)₃P, whereas the electron-rich ligand (4-CH₃C₆H₄)₃P gave the worst result.

The authors proposed that the reaction is initiated by gold-induced single electron transfer (SET) to the aryl diazonium salt, generating an aryl diazo radical and gold(II) species **A**.⁴⁵ Then, the phenyldiazonium radical recombines with the gold(II) center, which oxidizes the latter to gold(III) species **B**. Then, assisted by light irradiation, the gold(III) species delivers N₂ and the aryl gold(III) species **C**. In the next step, methanol adds to the π-activated alkyne to form vinyl gold species **D**. Reductive elimination then provides arylated enol ether **E**, which gives the final products upon hydrolysis.

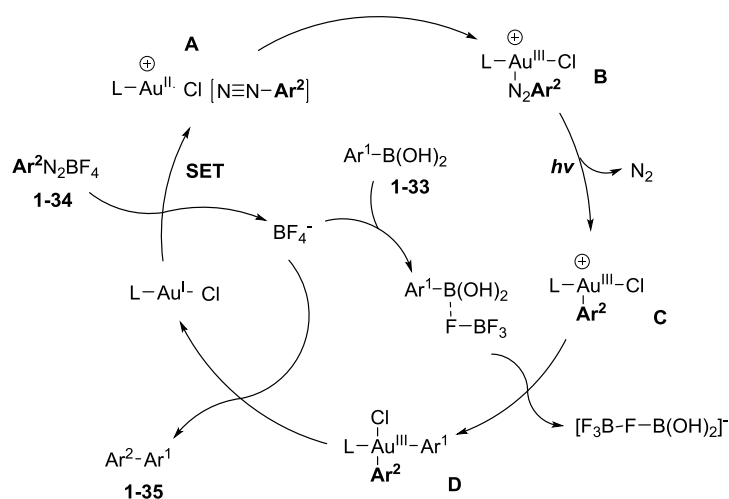
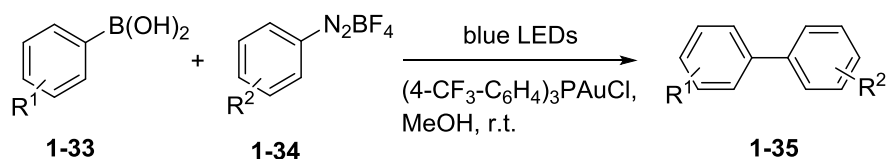
⁴⁵ (a) Zhdanko, A.; Maier, M. E. *Chem. Eur. J.* **2014**, *20*, 1918. (b) Lein, M.; Rudolph, M.; Hashmi, A. S. K.; Schwerdtfeger, P. *Organometallics* **2010**, *29*, 2206. (c) Krauter, C. M.; Hashmi, A. S. K.; Pernpointner, M. *ChemCatChem* **2010**, *2*, 1226. (d) Marion, N.; Ramón, R. S.; Nolan, S. P. *J. Am. Chem. Soc.* **2009**, *131*, 448. (e) Casado, R.; Contel, M.; Laguna, M.; Romero, P.; Sanz, S. *J. Am. Chem. Soc.* **2003**, *125*, 11925. (f) Mizushima, E.; Sato, K.; Hayashi, T.; Tanaka, M. *Angew. Chem. Int. Ed.* **2002**, *41*, 4563; *Angew. Chem.* **2002**, *114*, 4745. (g) Teles, J. H.; Brode, S.; Chabanas, M. *Angew. Chem. Int. Ed.* **1998**, *37*, 1415; *Angew. Chem.* **1998**, *110*, 1475. (h) Fukuda, Y.; Utimoto, K. *J. Org. Chem.* **1991**, *56*, 3729. (i) Galli, C. *Chem. Rev.* **1988**, *88*, 765.

In addition, they obtained a stable aryl gold(III) species with a P,N- bidentate ligand.⁴⁶ It's the first direct experimental evidence for the commonly postulated direct oxidative addition of an aryl diazonium salt to a pyridine phosphine gold(I) complex (Scheme 1-18).



Scheme 1-18. Synthesis of the P,N-chelate-stabilized gold(III) complex by direct oxidative addition of the phenyldiazonium salt to gold.

In 2017, Hashmi⁴⁷ reported another photosensitizer-free, visible light driven, gold-catalyzed C–C cross-couplings of arylboronic acids **1-33** and aryldiazonium salts **1-34** (Scheme 1-19). This reaction can be performed in very mild condition.



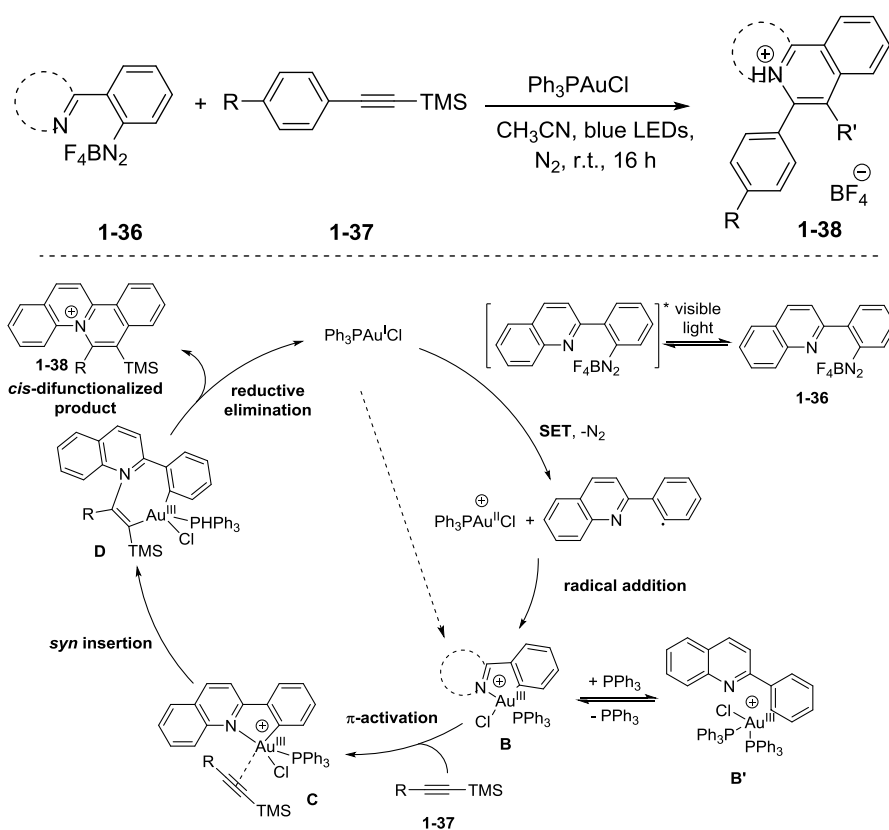
Scheme 1-19. Photosensitizer-free, gold-catalyzed C–C cross-coupling of boronic acids and diazonium salts enabled by visible light and proposed reaction mechanism.

⁴⁶ Huang, L.; Rominger, F.; Rudolph, M.; Hashmi, A. S. K. *Chem. Commun.* **2016**, 52, 6435.

⁴⁷ Witzel, S.; Xie, J.; Rudolph, M.; Hashmi, A. S. K. *Adv. Synth. Catal.* **2017**, 359, 1522.

Similar to their previous work,⁴⁸ the tris(4-trifluoromethyl) phosphinegold(I) chloride [(4-CF₃-C₆H₄)₃PAuCl] was used as gold catalyst. They proposed that it was a gold-induced single electron transfer to the aryldiazonium salt, and assisted by light irradiation, elimination of N₂ can afford aryl gold(III) species. After a transmetalation of the in situ activated arylboronic acid complex to give diaryl gold(III) species **D**, and reductive elimination from the Ar¹-Au(III)-Ar² intermediate delivers biaryl derivatives and completes the catalytic cycle.

In 2017, Man-Kin Wong⁴⁹ reported a photosensitizer-free visible light-mediated gold catalysed *cis*-difunctionalization of silylsubstituted alkynes (Scheme 1-20).



Scheme 1-20. Photosensitizer-free, visible light-mediated gold-catalysed alkyne *cis*-difunctionalization and proposed reaction mechanism.

Under visible light irradiation, the aryl diazonium salt is excited and reduced by single electron transfer from Au(I) catalyst, and form an aryl radical with the generation of a Au(II) species. Au(III) intermediate **B** can be formed by recombination of the Au(II) species and the aryl radical, and it can activate the silyl-substituted alkyne through π -activation to give

⁴⁸ Huang, L.; Rudolph, M.; Rominger, F.; Hashmi, A. S. K. *Angew. Chem. Int. Ed.* **2016**, *55*, 4808.

⁴⁹ Deng, J.-R.; Chan, W.-C.; Lai, N. C.-H.; Yang, B.; Tsang, C.-S.; Ko, B. C.-B.; Chan, S. L.-F.; Wong, M.-K. *Chem. Sci.*, **2017**, *8*, 7537.

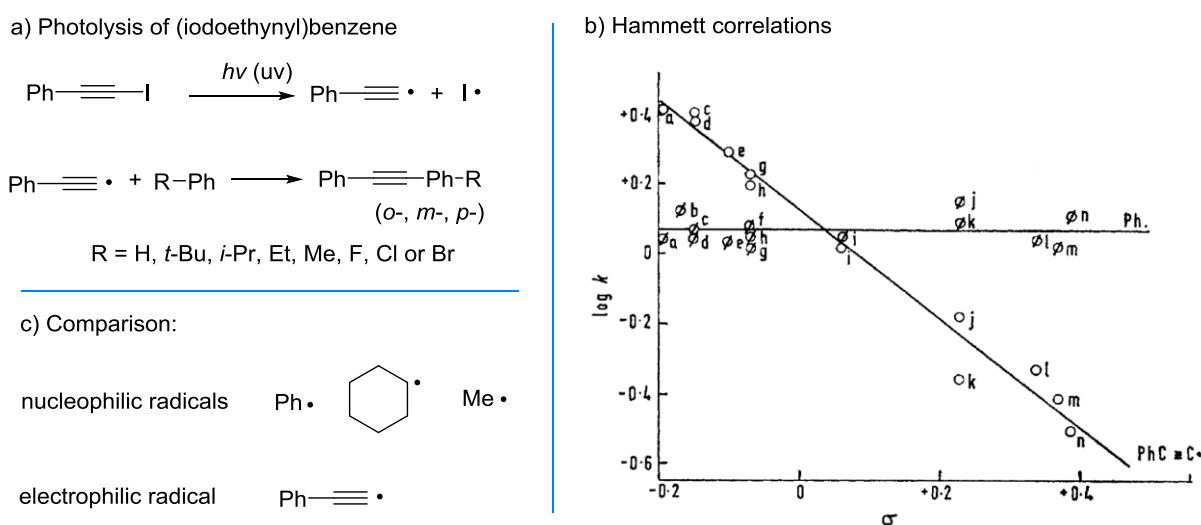
species **C**. After that, the π -activated alkyne can regioselectively insert the Au–N bond to form cis vinyl gold species **D**. Finally, a quinolizinium compound as the *cis*-difunctionalized product and the Au(I) catalyst can be provided through reductive elimination.

3 Iodoalkynes

The fact that iodoalkynes are much less reactive than aryl diazoniums, may bring new mode of activation of gold(I) complexes.

3.1 Alkynyl Radicals

In organic synthesis, very few examples of alkynyl radicals are reported, possibly due to their difficult generation and their very short life time. In 1970, Tiecco⁵⁰ reported that phenyl ethynyl radical can be generated by the photolysis of (iodoethynyl)benzene, and it can react with monosubstituted aromatic compounds through homolytic aromatic substitution to give three kinds of substitution products: *ortho*, *meta*, and *para* isomers (Scheme 1-21a).



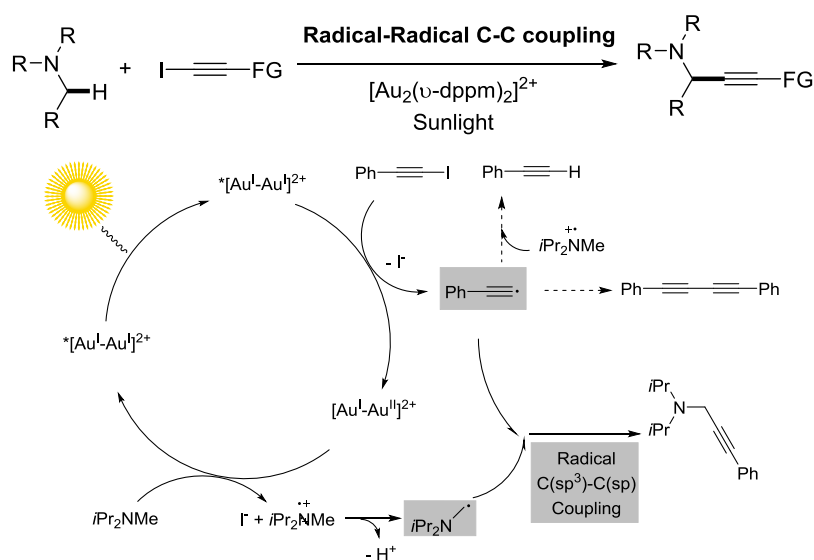
Scheme 1-21. a) Photolysis of (iodoethynyl)benzene, b) Hammett correlations for homolytic aromatic phenylethynylation *o* and phenylation ϕ : a, *p*-Bu^t; b, *p*-Me; c, *p*-Et; d, *p*-Pri; e, *m*-Bu^t; f, *m*-Me; g, *m*-Prⁱ; h, *m*-Et; i, *p*-F; j, *p*-Cl; k, *p*-Br; l, *m*-F; m, *m*-Cl; and n, *m*-Br, c) Comparison.

From the orientation and the relative reactivity data obtained from the reaction with several mono-substituted benzenes, Tiecco concluded that the phenylethynyl radical possesses an

⁵⁰ Tiecco, M. *J. Chem. Soc. B*, **1970**, 1413.

electrophilic character (Scheme 1-21b), because the Hammett plot of $\log k$ versus Hammett parameter σ has a negative ρ value. Comparatively, the phenyl radical, cyclohexyl radical, and methyl radical are nucleophilic radicals. The electrophilic character of phenylethynyl radical will give their specific properties (Scheme 1-21c).

In 2015, Hashmi⁵¹ reported a gold-catalyzed photoredox α -C(sp³)-H alkylation of tertiary aliphatic amines to provide propargylic amines with sunlight (Scheme 1-22).



Scheme 1-22. Gold-catalyzed radical C(sp³)-H alkylation of tertiary aliphatic amines and proposed mechanism.

In the presence of $[\text{Au}_2(\text{m-dppm})_2]^{2+}$ under sunlight, the iodoalkyne can generate an alkynyl radical. A C-C coupling of an α -aminoalkyl radical and an alkynyl radical is proposed for the C(sp³)-C(sp) bond formation. This C(sp³)-H alkylation reaction can be performed with highly regioselectivity and good functional-group compatibility under mild reaction conditions.

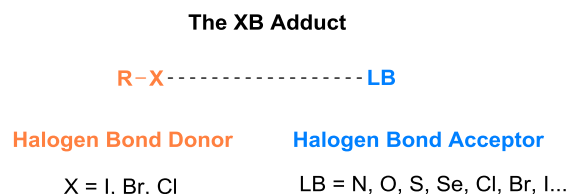
3.2 Halogen Bonding of (Iodoethynyl)benzene

Halogen bonding (XB) is an attractive non-covalent interaction between terminal halogen atoms in compounds of the type R-X and Lewis bases (LBs) (Scheme 1-23).⁵² R-X acts as

⁵¹ Xie, J.; Shi, S.; Zhang, T.; Mehrkens, N.; Rudolph, M.; Hashmi, A. S. K. *Angew. Chem. Int. Ed.*, **2015**, *54*, 6046.

⁵² (a) Cavallo, G.; Metrangolo, P.; Milani, R.; Pilati, T.; Priimagi, A.; Resnati, G.; Terraneo, G. *Chem. Rev.* **2016**, *116*, 2478. (b) Legon, A. C. *Phys. Chem. Chem. Phys.* **2010**, *12*, 7736. (c) Cavallo, G.; Metrangolo, P.; Pilati, T.;

the halogen-bond donor, where X is any halogen atom with an electrophilic region and R is a group covalently bound to X. LB is the halogen-bond acceptor, typically a molecular entity possessing at least one nucleophilic region.



Scheme 1-23. Introduction of the XB adduct.

Compared with other common intermolecular non-covalent interaction, hydrogen bonding, halogen bonding offers some potential advantageous features:⁵³

(1) because of sigma hole, halogen bonding has higher directionality, and a halogen atom can both donate and accept electronic density in a halogen bond;

(2) larger and more polarizable interacting atoms compared with hydrogen; The strength of halogen bonds ranges from ~ 2 kJ/mol to ~ 160 kJ/mol, equalling or exceeding that of hydrogen bonds (hydrogen bond energy is 5-30 kJ/mol);

(3) different solubility profiles, as halogen-bond donors are typically based on different fluorinated groups. Halogen bonding itself has been known for a long time and has attracted dramatical attention from chemists exploring crystal engineering, supramolecular chemistry, and drug design since the early 1990s.

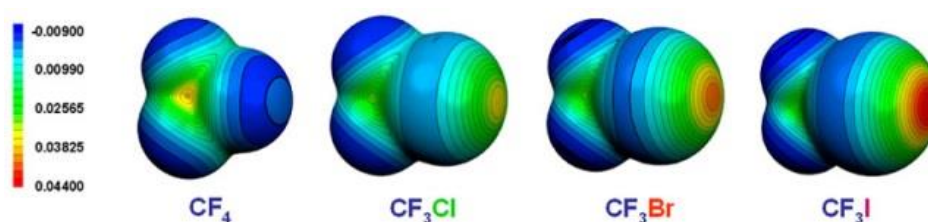
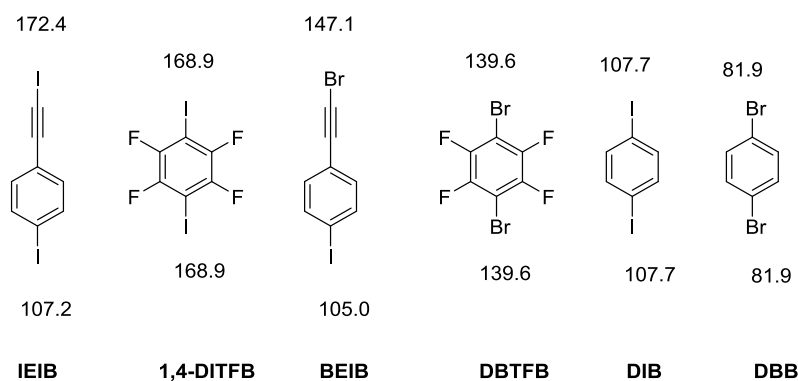


Figure 1-5. Ranking of halogen-bond donors.

The Figure 1-5 shows the halogen bond forming tendency,⁵⁴ the more red, the stronger tendency forming a halogen bond, so the I atom has the strongest tendency, and F atom has the weakest tendency.

Resnati, G.; Sansotera, M.; Terraneo, G. *Chem. Soc. Rev.* **2010**, *39*, 3772. (d) Metrangolo, P.; Meyer, F.; Pilati, T.; Resnati, G.; Terraneo, G. *Angew. Chem., Int. Ed.* **2008**, *47*, 6114.

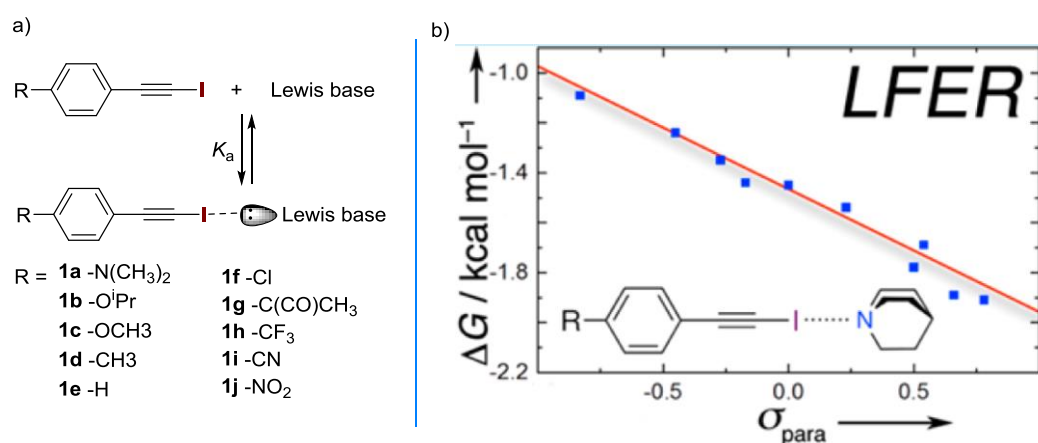
⁵³ Metrangolo, P.; Neukirch, H.; Pilati, T.; Resnati, G. *Acc. Chem. Res.* **2005**, *38*, 386.



Scheme 1-24. Halogen bond donor series paralleled the electrostatic potential on the donor halogen atom. Values of electrostatic potential energy surface are in kJ mol⁻¹.

Chemical structures of C(sp)-bonded XB donors (IEIB and BEIB), activated C(sp²)-bonded donors (1,4-DITFB and DBTFB), and nonactivated C(sp²)-bonded donors (DIB and DBB) were investigated by computational studies, by minimizing the molecular geometry and calculating the electrostatic potential energy surface $V_s(r)$ of each molecule (Scheme 1-24).⁵⁵ These calculations were performed by using DFT at the B3LYP/6-311+G** level with Spartan software (Spartan '08 © 1991–2009 Wavefunction Inc.) for the geometry optimization and for displaying the electrostatic potential energy surface. The maximum value of the potential, $V(r)$, corresponding to the depth of the σ -hole on each halogen atom, was determined for the six donors.

In 2014, Francois Diederich's group⁵⁶ reported the halogen bonding of (iodoethynyl)benzene derivatives in solution (Scheme 1-25).



⁵⁴ Clark, T.; Hennemann, M.; Murray, J. S.; Politzer, P. *J. Mol. Model.*, **2007**, *13*, 291.

⁵⁵ Aakeröy, C. B.; Baldrighi, M.; Desper, J.; Metrangolo, P.; Resnati, G. *Chem. Eur. J.* **2013**, *19*, 16240.

⁵⁶ Diederich, F. et al. *Org. Lett.*, **2014**, *16*, 4722.

It allows the construction of 2-fluoroalkylated 3-iodoquinoxalines in high yields under visible-light irradiation at room temperature. In this transformation, perfluoroalkyl iodides **1-40** act as halogen-bond donors, and organic bases and solvent MeCN maybe act as halogen-bond acceptors. Fluoroalkyl radicals can be generated by a visible-light-induced single electron transfer (SET) process. The fluoroalkyl radicals are trapped by *o*-diisocynoarenes to give quinoxaline derivatives.

Halogen bonding is a weak interaction of halogens with Lewis bases. There are some techniques for solution studies of XB (Figure 1-6).⁵⁸ Usually,

- 1) NMR is the most often used techniques to study XB;
- 2) UV–Vis spectroscopy is “inexpensive and straightforward...sometimes used, but it offer limited structural information”;
- 3) Infrared spectroscopy can also be used, it requires very low sample volume, but a big problem is the overlap of absorption bonding;
- 4) and calorimetry is insufficient in directly yielding atomic level information. Then we chose NMR titration experiments and UV-Vis experiments to investigate the XB.

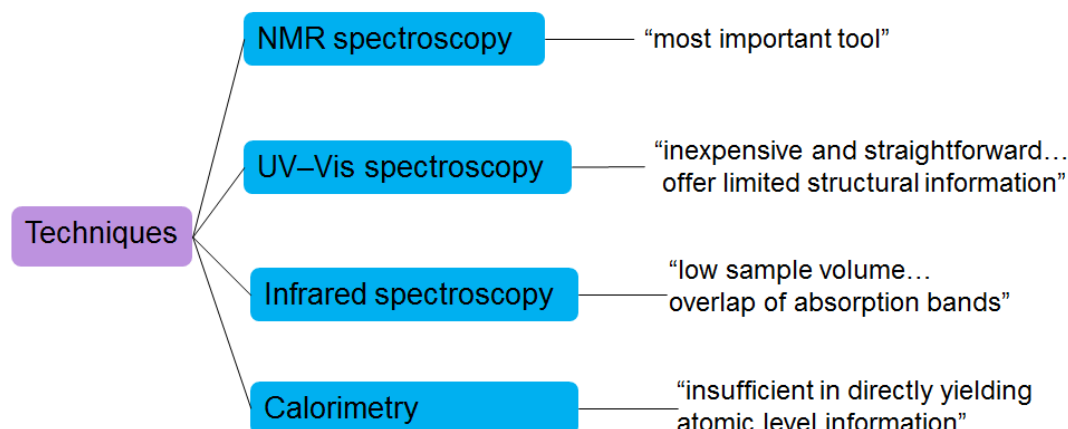
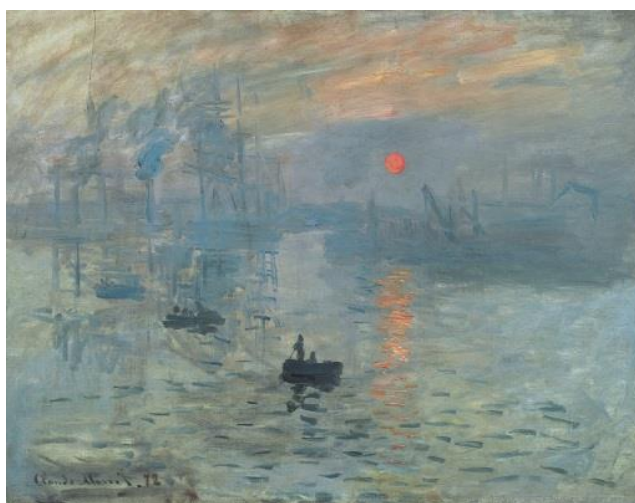


Figure 1-6. Techniques for Solution Studies of XB.

⁵⁸ Erdélyi, M. *Chem. Soc. Rev.* **2012**, *41*, 3547.

Chapter 2 Dual Photoredox/Gold Catalysis



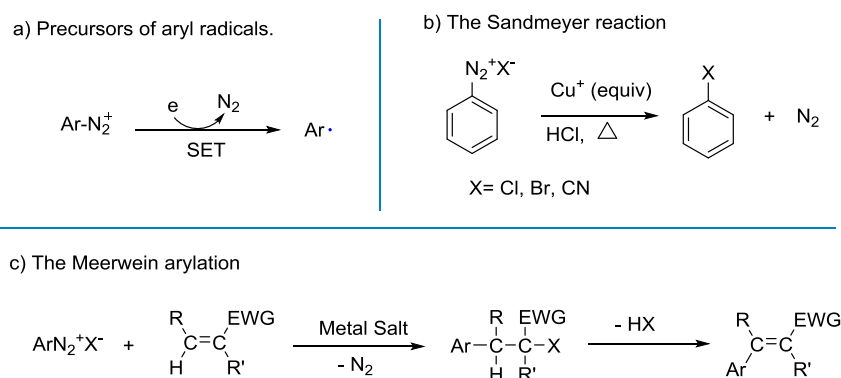
Impression, Sunrise, Claude Monet, 1872

1 Background: Aryl Diazonium Salts

A free radical⁵⁹ is an atom, molecule, or ion with an odd number of electrons. Organic free radicals are involved in the process of organic reactions, the production of synthetic materials and the healthy functioning of human body.

1.1 Two Types of Classic Name Reactions Involving Aryl Diazonium Salts

Diazonium salts,⁶⁰ presynthesized or generated in situ from anilines, are widely used as precursors of aryl fragments, as exemplified in the well-known Sandmeyer reactions⁶¹ and Meerwein arylation⁶² (Scheme 2-1). Although the mechanism of these reactions may be complex and not completely clear, the participation of aryl radicals is assumed and is very likely.



Scheme 2-1. Diazonium salts was used as precursors of aryl radicals.

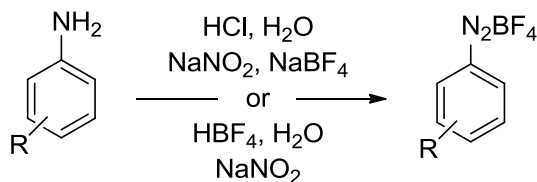
⁵⁹ (a) Gomberg, M. *J. Am. Chem. Soc.* **1900**, *20*, 757. (b) Gomberg, M. *Organic Radicals. Chem. Rev.* **1924**, *1*, 91. (c) Halliwell, B. and Gutteridge, J. M. C. *Free Radicals in Biology and Medicine*. 2nd ed.; Oxford: Clarendon, 1989. (d) Renaud, P.; Sibi, M. P. *Radicals in Organic Synthesis, Vol. 2*, 1st ed. Wiley-VCH, Weinheim, 2001. (e) Leffler, J. E. *An Introduction to Free Radicals*. New York: Wiley, 1993.

⁶⁰ Reviews on aryldiazonium salts: (a) Galli, C. *Chem. Rev.* **1988**, *88*, 765. (b) Mo, F.; Dong, G.; Zhang Y.; Wang, J. *Org. Biomol. Chem.* **2013**, *11*, 1582. (c) Hari, D. P.; König B. *Angew. Chem., Int. Ed.* **2013**, *52*, 4734. (d) Roglans, A.; Pla-Quintana, A.; Moreno-Mañas, M. *Chem. Rev.* **2006**, *106*, 4622. (e) Lindsay, R. J. In *Comprehensive Organic Chemistry*; Barton, S. D., Ollis, W. D., Sutherland, I. O., Eds.; Pergamon Press: Oxford, 1979; Vol. 2, p 154. (f) Zollinger, H. *Diazo Chemistry I: Aromatic and Heteroaromatic Compounds*; John Wiley & Sons: New York, 1994. (g) *The Chemistry of Diazonium and Diazo Groups*; Patai, S., Ed.; Wiley: New York, 1978. (h) Zollinger, H. *Angew. Chem., Int. Ed. Engl.* **1978**, *17*, 141. (i) Gloor, B.; Kaul, B. L.; Zollinger, H. *HCA*, **1972**, *55*, 1596.

⁶¹ (a) Sandmeyer, T. *Ber. Dtsch. Chem. Ges.* **1884**, *17*, 1633. (b) Sandmeyer, T. *Ber. Dtsch. Chem. Ges.* **1884**, *17*, 2650.

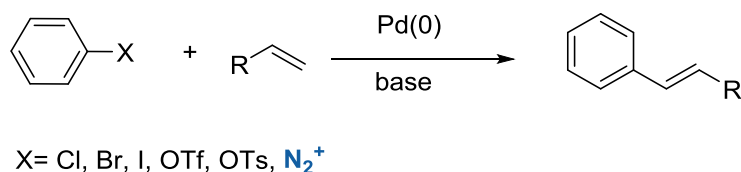
⁶² (a) Meerwein, H.; Buchner, E.; van Emsterk, K. *J. Prakt. Chem.* **1939**, *152*, 237. (b) Heinrich, M. R. *Chem. Eur. J.* **2009**, *15*, 820. (c) Doyle, M. P.; Siegfried, B.; Elliott, R. C.; Dellaria, J. F. *J. Org. Chem.* **1977**, *42*, 2431. (d) Raucher, S.; Koolpe, G. A. *J. Org. Chem.* **1983**, *48*, 2066.

The most widely used method for the synthesis of such aromatic diazonium salt is the diazotization of aromatic amines with sodium nitrite under HBF_4 or HCl/NaBF_4 conditions (Scheme 2-2).⁶³



Scheme 2-2. Synthesis of aromatic diazonium salt.

With the pioneering work of Richard F. Heck and Tsutomu Mizoroki in the field of Pd-catalyzed coupling reactions, the Heck-Mizoroki reaction has been extensively studied and expanded to include a wide variety of substrates (mainly due to its excellent efficiency and tolerance to different functional groups) in the 1960s and 1970s.⁶⁴ Now, the Heck–Mizoroki reaction has become one of the most important tools used by organic chemists to build C-C bonds. Its importance has been reflected in 2010 – Richard F. Heck, Ei-ichi Negishi and Akira Suzuki received the Nobel Chemistry Prize for their contribution of Pd-catalyzed cross-coupling reaction in organic synthesis.



Scheme 2-3. The Heck – Mastuda reaction.

In 1977, Tsutomu Matsuda firstly reported for the reaction of aromatic diazonium salts as arylating agents with olefins under the catalysis of Pd (Scheme 2-3). Aromatic diazonium salts have been used as reliable alternatives to conventional aromatic halides and oxygenated electrophiles in Pd-catalyzed Heck reactions due to their low cost and easiness of preparation.⁶⁵

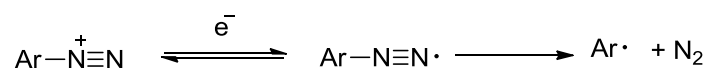
⁶³ Hanson, P.; Jones, J. R.; Taylor, A. B.; Walton, P. H.; Timms, A. W. *J. Chem. Soc., Perkin Trans. 2.* **2002**, 1135.

⁶⁴ de Meijere, A.; Meyer, F. E. *Angew. Chem. Int. Ed. Engl.*, **1995**, 33, 2379.

⁶⁵ (a) Kikukawa, K.; Kono, K.; Wada, F.; Matsuda, T. *Chem. Lett.* **1982**, 35. (b) Kikukawa, K.; Idemoto, T.; Katayama, A.; Kono, K.; Wada, F.; Matsuda, T. *J. Chem. Soc., Perkin Trans 1* **1987**, 1511. (c) Andrus, M. B.; Ma, Y.; Zang, Y.; Song, C. *Tetrahedron Lett.* **2002**, 43, 9137.

1.2 Reductive Potential of Aryl Diazonium Salts

Reductive potential is a measure of the tendency of a chemical species to acquire electrons and thereby be reduced. Reduction potential is measured in volts (V), or millivolts (mV). Each species has its own intrinsic reduction potential; the more positive the potential, the higher of the specie' affinity for electrons and tendency to be reduced.



The most direct way to reduce aromatic diazonium cations is by using an electrode. When an aromatic diazonium cation gets an electron, it forms an aromatic diazenyl radical, which is a very unstable specie and quickly eliminates nitrogen to form aryl radical. Electrochemical studies provide some basic information: diazonium salts are very easily reduced species (Table 2-1).

Table 2-1. Half-wave reduction potentials of arenediazonium ions in sulfolane.

Substituent	$E_{1/2}$ (vs SCE), V	Substituent	$E_{1/2}$ (vs SCE), V
<i>p</i> -NO ₂	+0.450	<i>p</i> -SO ₃ ⁻	+0.297
<i>p</i> -CN	+0.433	none	+0.295
<i>p</i> -Cl	+0.350	<i>p</i> -CH ₃	+0.250
<i>p</i> -Br	+0.383	<i>p</i> -OCH ₃	+0.140
<i>p</i> -I	+0.383	<i>p</i> -N(CH ₃) ₂	-0.095
<i>p</i> -CO ₂ ⁻	+0.328		

According to the results of Elofson and Gadallah,⁶⁶ the polarographic half-wave reduction potential of the phenyltetrafluoroborate diazonium salt in sulfolane is actually +0.295 V (compared to SCE, saturated calomel electrode). If the diazonium salt has a nitro substitution (*p*-nitro), $E_{1/2}$ will be increased to +0.450 V, and when the diazonium salt has a methoxyl substitution (*p*-methoxy), $E_{1/2}$ will be reduced to +0.140 V (examples of more substituents, see Table 2-1 for details). The above researchers found that there is a good linear relationship between the $E_{1/2}$ and the σ^+ substitution constant (Hammett substitution constant, which is used to describe the effect of the substituent on the electrical properties of the reactants) with a slope $\rho = 0.22$. This obtained correlation indicates that electron-withdrawing

⁶⁶ Elofson, R. M.; Gadallah, F. F. *J. Org. Chem.* **1969**, *34*, 854.

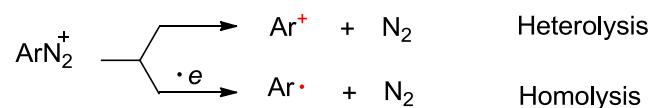
substituents facilitate the reduction of the diazonium salt, possibly due to the ability to stabilize the aromatic diazenyl radical. The above viewpoint has been confirmed by theoretical research.

Although the reaction of the aromatic diazonium salt on electrodes is rare, it is clearly concluded from the above-mentioned reductive potential on the electrode that: 1) diazonium salts have very low reductive potentials and are easily reduced, and 2) it is more advantageous for electron-donating substituents than electron-withdrawing substituents to be reduced to form aryl radicals.

1.3 Homolytic Dediazoniatio of Diazonium Salt

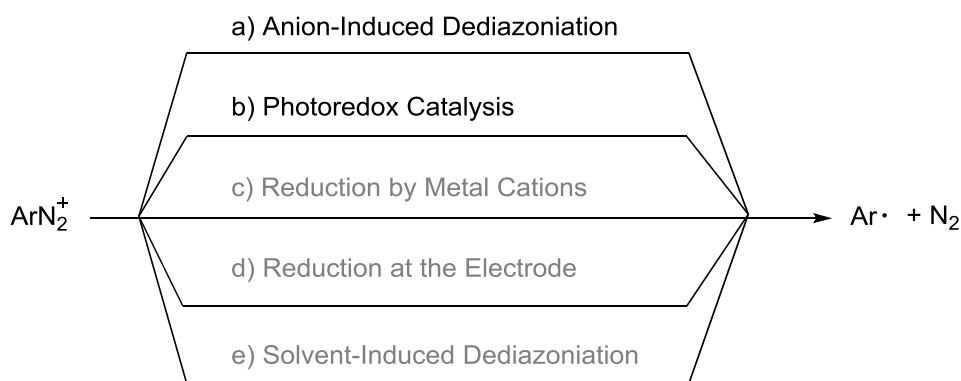
Aromatic diazonium salts have a long history and have recently been reemphasized with the rise of free radical chemistry. As mentioned above, the aromatic diazonium salt can be used as a precursor of an aryl radical (Ar^\cdot), which undergoes a single electron transfer (SET) and removes nitrogen to form an aryl radical (Ar^\cdot). It seems to be a very simple process, so what is it actually?

In order to answer this question, also because the release of nitrogen will be the critical step in the reaction of the aromatic diazonium salt, it is necessary to have a little deep understanding of how this step is taking place.



Scheme 2-4. The dediazoniatio reactions: which reaction type will predominate?

The release of nitrogen from the aromatic diazonium salt can take place through two distinct mechanism pathways (Scheme 2-4), ie heterolysis (form aryl cations) and homolysis (form aryl radicals). Although there are many factors (such as the electron donating ability of the solvent, the oxidation potential of the diazo cation, the presence of the additive, etc.) which will affect the path of the two mechanisms, in general, the homolysis will be the predominating pathway in dediazoniatio reactions of diazonium salt.

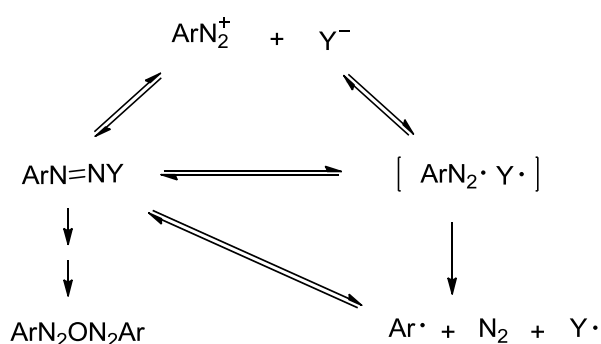


Scheme 2-5. Homolytic dediazonation pathways.

There are many approaches for the homolytic dediazonation reactions (Scheme 2-5), like anion-induced dediazonation, photoredox catalysis, reduction by metal cations, reduction at the electrode, solvent-induced dediazonation, and so on. The following discussion will focus on two main approaches: the anion-induced dediazonation and photoredox catalysis.

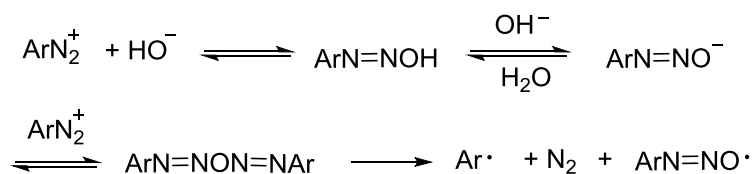
1.3.1 Anion-Induced Dediazonation

Anion-induced dediazonation is based on the redox potential of the electron donor particles. A nucleophilic material, which could be a counterion of diazonium ions, may impart an external atmosphere to or form a covalent adduct with ArN_2^+ due to favorable electrostatic interactions. The adduct may cleave under photochemical or thermal action, because of the instability of the nitrogen-containing fraction (Scheme 2-6).



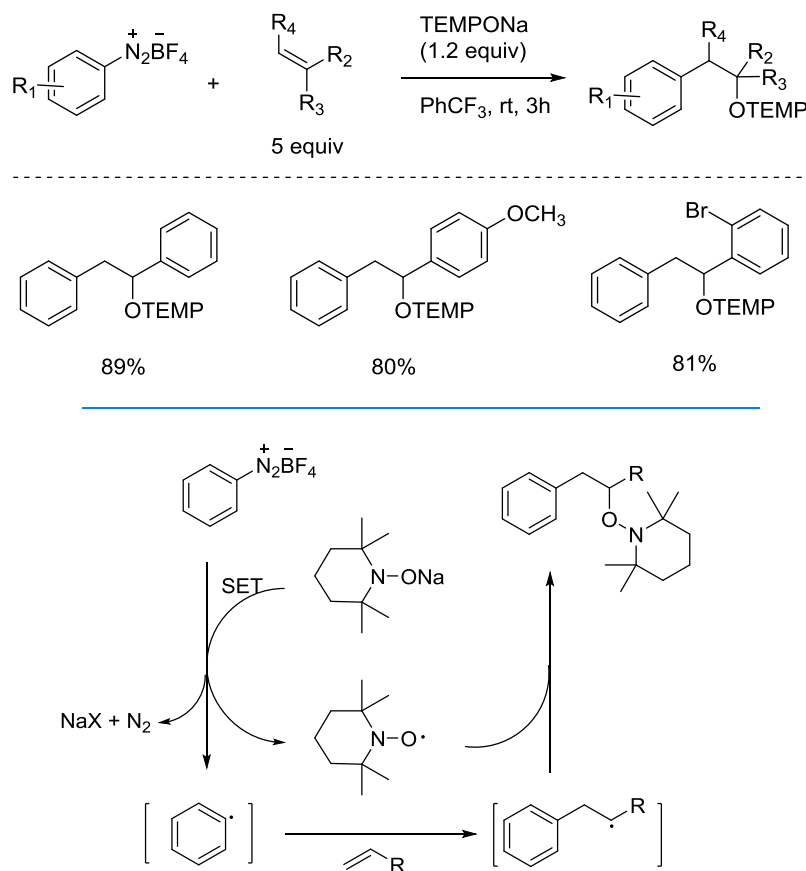
Scheme 2-6. The balance and cleavage of anions to diazonium ions.

The common anions (Y) are I^- , PhO^- , ArS^- , alkoxide(CH_3O^-), carboxylate(CH_3CO_2^-) ... In fact, the well-known Gomberg-Bachmann reaction is the OH^- induces dediazonation process (Scheme 2-7).



Scheme 2-7. OH⁻ induced dediazonation of the Gomberg-Bachmann reaction.

A remarkable example of anion-induced dediazonation was reported by Studer.⁶⁷ In 2012, Studer et al. reported a transition-metal free oxidative arylation of olefins with aromatic diazonium salts and TEMPONa (Scheme 2-8). This mechanism involves the addition of an aryl radical to an olefin, which is subsequently captured by TEMPO (2,2,6,6-tetramethylpiperidinoxyl, a common free radical scavenger) to give the corresponding oxidized arylation product. TEMPONa is used as a reducing reagent to convert the aromatic diazonium salt to the corresponding aryl radical via single electron transfer (SET). The TEMPO-based alkoxyamines product can be readily converted to more general and useful compounds via further chemical manipulation.

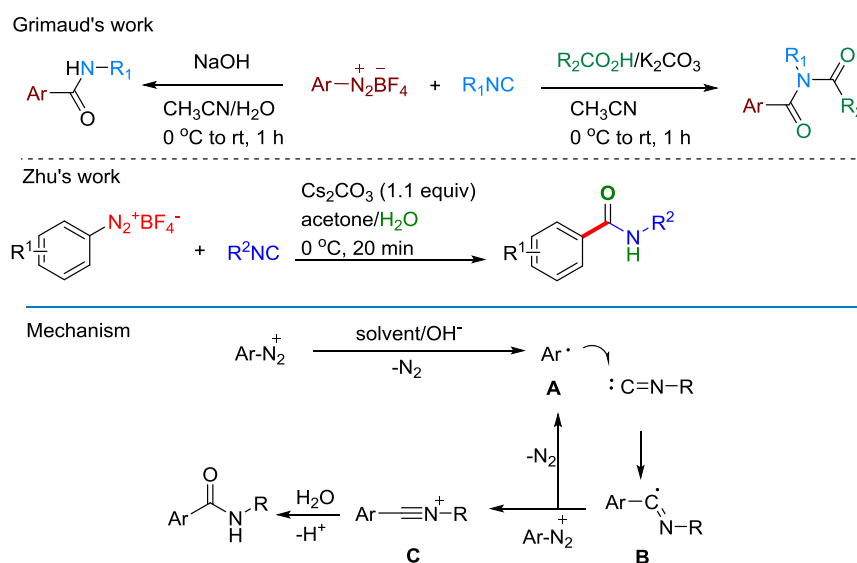


Scheme 2-8. Oxidative arylation of olefins with TEMPONa and aryl diazonium salts.

⁶⁷ Hartmann, M.; Li, Y.; Studer, A. *J. Am. Chem. Soc.* **2012**, *134*, 16516.

In 2013, the Grimaud⁶⁸ and the Zhu⁶⁹ groups reported a base and/or solvent-induced dediazonation of aryl diazonium salts (Scheme 2-9).

In a transition-metal-free carboxyamidation process, base and solvent induced aryl radical formation, followed by radical addition to isocyanide and single electron transfer (SET) oxidation, afford the corresponding arylcarboxyamides upon hydration of the nitrilium intermediate. This formal aminocarbonylation process occurs in the absence of CO and amines or anilines in aqueous media at 0 °C. Mechanistic studies suggest that radical intermediates are involved in the process.



Scheme 2-9. Base and/or solvent-induced dediazonation of aryl diazonium salts.

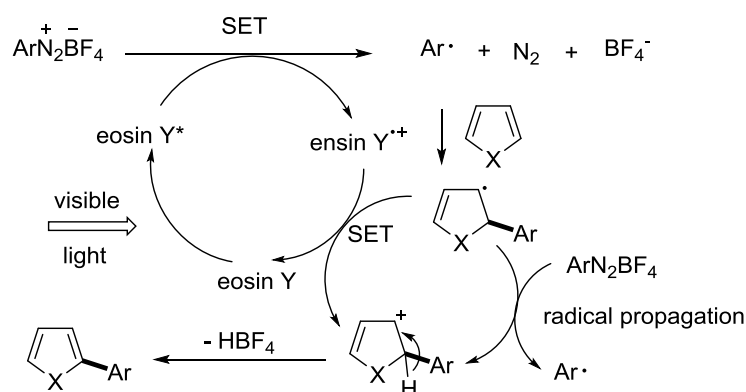
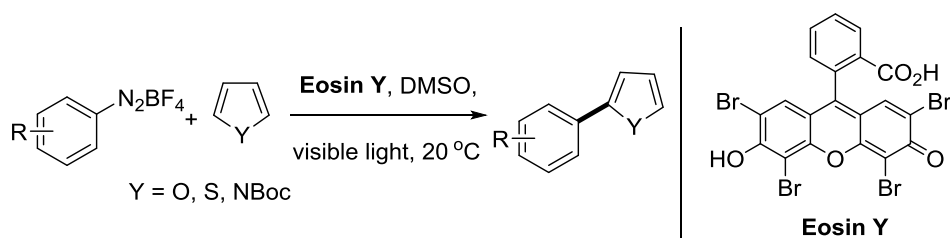
1.3.2 Photoredox Catalysis

In 2012, Burkhard König et al. reported a transition-metal-free, visible light-mediated direct C-H arylation of aryl diazonium salts with heteroarenes (Scheme 2-10).⁷⁰ This reaction does not require a transition metal catalyst or base and can be carried out smoothly at room temperature.

⁶⁸ Basavanag, U. M. V.; Dos Santos, A.; El Kaim, L.; Gámez-Montaño, R.; Grimaud, L. *Angew. Chem., Int. Ed.* **2013**, *52*, 7194.

⁶⁹ Xia, Z.; Zhu, Q. *Org. Lett.* **2013**, *15*, 4110.

⁷⁰ Hari, D. P.; Schroll, P.; König, B. *J. Am. Chem. Soc.* **2012**, *134*, 2958.



Scheme 2-10. Transition-metal-free, visible light-mediated direct C-H arylation of aryl diazonium salts with heteroarenes.

Compared to Sanford's ruthenium catalyst,⁷¹ this method uses Eosin Y as a photo-oxidation reduction catalyst and is believed to have undergone a free radical mechanism. This reaction can be effectively inhibited by 2,2,6,6-tetramethylpiperidinoxyl (TEMPO, a common free radical scavenger) and free radical intermediates are captured, it demonstrates the mechanism of free radicals. The detailed reaction mechanism is shown in the Scheme 2-10.

Recently, the groups of Glorius and Toste⁷² reported a redox-neutral approach, avoiding the use of strong external oxidants, by merging gold and visible light photoredox catalysis⁷³ in a dual catalytic event (see Chapter 1.2.3 Dual Gold/Photoredox Catalysis).⁷⁴

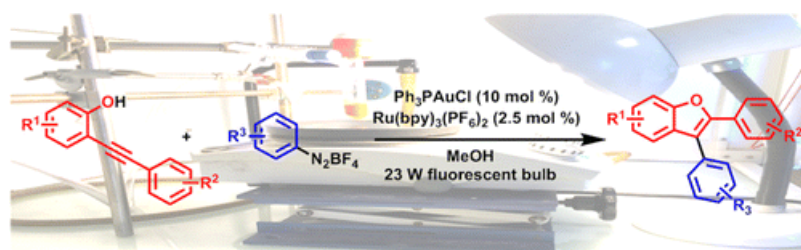
⁷¹ Kalyani, D.; McMurtrey, K. B.; Neufeldt, S. R.; Sanford, M. S. *J. Am. Chem. Soc.*, **2011**, *133*, 18566.

⁷² (a) Sahoo, B.; Hopkinson, M. N.; Glorius, F. *J. Am. Chem. Soc.* **2013**, *135*, 5505. (b) Shu, X.-z.; Zhang, M.; He, Y.; Frei, H.; Toste, F. D. *J. Am. Chem. Soc.* **2014**, *136*, 5844. (c) Hopkinson, M. N.; Sahoo, B.; Glorius, F. *Adv. Synth. Catal.* **2014**, *356*, 2794.

⁷³ For reviews on photoredox catalysis, see: (a) Prier, C. K.; Rankic, D. A.; MacMillan, D. W. C. *Chem. Rev.* **2013**, *113*, 5322. (b) Koike, T.; Akita, M. *Inorg. Chem. Front.* **2014**, *1*, 562. (c) Schultz, D. M.; Yoon, T. P. *Science* **2014**, *343*, 1239176. (d) Teplý, F. *Collect. Czech. Chem. Commun.* **2011**, *76*, 859. (e) Tucker, J. W.; Stephenson, C. R. J. *J. Org. Chem.* **2012**, *77*, 1617. For recent books, see: (f) *Chemical Photocatalysis*; König, B., Ed.; DeGruyter: Berlin, 2013. (g) *Photochemically generated intermediates in Synthesis*; Albin, A., Fagnoni, M., Eds.; John Wiley & Sons: Hoboken, NJ, 2013.

⁷⁴ For reviews, see: (a) Hopkinson, M. N.; Sahoo, B.; Li, J.-H.; Glorius, F. *Chem. - Eur. J.* **2014**, *20*, 3874. (b) Levin, M. D.; Kim, S.; Toste, F. D. *ACS Cent. Sci.* **2016**, *2*, 293. (c) Skubi, K. L.; Blum, T. R.; Yoon, T. P. *Chem. Rev.* **2016**, *116*, 10035.

In 2016, we reported a dual photoredox/gold catalysis arylation cyclization of *o*-alkynylphenols with aryl diazonium salts: a flexible synthesis of benzofurans (Scheme 2-11).⁷⁵ The reaction is proposed to proceed through a photoredox-promoted generation of a vinylgold(III) intermediate that undergoes reductive elimination to provide the heterocyclic coupling adduct.



Scheme 2-11. Dual Au and photoredox cyclization of *o*-alkynylphenols.

The following part will discuss more details about this work.

2 Project Aims and Introduction

In the past decade, homogeneous gold catalysts have received great attention. Most reports rely on the π -acidity of gold (I) or gold (III) complexes to activate C–C multiple bonds present on the substrate, such as olefins, allenes, and especially alkynes, to achieve nucleophilic attack.^{76,77}

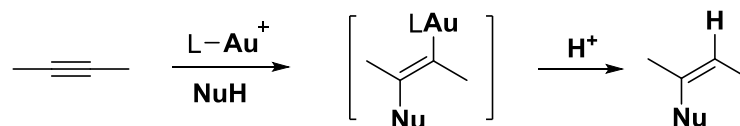
The thermodynamics of the π bond consumption to form a σ bond is particularly favorable. A large number of synthetic transformations are based on this process, usually consisting of an addition reaction. These methods of addition to the π moiety can involve highly reactive

⁷⁵ Xia, Z.; Khaled, O.; Mouriès-Mansuy, V.; Ollivier, C.; Fensterbank, L. *J. Org. Chem.* **2016**, *81*, 7182.

⁷⁶ For recent reviews on gold catalysis, see: (a) Dorel, R.; Echavarren, A. M. *Chem. Rev.* **2015**, *115*, 9028. (b) Jia M.; Bandini, M. *ACS Catal.* **2015**, *5*, 1638. (c) Qian, D.; Zhang, J. *Chem. Soc. Rev.* **2015**, *44*, 677. (d) See also a special Gold Catalysis issue of *Account of Chemical Research: Acc. Chem. Res.* **2014**, *47*, issue 3, Eds: Friend, C.; Hashmi, A. S. K. (e) Pflästerer, D.; Hashmi, A. S. K. *Chem. Soc. Rev.* **2016**, *45*, 1331. (f) Wei, Y.; Shi, M. *ACS Catal.* **2016**, *6*, 2515.

⁷⁷ For selected recent contributions on gold catalysis: (a) Maskiewicz, A.; Weibel, J.-M.; Pale, P.; Blanc, A. *Org. Lett.* **2016**, *18*, 844. (b) Kirillova, M. S.; Muratore, M. E.; Dorel, R.; Echavarren, A. M. *J. Am. Chem. Soc.* **2016**, *138*, 3671. (c) Khrakovsky, D. A.; Tao, C.; Johnson, M. L.; Thornbury, R. T.; Shevick, S. L.; Toste, D. J. *Angew. Chem. Int. Ed.* **2016**, *55*, 6079. (d) Carrèr, A.; Pean, C.; Perron-Sierra, F.; Mirguet, O.; Michelet, V. *Adv. Synth. Catal.* **2016**, *358*, 1540. (e) Jin, H.; Huang, L.; Xie, J.; Rudolph, M.; Rominger, F.; Hashmi, A. S. *Angew. Chemie, Int. Ed.* **2016**, *55*, 794. (f) Kothandaraman, P.; Zhao, Y.; Lee, B. R.; Ng, C. J. L.; Lee, J. Y.; Ayers, B. J.; Chan, P. W. H. *Adv. Synth. Catal.* **2016**, *358*, 1385. (g) Ding, D.; Mou, T.; Feng, M.; Jiang, X. *J. Am. Chem. Soc.* **2016**, *138*, 5218. (h) Singh, RahulKumar Rajmani; Liu, R.-S. *Adv. Synth. Catal.* **2016**, *358*, 1421. (i) Hosseyni, S.; Wojtas, L.; Li, M.; Shi, X. *J. Am. Chem. Soc.* **2016**, *138*, 3994.

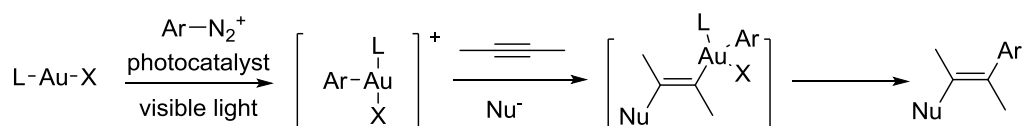
nucleophilic, electrophilic or free radical intermediates. Our team has devoted some of our efforts to developing multiple σ -binding sequences and highly modular precursors to achieve molecular complexity in one-pot operation over the past two decades.



Scheme 2-12. Gold-catalyzed nucleophilic addition to alkynes.

The preliminary triggering event for the catalytic cycle is the gold complex selective activation of carbon–carbon multiple bond. Although a variety of different intra- and intermolecular nucleophiles can be used in these processes, in most cases, nucleophilic attack will generate the organogold species, following undergoes protodemetalation⁷⁸ leading to hydrofunctionalized products (Scheme 2-12).

Without strong external oxidants, a redoxneutral approach by merging gold and visible-light photoredox catalysis⁷⁹ was extended to gold complexes by Glorius and Toste⁸⁰ (Scheme 2-13).



Scheme 2-13. Dual Au and photoredox catalytic difunctionalization of alkynes.

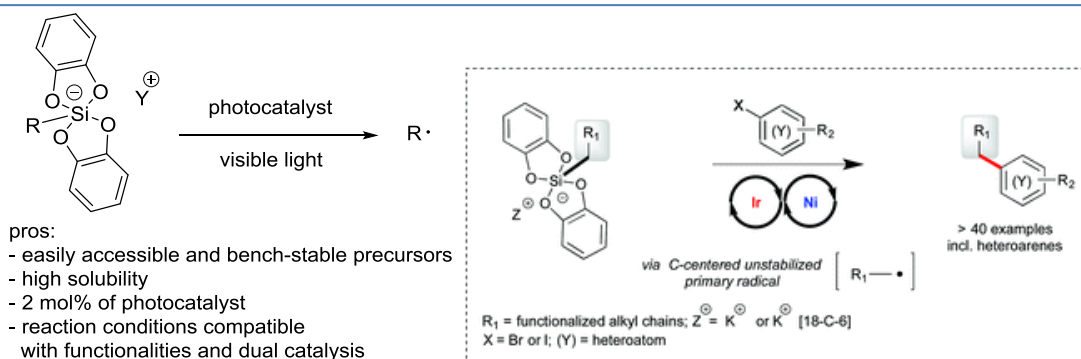
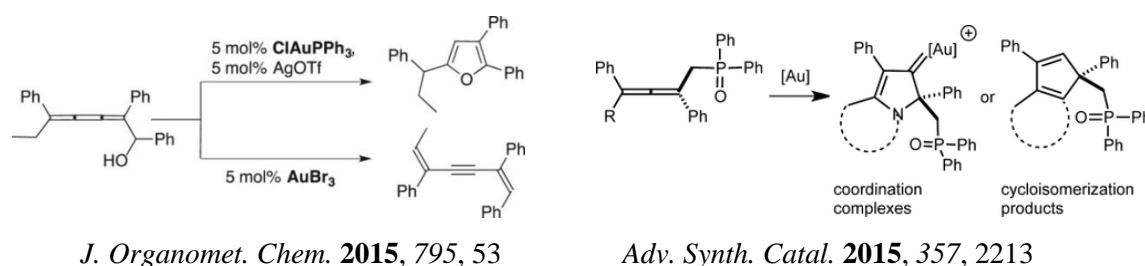
In these transformations, Au acts as a highly carbophilic π -Lewis acid, activating C–C multiple bonds toward intra- or intermolecular nucleophiles with often remarkable levels of chemo-, regio-, and/or stereocontrol. Whereas gold-catalyzed nucleophilic addition reactions

⁷⁸ For a insightful theoretical study of the protodeauration step, see: (a) BabaAhmadi, R.; Ghanbari, P.; Rajabi, N. A.; Hashmi, A. S. K.; Yates, B. F.; Ariafard, A. *Organometallics* **2015**, *34*, 3186 and references therein. (b) For a basicity scale of organogold compounds, see: Roth, K. E.; Blum, S. A. *Organometallics* **2010**, *29*, 1712.

⁷⁹ For reviews on photoredox catalysis: (a) Prier, C. K.; Rankic, D. A.; MacMillan, D. W. C. *Chem. Rev.* **2013**, *113*, 5322. (b) Koike, T.; Akita, M. *Inorg. Chem. Front.* **2014**, *1*, 562. (c) Schultz, D. M.; Yoon, T. P. *Science* **2014**, *343*, 1239176. (d) Teply, F. *Collect. Czech. Chem. Commun.* **2011**, *76*, 859. (e) Tucker, J. W.; Stephenson, C. R. J. *J. Org. Chem.* **2012**, *77*, 1617. For recent books, see: (f) *Chemical Photocatalysis* (Ed.: B. König), DeGruyter, Berlin, **2013**. (g) *Photochemically generated intermediates in Synthesis* (Eds.: A. Albini, M. Fagnoni) John Wiley & Sons, Hoboken, **2013**.

⁸⁰ (a) Sahoo, B.; Hopkinson, M. N.; Glorius, F. *J. Am. Chem. Soc.* **2013**, *135*, 5505. (b) Shu, X.-z.; Zhang, M.; He, Y.; Frei, H.; Toste, F. D. *J. Am. Chem. Soc.* **2014**, *136*, 5844. (c) Hopkinson, M. N.; Sahoo, B.; Glorius, F. *Adv. Synth. Catal.* **2014**, *356*, 2794.

to C–C multiple bonds typically result in hydrofunctionalization, the protodemetalation step in this process can be rerouted in favour of oxidative arylation in the presence of photoredox-generated aryl radicals. In this system, Au^I is oxidized in a stepwise fashion by photo-generated aryl radicals leading to cationic Au^{III} species, which already bears the aryl coupling partner. Coordination of the π -system and nucleophilic attack then lead selectively to the cross coupling product. Recently, DFT calculations⁸¹ and the isolation of arylgold(III) complexes⁸² under related experimental conditions has supported this proposed mechanism. Extensions of this process to alkynylgold and vinylgold intermediates have also been investigated.



Angew. Chem. Int. Ed. **2015**, 54, 11414.

Org. Chem. Front. **2016**, 3, 462.

Scheme 2-14. The gold catalysis and photoredox/organometallic dual catalysis reactions in our group.

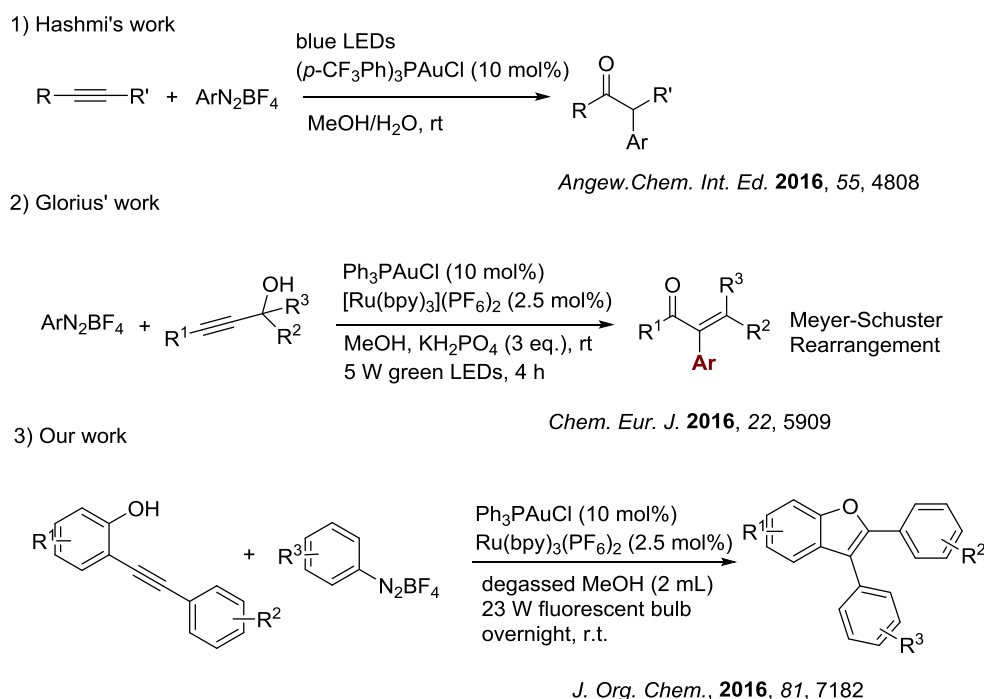
Due to our continuous interest in gold catalysis⁸³ and photoredox/organometallic dual catalysis reactions⁸⁴ (Scheme 2-14), we successfully developed a dual Au and photoredox catalytic intramolecular oxyarylation of *o*-alkynylphenol with aryldiazonium salts.

⁸¹ Zhang, Q.; Zhang, Z.-Q.; Fu, Y.; Fu H.-Z. *ACS Catal.* **2016**, 6, 798.

⁸² Huang, L.; Rominger, F.; Rudolph, M.; Hashmi, A. S. K. *Chem. Commun.* **2016**, 52, 6435.

⁸³ For recent contributions: (a) Nzulu, F.; Bontemps, A.; Robert, J.; Barbazanges, M.; Fensterbank, L.; Goddard, J.-P.; Malacria, M.; Ollivier, C.; Petit, M.; Rieger, J.; Stoffelbach, F. *Macromolecules* **2014**, 47, 6652. (b) Ferrand, L.; Das Neves, N.; Malacria, M.; Mouriès-Mansuy, V.; Ollivier, C.; Fensterbank, L. *J. Organomet. Chem.* **2015**, 795, 53. (c) Vanitcha, A.; Gontard, G.; Vanthuyne, N.; E. Derat, E.; Mouriès-Mansuy, V.; Fensterbank, L. *Adv. Synth. Catal.* **2015**, 357, 2213. (d) Vanitcha, A.; Damelincoirt, C.; Gontard, C.; Vanthuyne, N.; Mouriès-Mansuy, V.; Fensterbank, L. *Chem. Commun.* **2016**, 52, 6785.

In our study of these new dual catalytic events, two reports on dual photoredox/gold catalyzed alkyne bifunctionalization appeared in the literature (Scheme 2-15). Hashmi's research shows that under blue light LED illumination and without any photosensitizer, a gold-catalyzed intermolecular difunctionalized alkyne with aryldiazonium salts provides α -arylketones smoothly.⁸⁵ Soon, the Glorius group developed an aromatic version of the Meyer-Schuster rearrangement utilizing propargyl alcohol and aryldiazonium salts.⁸⁶



Scheme 2-15. Dual photoredox/gold catalysis difunctionalization of alkyne.

Benzofuran is the basic structure of many related compounds. For example, psoralen is a benzofuran derivative that occurs in several plants. Herein, we successfully developed a dual Au and photoredox catalytic intramolecular oxyarylation of *o*-alkynylphenol with aryldiazonium salts (Scheme 2-15c), coincidentally corresponding to one of our findings benzofuran.⁸⁷ This process involves the formation of new C–Nu and C=C bonds across the

⁸⁴ (a) Corcé, V.; Chamoreau, L. M.; Derat, E.; Goddard, J.-P.; Ollivier, C.; Fensterbank, L. *Angew. Chem. Int. Ed.* **2015**, *54*, 11414. (b) Lévêque, C.; Cheneberg, L.; Corcé, V.; Goddard, J.-P.; Ollivier, C.; Fensterbank, L. *Org. Chem. Front.* **2016**, *3*, 462.

⁸⁵ Huang, L.; Rudolph, M.; Rominger, F.; Hashmi, A. S. K. *Angew. Chem. Int. Ed.* **2016**, *55*, 4808.

⁸⁶ Tlahuext-Aca, A.; Hopkinson, M. N.; Garza-Sanchez, R. A.; Glorius, F. *Chem. Eur. J.* **2016**, *22*, 5909.

⁸⁷ These type of benzofurans have also been synthesized from 2-(arylethynyl)phenols by using other methods. See: (a) Arcadi, A.; Cacchi, S.; Fabrizi, G.; Marinelli, F.; Moro, L. *Synlett* **1999**, *1999*, 1432. (b) Hu, Y.; Nawoschik, K. J.; Liao, Y.; Ma, J.; Fathi, R.; Yang, Z. *J. Org. Chem.* **2004**, *69*, 2235. (c) Nakamura, M.; Ilies, L.; Otsubo, S.; Nakamura, E. *Angew. Chem., Int. Ed.* **2006**, *45*, 944. (d) Bernini, R.; Cacchi, S.; De Salve, I.;

alkyne and occurs at room temperature upon irradiation with a simple household light bulb. The full scope and limitations of this transformation are discussed below.

3 Results and Discussion

3.1 Optimization Studies

Initially, we choose 2-(phenylethynyl)phenol **2-1a** and *p*-tolylidiazonium salt **2-2a** (4 equiv) as the model substrates, in the presence of Ph₃PAuCl (10 mol %) and Ru(bpy)₃(PF₆)₂ (5 mol %), irradiated by visible light, degassed MeOH (0.1 M) used as solvent, it gave 73% yield of product **2-3a** (Table 2-2, entry 4). The cationic gold salt PPh₃AuNTf₂ or IPrAuCl gave the classical cycloisomerization **2-3a** rather than the arylated benzofuran (Table 2-2, entries 1 and 2).⁸⁸ Interestingly, in the absence of a photocatalyst or light, the reaction with PPh₃AuCl alone afforded only traces of arylative cyclization (entries 5 and 6).⁸⁹ Based on the analysis of the involved redox potentials, we added Eosin Y (E*_{ox} = -1.6 V vs SCE)⁹⁰ and Cu(dpp)₂PF₆·2H₂O (E*_{ox} = -1.11 V vs SCE)⁹¹ (5 mol %) into this reaction system, with or without PPh₃AuCl (entries 7–9) was tested, however, the yield could not be improved. The use of mixed solvents was not helpful either (entries 10–12), and decreasing the number of equivalents of diazonium salt led to lower yields (entries 13 and 14).

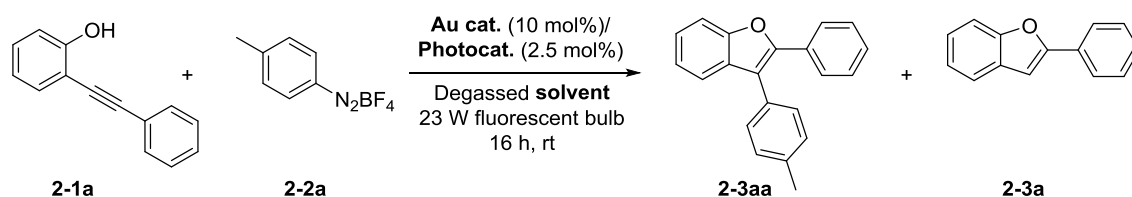
Fabrizi, G. *Synthesis* **2007**, 2007, 873. (e) Tsuji, H.; Mitsui, C.; Iliés, L.; Sato, Y.; Nakamura, E. *J. Am. Chem. Soc.* **2007**, 129, 11902. (f) Zhou, J.; Yang, W.; Wang, B.; Ren, H. *Angew. Chem., Int. Ed.* **2012**, 51, 12293.

⁸⁸ (a) Baralle, A.; Fensterbank, L.; Goddard, J.-P.; Ollivier, C. *Chem. Eur. J.* **2013**, 19, 10809. (b) For a review, see: Paria, S.; Reiser, O. *ChemCatChem* **2014**, 6, 2477.

⁸⁹ Huang, L.; Rudolph, M.; Rominger, F.; Hashmi, A. S. K. *Angew. Chem. Int. Ed.* **2016**, 55, 4808.

⁹⁰ Ravelli, D.; Fagnoni, M. *ChemCatChem* **2012**, 4, 169.

⁹¹ (a) Baralle, A.; Fensterbank, L.; Goddard, J.-P.; Ollivier, C. *Chem. - Eur. J.* **2013**, 19, 10809. (b) For a review, see: Paria, S.; Reiser, O. *ChemCatChem* **2014**, 6, 2477.

Table 2-2. Optimization of the Reaction Conditions.^a

Entry	Au cat.	Photocat.	Solvent	Yield of 3a ^b (%)
1	Ph ₃ PAuNTf ₂	Ru(bpy) ₃ (PF ₆) ₂	MeOH	> 5; (2-3a , 60)
2	Au(NHC)Cl	Ru(bpy) ₃ (PF ₆) ₂	MeOH	9; (2-3a , 35)
3	Ph ₃ PAuCl ^d	Ru(bpy) ₃ (PF ₆) ₂	MeOH	45; (2-3a , 40)
4	Ph₃PAuCl	Ru(bpy)₃(PF₆)₂	MeOH	75 (73)^c
5 ^γ (with light)	Ph ₃ PAuCl	none	MeOH	> 5; (2-3a , 28)
5 ^e	Ph ₃ PAuCl	none	MeOH	> 5; (2-3a , 30)
6 ^e	Ph ₃ PAuCl	Ru(bpy) ₃ (PF ₆) ₂	MeOH	> 5; (2-3a , 20)
7	Ph ₃ PAuCl	Eosin Y ^c	MeOH	8; (2-3a , 60)
8	-	Cu(dpp) ₂ PF ₆ ·2H ₂ O ^d	MeOH	>5; 2-3a not detected
9	Ph ₃ PAuCl	Cu(dpp) ₂ PF ₆ ·2H ₂ O ^d	MeOH	57
10	Ph ₃ PAuCl	Ru(bpy) ₃ (PF ₆) ₂	MeOH:MeCN(3:1)	60
11	Ph ₃ PAuCl	Ru(bpy) ₃ (PF ₆) ₂	MeOH:MeCN(4:1)	61
12	Ph ₃ PAuCl	Ru(bpy) ₃ (PF ₆) ₂	MeOH:MeCN(9:1)	66
13 ^f	Ph ₃ PAuCl	Ru(bpy) ₃ (PF ₆) ₂	MeOH	48
14 ^g	Ph ₃ PAuCl	Ru(bpy) ₃ (PF ₆) ₂	MeOH	39

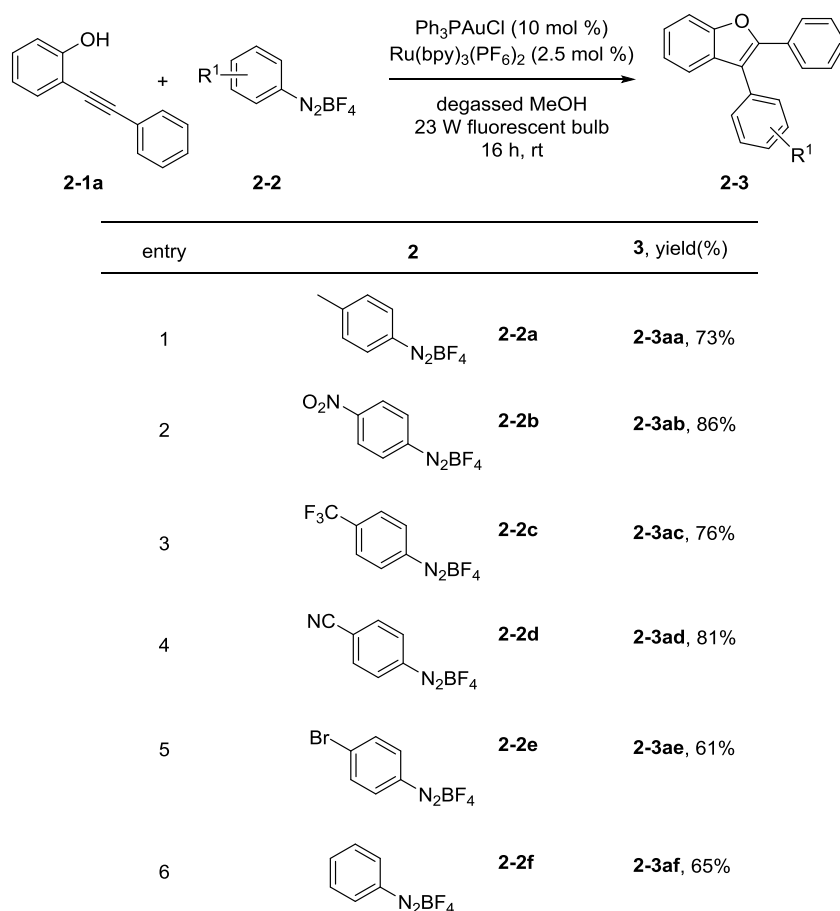
^a General conditions: **2-1a** (0.2 mmol, 0.1 M), [Au] catalyst (10 mol%), photocatalyst (2.5 mol%), **2-2a** (0.8 mmol), degassed solvent (2 mL), rt, 16 h, 23 W fluorescent light bulb. ^b Determined by ¹H NMR using butadiene sulfone as an internal standard. ^c Isolated yield. ^d 5 mol% used. ^e Reaction performed in the dark. ^f 3 equiv of **2-2a**. ^g 2 equiv of **2-2a**.

3.2 Scope and Limitations

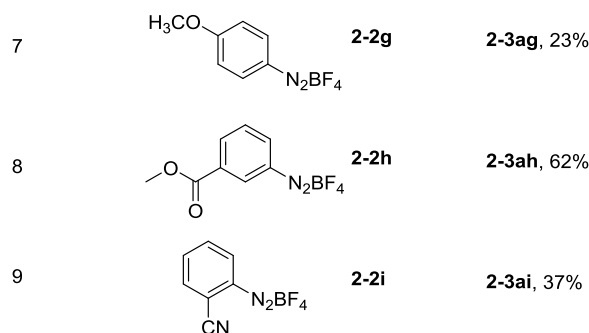
A series of substituted aryl diazonium tetrafluoroborates were reacted with 2-(phenylethynyl)phenol **2-1a** under the optimized reaction conditions as described in entry 3 of Table 2-3. Aryl diazonium tetrafluoroborates bearing electron-withdrawing groups in the para position, such as NO₂ (**2-2b**), CF₃ (**2-2c**), CN (**2-2d**), and Br (**2-2e**) groups afforded the corresponding arylated benzofurans **2-3ab**, **2-3ac**, **2-3ad**, and **2-3ae**, in moderate to good

yields. A good yield (65%) of 2,3-diphenylbenzofuran **3af**⁹² (entry 6) could be obtained when phenyldiazonium salt was subjected to the reaction. However, an electron-donating OCH₃ group led to a lower yield of coupling product **2-3ag** (23%, the rest is side product benzofuran), indicating that the reaction is significantly affected by the electronic density of the substrates. An aryldiazonium salt containing an ester group at the meta position was also tolerated well (**2-3ah**). But a substituent at the *ortho* position of the aryldiazonium salt resulted in a much lower yield (compare **2-3ad**, entry 4, vs **2-3ai**, entry 9).

Table 2-3. Scope of Aryl Diazonium Salts^a



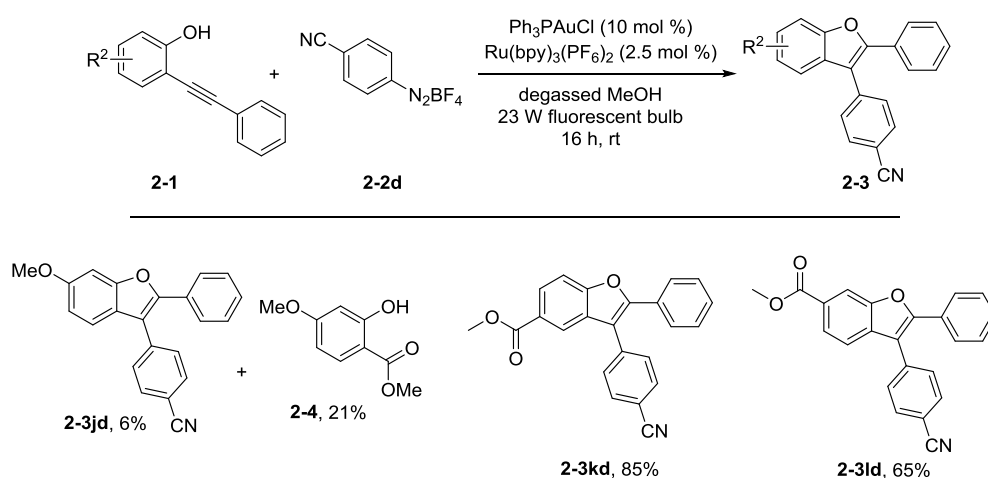
⁹² Experimental conditions by Glorius mention the use of 3 equiv. of KH₂PO₄. We obtained a better yield of **2-3af** (65% vs 53%) without this additive.



Reaction conditions: **2-1a** (0.2 mmol, 0.1 M) and **2-2** (4 equiv), Ph₃PAuCl (10 mol %), Ru(bpy)₃(PF₆)₂ (2.5 mol %), degassed methanol (2 mL) under Ar, rt, 16 h, 23 W fluorescent light bulb; isolated yields of **2-3**.

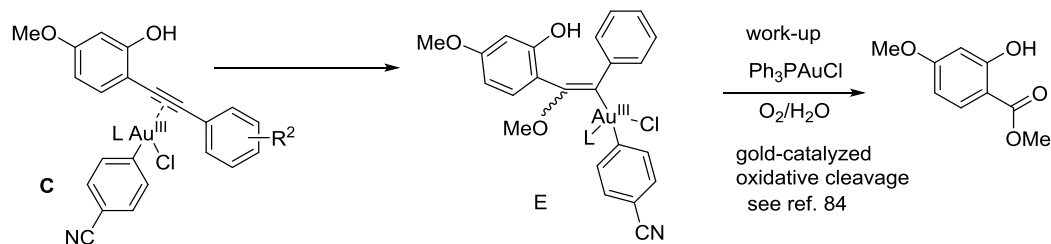
Substitution effect on both aromatic rings of *o*-alkynylphenol **1** was then investigated in reactions with aryl diazonium salts (Table 2-4). When the *o*-alkynylphenol **2-1j** bearing an electron-donating methoxy group in the *para* position to the alkyne, the known⁹³ ester **2-4** (21%) was isolated as the major product, the expected coupling benzofuran **2-3jd** was isolated in only 6% yield. This result is presumed from a preferential gold-catalyzed hydromethoxylation of the alkyne moiety [involving intermediate E (Scheme 2-18)], followed by a gold-catalyzed oxidative cleavage of the generated enol ether.⁹⁴ In contrast, when the 4-cyanophenyldiazonium salt reacts with the *o*-alkynylphenols with an electron-withdrawing ester group at the *para* or *meta* position, the corresponding arylated benzofurans could be isolated as in good yields (**2-3kd** and **2-3ld**).

Table 2-4. Influence of a substituent on the phenol moiety of *ortho*-alkynylphenols.

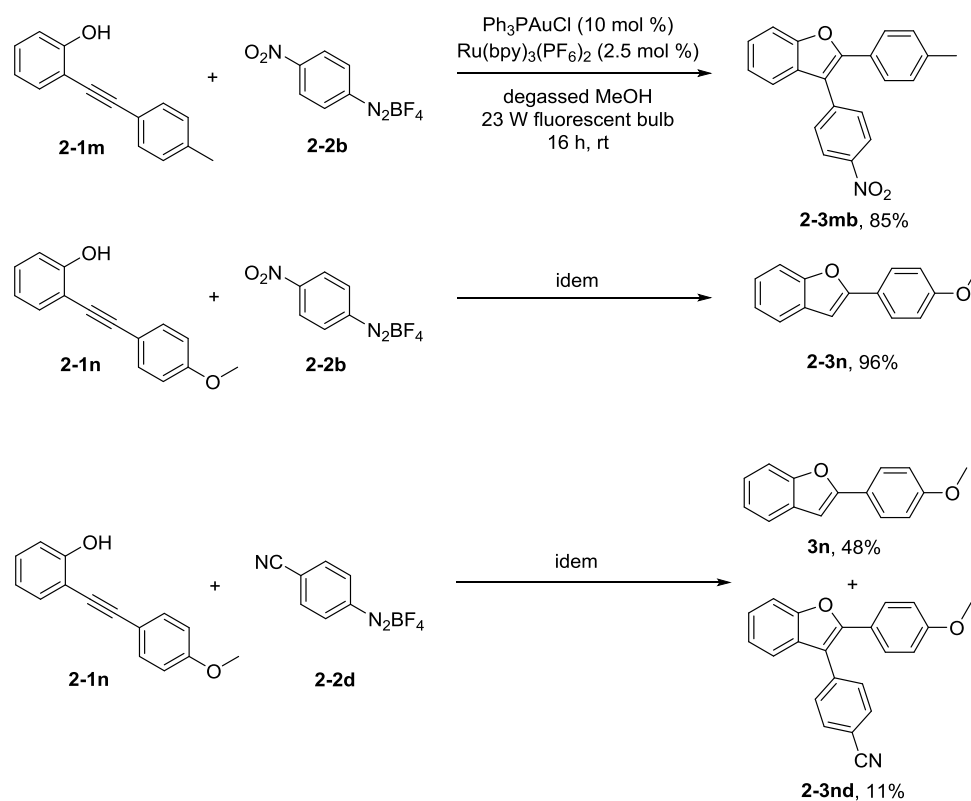


⁹³ CAS Registry No. 5446-02-6.

⁹⁴ Xing, D.; Guan, B.; Cai, G.; Fang, Z.; Yang, L.; Shi, Z. *Org. Lett.* **2006**, *8*, 693.



When *p*-nitrophenyldiazonium tetrafluoroborate reacted with *o*-alkynylphenol bearing a *p*-tolyl group attached to the alkyne, the corresponding 3-(4-nitrophenyl)-2-(*p*-tolyl)benzofuran **2-3mb** was afforded in 85% yield (Scheme 2-16). Again, when an *o*-alkynylphenol **2-1n** attached an electron donor (OMe), the unarylated 2-phenylbenzofuran **2-3n** was isolated in 96% yield, suggesting that the vinylgold intermediate undergoes competitive protodeauration. In similar case, when the *p*-cyanoaryldiazonium salt reacted with 2-((4-methoxyphenyl)ethynyl)phenol, the protodeaured product **2-3n** was formed in 48% yield, whereas the yield of the arylation product **2-3nd** was just 11%.



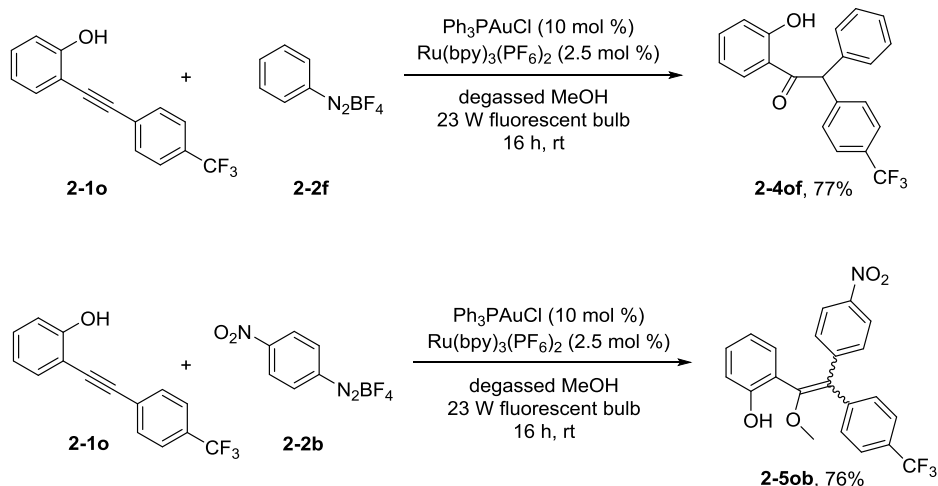
Scheme 2-16. Influence of an electron-donating substituent on the acetylene moiety of *ortho*-alkynylphenols.

The reaction between CF₃-alkynylphenol **2-1o** and aryldiazonium salt gave different results (Scheme 2-17). There was no benzofuran moiety formed, even though arylation happened

when phenyldiazonium salt **2-2f** was added. Instead, it gave an α,α' -bis-arylated ketone bearing a phenol moiety in good yield (77%). Base on the result that no cyclization of the phenol took place, it presumed that the vinylgold intermediate was trapped by methanol in the β position to gold,⁹⁵ the regioisomeric ketone structure of **2-5of** was proposed originating from the hydrolysis of the enol ether intermediate. Another similar reactivity was the reaction between 4-nitrophenyldiazonium salt **2-2b** and CF₃-alkynylphenol **2-1o**, the *E/Z* mixture of the more stable arylated enoethers **2-6ob** (76%) was obtained in this case. All these results suggest that the regioselectivity of the arylation step was influenced by electronic effects, and we will rationalize it below.

Finally, complex reaction mixtures were obtained when butyl-substituted and terminal *o*-alkynylphenols reacted with aryldiazonium salt **2-2d** under the same dual catalysis conditions.

The reaction of butyl-substituted *o*-alkynylphenol and aryldiazonium **2-2d** gave two main products which contains minor impurities. The expected arylyative cyclization product [4-(2-butylbenzofuran-3-yl)benzotrile, <15%] and 4-pentanoylbenzotrile could be identified, but the mechanism is still unclear (<16%), a sequential addition of the aryl radical to the alkyne moiety and a subsequent gold-catalyzed oxidative cleavage of the generated double bond maybe responsible for this result.⁹⁶

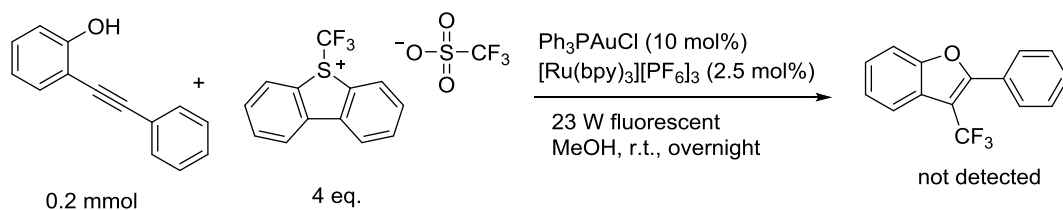


Scheme 2-17. Influence of an electron-withdrawing substituent on the acetylene moiety of *ortho*-alkynylphenols.

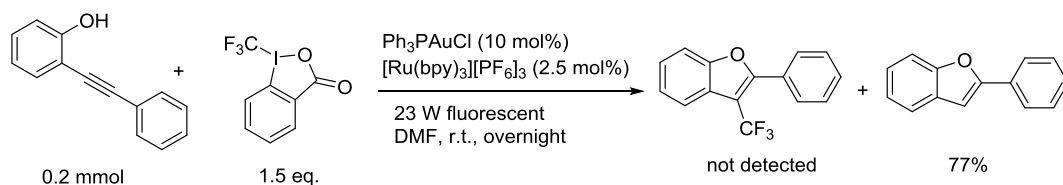
⁹⁵ (a) Huang, L.; Rudolph, M.; Rominger, F.; Hashmi, A. S. K. *Angew.Chem. Int. Ed.* **2016**, *55*, 4808. (b) Tlahuext-Aca, A.; Hopkinson, M. N.; Garza-Sanchez, R. A.; Glorius, F. *Chem. Eur. J.* **2016**, *22*, 5909.

⁹⁶ Xing, D.; Guan, B.; Cai, G.; Fang, Z.; Yang, L.; Shi, Z. *Org. Lett.* **2006**, *8*, 693.

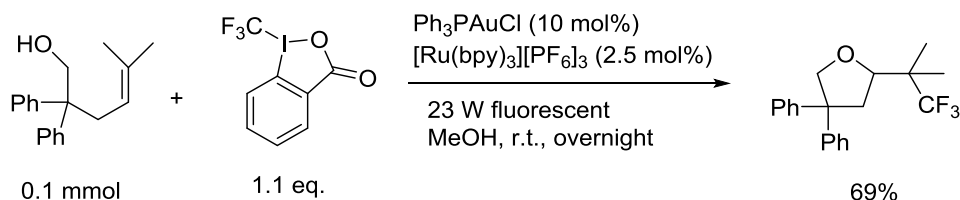
Other similar reactions tried



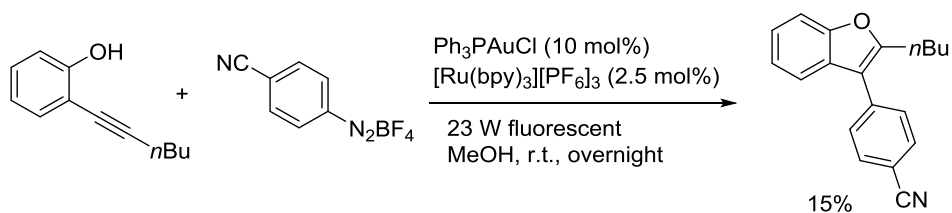
Replace aryl diazonium salt with Umemoto reagent, the desired trifluoromethylation did not occur.



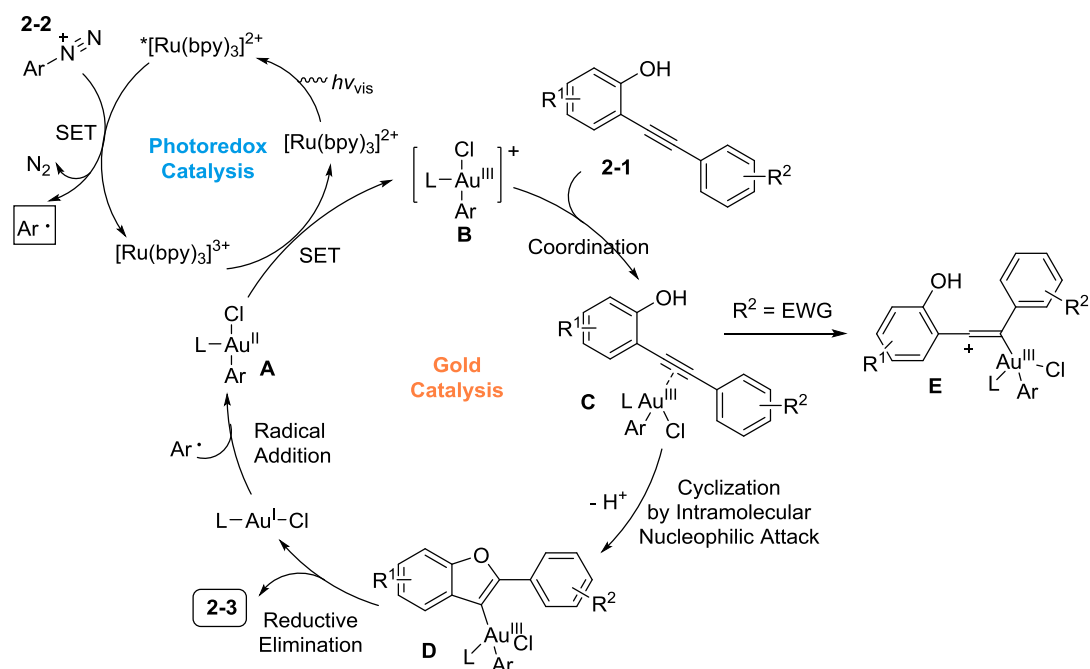
No reaction was observed with the Togni Reagent II, instead the protodeauration cyclization product was obtained as 77% yield, it comes from the gold catalyzed cyclization of *o*-alkynylphenol.



In the presence of gold catalyst and ruthenium photocatalyst under visible light irradiation, the 5-methyl-2,2-diphenylhex-4-en-1-ol reacted with Togni Reagent II to give the corresponding trifluoromethylation cyclization product as 69% yield, the proposed mechanism is similar to photoredox/gold catalysis, we try to develop a new reaction pathway, so we did not continue our studies of this reaction.



5of). Reductive elimination would still take place to give arylation and propagate the catalytic cycle.



Scheme 2-18. Proposed reaction mechanism.

3.4 Conclusion

In summary, we have developed a novel photoredox/gold catalysis of C3 benzofuran derivatives by arylation cyclization of *o*-alkynylphenol with aryl diazonium salts. A range of aryl diazonium salts react with *o*-alkynylphenol to afford diversified C3-aryl benzofurans in good to excellent yields at room temperature in the absence of base and/or additives. This reaction proceeds through auroated heterenes, i.e., the vinylgold(III) intermediates formed by 5-endo-dig cyclization of intramolecular nucleophilic attack. This principle provides a simple approach to benzofuran derivatives under mild conditions and extended application of the vinylgold(III) intermediates as well. This work constitutes one more example of a successful dual catalytic approach relying in part on an efficient photoredox-catalyzed event and augurs well for further exciting developments in this domain.

4 Experimental Section

4.1 General Experimental Details

All reactions involving air sensitive reagents or intermediates were carried out in pre-heated glassware under an argon atmosphere using standard *Schlenk* techniques. All solvents and chemicals were used as received from the suppliers (*Alfa Aesar*, *Sigma Aldrich*). Methanol and acetonitrile were purified by mean of distillation under dry Argon atmosphere on calcium hydride. Organic solutions were concentrated under reduced pressure on a Büchi rotary evaporatory. The reactions were irradiated by a standard household lamp with a 23 W fluorescent light bulb. Aryl diazonium tetrafluoroborates **2-2a-2i** were synthesized following the procedure of Hanson.⁹⁹ Photocatalysts [Ru(bpy)₃]₂(PF₆)₂ (bpy=2,2'-bipyridine) and Cu(dpp)₂PF₆·2H₂O were prepared according to the procedure of Yoon¹⁰⁰ and Meyer¹⁰¹ respectively. The gold(I) complexes [Ph₃PAu]NTf₂ and IPrAuCl (IPr = 1,3-bis(2,6-diisopropylphenyl)imidazol-2-ylidene) were obtained by the procedures of Gagosz¹⁰² and Nolan¹⁰³ respectively. All other metal complexes were commercially available and used as received. Chromatographic purifications of products were accomplished using force-flow chromatography (FC) on Davisil (LC60A) SI 60 Å (40 – 63 µm) silica gel according to the method of Still.¹⁰⁴ Thin layer chromatography (TLC) was performed on Merck 60 F254 silica gel plates. TLC visualization was performed by fluorescence quenching (λ = 254 nm). Filtrations through Celite were performed using Hyflo Super Cel from Fluka. ¹H NMR spectra were recorded on a Bruker 400 AVANCE or 300 AVANCE (400 and 300 MHz respectively) and are referenced relative to residual CDCl₃ protons signals at δ 7.26 ppm. ¹³C NMR spectra were recorded on a Bruker 400 AVANCE or 300 AVANCE (100 and 75 MHz respectively) and are referenced relative to CDCl₃ at δ 77.00 ppm. ¹⁹F NMR spectra were recorded on a Bruker 400 AVANCE (376 MHz) and are referenced relative to CFC₃ at δ 0.00 ppm. Data are reported as follows: chemical shift (δ ppm), multiplicity (s = singlet, d = doublet, t = triplet, q = quartet, qt = quintuplet, m = multiplet, bs = broad signal), coupling

⁹⁹ Hanson, P.; Jones, J. R.; Taylor, A. B.; Walton, P. H.; Timms, A. W. *J. Chem. Soc., Perkin Trans. 2* **2002**, 1135.

¹⁰⁰ Ishay, M. A.; Lu, Z.; Yoon, T. P. *J. Am. Chem. Soc.* **2010**, *132*, 8572.

¹⁰¹ Ruthkosky, M.; Castellano, F. N.; Meyer, G. J. *Inorg. Chem.* **1996**, *35*, 6406.

¹⁰² Mezailles, N.; Ricard, L.; Gagosz, F. *Org. Lett.* **2005**, *7*, 4133.

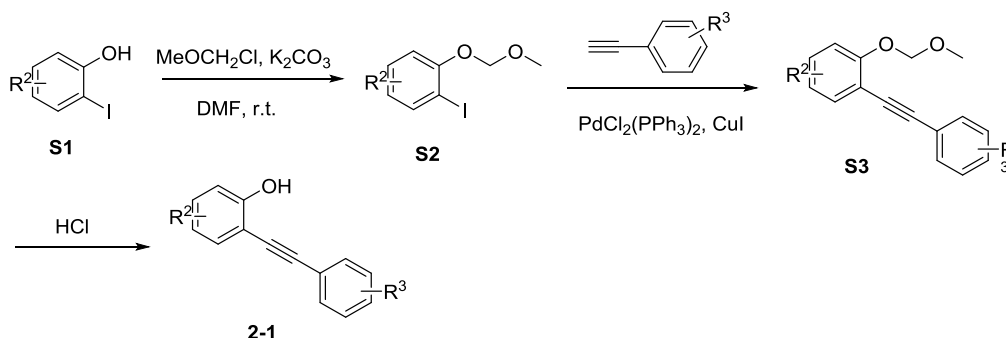
¹⁰³ (a) de Fremont, P.; Scott, N. M.; Stevens, E. D.; Nolan, S. P. *Organometallics* **2005**, *24*, 2411. (b) de Fremont, P.; Scott, N. M.; Stevens, E. D.; Ramnial, T.; Lightbody, O. C.; MacDonald, C. L. B.; Clyburne, J. A. C.; Abernethy, C. D.; Nolan, S. P. *Organometallics* **2005**, *24*, 6301.

¹⁰⁴ Still, W. C.; Kahn, M.; Mitra, A. J. *J. Org. Chem.* **1978**, *43*, 2923.

constant (Hz) and integration. IR spectra were recorded on a Bruker Tensor 27 (ATR diamond) and are reported in terms of frequency of absorption (cm^{-1}). High resolution mass spectrometries were performed on a microTOF (ESI).

4.2 General Procedure

General Procedure 1 (GP1). Synthesis of 2-(phenylethynyl)phenol **2-1a**.¹⁰⁵

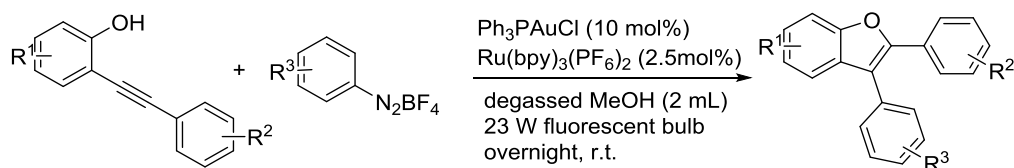


MOMCl (1.1 g, 13.6 mmol, 1.5 equiv.) was added to a mixture of 2-iodo phenol **S1** (2 g, 9.1 mmol, 1 equiv.) and K₂CO₃ (5.0 g, 36.36 mmol, 4 equiv.) in DMF (8 mL). The mixture was stirred at room temperature 2h. The completion of the reaction was monitored by TLC (Pent/Et₂O: 9/1). The solution was diluted with diethyl ether (100 mL) and 60 mL of water were added. The layers were separated and the aqueous phase was extracted with diethyl ether (3 × 30 mL). The combined organic layers were washed with brine, dried over MgSO₄, filtered and concentrated under reduced pressure to afford the iodide **S2a** (2.4 g, quant). The latter was engaged without purification in the alkylation of alkyne following a Sonogashira process. To a solution of phenylacetylene (1.0 g, 10.0 mmol, 1.1 equiv.) and **S2a** (2.4 g, 9.1 mmol, 1.0 equiv.) in triethylamine (90 mL), PdCl₂(PPh₃)₂ (126.3 mg, 0.18 mmol, 2 mol%) and CuI (34.3 mg, 0.18 mmol, 2 mol%) were added. The mixture was stirred at 65°C until complete consumption of **S2a** was observed by TLC (Pent/Et₂O: 9/1). The reaction mixture was warmed to room temperature, diethyl ether was added (50 mL) and the mixture was filtrated through a plug of cotton wool. After removal of the solvent, the residue was purified by silica gel chromatography (Pent/Et₂O: 9/1) to afford **S3a** (1.95 g, 91%). The deprotection of MOM was conducted by added HCl (0.85 mL, 9.0 mmol, 6N) to a solution of **S3a** (1.95 g, 8.2 mmol) in MeOH (15 mL). The reaction mixture was stirred until the deprotection was completed. The mixture was diluted with water (50 mL) and diethyl ether (30 mL). The layers

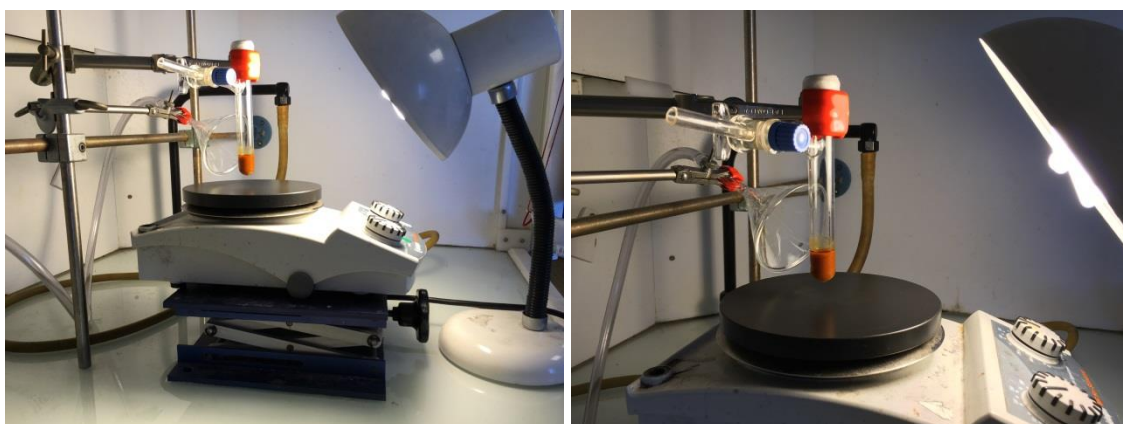
¹⁰⁵ Hashmi, A. S. K.; Ramamurthi, T. D.; Rominger, F. *Adv. Synth. Catal.* **2010**, 352, 971.

were separated and the aqueous phase was extracted with diethyl ether (3×30 mL). The combined organic layers were washed with brine, dried over Na_2SO_4 , filtered and concentrated under reduced pressure to afford **2-1a** as a yellow solid (1.3 g, 82%) after purification by flash Chromatography (Pent/ Et_2O : 9/1).

General Procedure 2 (GP2). *Arylative Cyclization of Ortho-Alkynylphenols with Aryl Diazonium Salts.*



The photocatalyst $[\text{Ru}(\text{bpy})_3](\text{PF}_6)_2$ (4.3 mg, 0.005 mmol, 2.5 mol%), the gold(I) complex Ph_3PAuCl (9.9 mg, 0.02 mmol, 10 mol%), the appropriate diazonium salt **2-2** (0.8 mmol) and ortho-alkynylphenol derivative **2-1** (0.2 mmol, 0.1 M) were introduced in a *schlenk* tube equipped with a magnetic stirring bar in which MeOH (2 mL) was added. The mixture was degassed using three freeze pump-thaw cycles then was irradiated with a 23 W fluorescent light bulb (~10 cm away from the glassware). If necessary, the air flowing can be used to cool down the *schlenk* tube) for 16 h (unless mentioned). The reaction was quenched with water (2 mL) and a saturated aqueous K_2CO_3 solution (1 mL) and the solution was extracted Et_2O (4×5 mL). The combined organic layer was dried over Na_2SO_4 , filtered and concentrated under reduced pressure to give the crude product. The residue was purified by FC on silica gel to afford the desired product.

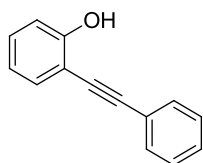


4.3 Compound Characterizations

A. Synthesis of *o*-alkynylphenol derivatives as substrates.

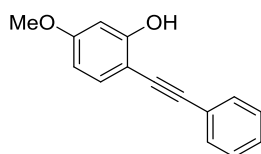
All *o*-alkynylphenol substrates were prepared according to the procedure reported by Hashmi et al.¹⁰⁶ and based on the synthesis of 2-(phenylethynyl)phenol **2-1a**, as summarized before part in **General Procedure 1 (GP1)**.

2-(Phenylethynyl)phenol (**2-1a**).



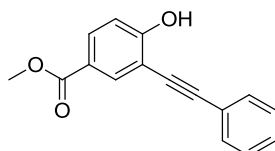
Following general procedure GP1 with 2-iodophenol (2 g, 9.1 mmol) and phenylacetylen (1.0 g, 9.1 mmol) to afford **2-1a** (1.3 g, 74% over three steps). The spectroscopic data match those previously reported in the literature.¹⁰⁷ ¹H NMR (300 MHz, CDCl₃) δ 7.60-7.56 (m, 2H), 7.46 (dd, *J* = 7.8, 1.8 Hz, 1H), 7.43-7.39 (m, 3H), 7.33-7.27 (m, 1H), 7.02 (dd, *J* = 8.1, 0.9 Hz, 1H), 6.94 (td, *J* = 7.5, 1.2 Hz, 1H), 5.87 (s, 1H).

5-Methoxy-2-(phenylethynyl)phenol (**2-1j**).



Following general procedure reported by A. J. Frontier *et al.*¹⁰⁸ with 2-iodo-5-methoxyphenol and phenylacetylen. The spectroscopic data match those previously reported in the literature.¹⁰⁹ ¹H NMR (300 MHz, CDCl₃) 7.54-7.51 (m, 2H), 7.32-7.27 (m, 4H), 6.56 (d, *J* = 2.4 Hz, 1H), 6.50 (dd, *J* = 6.3, 2.4 Hz, 1H), 5.87 (bs, 1H), 3.81 (s, 3H).

Methyl 4-hydroxy-3-(phenylethynyl)benzoate (**2-1k**).



¹⁰⁶ Hashmi, A. S. K.; Ramamurthi, T. D.; Rominger, F. *Adv. Synth. Catal.* **2010**, 352, 971.

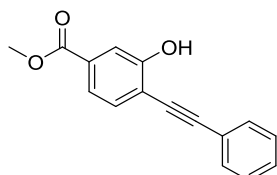
¹⁰⁷ Hashmi, A. S. K.; Ramamurthi, T. D.; Rominger, F. *Adv. Synth. Catal.* **2010**, 352, 971.

¹⁰⁸ Malona, J. A.; Cariou, K.; Spencer, III, W. T.; Frontier, A. J. *J. Org. Chem.* **2012**, 77, 1891.

¹⁰⁹ Auzias, M. G.; Neuburger, M.; Wegner, H. A. *Synlett* **2010**, 16, 2443.

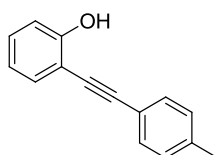
Following general procedure GP1 with methyl 4-hydroxy-3-iodobenzoate (556 mg, 2 mmol) and phenylacetylen (224.7 mg, 2.2 mmol) to afford **2-1k** (413.7 mg, 82% over three steps). The spectroscopic data match those previously reported in the literature.¹¹⁰ ¹H NMR (300 MHz, CDCl₃) δ 8.15 (d, *J* = 2.1 Hz, 1H), 7.96 (dd, *J* = 8.7, 2.1 Hz, 1H), 7.57-7.53 (m, 2H), 7.41-7.38 (m, 3H), 7.02 (d, *J* = 8.7 Hz, 1H), 6.26 (s, 1H), 3.90 (s, 3H).

Methyl 3-hydroxy-4-(phenylethynyl)benzoate (2-1l).



Following general procedure GP1 with methyl 3-hydroxy-4-iodobenzoate (556 mg, 2 mmol) and phenylacetylen (224.7 mg, 2.2 mmol) to afford **2-1l** (454 mg, 90% over three steps). Mp 204 °C. ¹H NMR (300 MHz, CDCl₃) δ 7.65 (d, *J* = 1.5 Hz, 1H), 7.61-7.54 (m, 3H), 7.43 (d, *J* = 8.1 Hz, 1H), 7.40-7.38 (m, 3H), 5.95 (s, 1H), 3.92 (s, 3H); ¹³C NMR (75 MHz, CDCl₃) δ 166.3, 156.3, 131.7, 131.7, 131.6, 129.3, 128.6, 121.9, 121.5, 115.8, 114.3, 98.7, 82.5, 52.3. IR (neat): 3407, 2961, 2922, 2853, 1711, 1607, 1573, 1428, 1292, 1244, 1201, 1094, 986, 915, 881, 799, 755, 692, 590 cm⁻¹. HRMS calc. for [C₁₆H₁₂NaO₃]⁺ 275.0684; found 275.0679.

2-(p-Tolyethynyl)phenol (2-1m).

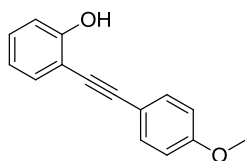


Following general procedure GP1 with 2-iodophenol (440 mg, 2 mmol) and 4-ethynyltoluene (255 mg, 2.2 mmol) to afford **2-1m** (292 mg, 70% over three steps). The spectroscopic data match those previously reported in the literature.¹¹¹ ¹H NMR (300 MHz, CDCl₃) δ 7.46-7.40 (m, 3H), 7.30-7.24 (m, 1H), 7.20-7.17 (m, 2H), 6.99 (bdd, *J* = 8.4, 1.2 Hz, 1H), 6.91 (td, *J* = 7.5, 1.2 Hz, 1H), 5.85 (s, 1H), 2.39 (s, 3H).

¹¹⁰ Boyer, A.; Isono, N.; Lackner, S.; Lautens, M. *Tetrahedron* **2010**, *66*, 6468.

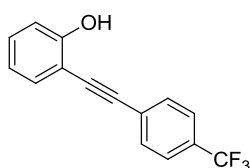
¹¹¹ Martínez, C.; Álvarez, R.; Aurrecochea, J. M. *Org. Lett.* **2009**, *11*, 1083.

2-((4-Methoxyphenyl)ethynyl)phenol (**2-1n**).



Following general procedure GP1 with 2-iodophenol (440 mg, 2 mmol) and 4-ethynylanisole (291 mg, 2.2 mmol) to afford **2-1n** (292 mg, 65% over three steps). The spectroscopic data match those previously reported in the literature.¹¹² ¹H NMR (300 MHz, CDCl₃) δ 7.82-7.79 (m, 2H), 7.58-7.50 (m, 2H), 7.26-7.20 (m, 2H), 7.00-6.97 (m, 2H), 6.89 (s, 1H), 3.87 (s, 3H).

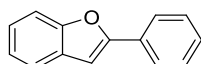
2-((4-(Trifluoromethyl)phenyl)ethynyl)phenol (**2-1o**).



Following general procedure GP1 with 2-iodophenol (440 mg, 2 mmol) and 4-(trifluoromethyl)phenylacetylene (374 mg, 2.2 mmol) to afford **2-1o** (424 mg, 81% over three steps). The spectroscopic data match those previously reported in the literature.¹¹³ ¹H NMR (300 MHz, CDCl₃) δ 7.64 (m, 4H), 7.44 (dd, *J* = 7.8, 1.5 Hz, 1H), 7.31 (bs, 1H), 7.00 (bd, *J* = 8.1 Hz, 1H), 6.94 (bt, *J* = 7.5 Hz, 1H), 5.76 (s, 1H).

B. Products of arylation cyclization of ortho-alkynylphenols

2-Phenylbenzofuran (**2-3a**).



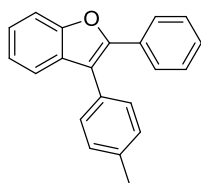
The spectroscopic data match those previously reported in the literature.¹¹⁴ ¹H NMR (300 MHz, CDCl₃) δ 7.88 (dd, *J* = 8.4, 1.5 Hz, 2H), 7.59 (dd, *J* = 7.8, 1.8 Hz, 1H), 7.54 (d, *J* = 8.4 Hz, 1H), 7.46 (t, *J* = 7.5 Hz, 2H), 7.32-7.21 (m, 3H), 7.03 (s, 1H).

2-Phenyl-3-(*p*-tolyl)benzofuran (**2-3aa**).

¹¹² Fischer, J.; Savage, G. Paul.; Coster, M. J. *Org. Lett.* **2011**, *13*, 3376.

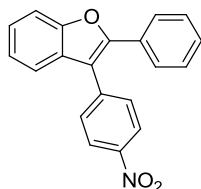
¹¹³ Liao, Y.; Smith, J.; Fathi, R.; Yang, Z. *Org. Lett.* **2005**, *7*, 2707.

¹¹⁴ Hiroya, K.; Itoh, S.; Sakamoto, T. *Tetrahedron* **2005**, *61*, 10958.



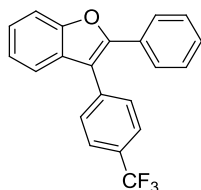
Following general procedure GP2 with *ortho*-alkynylphenol **2-1a** (38.8 mg, 0.2 mmol) and aryldiazonium **2-2a** (165 mg, 0.8 mmol). The crude product was purified by flash column chromatography (Pent/Et₂O, 100:1) to afford **2-3aa** as a yellow solid (42 mg, 73%). The spectroscopic data match those previously reported in the literature.¹¹⁵ ¹H NMR (300 MHz, CDCl₃) δ 7.68-7.65 (m, 2H), 7.55-7.47 (m, 2H), 7.36 (dd, *J* = 6.0, 1.8 Hz, 2H), 7.34- 7.19 (m, 7H), 2.43 (s, 3H). ¹³C NMR (101 MHz, CDCl₃) δ 154.0, 150.3, 137.3, 130.8, 130.4, 129.7, 129.7, 129.6, 128.4, 128.2, 127.0, 124.6, 122.8, 120.1, 117.5, 111.1, 21.4.

3-(4-Nitrophenyl)-2-phenylbenzofuran (2-3ab).



Following general procedure GP2 with *ortho*-alkynylphenol **2-1a** (38.8 mg, 0.2 mmol) and aryldiazonium **2-2b** (190 mg, 0.8 mmol). The crude product was purified by flash column chromatography (Pent/Et₂O, 100:1) to afford **2-3ab** as a yellow solid (54 mg, 86%). The spectroscopic data match those previously reported in the literature.¹¹⁵ ¹H NMR (300 MHz, CDCl₃) δ 8.26 (d, *J* = 8.7 Hz, 2H), 7.70 (d, *J* = 8.7 Hz, 2H), 7.63-7.59 (m, 3H), 7.53-7.50 (m, 1H), 7.47-7.36 (m, 4H), 7.33-7.27 (m, 1H). ¹³C NMR (75 MHz, CDCl₃) δ 154.1, 151.9, 147.1, 140.2, 130.4, 129.8, 129.1, 128.9, 128.7, 127.4, 125.2, 124.2, 123.4, 119.4, 115.4, 111.4.

2-Phenyl-3-(4-(trifluoromethyl)phenyl)benzofuran (2-3ac).

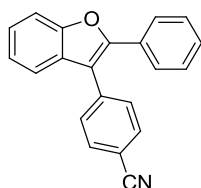


Following general procedure GP2 with *ortho*-alkynylphenol **2-1a** (38.8 mg, 0.2 mmol) and aryldiazonium **2-2c** (208 mg, 0.8 mmol). The crude product was purified by flash column chromatography (Pent/Et₂O, 100:0) to afford **2-3ac** as a white solid (51 mg, 76%). The

¹¹⁵ Hu, Y.; Nawoschik, K. J.; Liao, Y.; Ma, J.; Fathi, R.; Yang, Z. *J. Org. Chem.* **2004**, *69*, 2235.

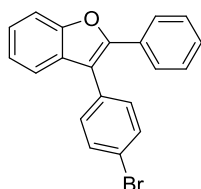
spectroscopic data match those previously reported in the literature.¹¹⁶ ¹H NMR (300 MHz, CDCl₃) δ 7.78-7.72 (m, 2H), 7.65-7.57 (m, 4H), 7.49 (d, *J* = 7.5 Hz, 1H), 7.39-7.26 (m, 6H). ¹³C NMR (101 MHz, CDCl₃) δ 154.1, 151.3, 136.9, 130.2, 130.1, 129.6, 128.8, 128.7, 128.6, 128.5, 127.2, 125.9 (q, *J*_{C-F} = 4.0 Hz), 125.0, 124.9, 124.2 (q, *J*_{CF3} = 270.7 Hz), 123.3, 122.9, 120.9, 119.7, 116.1, 111.3; ¹⁹F NMR (282 MHz, CDCl₃) δ -62.43.

4-(2-Phenylbenzofuran-3-yl)benzonitrile (2-3ad).



Following general procedure GP2 with *ortho*-alkynylphenol **2-1a** (38.8 mg, 0.2 mmol) and aryldiazonium **2-2d** (174 mg, 0.8 mmol). The crude product was purified by flash column chromatography (Pent/Et₂O, 100:1) to afford **2-3ad** as a colourless solid (48 mg, 81%). The spectroscopic data match those previously reported in the literature.¹¹⁷ ¹H NMR (300 MHz, CDCl₃) δ 7.77 (d, *J* = 8.1 Hz, 2H), 7.75-7.57 (m, 4H), 7.50 (dt, *J* = 7.5, 1.2, 0.6 Hz, 1H), 7.41-7.34 (m, 4H), 7.31-7.26 (m, 1H). ¹³C NMR (75 MHz, CDCl₃) δ 154.2, 151.7, 138.2, 132.8, 130.4, 129.9, 129.1, 128.7, 127.4, 125.2, 123.4, 119.5, 118.8, 115.8, 111.4, 111.3.

3-(4-Bromophenyl)-2-phenylbenzofuran (2-3ae).



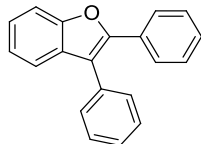
Following general procedure GP2 with *ortho*-alkynylphenol **2-1a** (38.8 mg, 0.2 mmol) and aryldiazonium **2-2e** (217 mg, 0.8 mmol). The crude product was purified by flash column chromatography (Pent/Et₂O, 100:0) to afford **2-3ae** as a white solid (43 mg, 61%). Mp 120 °C. ¹H NMR (300 MHz, CDCl₃) δ 7.67-7.55 (m, 5H), 7.48 (dd, *J* = 7.5, 1.2 Hz, 1H), 7.41-7.23 (m, 7H). ¹³C NMR (75 MHz, CDCl₃) δ 154.0, 150.8, 132.2, 131.9, 131.4, 130.4, 129.8, 128.6, 128.5, 127.1, 124.9, 123.1, 121.7, 119.7, 116.3, 111.2. IR (neat): 2363, 2328, 1487,

¹¹⁶ Han, J.-S.; Chen, S.-Q.; Zhong, P.; Zhang, X.-H. *Synthetic communications* **2014**, *44*, 3148.

¹¹⁷ Markina, N. A.; Chen, Y.; Larock, R. C. *Tetrahedron* **2013**, *69*, 2701.

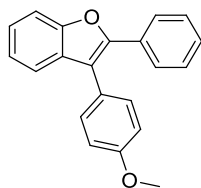
1445, 1380, 1256, 1206, 1064, 1001, 956, 839, 804, 741, 681, 606 cm^{-1} . MS (EI, 70 eV) m/z 350 (**2-3ae** (^{81}Br)), 348 (**2-3ae** (^{79}Br)), 270 (**2-3ae** – Br + H).

2,3-Diphenylbenzofuran (2-3af).



Following general procedure GP2 with *ortho*-alkynylphenol **2-1a** (38.8 mg, 0.2 mmol) and aryldiazonium **2-2f** (154 mg, 0.8 mmol). The crude product was purified by flash column chromatography (Pent/Et₂O, 100:0) to afford **2-3af** as a colourless oil (35 mg, 65%). The spectroscopic data match those previously reported in the literature.¹¹⁸ ¹H NMR (300 MHz, CDCl₃) δ 7.68 (dd, $J = 7.2, 2.7$ Hz, 2H), 7.57 (d, $J = 7.8$ Hz, 1H), 7.51-7.42 (m, 6H), 7.35-7.22 (m, 5H). ¹³C NMR (75 MHz, CDCl₃) δ 154.0, 150.5, 132.9, 130.7, 130.3, 129.8, 129.0, 128.4, 128.3, 127.6, 127.0, 124.7, 122.9, 120.0, 117.5, 111.1.

3-(4-Methoxyphenyl)-2-phenylbenzofuran (2-3ag).

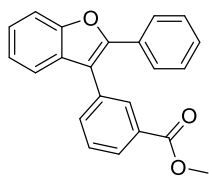


Following general procedure GP2 with *ortho*-alkynylphenol **2-1a** (38.8 mg, 0.2 mmol) and aryldiazonium **2-2g** (178 mg, 0.8 mmol). The crude product was purified by flash column chromatography (Pent/Et₂O, 100:0) to afford **2-3ag** as a white solid (14 mg, 23%). The spectroscopic data match those previously reported in the literature.¹¹⁹ ¹H NMR (300 MHz, CDCl₃) δ 7.68 (dd, $J = 8.1, 2.1$ Hz, 2H), 7.56 (d, $J = 8.1$ Hz, 1H), 7.51-7.48 (m, 1H), 7.44 (d, $J = 8.7$ Hz, 2H), 7.33-7.24 (m, 5H), 7.02 (d, $J = 8.4$ Hz, 2H), 3.89 (s, 3H). ¹³C NMR (75 MHz, CDCl₃) δ 159.1, 154.0, 150.8, 130.9, 130.8, 130.5, 128.4, 128.2, 126.9, 124.9, 124.6, 122.8, 120.0, 117.1, 114.5, 111.1, 55.3.

¹¹⁸ Han, J.-S.; Chen, S.-Q.; Zhong, P.; Zhang, X.-H. *Synth. Commun.* **2014**, *44*, 3148.

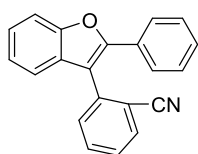
¹¹⁹ Hu, Y.; Nawoschik, K. J.; Liao, Y.; Ma, J.; Fathi, R.; Yang, Z. *J. Org. Chem.* **2004**, *69*, 2235.

3-(2-Phenylbenzofuran-3-yl)benzoate (2-3ah).



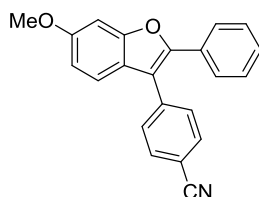
Following general procedure GP2 with *ortho*-alkynylphenol **2-1a** (38.8 mg, 0.2 mmol) and aryldiazonium **2-2h** (200 mg, 0.8 mmol). The crude product was purified by flash column chromatography (Pent/Et₂O, 100:1) to afford **2-3ah** as a colourless oil (41 mg, 62%). ¹H NMR (300 MHz, CDCl₃) δ 8.23-8.22 (m, 1H), 8.11-8.08 (m, 1H), 7.69-7.46 (m, 6H), 7.38-7.28 (m, 4H), 7.26-7.23 (m, 1H), 3.93 (s, 3H). ¹³C NMR (75 MHz, CDCl₃) δ 166.8, 154.0, 150.9, 134.4, 133.3, 131.0, 130.8, 130.3, 129.9, 129.1, 128.8, 128.6, 128.5, 127.0, 124.9, 123.1, 119.8, 116.5, 111.2, 52.2. IR (neat): 2963, 2923, 2854, 1726, 1453, 1376, 1295, 1261, 1195, 1112, 1073, 750, 634 cm⁻¹. HRMS calc. for [C₂₂H₁₆NaO₃]⁺ 351.0997; found 351,0992.

2-(2-Phenylbenzofuran-3-yl)benzonitrile (2-3ai).



Following general procedure GP2 with *ortho*-alkynylphenol **2-1a** (38.8 mg, 0.2 mmol) and aryldiazonium **2-2i** (174 mg, 0.8 mmol). The crude product was purified by flash column chromatography (Pent/Et₂O, 100:1) to afford **2-3ai** as a yellow oil (22 mg, 37%). ¹H NMR (300 MHz, CDCl₃) δ 7.83 (dd, *J* = 7.2, 1.5 Hz, 1H), 7.72 (td, *J* = 7.5, 1.5 Hz, 1H), 7.63-7.52 (m, 4H), 7.40-7.24 (m, 7H). ¹³C NMR (101 MHz, CDCl₃) δ 154.0, 152.2, 137.0, 133.9, 133.2, 131.6, 130.1, 129.5, 128.9, 128.7, 128.4, 126.8, 125.1, 125.1, 123.3, 119.6, 117.6, 113.8, 111.4. IR (neat): 2963, 2922, 2854, 1455, 1374, 1258, 1204, 1108, 754, 692, cm⁻¹. HRMS calc. for [C₂₁H₁₃NNaO]⁺ 318.0895; found 318.0889.

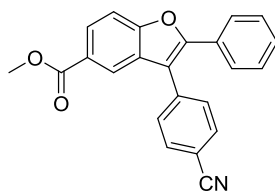
6-Methoxy-3-(4-methylphenyl)-2-phenyl-benzofuran (2-3jd)



Following general procedure GP2 with *ortho*-alkynylphenol **2-1j** (37.6 mg, 0.17 mmol) and aryldiazonium **2-2d** (173 mg, 0.8 mmol). A mixture of products **2-4** and **2-3jd** were obtained

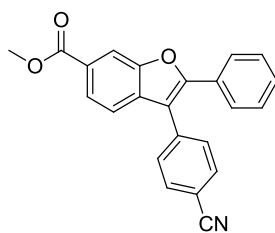
and purified by flash column chromatography (Pent/Et₂O, 100:6) to afford **2-4** as a colourless oil (6.4 mg, 21%) and **2-3jd** as a colourless oil in the presence of a trace of **2-4** (3 mg, 6%). Compound **2-4** is commercial available and the spectroscopic data match those previously reported in the literature. Compound **2-4**: ¹H NMR (400 MHz, CDCl₃) δ 11.0 Hz (s, 1H), 7.73 (dd, *J* = 8.0, 0.4 Hz, 1H), 6.45-6.42 (m, 2H), 3.91 (s, 3H), 3.82 (s, 3H). ¹³C NMR (101 MHz, CDCl₃) δ 170.4, 165.6, 163.8, 131.2, 107.6, 105.4, 100.7, 55.5, 51.9. Compound **2-3jd**: ¹H NMR (400 MHz, CDCl₃) δ 7.74 (d, *J* = 8.8 Hz, 2H), 7.62 (d, *J* = 8.4 Hz, 2H), 7.57-7.54 (m, 2H), 7.36-7.33 (m, 4H), 7.11 (d, *J* = 2.0 Hz, 1H), 6.91 (dd, *J* = 8.4, 2.0 Hz, 1H), 3.90 (s, 3H). ¹³C NMR (101 MHz, CDCl₃) δ 158.7, 155.2, 150.7, 138.3, 132.7, 130.3, 130.1, 128.7, 128.7, 127.0, 122.5, 119.7, 118.8, 115.7, 112.4, 111.2, 95.9, 55.8. IR (neat): 3735, 3629, 2916, 2843, 2364, 2328, 2227, 1669, 1617, 1494, 1440, 1347, 1271, 1196, 1153, 1114, 1068, 1026, 971, 877, 833, 769, 695, 640, 586 cm⁻¹. HRMS calc. for [C₂₂H₁₅NNaO₂]⁺ 348.0995; found 348.0983.

Methyl 3-(4-cyanophenyl)-2-phenylbenzofuran-5-carboxylate (2-3kd).



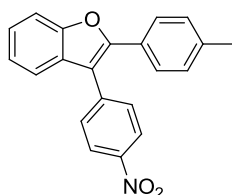
Following general procedure GP2 with *ortho*-alkynylphenol **2-1k** (50 mg, 0.2 mmol) and aryldiazonium **2-2d** (174 mg, 0.8 mmol). The crude product was purified by flash column chromatography (Pent/Et₂O, 100:4) to afford **2-3kd** as a white solid (60 mg, 85%). Mp 215 °C. ¹H NMR (300 MHz, CDCl₃) δ 8.19 (dd, *J* = 1.8, 0.6 Hz, 1H), 8.10 (dd, *J* = 8.4, 1.5 Hz, 1H), 7.79-7.76 (m, 2H), 7.64- 7.58 (m, 5H), 7.38-7.36 (m, 3H), 3.93 (s, 3H). ¹³C NMR (75 MHz, CDCl₃) δ 166.9, 156.6, 153.0, 137.3, 132.9, 130.4, 129.5, 129.3, 129.2, 128.8, 127.4, 126.9, 125.8, 121.9, 118.6, 116.0, 111.7, 111.3, 52.2. IR (neat): 2923, 2853, 2228, 1718, 1606, 1437, 1372, 1293, 1242, 1200, 1098, 991, 918, 848, 763, 692, cm⁻¹. HRMS calc. for [C₂₃H₁₅NNaO₃]⁺ 376.0950; found 376.0944.

Methyl 3-(4-cyanophenyl)-2-phenylbenzofuran-6-carboxylate (2-3ld).



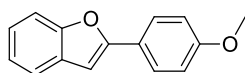
Following general procedure GP2 with *ortho*-alkynylphenol **2-1l** (50 mg, 0.2 mmol) and aryldiazonium **2-2d** (174 mg, 0.8 mmol). The crude product was purified by flash column chromatography (Pent/Et₂O, 100:4) to afford **2-3ld** as a white solid (46 mg, 65%). Mp 148 °C. ¹H NMR (300 MHz, CDCl₃) δ 8.26 (dd, *J* = 1.2, 0.6 Hz, 1H), 7.99 (dd, *J* = 6.9, 1.5 Hz, 1H), 7.78-7.75 (m, 2H), 7.63-7.58 (m, 4H), 7.50 (dd, *J* = 8.1, 0.6 Hz, 1H), 7.39-7.36 (m, 3H), 3.97 (s, 3H). ¹³C NMR (75 MHz, CDCl₃) δ 166.9, 154.5, 153.5, 137.4, 133.2, 132.9, 130.4, 129.7, 129.3, 128.8, 127.5, 127.0, 124.8, 119.0, 118.6, 115.8, 113.0, 111.7, 52.3. IR (neat): 2952, 2366, 2228, 1705, 1613, 1496, 1428, 1367, 1287, 1222, 1192, 1072, 974, 909, 869, 833, 760, 731, 686, 626 cm⁻¹. HRMS calc. for [C₂₃H₁₅NNaO₃]⁺ 376.0950; found 376.0944.

3-(4-Nitrophenyl)-2-(p-tolyl)benzofuran (2-3mb).



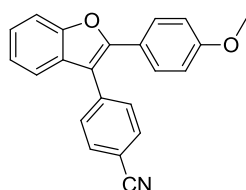
Following general procedure GP2 with *ortho*-alkynylphenol **2-1m** (42 mg, 0.2 mmol) and aryldiazonium **2-2b** (189 mg, 0.8 mmol). The crude product was purified by flash column chromatography (Pent/Et₂O, 100:1) to afford **2-3mb** as a yellow oil (56 mg, 85%). ¹H NMR (300 MHz, CDCl₃) δ 8.31 (d, *J* = 8.7 Hz, 2H), 7.69 (dd, *J* = 6.9, 1.8 Hz, 2H), 7.58 (d, *J* = 8.1 Hz, 1H), 7.52-7.48 (m, 3H), 7.39-7.34 (m, 1H), 7.31-7.26 (m, 1H), 7.17 (d, *J* = 8.1 Hz, 2H), 2.38 (s, 3H). ¹³C NMR (75 MHz, CDCl₃) δ 154.1, 152.3, 147.0, 140.4, 139.4, 130.4, 129.4, 129.0, 127.4, 126.9, 125.0, 124.2, 123.4, 119.3, 114.8, 111.4, 21.4. IR (neat): 2364, 2329, 1603, 1515, 1456, 1347, 1257, 1071, 859, 822, 750, 654, 610 cm⁻¹. HRMS calc. for [C₂₁H₁₅NNaO₃]⁺ 352.0944; found 352.0944.

2-(4-Methoxyphenyl)benzofuran (2-3n).



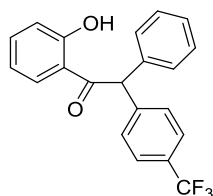
Following general procedure GP2 with *ortho*-alkynylphenol **2-1n** (45 mg, 0.2 mmol) and aryldiazonium **2-2b** (189 mg, 0.8 mmol) or **2-2d** (173 mg, 0.8 mmol). The crude product was purified by flash column chromatography (Pent/Et₂O, 100:6) to afford **2-3n** as a white solid (43 mg, 96%) and (21 mg, 48%) respectively. The spectroscopic data match those previously reported in the literature.¹²⁰ ¹H NMR (300 MHz, CDCl₃) δ 7.83-7.78 (m, 2H), 7.58-7.49 (m, 2H), 7.29-7.20 (m, 2H), 7.01-6.96 (m, 2H), 6.89 (s, 1H), 3.87 (s, 3H); ¹³C NMR (75 MHz, CDCl₃) δ 160.0, 156.1, 154.7, 129.5, 126.4, 123.7, 123.4, 122.8, 120.6, 114.3, 111.0, 99.7, 76.6, 55.4.

4-(2-(4-Methoxyphenyl)benzofuran-3-yl)benzonitrile (2-3nd).



Following general procedure GP2 with *ortho*-alkynylphenol **2-1n** (45 mg, 0.2 mmol) and aryldiazonium **2-2d** (173 mg, 0.8 mmol). The crude product was purified by flash column chromatography (Pent/Et₂O, 100:6) to afford **2-3nd** as a colourless oil (7 mg, 11%). ¹H NMR (400 MHz, CDCl₃) δ 7.75-7.73 (m, 2H), 7.64-7.62 (m, 2H), 7.57-7.52 (m, 3H), 7.49-7.47 (m, 1H), 7.37-7.32 (m, 1H), 7.29-7.25 (m, 1H), 6.89 (dd, *J* = 6.8, 2.0 Hz, 2H), 3.84 (s, 3H); ¹³C NMR (101 MHz, CDCl₃) δ 191.6, 160.3, 154.0, 151.9, 138.5, 132.7, 130.4, 129.2, 128.9, 124.8, 123.3, 122.4, 119.2, 118.9, 114.2, 111.3, 111.0, 55.3. IR (neat): 3053, 2965, 2923, 2848, 2226, 1608, 1507, 1452, 1373, 1302, 1253, 1175, 1111, 1071, 1027, 963, 838, 747, 599 cm⁻¹. HRMS calc. for [C₂₂H₁₅NNaO₂]⁺ 348.0995; found 348.0982.

Compound (2-5of).

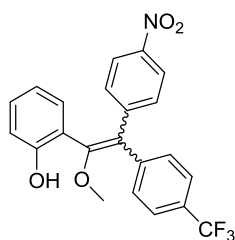


Following general procedure GP2 with *ortho*-alkynylphenol **2-1o** (52 mg, 0.2 mmol) and aryldiazonium **2-2f** (154 mg, 0.8 mmol). The crude product was purified by flash column chromatography (Pent/Et₂O, 100:1) to afford the ketone **2-5of** (present in the enol form) as a colourless oil (55 mg, 77%). ¹H NMR (300 MHz, CDCl₃) δ 12.15 (s, 1H), 7.81-7.78 (dd, *J* =

¹²⁰ Jaseer, E. A.; Prasad, D. J. C.; Sekar, G. *Tetrahedron* **2010**, *66*, 2077.

8.1, 1.8 Hz, 1H), 7.62-7.59 (d, $J = 8.1$ Hz, 1H), 7.49-7.27 (m, 9H), 7.02-6.99 (dd, $J = 8.4, 1.2$ Hz, 1H), 6.86-6.81 (td, $J = 7.2, 1.2$ Hz, 1H), 6.13 (s, 1H). ^{13}C NMR (75 MHz, CDCl_3) δ 203.6, 163.4, 142.6, 137.8, 136.8, 130.5, 129.6, 129.2, 128.9, 127.8, 125.6 (q, $J_{\text{C-F}} = 3.7$ Hz), 119.2, 118.9, 118.8, 58.6. Two carbons are missing. ^{19}F NMR (282 MHz, CDCl_3) δ -62.57. IR (neat): 2924, 1710, 1640, 1576, 1487, 1447, 1414, 1361, 1321, 1226, 1162, 1119, 1066, 1007, 797, 746, 698, 637 cm^{-1} . HRMS calc. for $[\text{C}_{21}\text{H}_{15}\text{F}_3\text{NaO}_2]^+$ 379.0916; found 379.0926.

Compound (2-6ob).



Following general procedure GP2 with *ortho*-alkynylphenol **2-1o** (52 mg, 0.2 mmol) and aryldiazonium **2-2b** (189 mg, 0.8 mmol). The crude product was purified by flash column chromatography (Pent/ Et_2O , 100:3) to afford the enol ether **6ob** as a yellow oil (62.7 mg, 76%). ^1H NMR (300 MHz, CDCl_3) δ 11.98 (s, 0.05H), 8.22-8.19 (m, 1.06H), 7.96 (dd, $J = 6.9, 1.5$ Hz, 0.96H), 7.64-7.61 (m, 1.16H), 7.46-7.36 (m, 3.48H), 7.27-7.22 (m, 1H), 7.11-7.05 (m, 2H), 6.93-6.88 (m, 2H), 6.76-6.70 (m, 1H), 6.03-5.97 (m, 0.96H), 3.58-3.57 (m, 3H). ^{13}C NMR (75 MHz, CDCl_3) δ 154.5, 154.4, 152.7, 146.9, 146.3, 142.9, 131.8, 131.8, 131.6, 130.8 (q, $J_{\text{C-F}} = 34.1$ Hz), 125.3 (q, $J_{\text{C-F}} = 3.7$ Hz), 125.1 (q, $J_{\text{C-F}} = 4.0$ Hz), 124.1, 123.4, 123.3, 120.8, 120.7, 118.9, 118.8, 116.5, 116.4, 57.9, 57.8. ^{19}F NMR (282 MHz, CDCl_3) δ -62.59, -62.62. IR (neat): 2935, 2844, 1703, 1586, 1513, 1449, 1406, 1322, 1163, 1114, 1069, 1009, 843, 753, 701, 639 cm^{-1} . HRMS calc. for $[\text{C}_{22}\text{H}_{16}\text{F}_3\text{NNaO}_4]^+$ 438.0924; found 438.0940.

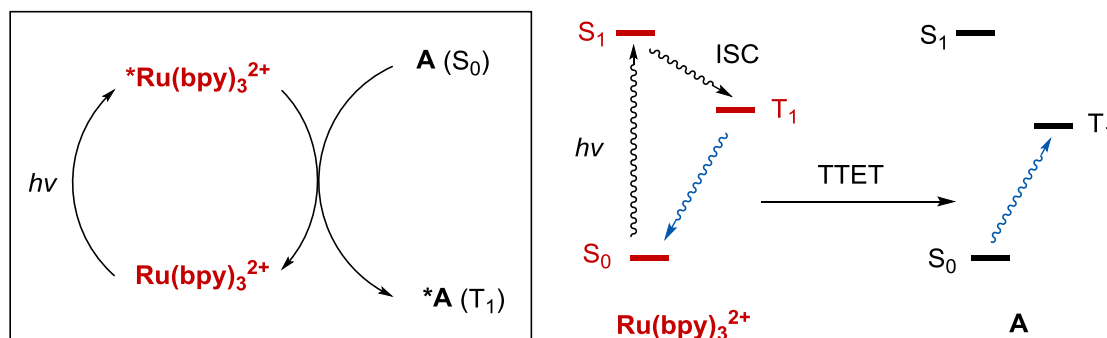
Chapter 3 Photosensitized Gold Catalysis



Three Goldfish, Zhonghua Xia, 2018

1 Background on Energy Transfer Process on Photocatalytic System

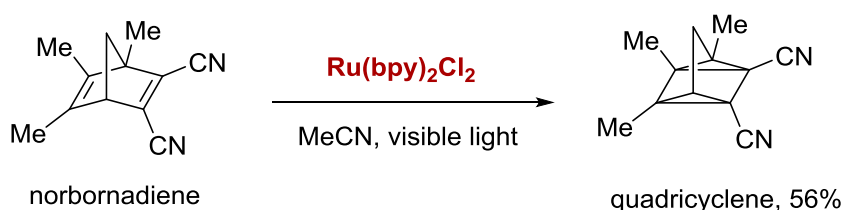
The photoredox catalysis with transition metal complexes has recently received extensive attention, because it could promote various new carbon-carbon bond formation reactions. Most of these photoredox reactions far rely on the ability of photoexcited catalysts to engage in electron transfer with organic molecules. However, a fundamental different pathway for decay of photoexcited states is energy transfer.



Scheme 3-1. Triplet-triplet energy transfer from $*\text{Ru}(\text{bpy})_3^{2+}$ to acceptor **A**.

For example, irradiation of $\text{Ru}(\text{bpy})_3^{2+}$ excites the complex from its ground singlet state (S_0) to its lowest singlet excited state (S_1) (Scheme 3-1). The long-lived lowest-energy triplet state (T_1) could be generated from intersystem crossing (ISC). The triplet excited state of $\text{Ru}(\text{bpy})_3^{2+}$ may both engage in electron transfer triplet-triplet energy transfer (TTET). In this process of TTET, decay of $*\text{Ru}(\text{bpy})_3^{2+}$ from its triplet state to its ground singlet state can activate another molecule **A** from its ground singlet state S_0 to its lowest-energy triplet state T_1 .¹²¹

Just only a handful of organic transformations have been achieved to employ the triplet-triplet energy transfer from visible light photocatalysts. In an early example using this pathway, the substituted norbornadiene is converted to quadricyclene (Scheme 3-2).¹²²



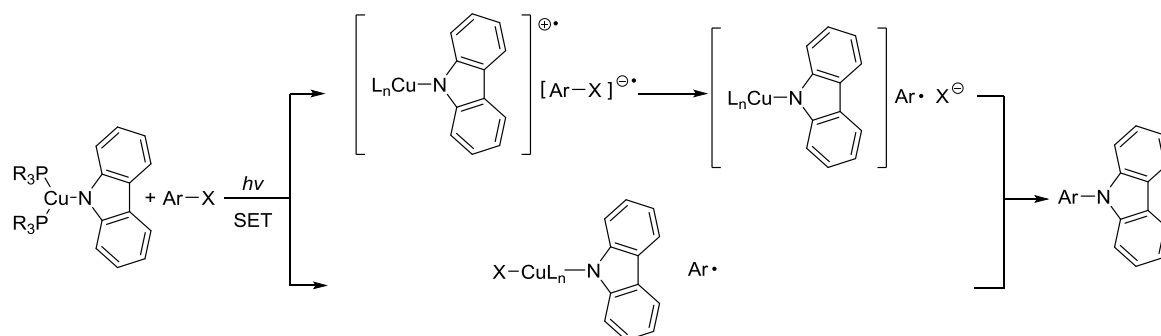
Scheme 3-2. Formation of quadricyclene.

¹²¹ Prier, C. K.; Rankic, D. A.; MacMillan, D. W. C. *Chem. Rev.* **2013**, *113*, 5322.

¹²² Ikezawa, H.; Kutal, C.; Yasufuku, K.; Yamazaki, H. *J. Am. Chem. Soc.* **1986**, *108*, 1589.

After the energy transfer from $*\text{Ru}(\text{bpy})_3^{2+}$ to the norbornadiene, the triplet state of norbornadiene undergoes bond rearrangement to give quadricyclene. As both the oxidation ($E_{1/2}^{+1/0} = +1.82 \text{ V vs SCE}$) and reduction potentials ($E_{1/2}^{0/-1} = -1.39 \text{ V vs SCE}$) of norbornadiene are higher than those of $*\text{Ru}(\text{bpy})_3^{2+}$, the electron-transfer pathways are not possible in this transformation.

In 2012, Fu and Peters¹²³ demonstrated that a radical pathway for photoinduced Ullmann C–N bond formation via a copper–carbazolide complex (Scheme 3-3). Usually, the classic Ullmann C–N coupling reaction was believed to undergo C–X cleavage via concerted oxidative addition to copper. Their mechanistic studies suggested that, under very mild conditions, photochemical initiation can lead to C–N bond formation with carbazole. Indeed, their findings open the door to the development of practical photoinduced, copper-catalyzed C–N bond-forming processes.



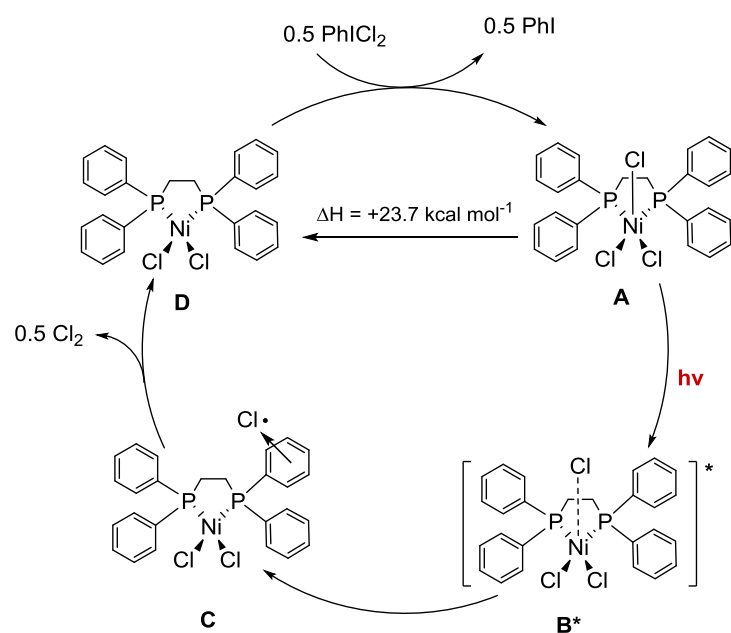
Scheme 3-3. Outline of a possible pathway for photoinduced Ullmann C–N bond formation via a copper–carbazolide complex.

In 2015, Nocera¹²⁴ achieved a halogen photoelimination from mononuclear Ni(III) complexes with visible light (Scheme 3-4).

Ni(III) trichloride complex $\text{NiCl}_3(\text{dppe})$ (**A**) (dppe = bis(diphenylphosphino)ethane) can be prepared by treating $\text{NiCl}_2(\text{dppe})$ (**D**) with 0.5 equiv of PhICl_2 . The photoreaction is substantially endothermic, which stores $23.7 \text{ kcal mol}^{-1}$. Photon absorption by $\text{NiCl}_3(\text{dppe})$ (**A**) provides access to $\text{NiCl}_3(\text{dppe})^*$ (**B***), which undergoes the photodissociation of chlorine atom. The resulting intermediate **C** leads to $\text{NiCl}_2(\text{dppe})$ (**D**) and Cl_2 through elimination chemistry.

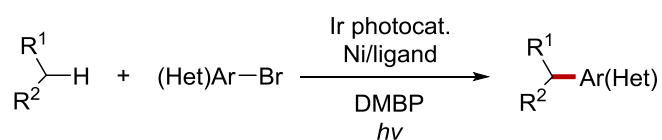
¹²³ For a seminal report with direct irradiation, see: Creutz, S. E.; Lotito, K. J.; Fu, G. C.; Peters, J. C. Photoinduced Ullmann C–N coupling: demonstrating the viability of a radical pathway. *Science* **2012**, 338, 647.

¹²⁴ Hwang, S. J.; Powers, D. C.; Maher, A. G.; Anderson, B. L.; Hadt, R. G.; Zheng, S.-L.; Chen, Y.-S.; Nocera, D. G. Trap-free halogen photoelimination from mononuclear Ni(III) complexes. *J. Am. Chem. Soc.* **2015**, 137, 6472.

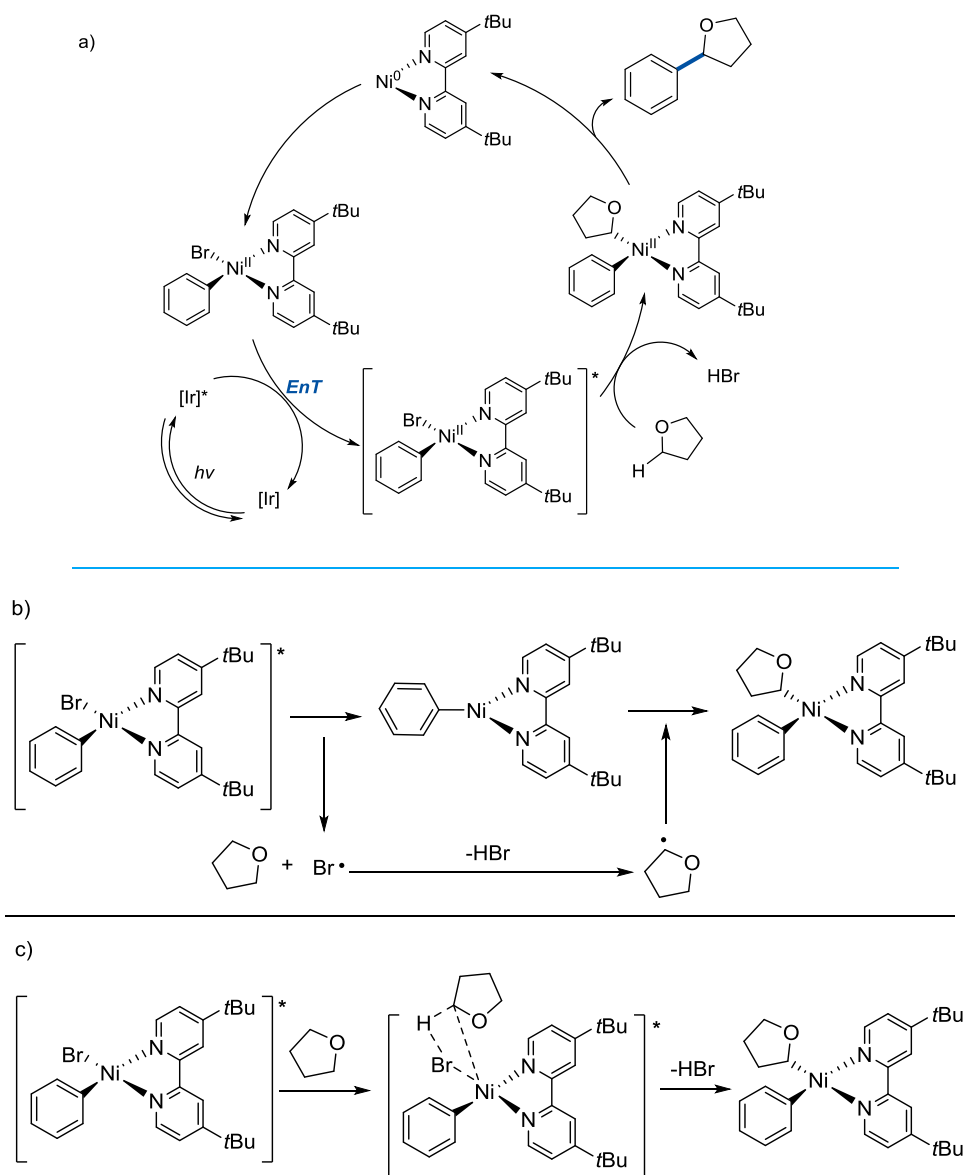


Scheme 3-4. Proposed photoreduction of complex **A**.

In 2017, Molander¹²⁵ reported a photochemical nickel-catalyzed coupling of (hetero)aryl bromides with activated α -heterosubstituted or benzylic $C(sp^3)$ -H bonds (Scheme 3-5). The mechanistic studies suggest that an energy-transfer pathway involved in which an excited-state nickel complex initiates C-H functionalization.



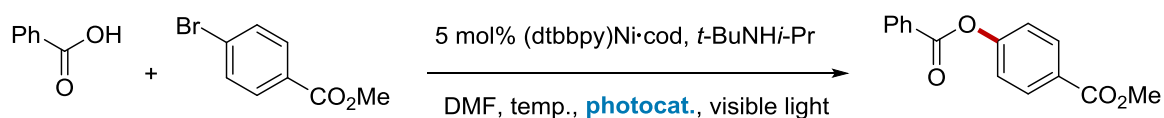
¹²⁵ Heitz, D. R.; Tellis, J. C.; Molander, G. A. *J. Am. Chem. Soc.*, **2016**, *138*, 12715.



Scheme 3-5. Ni-catalyzed C(sp³)-H arylation via energy transfer and H-atom abstraction, EnT = triplet-triplet energy transfer.

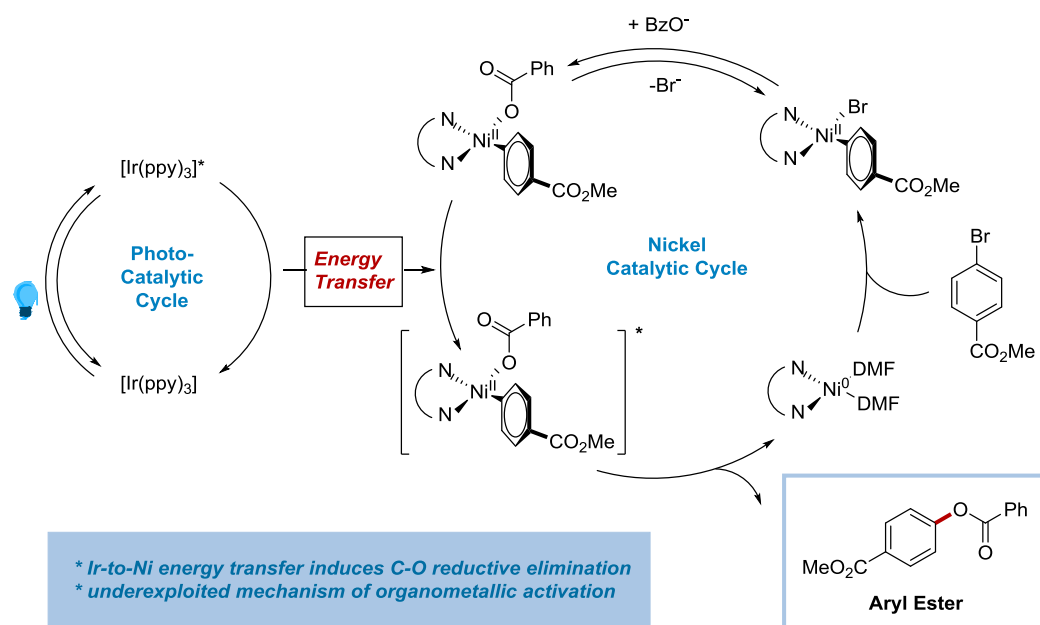
Mechanistic investigations suggest that an excited-state nickel complex undergoes a Ni–Br homolysis event (Scheme 3-5a, b). The resultant bromine radical can abstract weak C(sp³)-H bonds to generate reactive alkyl radicals that can be engaged in Ni-catalyzed arylation. Evidence suggests that the iridium photocatalyst facilitates nickel excitation and bromine radical generation via triplet–triplet energy transfer. When the excitation into a higher energy singlet excited state via UV irradiation, an alternative pathway is accessible, which undergoes intersystem crossing and relax nonradiatively to the same active excited state (Scheme 3-5a, c).

Recently, McCusker and MacMillan¹²⁶ reported a energy transfer-mediated organometallic catalysis through electronically excited nickel(II) by photosensitization to couple aryl halides with carboxylic acids. The proposed energy transfer-driven catalytic cycle is shown in Scheme 3-6.



Ir(ppy)₃ (1), 18 hr: **85% yield**
Ph₂C=O (2), 18 hr: **25% yield**
no photocat., 120 hr: **45% yield**

catalytically active excited state accessed by sensitization or by direct excitation



Scheme 3-6. Photosensitized nickel catalysis and proposed mechanism.

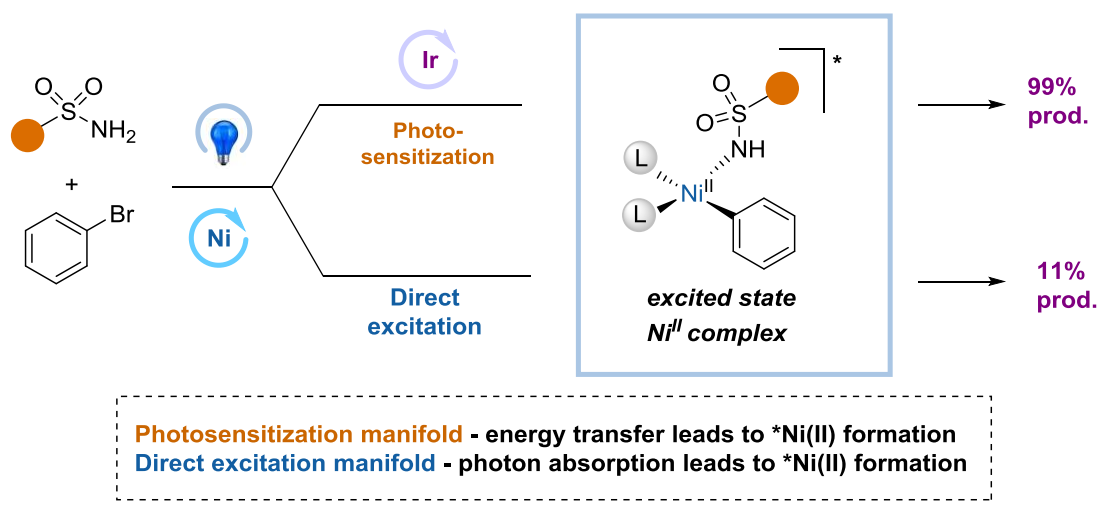
At beginning, oxidative addition of an aryl halide to dtbbpy·Ni(0) provides aryl–Ni(II) species. Coordination of a carboxylate nucleophile benzoate rapidly yields the aryl–Ni(II) carboxylate. Under the visible light irradiation, energy transfer from Ir(ppy)₃ to aryl–Ni(II) carboxylate to produce electronically excited Ni(II) species. The O-aryl ester product is formed from reductive elimination from excited Ni(II) species, and regenerating Ni(0) species.

¹²⁶ (a) Welin, E. R.; Le, C.; Arias-Rotondo, D. M.; McCusker, J. K.; MacMillan, D. W. C. Photosensitized energy transfer-mediated organometallic catalysis through electronically excited nickel(II). *Science* **2017**, 355, 380. (b) Kim, T.; McCarver, S. J.; Lee, C.; MacMillan, D. W. C. *Angew. Chem. Int. Ed.* **2018**, 57, 3488.

In 2018, MacMillan reported a photosensitized nickel catalytic sulfonamidation of aryl and heteroaryl halides. This method provides generic nickel-catalyzed access to a wide range of N-aryl and N-heteroaryl sulfonamide motifs, which are broadly represented in drug discovery. The control experiments revealed that the presence of both nickel and visible light were critical to product formation (Table 3-1). However, in the absence of photocatalyst, there was still 11% of product obtained through irradiation with blue LED light. It demonstrates that an energy-transfer mechanism may be operative in the presence of the photocatalyst.

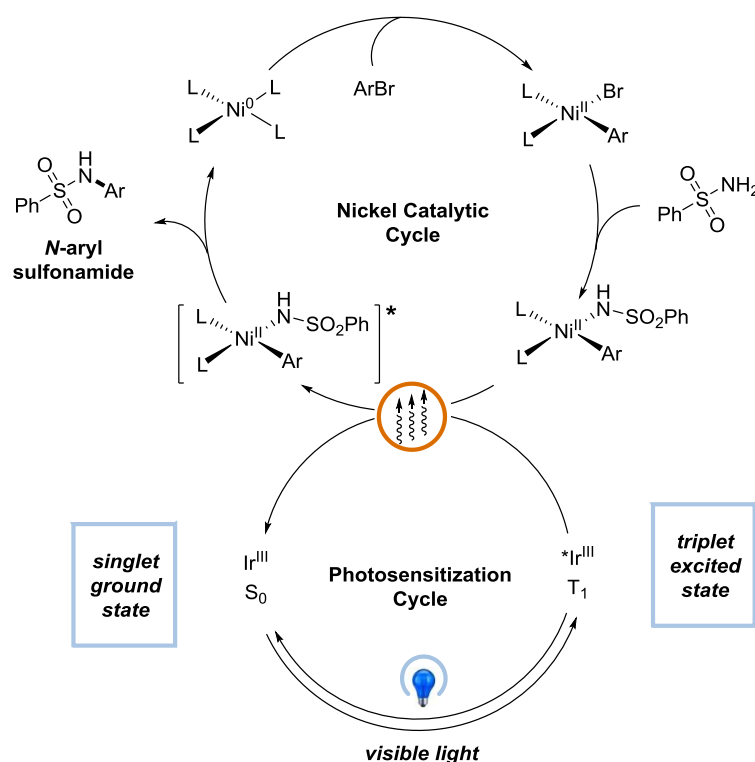
Table 3-1. C-N sulfonamidation control experiments.^[a]

Entry	Conditions	Yield [%] ^[b]
1	as shown	99
2	no light	0
3	no nickel	0
4	no photocatalyst	11
5	benzophenone (0.5%) as photocatalyst	18
6	no photocatalyst, no light	0



^[a] Performed with Ir(ppy)₂(bpy)PF₆ (0.05 mol%), Ni(cod)₂ (5 mol%), TMG (1.5 equiv), aryl halide (1.0 equiv), and benzenesulfonamide (1.5 equiv). ^[b] Yields were obtained by ¹H NMR analysis.

The proposed mechanism for this sulfonamidation method is outlined in Scheme 3-7. Firstly, oxidative addition of the Ni(0) complex to the electrophile aryl halide generates the Ni(II)-aryl complex. Ni(II)-aryl amido complex can be formed by ligand exchange with benzenesulfonamide and deprotonation. Meanwhile, under the visible light irradiation, the ground state of iridium(III) photocatalyst Ir(ppy)₂(bpy)PF₆ (ppy=2-phenylpyridine; bpy=bipyridine) produces the long-lived triplet photoexcited state *Ir(III) (t=0.3 ms).¹²⁷ Energy transfer from excited-state Ir system to the Ni(II)-aryl amido complex forms the excited nickel complex, followed by reductive elimination to deliver the N-aryl sulfonamide product and regenerate the Ni(0) catalyst.



Scheme 3-7. Photosensitized nickel catalytic sulfonamidation and proposed mechanism.

2 Project Aims and Introduction

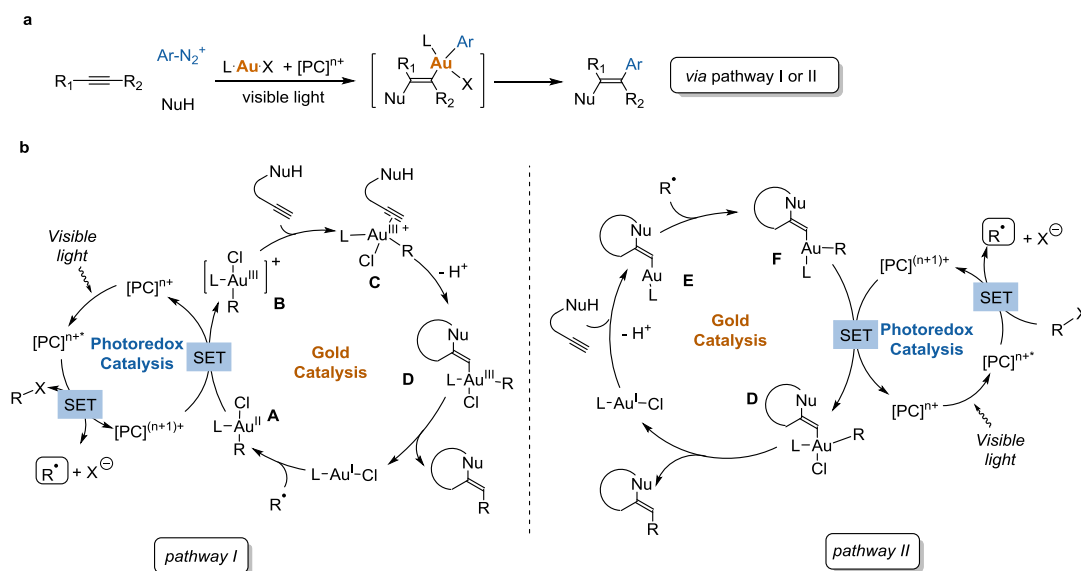
Following the principle of step economy¹²⁸ and also for higher levels of molecular complexity, some in situ post-functionalization reactions of organic gold intermediates,¹²⁹ such as electrophilic halogenation or cross-coupling reactions, have been designed. The cross-

¹²⁷ Ochola, J. R.; Wolf, M. O. *Org. Biomol. Chem.* **2016**, *14*, 9088.

¹²⁸ (a) Wender, P. A. *Tetrahedron* **2013**, *69*, 7529. (b) Newhouse, T.; Baran, P. S.; Hoffmann, R. W. *Chem. Soc. Rev.* **2009**, *38*, 3010.

¹²⁹ Liu, L.-P.; Hammond, G. *Chem. Soc. Rev.* **2012**, *41*, 3129.

coupling reactions have to undergo the addition of Au (I) to Au (III), which requires stoichiometric oxidants, transmetalation and reductive elimination cycle.¹³⁰ Glorius¹³¹ and Toste¹³² have made significant advances in this field by circumventing the burden of stoichiometric oxidants by combining gold catalysis with photocatalytic oxidation catalysis to ensure the oxidation states shuttle (Scheme 3-8a).¹³³



Scheme 3-8. Dual Au and photoredox catalytic difunctionalization of alkynes and mechanism manifolds in dual Au-photoredox catalysis.

Taking advantage of low reductive potential of aryl diazonium salts, arylation cyclization and related transformations as well as cross coupling processes involving aryl diazonium salts have been devised.¹³⁴ Two mechanisms have been proposed for these transformations

¹³⁰ (a) Zheng, Z.; Wang, Z.; Wang, Y.; Zhang, L. *Chem. Soc. Rev.* **2016**, *45*, 4448. (b) Hopkinson, M. N.; Tlahuext-Aca, A.; Glorius, F. *Acc. Chem. Res.* **2016**, *49*, 2261.

¹³¹ (a) Sahoo, B.; Hopkinson, M. N.; Glorius, F. *J. Am. Chem. Soc.* **2013**, *135*, 5505. (b) Hopkinson, M. N.; Sahoo, B.; Glorius, F. *Adv. Synth. Catal.* **2014**, *356*, 2794. (c) Tlahuext-Aca, A.; Hopkinson, M. N.; Sahoo, B.; Glorius, F. *Chem. Sci.* **2016**, *7*, 89.

¹³² (a) Shu, X.-z.; Zhang, M.; Frei, H.; Toste, F. D. *J. Am. Chem. Soc.* **2014**, *136*, 5844. (b) He, Y.; Wu, H.; Toste, F. D. *Chem. Sci.* **2015**, *7*, 1194. (c) Kim, S.; Rojas-Martin, J.; Toste, F. D. *Chem. Sci.* **2016**, *7*, 85.

¹³³ For reviews, see: (a) Levin, M. D.; Kim, S.; Toste, F. D. *ACS Cent. Sci.* **2016**, *2*, 293. (b) Skubi, K. L.; Blum, T. R.; Yoon, T. P. *Chem. Rev.* **2016**, *116*, 10035. (c) Toth, B. L.; Tischler, O.; Novak, Z. *Tetrahedron Lett.* **2016**, *57*, 4505. (d) Twilton, J.; Le, C.; Zhang, P.; R. W. Evans, D. W. C. MacMillan, *Nat. Rev. Chem.* **2017**, *1*, 0052. (e) Zhang, M.; Zhu, C.; Ye, L.-W. *Synthesis* **2017**, *49*, 1150.

¹³⁴ (a) Patil, D. V.; Yun, H.; Shin, S. *Adv. Synth. Catal.* **2015**, *357*, 2622. (b) Um, J.; Yun, H.; Shin, S. *Org. Lett.* **2016**, *18*, 484. (c) Huang, L.; Rudolph, M.; Rominger, F.; Hashmi, A. S. K. *Angew. Chem. Int. Ed.* **2016**, *55*, 4808. (d) Tlahuext-Aca, A.; Hopkinson, M. N.; Garza-Sanchez, R. A.; Glorius, F. *Chem. Eur. J.* **2016**, *22*, 5909. (e) Alcaide, B.; Almendros, P.; Busto, E.; Luna, A. *Adv. Synth. Catal.* **2016**, *358*, 1526. (f) Cornilleau, T.;

(Scheme 3-8b). In pathway I, a free radical derived from a photoredox cycle is added to the gold (I) precatalyst to give a transient gold (II) complex **A**, the gold (II) complex **A** can be further oxidized by a photoredox cycle to give a gold (III) salt **B**. The latter will coordinate the unsaturation of the precursor and the nucleophilic addition or cyclization of the resulting complex **C** to give an alkyl or vinyl gold (I) intermediate **D**. Reduction elimination to give the final product and regenerates the gold (I) complexes. Alternatively, pathway II involves a radical addition onto the alkyl or vinyl gold (I) intermediate **E** before than the gold(I) complexes. The key gold(III) intermediate **D** is reached after the oxidation of the transitory gold (II) complex **F**. Recent stoichiometric reactions and calculations favor the pathway I.¹³⁵

Utilizing these transformations to other partners has appeared to be highly desirable, it prompts us to develop some new alkynylation cyclization processes that correspond to the formal Csp^2 - Csp cross-coupling reaction, as there are few precedents in this type of dual catalytic conversion.¹³⁶ Therefore, in our previous studies on dual photoredox/gold catalyzed arylation cyclization of *o*-alkynylphenols which leads to benzofurans,¹³⁷ we replace aryl diazoniums by alkynyl iodide partners will form the basis for proper exploration and provide valuable scaffolds. We also realized that the reactivity of alkynyl iodide is much lower than that of aryl diazonium, and we may have to design a new gold(I) complex activation mode to facilitate the C-C bond formation step. In fact, gold (I) complexes are well known for their reluctance to oxidize. Only use special electrophiles and / or conditions to make it feasible. For example, Toste indicates that CF_3I is added to the arylgold(I) complex under UV irradiation.¹³⁸ Cyclometallated Au(III) intermediates can be generated by oxidative addition of substrates bearing a directing group. Recently, cross couplings reactions through an Au(I)/Au(III) catalytic cycle have been shown to be promoted by bidentate ligands on gold (I) with specific characteristics.¹³⁹

Hermange, P.; Fouquet, E. *Chem. Commun.* **2016**, 52, 10040. (g) Gauchot, V.; Lee, A.-L. *Chem. Commun.* **2016**, 52, 10163. (h) Gauchot, V.; Sutherland, D. R.; Lee, A.-L. *Chem. Sci.* **2017**, 8, 2885.

¹³⁵ (a) Tlahuext-Aca, A.; Hopkinson, M. N.; Daniliuc, C. G.; Glorius, F. Oxidative addition to gold(I) by photoredox catalysis: straightforward access to diverse (*C,N*)-cyclometalated gold(III) complexes. *Chem. Eur. J.* **2016**, 22, 11587. (b) Zhang, Q.; Zhang, Z.-Q.; Fu, Y.; Yu, H.-Z. Mechanism of the visible light-mediated gold-catalyzed oxyarylation reaction of alkenes. *ACS Catal.* **2016**, 6, 798.

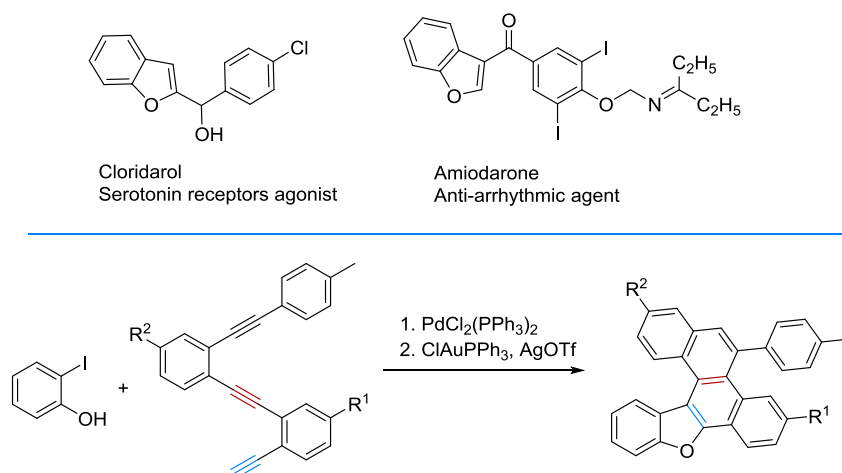
¹³⁶ For a dual catalysis example on a different system (aryldiazonium-TMS-alkyne), see: Kim, S., Rojas-Martin, J. & Toste, F. D. Visible light-mediated gold-catalysed carbon(sp^2)-carbon(sp) coupling. *Chem. Sci.* **2016**, 7, 85.

¹³⁷ Xia, Z.; Khaled, O.; Mouriès-Mansuy, V.; Ollivier, C.; Fensterbank, L. *J. Org. Chem.* **2016**, 81, 7182.

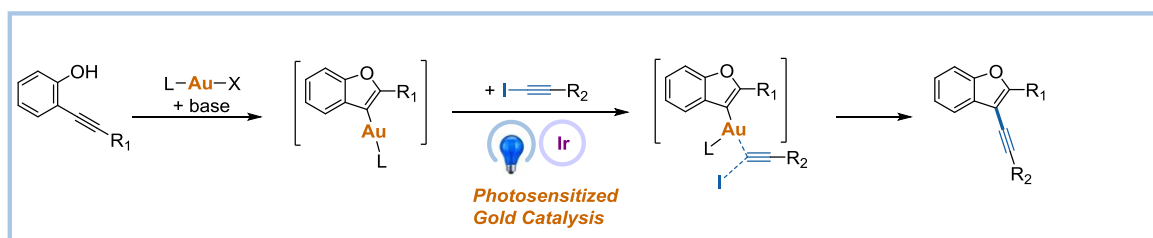
¹³⁸ Winston, M. S.; Wolf, W. J.; Toste, F. D. *J. Am. Chem. Soc.* **2015**, 137, 7921.

¹³⁹ Zeineddine, A.; Estévez, L.; Mallet-Ladeira, S.; Miqueu, K.; Amgoune, A.; Bourissou, D. *Nat. Comm.*, **2017**, 8, 565.

Benzofuran derivatives are important heterocyclic compounds, some of them possess biological activities, for example, the cloridarol is a serotonin receptors agonist, the amiodarone is an anti-arrhythmic agent. In 2012, Alabugin reported a gold catalyzed selective “all-endo” cascade, and get benzofuran-fused chrysenes derivatives.¹⁴⁰



In this work, we developed a new C-C bond formation pattern at a gold(I) complex by photo-induced energy transfer to promote oxidative addition, it's a new reactions for the synthesis of benzofuran derivatives.



Scheme 3-9. This work: dual Au and photoinduced alkylnylative O-cyclization via photosensitized oxidative addition.

3 Results and Discussion

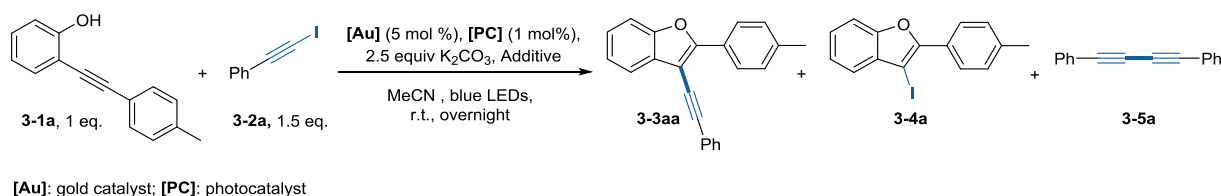
3.1 Optimization Studies

We initiated our work by examining the model reaction between 2-(phenylethynyl)phenol **3-1a** and (iodoethynyl)benzene **3-2a** under various conditions. Following the previous arylation protocol which relies on using a catalytic mixture of Ru(bpy)₃²⁺ and PPh₃AuCl in

¹⁴⁰ Byers, P. M.; Rashid, J. I.; Mohamed, R. K.; Alabugin, I. V. *Org. Lett.*, **2012**, *14*, 6032.

MeOH leads to negative results. Fortunately, when replace the solvent with acetonitrile, and add a base into it, the benzofuran **3-3aa** could be obtained as 15% (Table 1, entry 1). By using Ir[dF(CF₃)ppy]₂(dtbbpy)PF₆ (**[Ir-F]**) as photocatalyst, the yield of **3-3aa** was increased to 26% (entry 3). By switching PPh₃AuCl to (*p*-CF₃Ph)₃PAuCl [**Au-CF₃**], a substantial gain of yield was observed (56% of **3-3aa**). Finally, after substantial optimization, the best result since a 71% isolated yield of **3-3aa** was obtained when combine [**Au-CF₃**] (5 mol %), (**[Ir-F]**) (1 mol%), 1,10-phenanthroline (10 mol%), K₂CO₃ (2.5 equiv) in degassed MeCN at r.t. overnight under blue LEDs light (entry 5). Interestingly, the reaction can work without a photocatalyst (entry 8) and it is not beneficial to use a more reducing photocatalyst such as fac-Ir(ppy)₃ (entry 2). A control experiment on the action of 1,10-phenanthroline was also carried out. A stoichiometric amount of 1,10-phenanthroline proved to be detrimental to the yield (entry 6), but other amines such as the quinuclidine ring (entry 7) or TMEDA, DABCO, DBU (see SI-III4) can also be used to improve the reaction. In sharp contrast, in the absence of a base (K₂CO₃, item 11), a gold catalyst (*p*-CF₃Ph)₃PAuCl (entry 10) or light (entry 12), the desired product could not be obtained. Finally, it is worth noting that under almost all conditions, 3-iodo-2-phenylbenzofuran **3-4a** and diyne **3-5a** are by-products. Further, when (bromoethynyl)benzene **3-2a-Br** was reacted, only 9% of **3-3aa** was obtained.

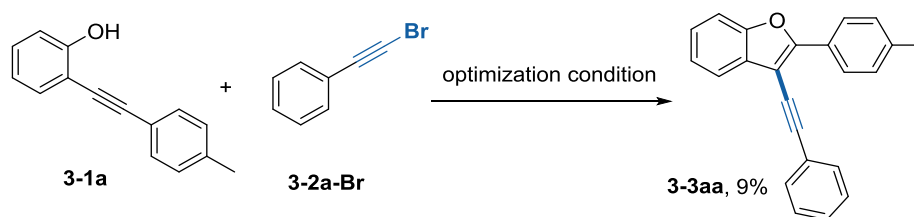
Table 3-2. Defining the key parameters of the alkynative cyclization^a



Entry	[Au]	[PC]	Additive, 10 mol%	3-3aa yield (%) ^c	3-4a yield (%)
1 ^b	PPh ₃ AuCl	Ru(bpy) ₃ (PF ₆) ₂	-	15	21
2 ^b	PPh ₃ AuCl	fac-Ir(ppy) ₃	-	8	22
3 ^b	PPh ₃ AuCl	[Ir-F]	-	26	33
4	[Au-CF₃]	[Ir-F]	-	56	22
5	[Au-CF₃]	[Ir-F]	phen.	72 (71)	15
6	[Au-CF₃]	[Ir-F]	phen. (1 equiv)	25	25
7	[Au-CF₃]	[Ir-F]	quinuclidine	65	19
8	[Au-CF₃]	-	phen.	26	29
9	[Au-CF₃]	-	-	11	29

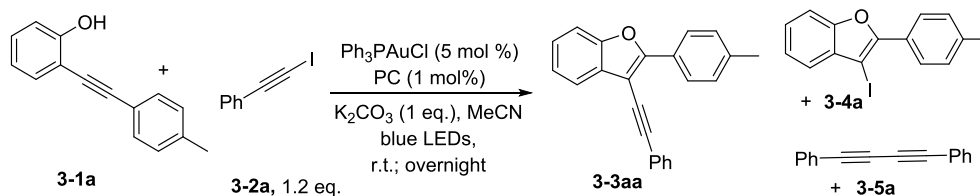
10	-	[Ir-F]	phen.	-	8
11 ^d	[Au-CF₃]	[Ir-F]	phen.	-	27
12 ^e	[Au-CF₃]	[Ir-F]	phen.	-	16

^a **[Au-CF₃]** = (*p*-CF₃Ph)₃PAuCl; **[Ir-F]** = Ir[dF(CF₃)ppy]₂(dtbbpy)PF₆; phen. = 1,10-phenanthroline. ^b Only 1 equiv of K₂CO₃ was used. ^c Yields are determined by ¹H NMR using 1,3,5-trimethoxybenzene as internal standard, yield in parentheses is isolated yield. ^d No K₂CO₃. ^e No light.



The detail optimization studies will be discussed below.

3.3.1 Screening of Photocatalysts



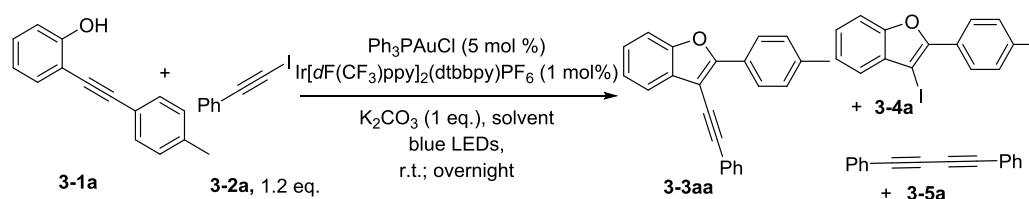
Entry	PC (1 mol%)	E* _{1/2} (V vs SCE)	Yield of 3-3aa
1	Ir[dF(CF₃)ppy]₂(dtbbpy)PF₆	-0.89	26%
2	Ru(bpy) ₃ (PF ₆) ₂	-0.81	15%
3	[Au ₂ (<i>u</i> -dppm) ₂](OTf) ₂	-1.6	6%
4	<i>fac</i> -Ir(ppy) ₃	-1.73	8%

Reaction conditions: **3-1a** (0.1 mmol, 0.05 M), **3-2a** (1.2 equiv), Ph₃PAuCl catalyst (5 mol %), photocatalyst (1 mol %), K₂CO₃ (1 equiv), degassed MeCN (2 mL), r.t., overnight, blue LEDs light. Yields are determined by ¹H NMR using 1,3,5-trimethoxybenzene as an internal standard.

Firstly, we screened photocatalysts, like Ir[dF(CF₃)ppy]₂(dtbbpy)PF₆ (**[Ir-F]**), Ru complex, [Au₂(*u*-dppm)₂](OTf)₂, and *fac*-Ir(ppy)₃ {Tris[2-phenylpyridinato-C2,N]iridium(III)}, it showed that the **[Ir-F]** complex can get the best yield. But if we consider the reductive potential of these three photocatalysts, we can't find the connection between the reductive

potentials and yields. Also, the reductive potential of iodoethynylbenzene ($E_{1/2}(\mathbf{2a}) = -1.39$ V vs SCE, MeCN as solvent) is significantly higher than **[Ir-F]** catalyst ($E^*_{1/2} = -0.89$ V vs SCE, MeCN as solvent), a photoreductive formation of an alkynyl radical appeared quite unlikely.

3.3.2 Screening of Solvents

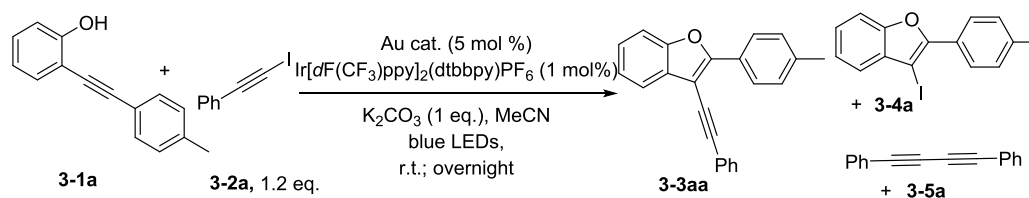


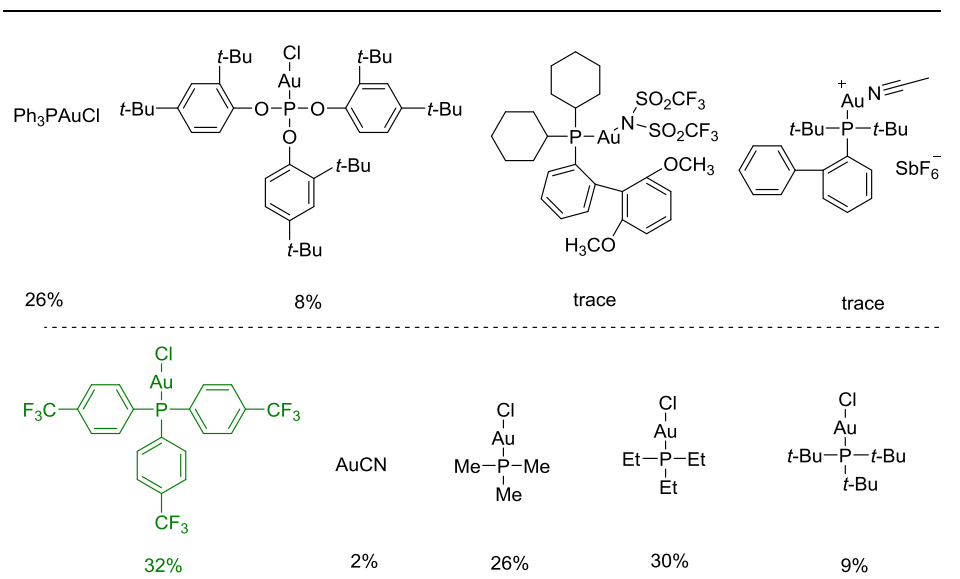
Entry	Solvent (2 mL)	Yield of 3-3aa
1	MeCN	26%
2	MeOH	<1%
3	DCM	5%
4	PhCF ₃	3%

Reaction conditions: **3-1a** (0.1 mmol, 0.05 M), **3-2a** (1.2 equiv), Ph₃PAuCl catalyst (5 mol %), Ir[dF(CF₃)ppy]₂(dtbbpy)PF₆ (1 mol%), K₂CO₃ (1 equiv), degassed solvent (2 mL), r.t., overnight, blue LEDs light. Yields are determined by ¹H NMR using 1,3,5-trimethoxybenzene as an internal standard.

The solvent MeOH used in previous arylation protocol did not prove to be suitable for this reaction, the optimal solvent is MeCN.

3.3.3 Screening of Au Catalysts

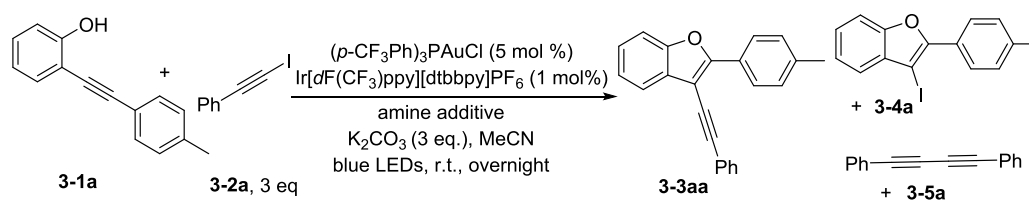


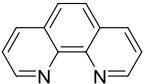
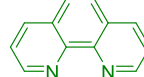
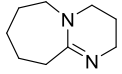
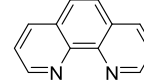
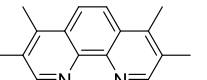
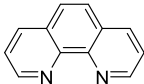
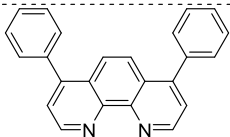
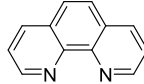
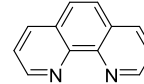


Reaction conditions: **3-1a** (0.1 mmol, 0.05 M), **3-2a** (1.2 equiv), [Au] catalyst (5 mol %), Ir[dF(CF₃)ppy]₂(dtbbpy)PF₆ (1 mol%), K₂CO₃ (1 equiv), degassed MeCN (2 mL), r.t., overnight, blue LEDs light. Yields are determined by ¹H NMR using 1,3,5-trimethoxybenzene as an internal standard.

The electronic property and bulk of the ligands can affect the efficiency of the gold catalyst. After screened various gold complexes, it showed that the (*p*-CF₃Ph)₃PAuCl got the best yield.

3.3.4 Screening of Amines

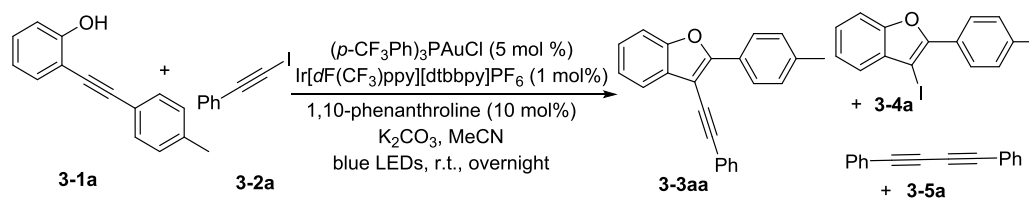


entry	amines (mol%)	yield of 3-3aa (%)	entry	amines (mol%)	yield of 3-3aa (%)
1	 (20)	25	7	 (5)	59
2	 (20)	39	8	 (10)	66
3	 (DBU, 20)	60	9	 (20)	63
4	 (20)	50	10	 (40)	62
5	 (20)	52	11	 (60)	56
6	 (DABCO, 20)	41	12	 (100)	52

Reaction conditions: **3-1a** (0.1 mmol, 0.05 M), **3-2a** (3 equiv), (*p*-CF₃Ph)₃PAuCl (5 mol %), Ir[dF(CF₃)ppy]₂(dtbbpy)PF₆ (1 mol%), K₂CO₃ (3 equiv), degassed MeCN (2 mL), r.t., overnight, blue LEDs light. Yields are determined by ¹H NMR using 1,3,5-trimethoxybenzene as an internal standard.

Then some diamines were added into this system. Fortunately, they worked. The addition of 1,10-phenanthroline allowed a significant yield increase. The reason for this is not clearly established and several hypotheses are standing. For instance, some halogen bonding between phenanthroline and the alkynyl iodides **2**, or these amines used as weak organic bases. More detail about it will be discussed in the mechanism part.

3.3.5 Screening of Reagents Ratio



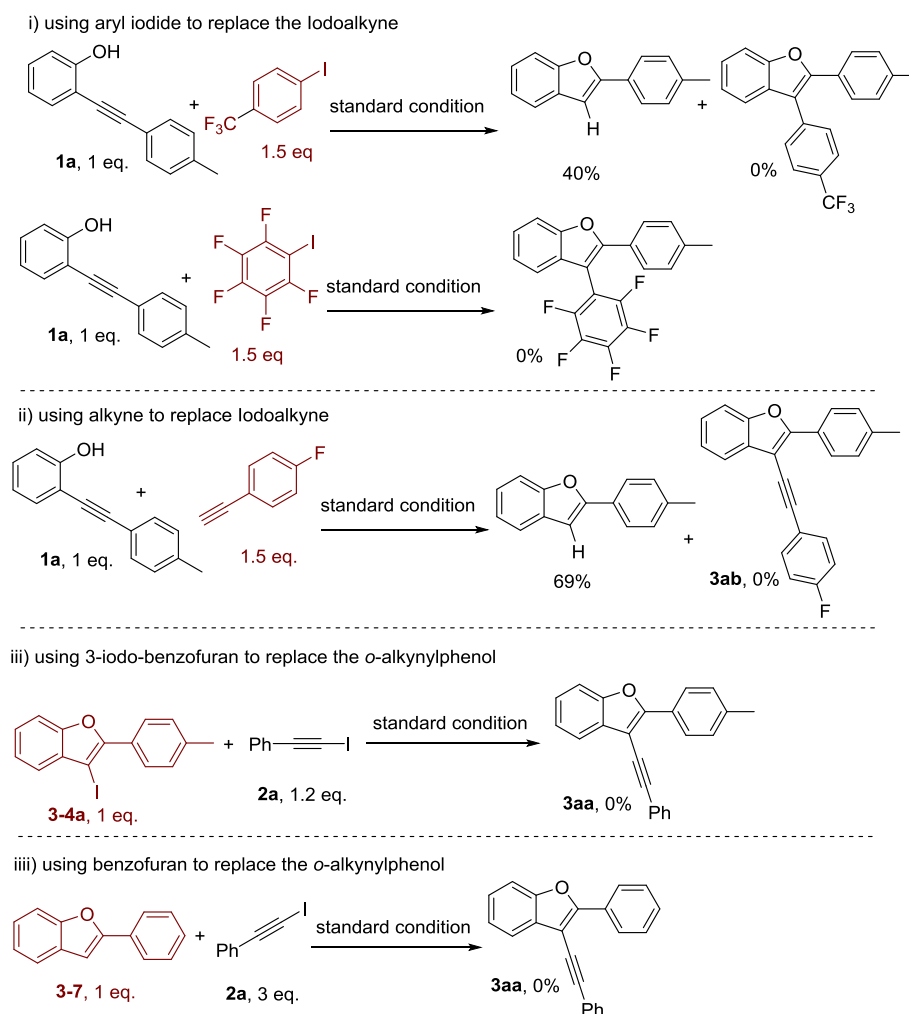
entry	Ph—C≡C—I 3-2a (eq.)	K ₂ CO ₃ (eq.)	yield of 3-3aa (%)
1	1.2	2	55
2	1.5	2	59
3	1.5	2.5	72
4	2	3	72
5	3	4	68
6	4	5	32

Reaction conditions: **3-1a** (0.1 mmol, 0.05 M), **3-2a** (equiv), (*p*-CF₃Ph)₃PAuCl (5 mol %), Ir[dF(CF₃)ppy]₂(dtbbpy)PF₆ (1 mol%), K₂CO₃ (equiv), degassed MeCN (2 mL), r.t., overnight, blue LEDs light. Yields are determined by ¹H NMR using 1,3,5-trimethoxybenzene as an internal standard.

Then the ratio of iodoethynyl benzene and K₂CO₃ was screened. When the number of equivalents of **2a** and K₂CO₃ decreased to 1.5 and 2.5, separately, the optimal reaction condition was obtained.

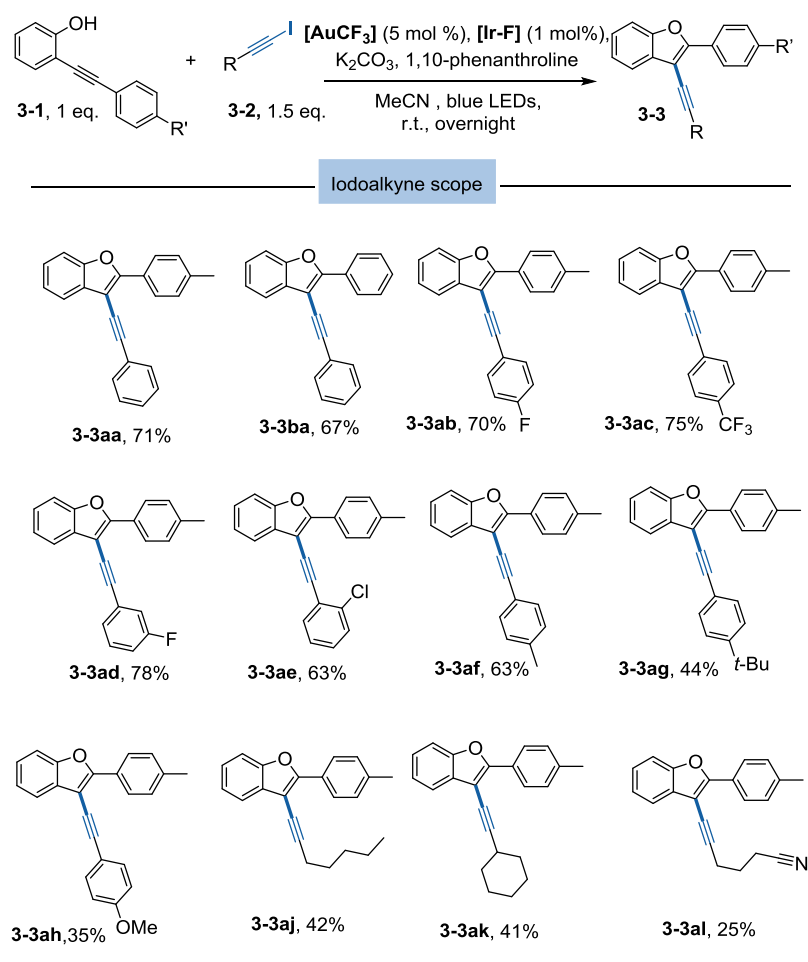
3.3.6 Starting Material Replacement Experiments

Several starting material replacement experiments were run to check the mechanism and explain the formation of the side products, but the cross coupling product was not detected in any of them. The unique property of iodoalkynes is necessary of this dual Au and photoinduced cyclization, aryl iodides and arylacetylenes are not suitable for this reaction. The side products **3-4a** and **3-7** can not participate in further reaction to generate the cross coupling compound **3-3**.



3.2 Scopes and Limitations

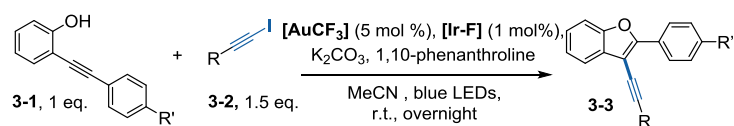
We then explored the scope of this transformation. A series of substituted aryl iodoalkynes **3-2** were reacted with 2-(phenylethynyl)phenols **3-1** under the optimized reaction conditions (Table 2). Aryl iodoethynyl bearing electron-withdrawing groups in the *para* position, such as F and CF_3 afforded corresponding benzofurans **3-3ab** and **3-3ac** in good yields. *Meta* F or *ortho* Cl substituted aryl iodoalkynes reacted smoothly with 2-(phenylethynyl)phenol **3-1a**, providing **3-3ad** and **3-3ae** in 78% and 63% yields, respectively. The presence of electron donating groups (-Me, -*t*-Bu, -OMe) or no substitution furnished the alkynylbenzofurans in slightly lower (**3-3af**, **3-3ag** and **3-3ba**) to moderate (**3-3ah**) yields. No reaction was observed with an iodoalkyne bearing a 4-nitro arylgroup. Instead, the protodeauration cyclization product **3-9** was obtained. In addition, alkylalkynes bearing *n*-pentyl, cyclohexyl, and 3-nitrile butyl groups could be incorporated into the benzofurans scaffold (**3-3aj-3al**) from the corresponding alkyl iodoalkynes, albeit in significantly lower yields (25–42 % yield).

Table 3-3. Scope of Iodoalkyne Substrates^a

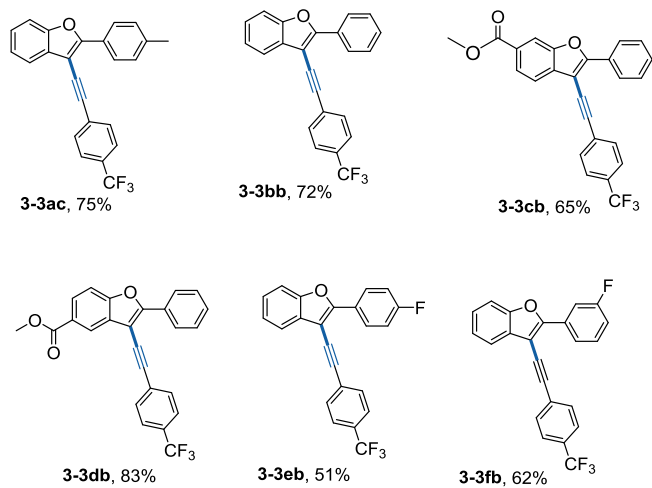
^a 5 mol % $[\text{AuCF}_3]$ = (*p*-CF₃Ph)₃PAuCl, 1 mol% $[\text{Ir-F}]$ = Ir[dF(CF₃)ppy]₂(dtbbpy)PF₆, K₂CO₃ (2.5 eq.), 1,10-phenanthroline (10 mol%) MeCN, blue LEDs, r.t.; overnight.

The effect of substitution on both aromatic rings of *o*-alkynylphenols **3-1** was then investigated in reactions with 1-(iodoethynyl)-4-(trifluoromethyl)benzene **3-2c** (Table 3). Arylalkynes with no substitution or bearing a CH₃, F group at the *para* or *meta* position to the alkyne gave good yields of benzofurans (**3-3bb**, **3-3ac**, **3-3eb** and **3-3fb**). Similarly, precursors with an electron-withdrawing ester group on the phenol moiety at the *para* or *meta* position of the alkyne, delivered the corresponding ethynylbenzofurans in good yields (**3-3cb** and **3-3db**, Table 3).

Table 3-4. Scope of *o*-Alkynylphenol Compounds^a

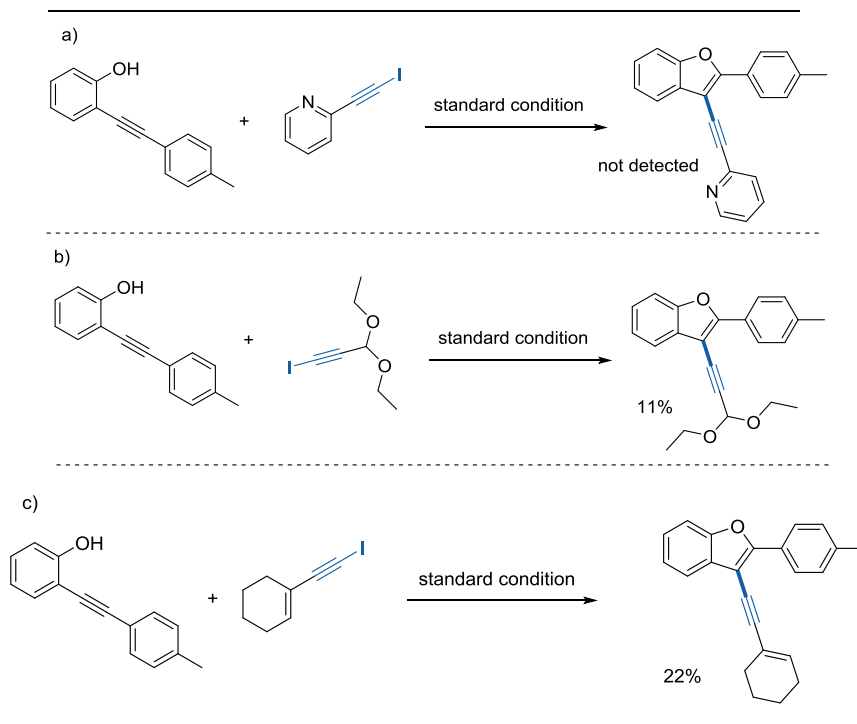


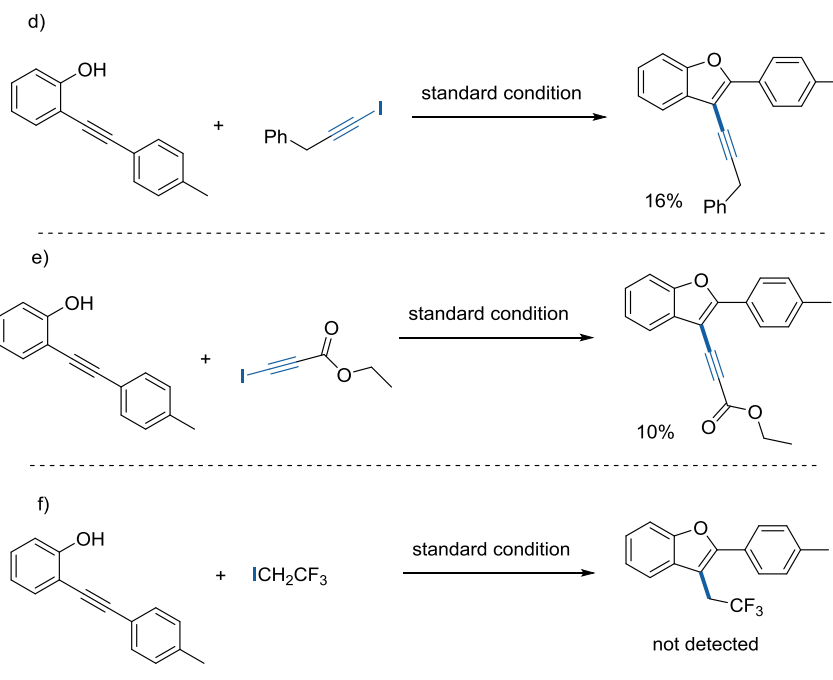
o-Alkynylphenol scope



^a 5 mol % $[\text{AuCF}_3] = (p\text{-CF}_3\text{Ph})_3\text{PAuCl}$, 1 mol% $[\text{Ir-F}] = \text{Ir}[d\text{F}(\text{CF}_3)\text{ppy}]_2(\text{dtbbpy})\text{PF}_6$, K_2CO_3 (2.5 eq.), 1,10-phenanthroline (10 mol%) MeCN, blue LEDs, r.t.; overnight.

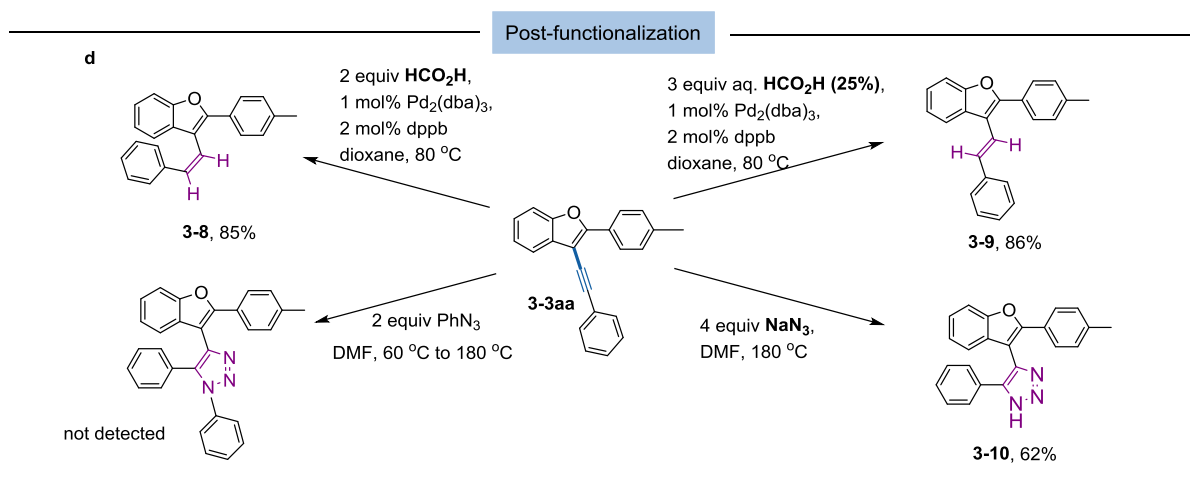
Except previous examples, some other iodoalkyne derivatives were performed in standard reaction conditions. Due to their structures, some of them got very low yields (with side product benzofuran), and others did not work at all.





3.3 Post-functionalization

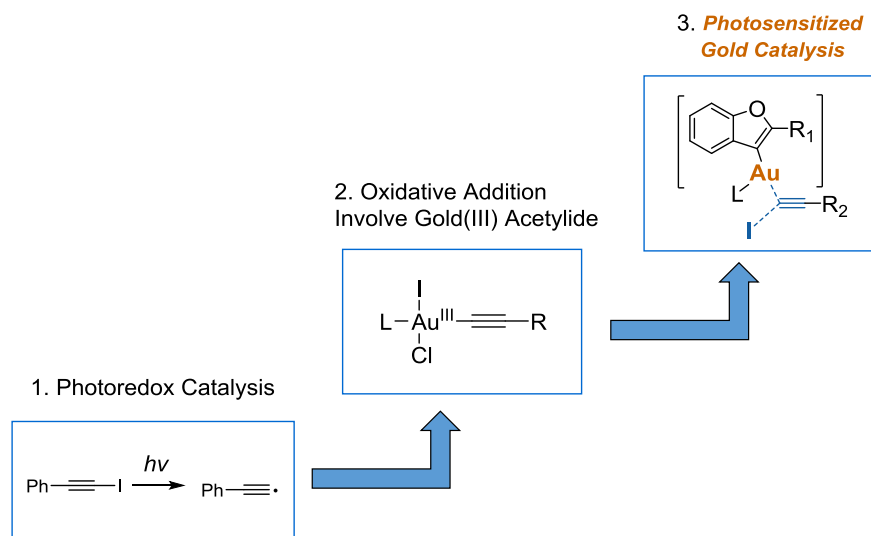
The benzofurans **3-3** are valuable scaffolds for further elaboration notably through the potential reactivity of the alkyne moiety. For instance, the product **3-3aa** can be hydrogenated by formic acid under palladium(0) catalysis.¹⁴¹ Depending on the reaction conditions *Z*-alkene **3-8** or the *E*-isomer **3-9** can be selectively obtained. Triazole **3-10** could also be formed in thermal conditions through a Huisgen type of reaction between **3-3aa** and sodium azide.



Scheme 3-10. Post-functionalization of benzofurans **3-3**.

¹⁴¹ Shen, R.; Chen, T.; Zhao, Y.; Qiu, R.; Zhou, Y.; Yin, S.; Wang, X.; Goto, M.; Han, L.-B. *J. Am. Chem. Soc.* **2011**, *133*, 17037.

4 Mechanism Investigation



Scheme 3-11. Three mechanism pathways.

The mechanism studies include three parts: photoredox catalysis, oxidative addition involve gold(III) acetylide and photosensitized gold catalysis (Scheme 3-11). These three pathways will be discussed in the following.

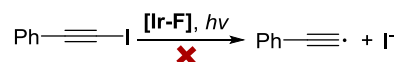
4.1 Photoredox Catalysis

This preliminary set of findings drove us to delineate a plausible mechanism for further optimization of the reaction. We first considered the addition of a radical intermediate stemming from the photocatalytic cycle to produce the corresponding intermediate of type **B** through **A** (Scheme 3-8b, pathway I).

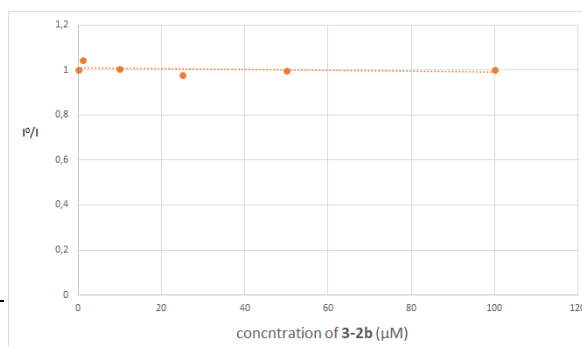
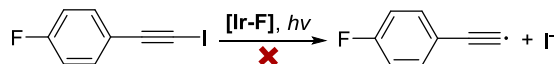
4.1.1 Investigation of Halogen Bonding

Alkynyl radicals indeed remain elusive species but they have been mentioned sporadically in the literature to be generated from alkynyl iodides.¹⁷ Nevertheless, by using alkynyl iodide **3-2b** as a probe because it bears a fluorine label, this hypothesis was rapidly discarded. First, as the reductive potential of 1-fluoro-4-(iodoethynyl)benzene ($E_{1/2}(\mathbf{3-2b}) = -1.47$ V vs SCE) is significantly higher than **[Ir-F]** catalyst ($E^*_{1/2} = -0.89$ V vs SCE), photoreductive formation of an alkynyl radical appeared quite unlikely (Scheme 3-9). This was corroborated by fluorescence quenching studies which showed no quench of excited **[Ir-F]**, noted **[Ir-F]***, by **3-2b** therefore precluding a direct photocatalyzed electron transfer event (Scheme 3-12).

$E^*_{\text{red}}(\mathbf{3-2a}) = -1.39 \text{ V vs SCE}$

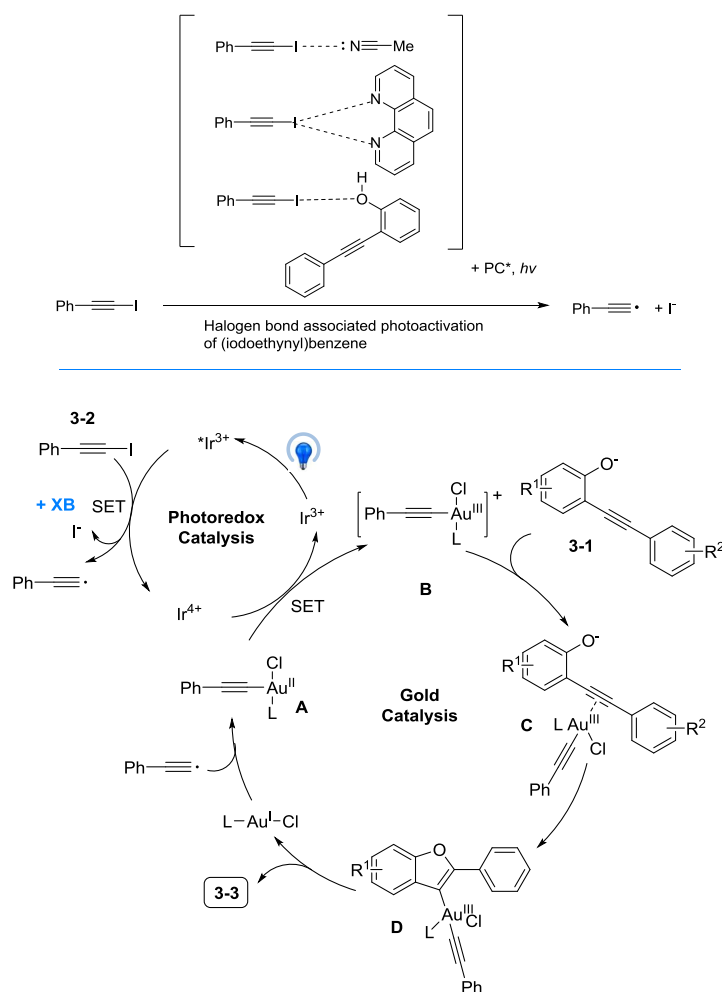


$E^*_{\text{red}}(\mathbf{3-2b}) = -1.47 \text{ V vs SCE}$

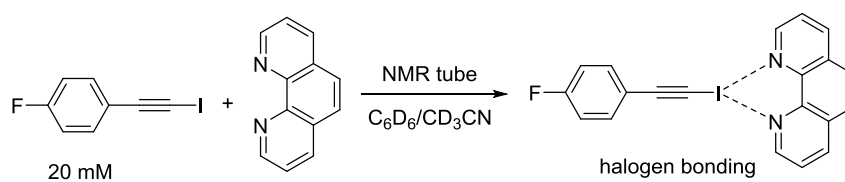


Scheme 3-12. Reductive potential and fluorescence quenching studies of **3-2b**.

Based on the comparison of the redox potentials, the Ir photocatalyst cannot reduce iodoalkyne **3-2**. However we wondered if halogen bonding between iodoalkyne **3-2** and phen or *o*-alkynylphenol in MeCN could take place and render possible the formation of alkynyl radical (Scheme 3-13). NMR titration experiment is the most often used techniques to study halogen bonding.

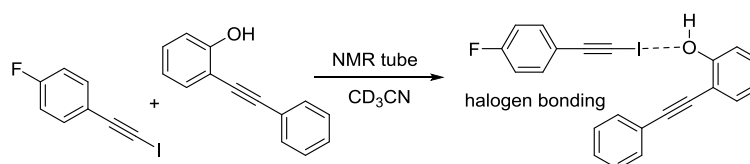


Scheme 3-13. Dual gold and halogen-bond-assisted photoredox catalysis.

Table 3-5. NMR titration experiments of iodoalkyne and phen in C₆D₆ and CD₃CN

Entry	<i>c</i> (Phen) (mM)	$\Delta\delta$ ¹⁹ F shift (ppm) in C ₆ D ₆	$\Delta\delta$ ¹⁹ F shift (ppm) in CD ₃ CN
1	0	0	0
2	10	0.02	0
3	20	0.03	0
4	50	0.15	0
5	100	0.32	0.01
6	150	0.35	0.04

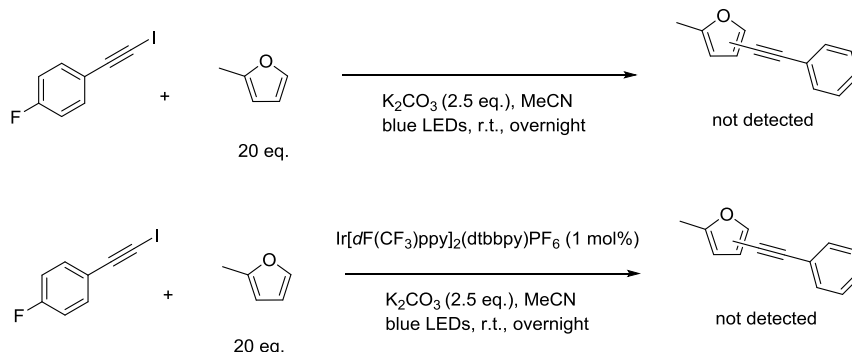
The NMR titration experiments in C₆D₆ and CD₃CN indicate that 1) halogen bonding probably exists between iodoalkyne and phen in C₆D₆, 2) and the solvent can affect the halogen bonding.

Table 3-6. NMR Titration experiments of iodoalkyne and *o*-alkynylphenol in CD₃CN.

Entry	<i>c</i> (phenol) (mM)	$\Delta\delta$ ¹⁹ F shift (ppm) in CD ₃ CN
1	0	0
2	20	0.01
3	40	0.01
4	100	0.01
5	200	0.02

As the $\Delta\delta$ ¹⁹F shift is very small, the NMR titration experiments in CD₃CN are difficult to prove the existence of halogen bonding between iodoalkyne **3-2** and *o*-alkynylphenol (Table 3-6).

In order to trap the possible alkynyl radical, we designed a cross coupling experiment between iodoalkyne and 2-methylfuran. However, the attempt of trapping alkyl radical did not succeed.



4.1.2 Investigated on the Role of 1,10-Phenanthroline

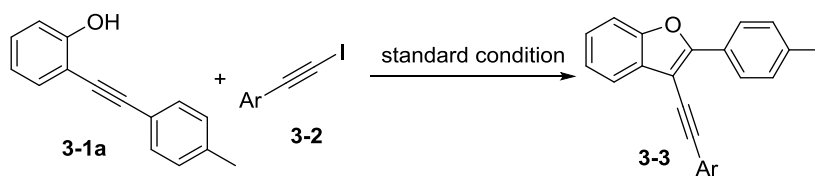
The adjunction of 1,10-phenanthroline allowed to observe a significant yield increase whatever the followed pathway. Compare for instance entry 4 vs 5 of Table 3-2 or entry 8 vs 9 of Table 3-2. The reason for this is not clearly established and several hypotheses are standing. Just like previous discussion, the halogen bonding between phenanthroline and the alkynyl iodides **3-2**, which are known halogen bonding donors,¹⁴² might be at play and explain the increased reactivity of the system. Except halogen bonding, several other hypotheses are investigated below.

a) Experiment with and without Phenanthroline

Two *Schlenk* tubes were labeled as **A** and **B**. Tube **A** followed the General Procedure 4 (GP4), tube **B** followed the General Procedure 4 (GP4), just without phen.

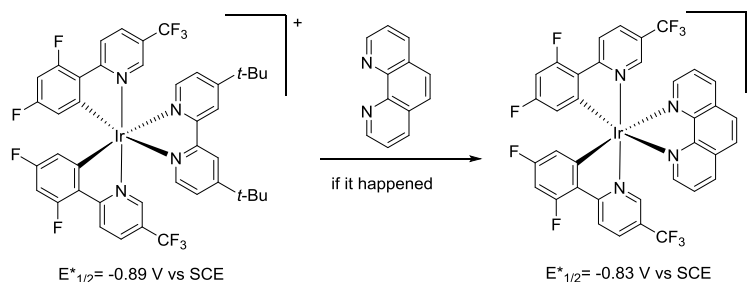
This series of experiments show a general positive effect of the presence of phenanthroline.

¹⁴² Dumele, O.; Wu, D.; Trapp, N.; Goroff, N.; Diederich, F. Halogen Bonding of (Iodoethynyl)benzene Derivatives in Solution. *Org. Lett.* **2014**, *16*, 4722.



entry	3-2	tube A tube B	yield of 3-3
1		with phen	72% (¹ H NMR)
		no phen	56% (¹ H NMR)
2		with phen	63% (¹ H NMR)
		no phen	61% (¹ H NMR)
3		with phen	65% (isolated)
		no phen	60% (isolated)
4		with phen	37% (¹ H NMR)
		no phen	25% (¹ H NMR)

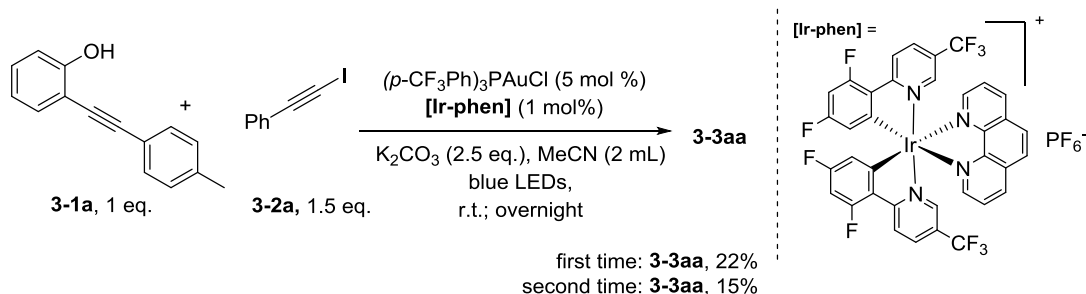
b) Does Phen Coordinate With Ir Catalyst?



Even if the ligand dtbbpy of **[Ir-F]** was replaced by phen, the reductive potential of resulting **[Ir-F]** ($E^*_{1/2} = -0.83 \text{ V vs SCE}$)¹⁴³ is lower than the original one ($E^*_{1/2} = -0.89 \text{ V vs SCE}$), both of them can not reduce iodoethynyl benzene ($E_{1/2}(\mathbf{3-2a}) = -1.39 \text{ V vs SCE}$) and bromoethynyl benzene ($E_{1/2}(\mathbf{3-2a-Br}) = -1.60 \text{ V vs SCE}$). Considering the reductive potential of iodoalkynes and photocatalyst **[Ir-F]**, photoreductive formation of the corresponding alkynyl radical appeared quite unlikely.

¹⁴³ Singh, A.; Teegardin, K.; Kelly, M.; Prasad, K. S.; Krishnan, S.; Weaver, J. D. *J. Organomet. Chem.* **2015**, 776, 51.

Moreover, the **[Ir-phen]** photocatalyst was synthesized according to the procedure reported by Weaver.¹⁴⁴ This **[Ir-phen]** photocatalyst did not prove very efficient, so the replacement of dtbbpy by phen does not appear as the explanation of the yield improvement.



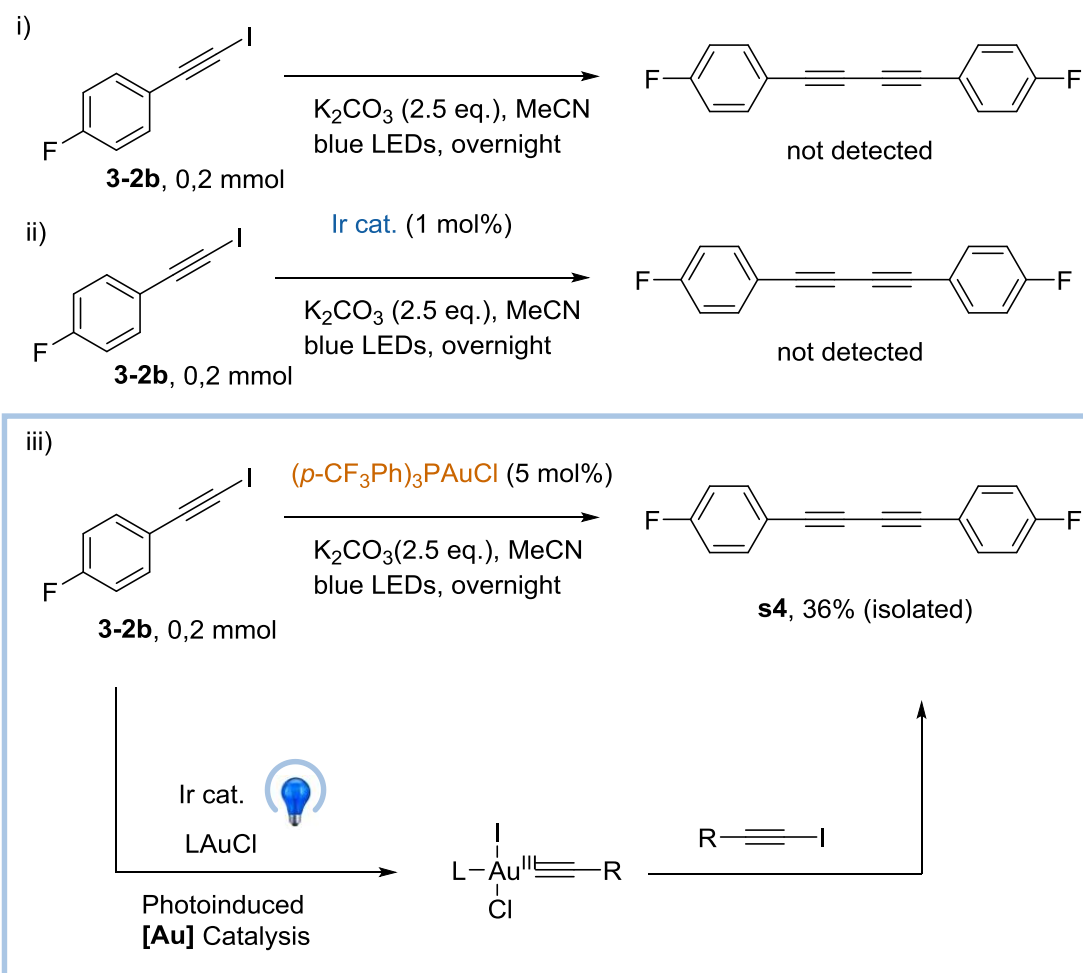
Conclusion of part 1: with our first hypothesis, it is difficult to prove the mechanism of the photoredox catalysis, it is also difficult to prove the existence of halogen bonding in our reaction.

4.2 Oxidative Addition Involve Gold(III) Acetylide

To support the plausible formation of gold(III) acetylide intermediate, several experiments are performed.

¹⁴⁴ Singh, A.; Teegardin, K.; Kelly, M.; Prasad, K. S.; Krishnan, S.; Weaver, J. D. *J. Organomet. Chem.* **2015**, 776, 51.

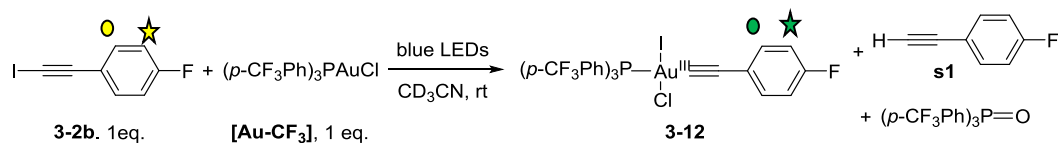
4.2.1 Formation of Dialkyne



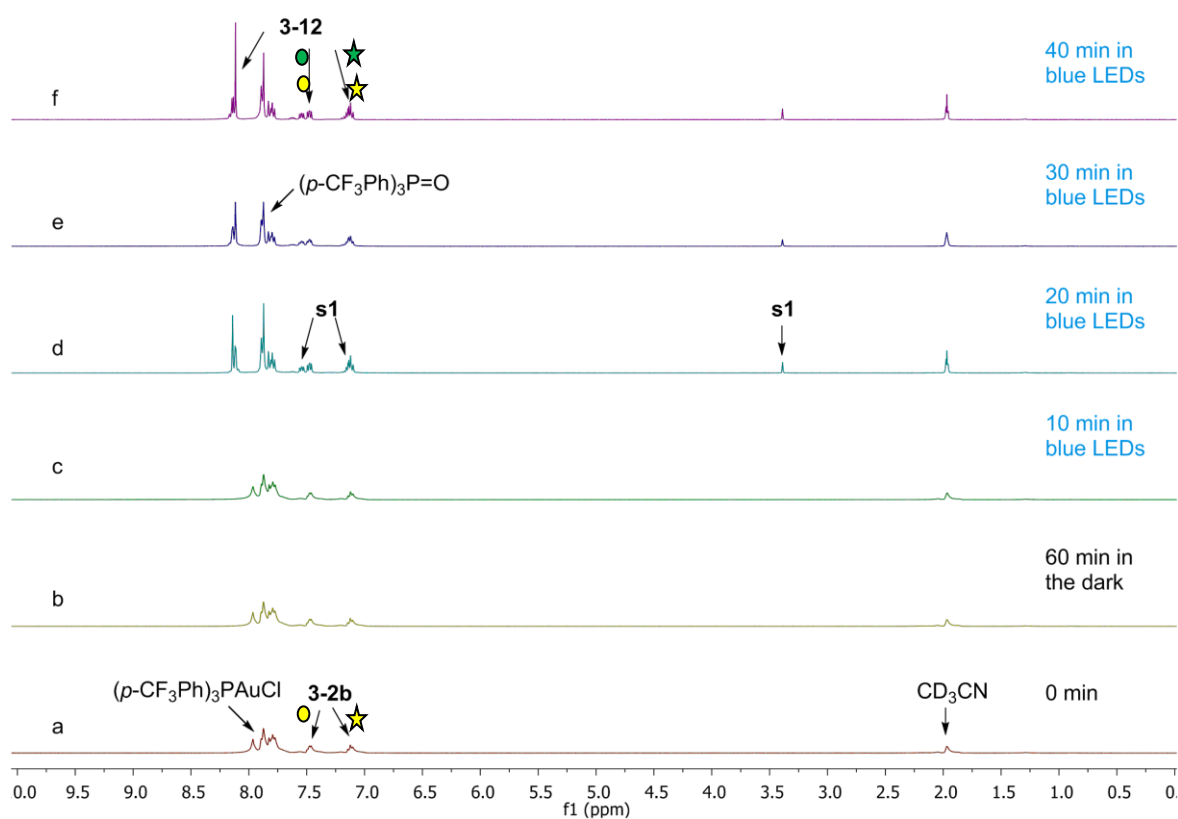
Reaction conditions: **3-2b** (0.2 mmol, 0.1 M), (*p*-CF₃Ph)₃PAuCl (5 mol %), Ir[dF(CF₃)ppy]₂(dtbbpy)PF₆ (1 mol%), K₂CO₃ (2.5 equiv), degassed MeCN (2 mL), r.t., overnight, blue LEDs light.

We did a series of control experiments about the Ir photocatalyst and Au catalyst on the dialkyne formation. Dialkyne 1,4-bis(4-fluorophenyl)buta-1,3-diyne could be formed only in the presence of the gold catalyst. These experiments reminded us that the diyne compound **s4** maybe came from a gold(III) acetylide intermediate, which was generated from a photoinduced gold catalysis process, also the side product diyne **3-5** maybe came from the similar pathway. These interesting experiments attracted more our attention to the role of gold catalyst in this reaction.

4.2.2 NMR Monitoring Experiment of 3-2b and Au(I) Complex

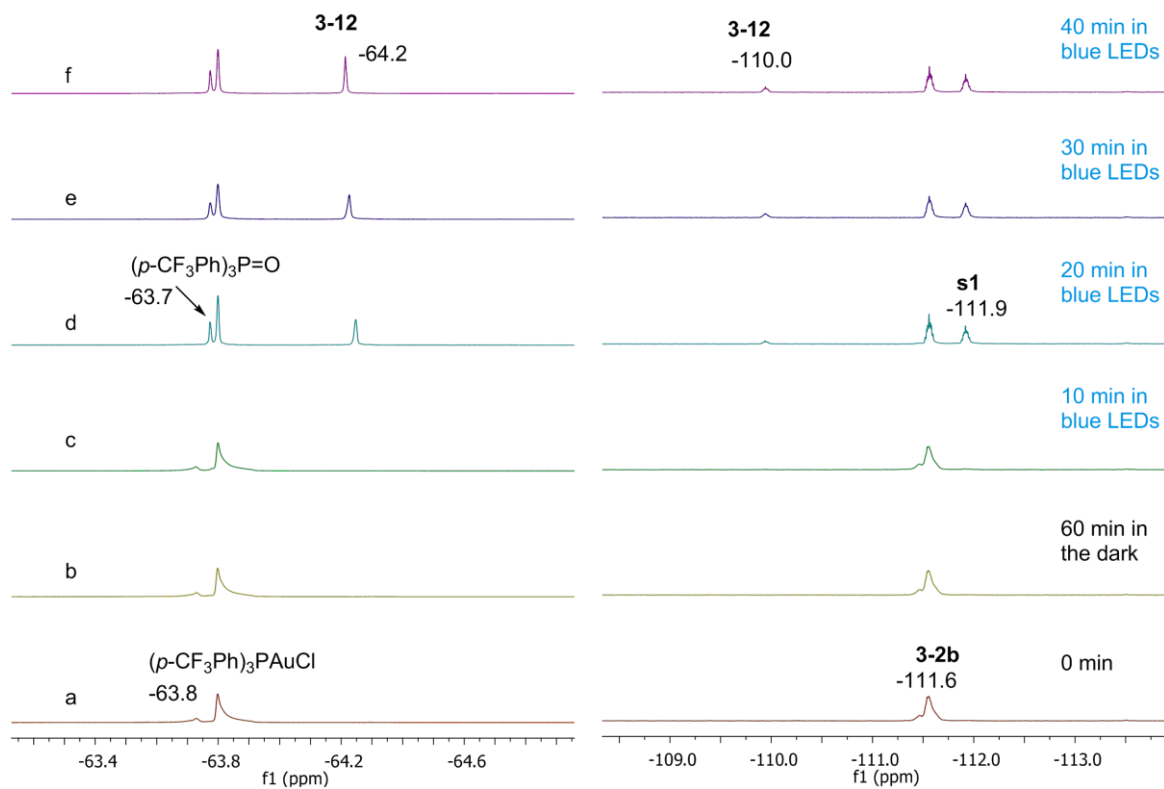


We also considered a different pathway, not connected to the generation of a radical species, and relying on the formation of a gold(III) intermediate of type **B** (Scheme 3-8). This hypothesis came from the following series of observations. While a mixture of alkyne **3-2b** and gold complex [Au-CF₃] ([Au-CF₃] = (p-CF₃Ph)₃PAuCl) remained unreacted for a few hours at room temperature as judged from ¹⁹F and ³¹P NMR monitoring, blue LEDs irradiation of the same mixture showed some partial conversion of the initial gold complex to a new gold species, which salient features after 20 min of irradiation, showed a broad resonance at 42 ppm in ³¹P NMR (CD₃CN) and two new signals at -64.2 ppm (broad peak) as well as a triplet (*J* = 2.4 Hz) at -110 ppm in ¹⁹F NMR. Based on the downfield shift of the ³¹P resonance (from 33.5 ppm for [Au-CF₃] to 42 ppm) and by analogy with literature,¹⁴⁵ we hypothesized the formation of a putative gold(III) intermediate like **3-12**.

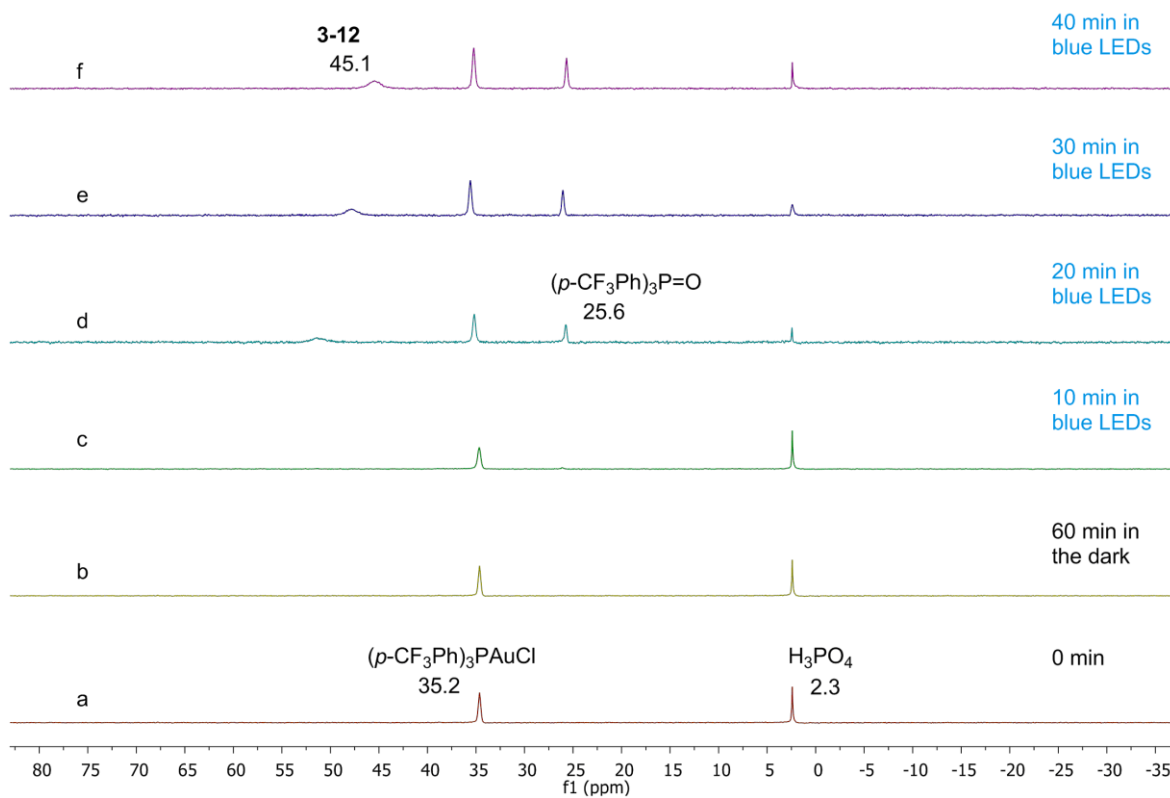


¹⁴⁵ Leyva-Pérez, A.; Doménech-Carbó, A.; Corma, A. *Nat. Commun.* **2015**, 6703.

¹H-NMR



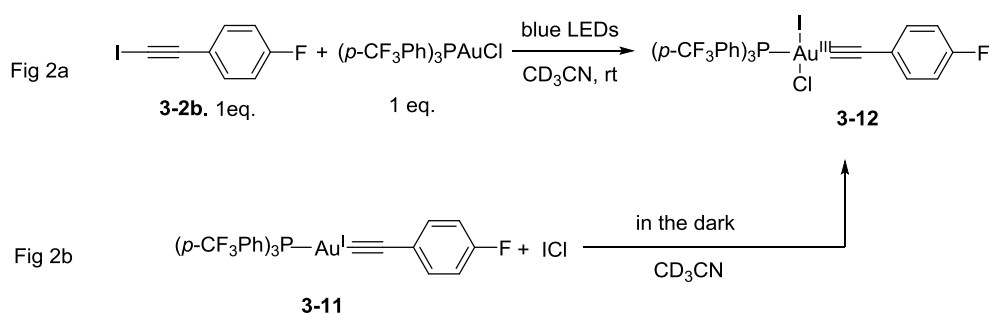
¹⁹F-NMR



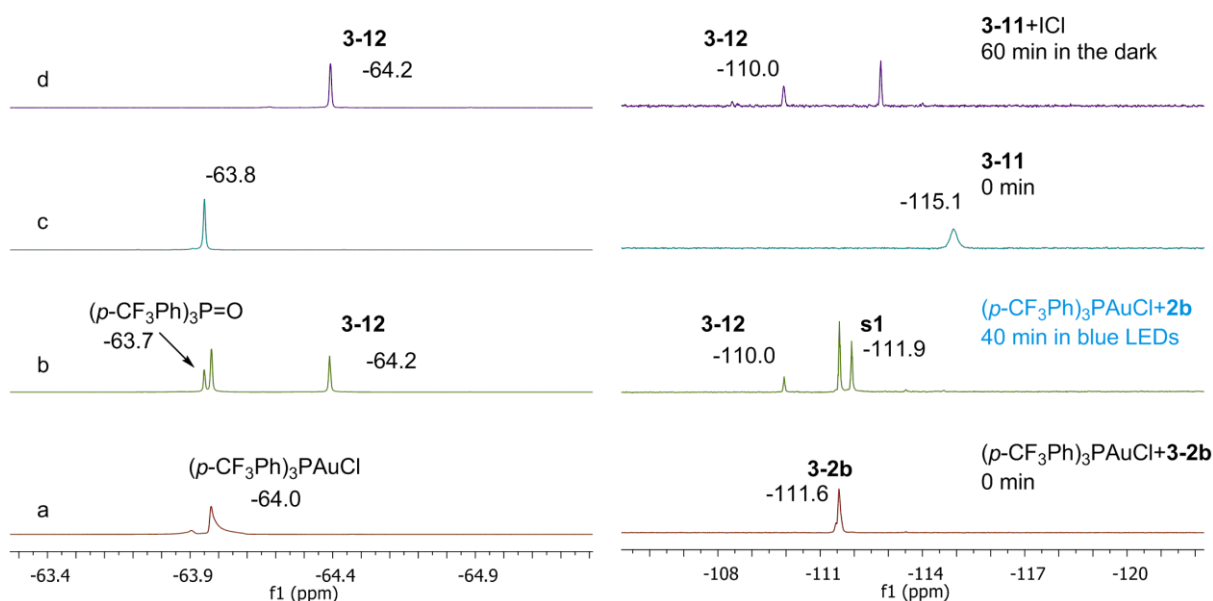
³¹P-NMR

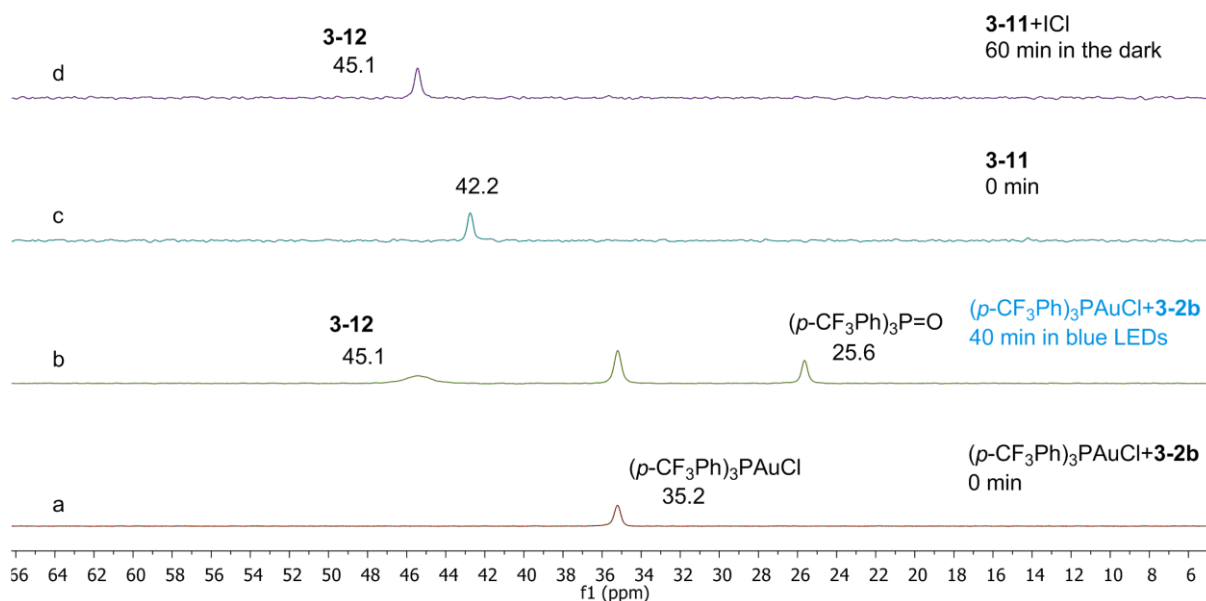
Due to possible interactions between the phosphine oxide and gold(III) acetylide **3-12**, the ³¹P NMR peak of Au(III) acetylide **3-12** may shift. Also due to extreme sensitivity to moisture, air and light, we could not isolate or detect the unstable gold(III) acetylide intermediate **3-12**. It was not detected either by ESI-MS or the mixture, it gets hydrolyzed forming phosphine oxide and terminal alkyne **s1**.

4.2.3 Cross Checking of the Gold(III) Acetylide Structure **3-12**



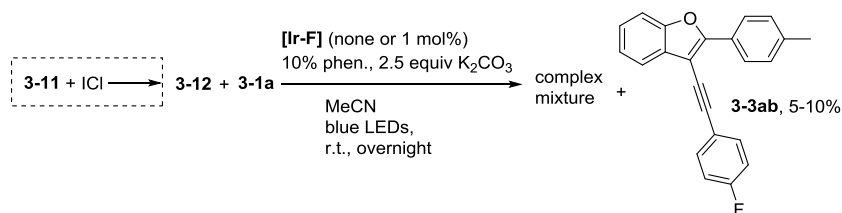
Structure of **3-12** could be cross checked by preparing it through a different route. Addition of ICl to freshly prepared gold acetylide **3-11** gave instantaneously a new complex featuring the same NMR signatures as **3-12** (see below). Intermediate complex **3-12** proved to be extremely sensitive to air and moisture and we could not isolate and further characterize it.





³¹P NMR monitoring of **Fig 2a** and **Fig 2b**

4.2.4 Generation of the Possible Gold(III) Acetylide Intermediate **3-12** under Standard Condition



We ran the following experiments. Freshly prepared **3-12** (0.67 equiv) was introduced to a mixture of phenol **3-1a** (1.0 equiv), K_2CO_3 (2.5 equiv), phenanthroline (10 mol%) with **[Ir-F]** (1 mol%) or without **[Ir-F]**. A complex mixture was formed showing nevertheless the formation of benzofuran **3-3ab** as minor product (< 10 %). This mitigated result cast some doubt about the real involvement of a gold species such as **3-12** in the efficient formation of benzofurans **3-3**.

4.3 Photosensitized Gold Catalysis

Based on all literature reports,¹⁴⁶ a vinyl gold(III) intermediate of type **D** of Scheme 3-8b (pathway II) which would undergo reductive elimination to provide benzofurans **3-3** is presumably involved.

4.3.1 NMR Monitoring Experiments of Vinylgold(I) Intermediate

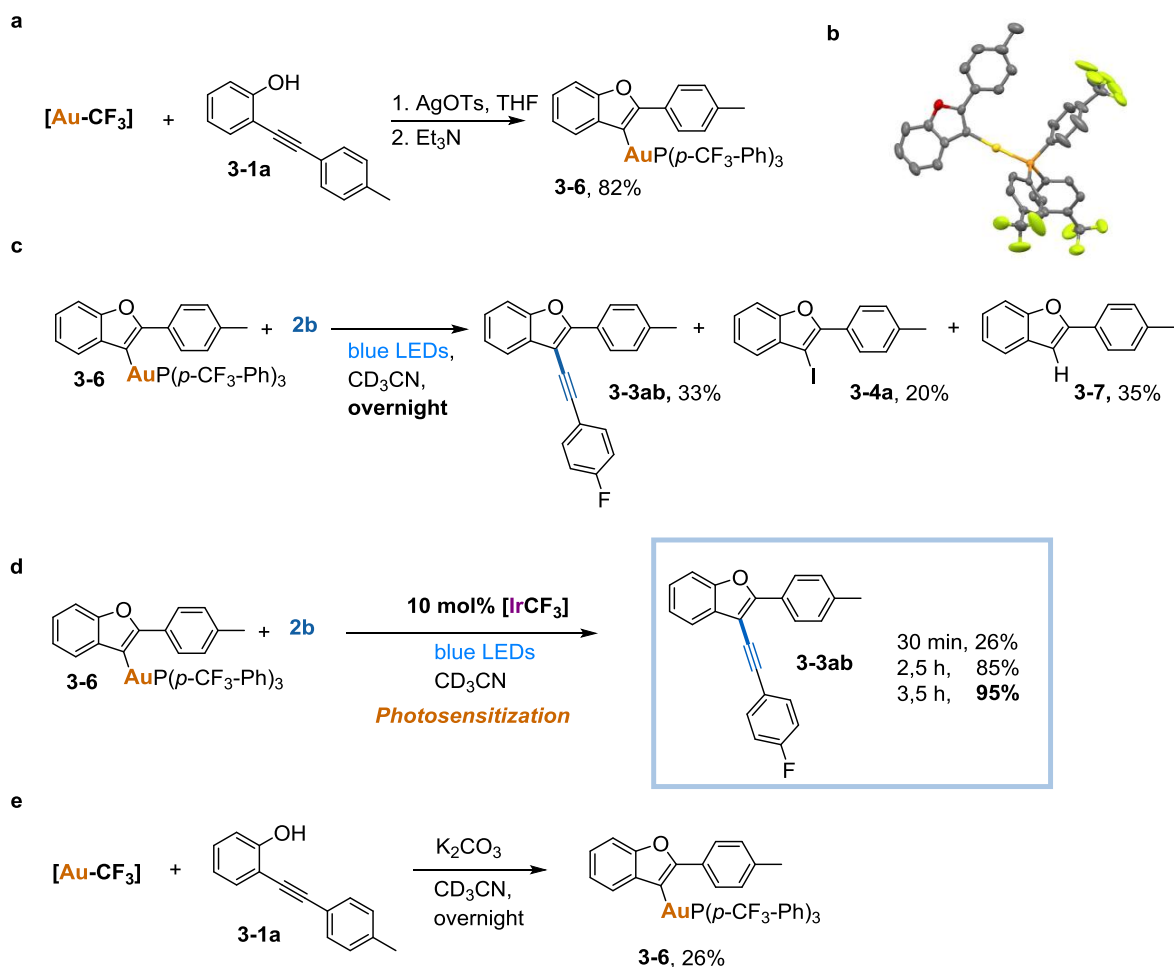


Figure 3-1. A vinylgold(I) as plausible intermediate. **a** Preparation of vinylgold(I) **3-6**. **b** XRD structure of complex **3-6**. **c** Alkylation from **3-2b** and **3-6** under blue LEDs irradiation. **d** Alkylation from **3-2b** and **3-6** under blue LEDs irradiation in the presence of iridium photocatalyst. **e** Formation of vinylgold(I) **3-6** in the reaction conditions.

¹⁴⁶ (a) Zheng, Z.; Wang, Z.; Wang, Y.; Zhang, L. *Chem. Soc. Rev.* **2016**, *45*, 4448. (b) Twilton, J.; Le, C.; Zhang, P.; Evans, R. W.; MacMillan, D. W. C. *Nat. Rev. Chem.* **2017**, *1*, 0052. (c) For reviews, see: Levin, M. D.; Kim, S.; Toste, F. D. *ACS Cent. Sci.* **2016**, *2*, 293.

We prepared vinylgold(I) **3-6** in 82% yield by an independent route¹⁴⁷ as shown in Figures 3-1a. X-ray diffraction analysis of suitable crystals of **3-6** confirmed its structure and provided useful structural data for further modeling studies.

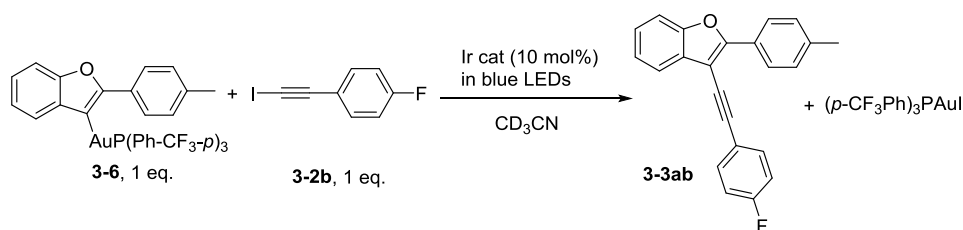
When confronted to one equiv of alkynyl iodide **3-2b**, no conversion was observed after a few hours at room temperature. Here also, blue LEDs irradiation changed the scenario. Little conversion (< 10 %) was observed after 2 h at room temperature. Overnight irradiation resulted in the formation of **3-3ab** in 33% (accompanied by 20% of **3-4a** and 35% of protodeauration product **3-7** as determined by ¹H NMR, see Figure 3-1c).

However, addition of 10 mol% of **[Ir-F]** dramatically altered the outcome and yielded benzofuran **3-3ab** almost quantitatively (Figure 3-1d). Therefore, experimental conditions to trigger the key C-C bond formation were found. Although, the benzofuran formation could be achieved without photocatalyst **[Ir-F]** (Figure 3c) which brings another rationalization for the finding of entries 8 and 9 of Table 1, it appears highly accelerated in its presence.

Another important point to check was the formation of **3-6** in the reaction conditions. This was achieved by exposing phenol **3-1a** to a stoichiometric amount of **[Au-CF₃]** in CD₃CN overnight. After overnight reaction time in the dark, the formation of vinylgold(I) **3-6** was observed by NMR in 26% yield. (Figure 3-1e).

The following are the NMR monitoring experiments of vinylgold(I) intermediate.

a) NMR Monitoring Experiment of the Reaction Between Vinylgold(I) **3-6** and **3-2b**



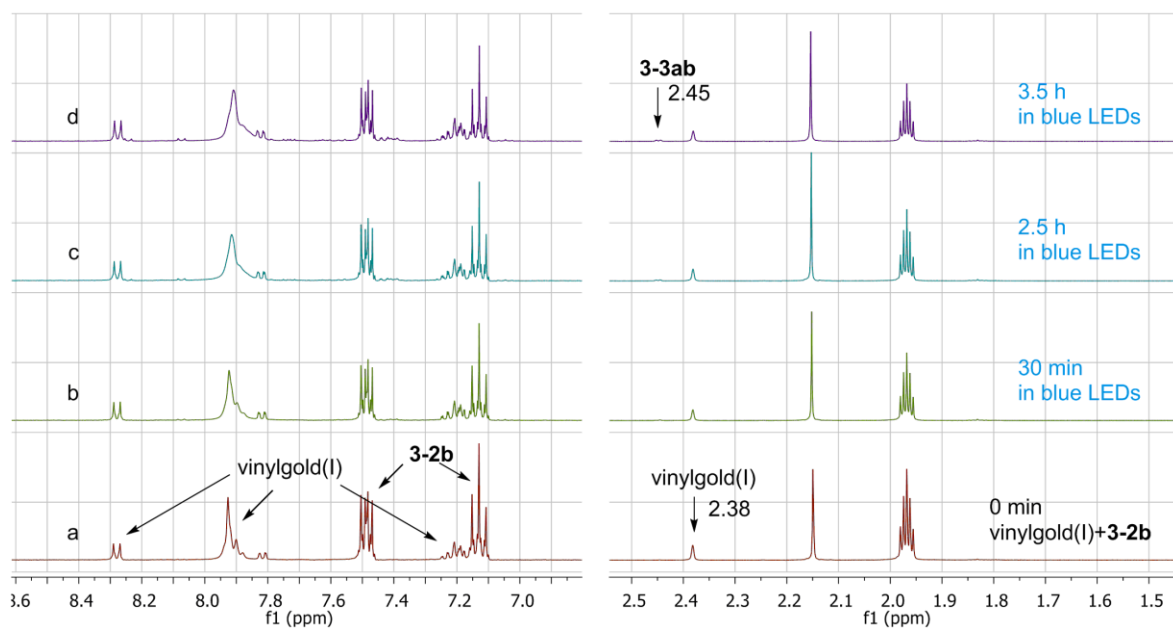
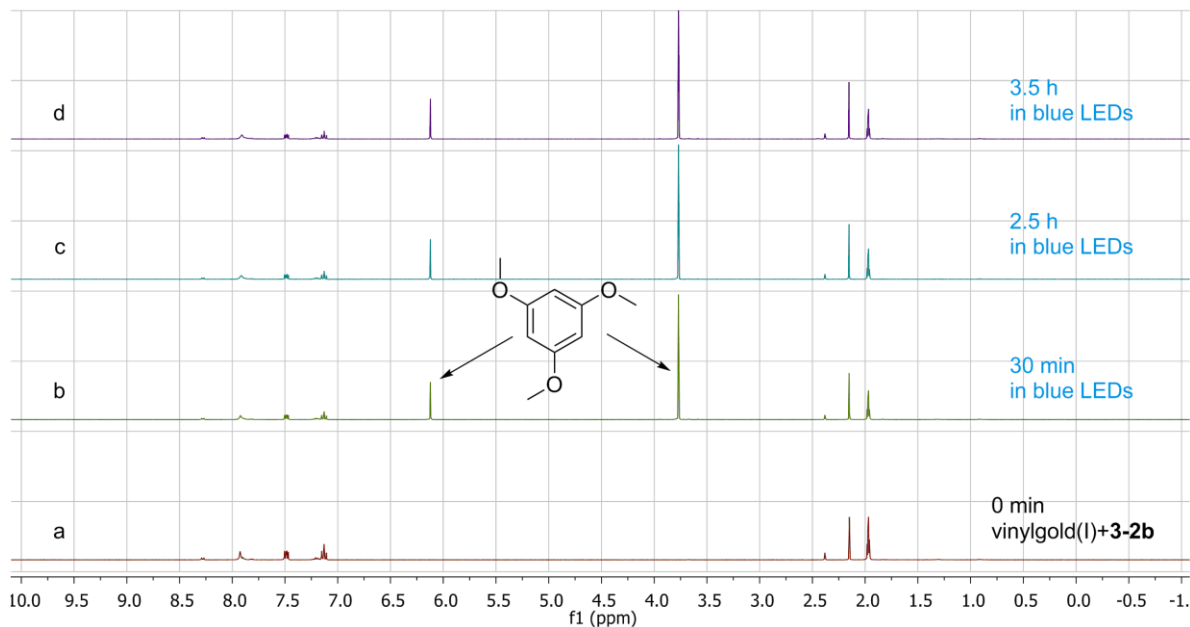
Tube A: The vinylgold(I) compound **3-6** was treated with a stoichiometric amount of iodoalkyne **3-2b** in CD₃CN, stirring in blue LEDs light for 30 min, 2.5 h and 3.5 h, followed by ¹H-NMR, ¹⁹F-NMR and ³¹P-NMR analysis. The yields are the averages of two times.

Tube B corresponds to the experiment in Figure 3-1d, the vinylgold(I) compound **3-6** and photocatalyst Ir[dF(CF₃)ppy]₂(dtbbpy)PF₆ was treated with a stoichiometric amount of iodoalkyne **3-2b** in CD₃CN for 30 min, 2.5 h and 3.5 h, followed by ¹H-NMR, ¹⁹F-NMR and ³¹P-NMR analysis.

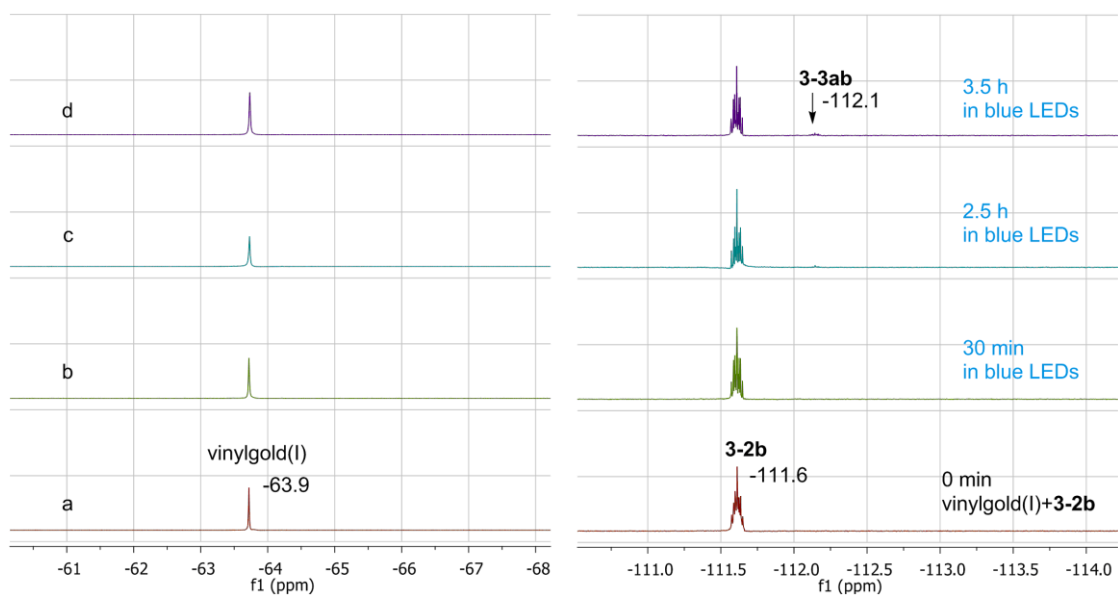
¹⁴⁷ Hashmi, A. S. K.; Ramamurthi, T. D.; Rominger, F. *Adv. Synth. Catal.* **2010**, 352, 971.

Yield of **3ab** in Tube A and Tube B under blue LEDs light

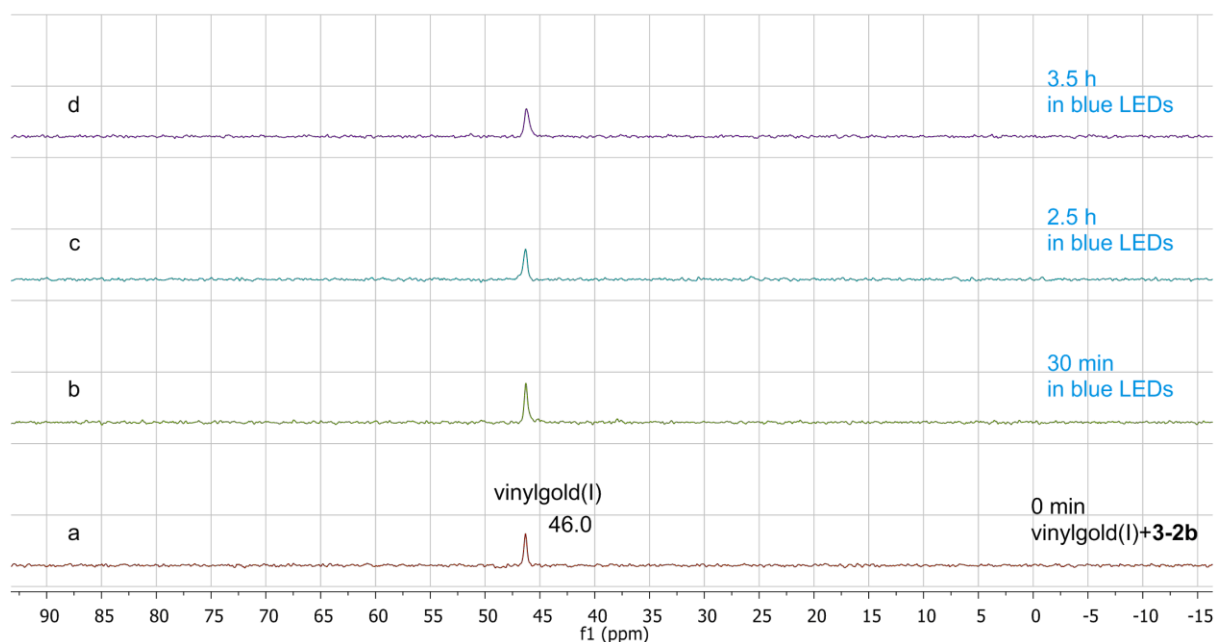
Time	Tube A (without Ir cat, two times)	Tube B (with Ir cat)
30 min	1%	26%
2.5 h	3%	85%
3.5 h	5%	95%



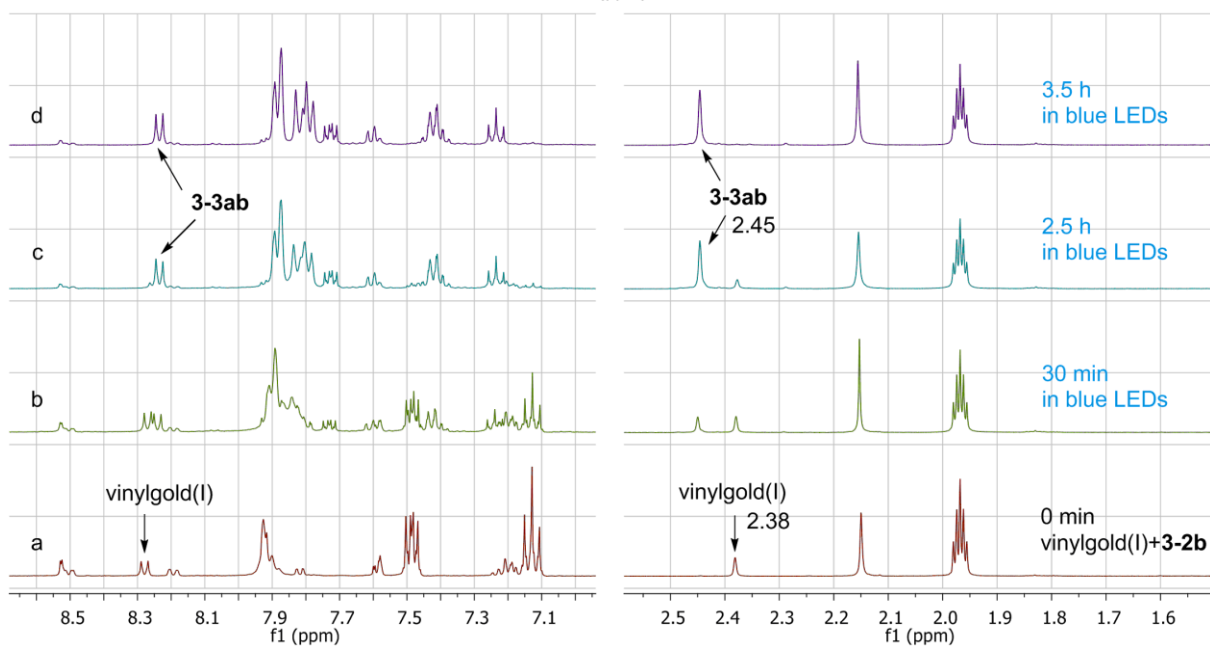
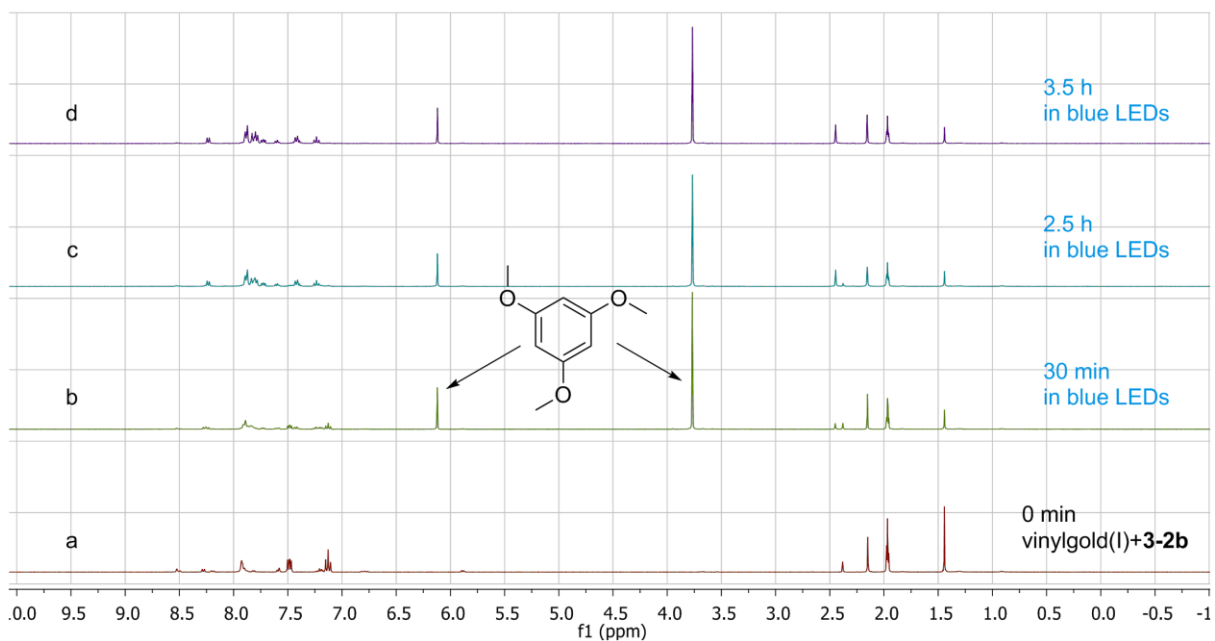
Tube A: $^1\text{H-NMR}$



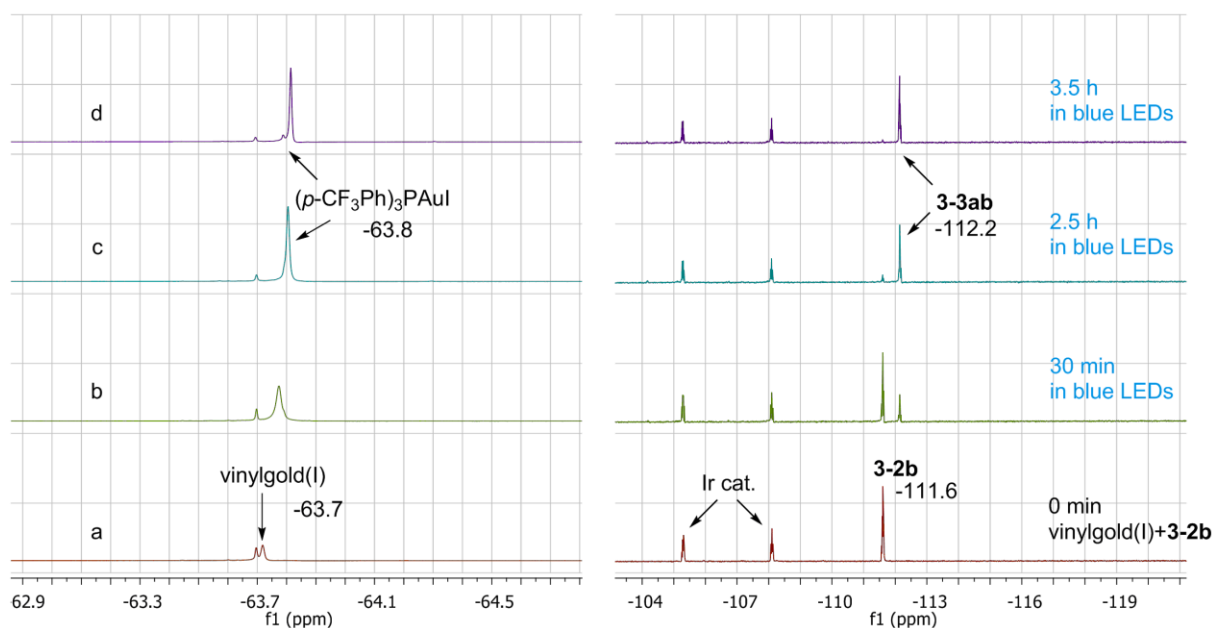
Tube A: ^{19}F -NMR



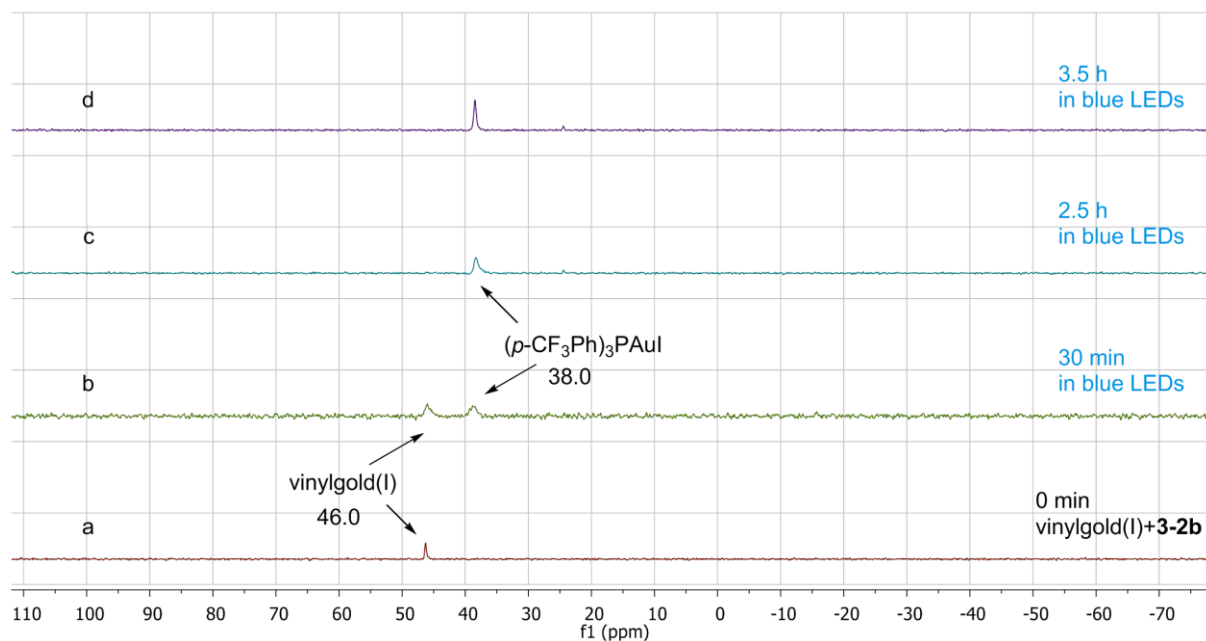
Tube A: ^{31}P -NMR



Tube B: $^1\text{H-NMR}$

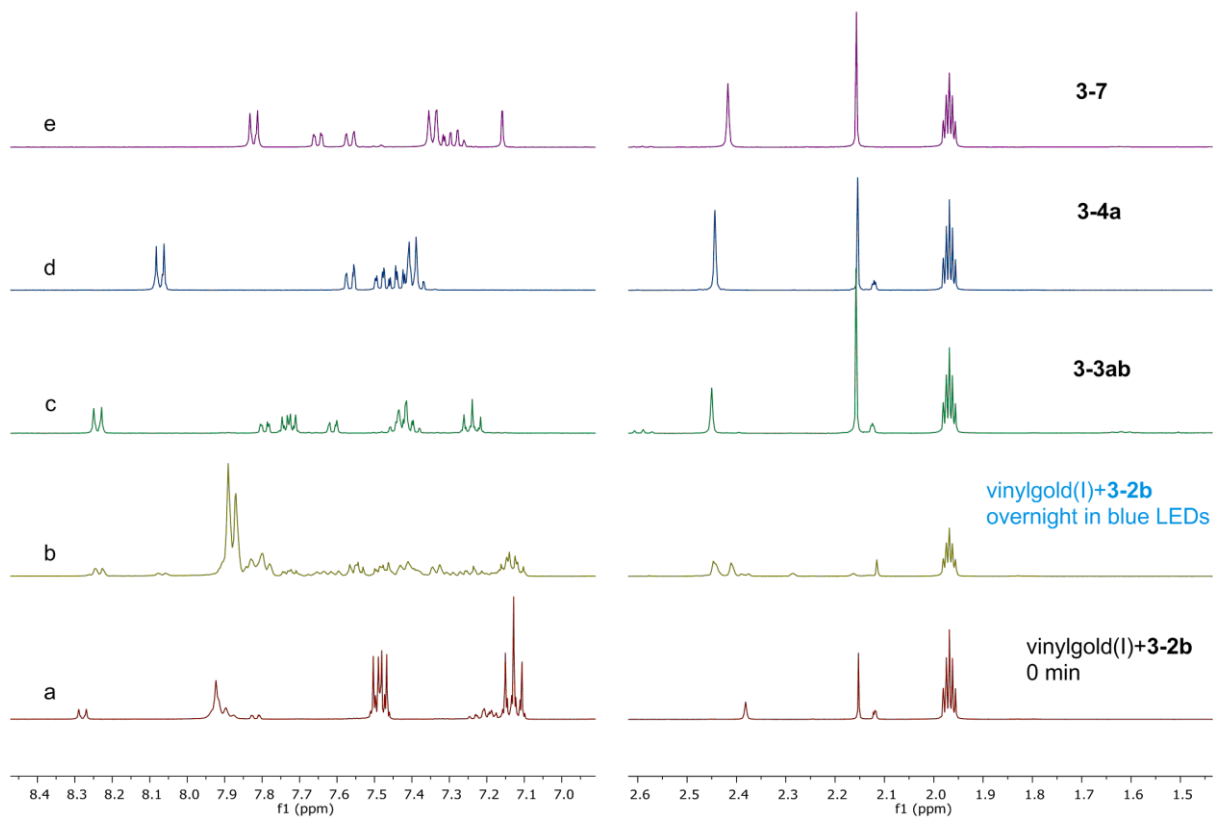
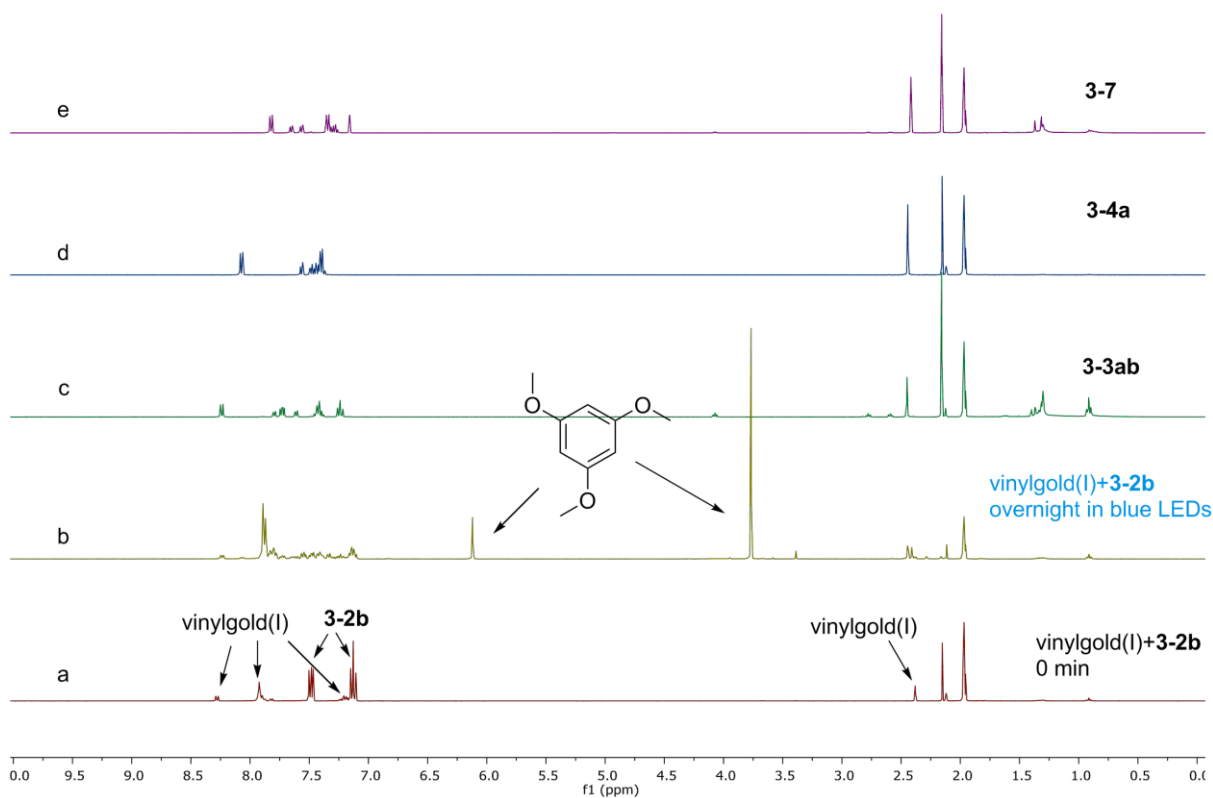


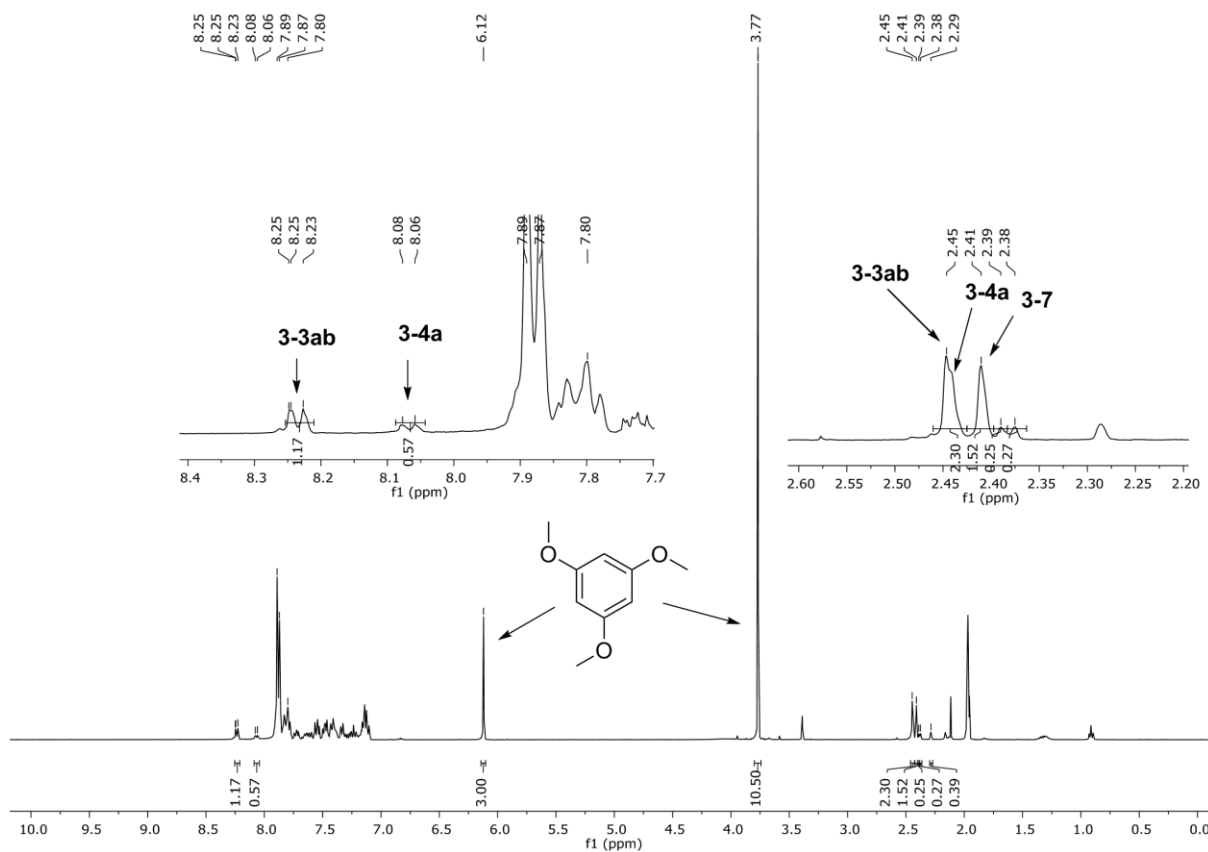
Tube B: ^{19}F -NMR



Tube B: ^{31}P -NMR

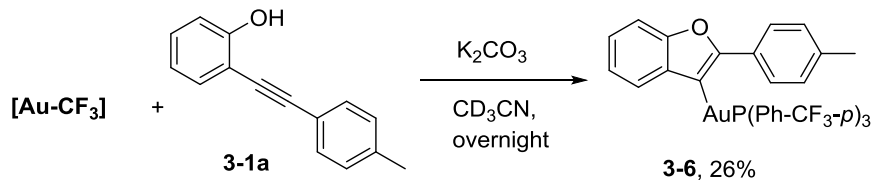
Tube C corresponds to the experiment in Figure 3-1c, the vinylgold(I) compound **3-6** was treated with a stoichiometric amount of iodoalkyne **3-2b** in CD_3CN , stirring in blue LEDs light for overnight, do ^1H -NMR, ^{19}F -NMR and ^{31}P -NMR analysis. After comparing the pure ^1H -NMR spectrum of **3-3ab**, **3-4a** and **3-7**, it shows that the generated **3-3ab** is 33% yield, accompanied by 20% of **3-4a** and 35% of protodeauration product **3-7**.



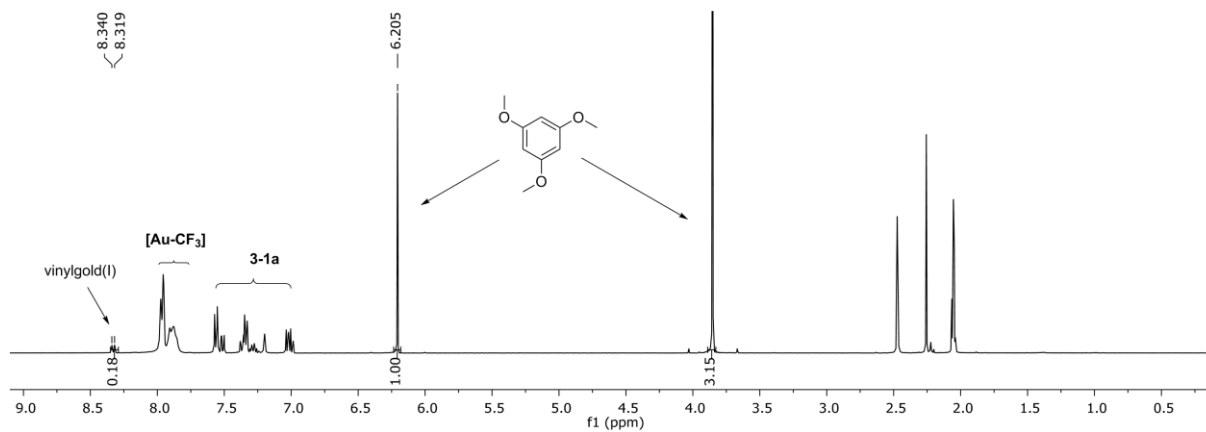


Tube C: $^1\text{H-NMR}$

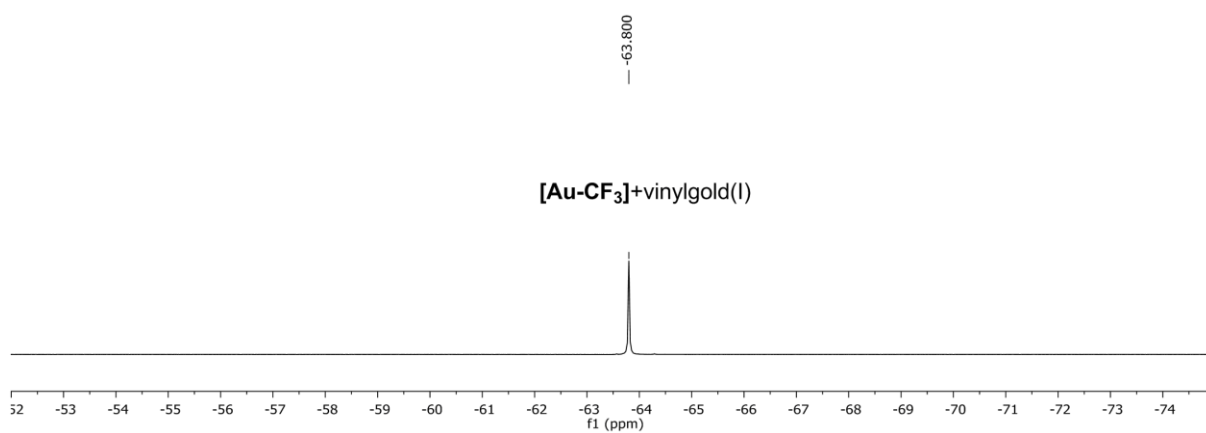
b) Formation of Vinylgold(I) 3-6 under Standard Conditions



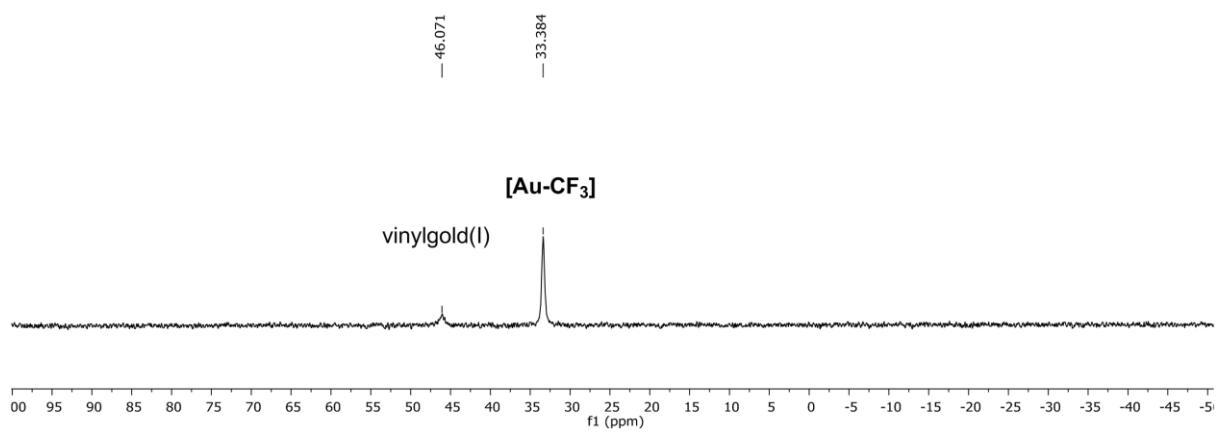
Tube D corresponds to the experiment in Figure 3-1e, phenol **1a** and K_2CO_3 were treated with a stoichiometric amount of $(p\text{-CF}_3\text{Ph})_3\text{PAuCl}$ in CD_3CN in a NMR tube, stirring it for overnight in the dark. Add 1,3,5-trimethoxybenzene (0.019 mmol) as internal standard into Tube D, do $^1\text{H-NMR}$, $^{19}\text{F-NMR}$ and $^{31}\text{P-NMR}$ analysis, the formation of vinylgold(I) **6** was observed by NMR in 26% yield.



Tube D: ¹H-NMR



Tube D: ¹⁹F-NMR



Tube D: ³¹P-NMR

4.3.2 Fluorescence Quenching Study

The possibility of an energy transfer to vinylgold(I) **3-6** starting from the long-lived triplet state $^3[\text{Ir-F}]$ (3T_1) was confirmed by steady state fluorescence quenching studies of $[\text{Ir-F}]$ by vinylgold(I) **3-6** which exhibited a significant decrease of fluorescence intensity upon gradual addition of **3-6**. A plot of the intensity ratio I^0/I versus the concentration of **3-6** showed a linear relation, following the Stern–Volmer law which allowed to determine a bimolecular quenching constants $k_q = 3.8 \cdot 10^8 \text{ l}\cdot\text{mol}^{-1}\cdot\text{s}^{-1}$.

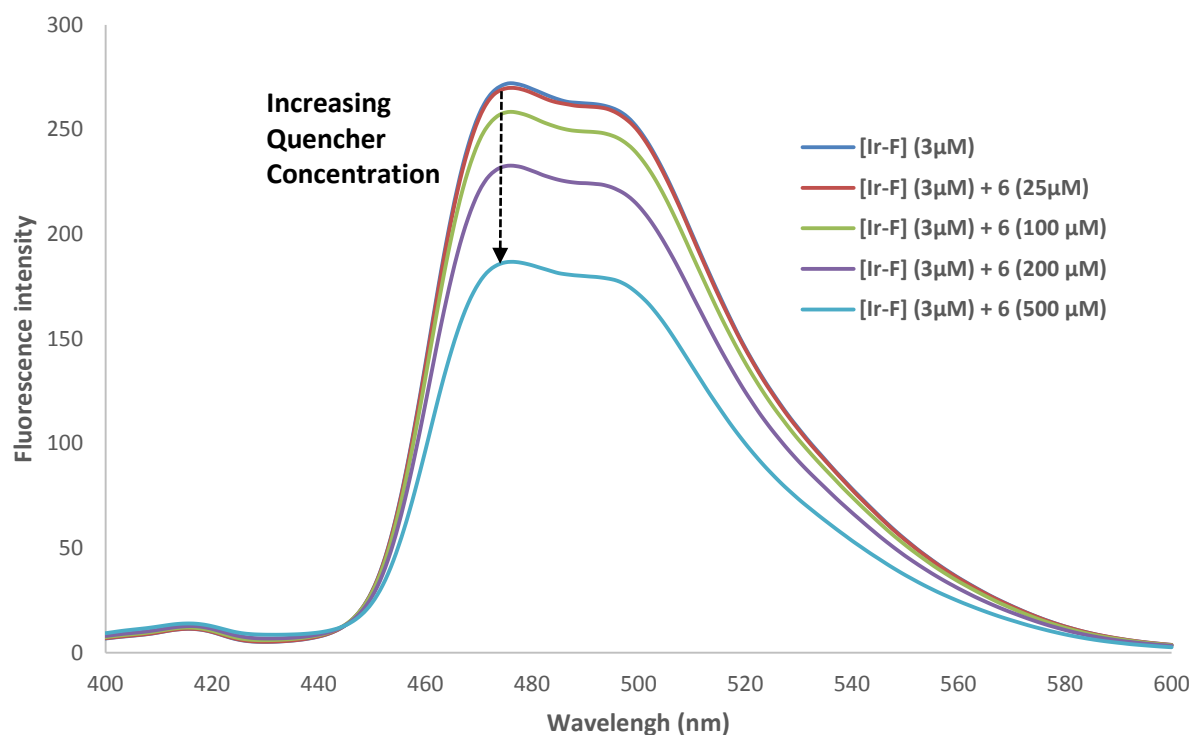


Figure 3-2. Fluorescence spectra, fluorescence quenching studies of $[\text{Ir-F}]$ by vinylgold(I) **3-6** which exhibited a significant decrease of fluorescence intensity upon gradual addition of **3-6**. This work was done by Dr. Vincent Corcé.

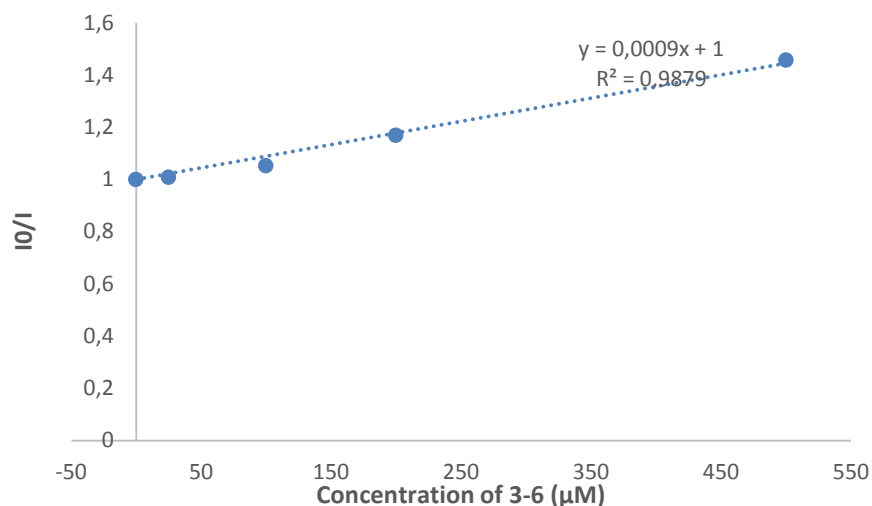


Figure 3-3. Stern-Volmer plot, A plot of the intensity ratio I^0/I versus the concentration of **3-6** showed a linear relation, following the Stern–Volmer law which allowed to determine a bimolecular quenching constants $k_q = 3.8 \cdot 10^8 \text{ l.mol}^{-1} \cdot \text{s}^{-1}$. This work was done by Dr. Vincent Corcé.

4.3.3 Theoretical Studies

Inspired by a recent report on "excited-state organometallic catalysis" by McCusker and MacMillan,¹⁴⁸ who reported an energy-transfer mediated reductive elimination on an excited arylnickel(II) intermediate, we considered the possible implication of an excited state of **3-6**.

A direct excitation of **3-6** by blue LEDs does not seem very likely as the reaction yield decreases dramatically when no photocatalyst [**Ir-F**] is added to the mixture (entries 8 and 9, Table 3-2). We have accordingly focused on the possibility of an energy transfer to **3-6** starting from the long-lived triplet state $^3[\text{Ir-F}]$ (3T_1). This was supported by calculations. The spin density of $^3[\text{Ir-F}]$ was indeed compared either isolated or in the vicinity of **3-6** (Figure 3-4 and Experiment Part for calculation details). As observed in Figure 3-4, part of the $^3[\text{Ir-F}]$ spin density is transferred to the approaching furan moiety of the gold complex **3-6**, intimating that energy transfer is taking place. This would lead to the formation of **3-6** in an excited electronic state which may further react with iodoethynyl benzene **3-2a**. Note that the same calculations performed on $^3[\text{Ir-F}]$ approached by **3-2a** show that no transfer is occurring on **3-2a** (see Experiment Part for details). This finding agrees well with the quenching studies done on [**Ir-F**] in presence of **3-6** or **3-2a**. To determine which electronic states of **3-6** are

¹⁴⁸ (a) Welin, E. R.; Le, C.; Arias-Rotondo, D. M.; McCusker, J. K.; MacMillan, D. W. C. Photosensitized energy transfer-mediated organometallic catalysis through electronically excited nickel(II). *Science* **2017**, 355, 380. (b) Kim, T.; McCarver, S. J.; Lee, C.; MacMillan, D. W. C. *Angew. Chem. Int. Ed.* **2018**, 57, 3488.

accessible via this energy transfer, time-dependent DFT (TD-DFT) calculations were carried out. Results show that only the 3T_1 excited state **3-6** is accessible within the blue LEDs energy range (470 nm, see Experiment Part for calculations details).

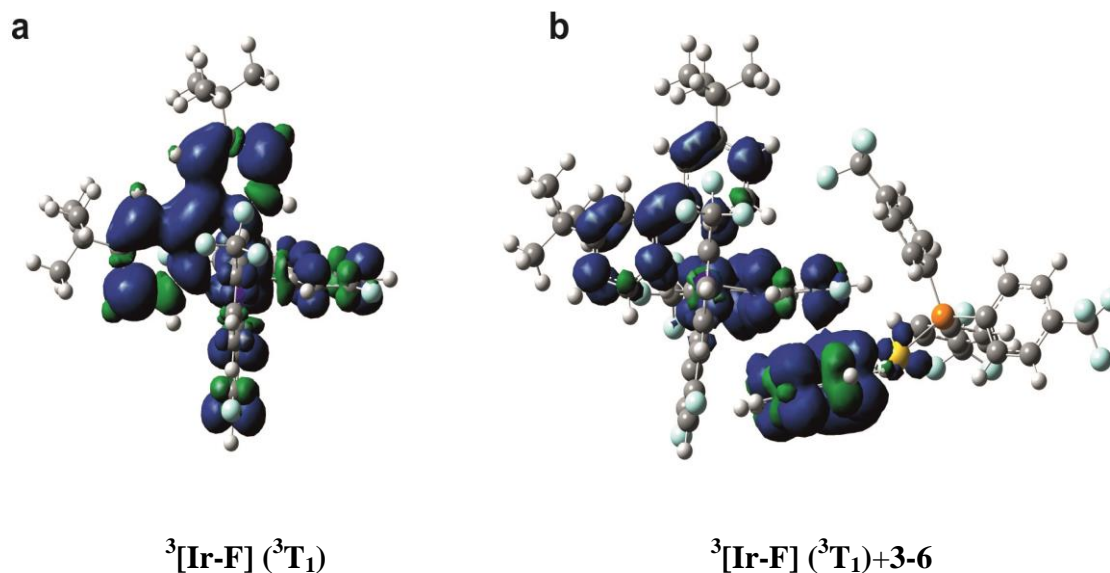


Figure 3-4. Spin density isosurface (isovalue 0.0006 a.u.). **a** Isolated $^3[\text{Ir-F}]$ complex. **b** $[\text{Ir-F}]^*$ (3T_1) in the vicinity of **3-6**. This work was done by Dr. Yves Gimbert and Dr. Héloïse Dossmann.

Following these findings, we have therefore conducted a detailed theoretical study of the reaction of **3-6** with **3-2a** with **3-6** in its 3T_1 excited state. The ground state reactivity of **3-6** was also checked in order to help rationalizing the role of blue LEDs in the mechanism efficiency. For the sake of clarity, we will now refer to **3-6** either as $^1\mathbf{3-6}$ or as $^3\mathbf{3-6}$ to unambiguously indicate respectively to the 1S_0 ground state or the 3T_1 excited state of **3-6**. All calculations presented below were obtained at the PBE0/SDD(Au), 6-311G*(I), 6-31G** (other atoms) level of theory, taking into account solvent effects by SMD procedure. If not stated otherwise, reported energies are ΔG_{MeCN} .

On the ground state singlet potential energy surface, the reaction pathway was quite straightforward to determine. A gold(III) complex, $^1\mathbf{I}$, could indeed easily be localized (Figure 3-5). Although it undergoes a highly exothermic reductive elimination to give **3-3aa** (-47.2 kcal/mol with a barrier of 10.5 kcal/mol), its formation cost is prohibitive: almost 28 kcal/mol (Figure 3-5). This renders the overall pathway unlikely.

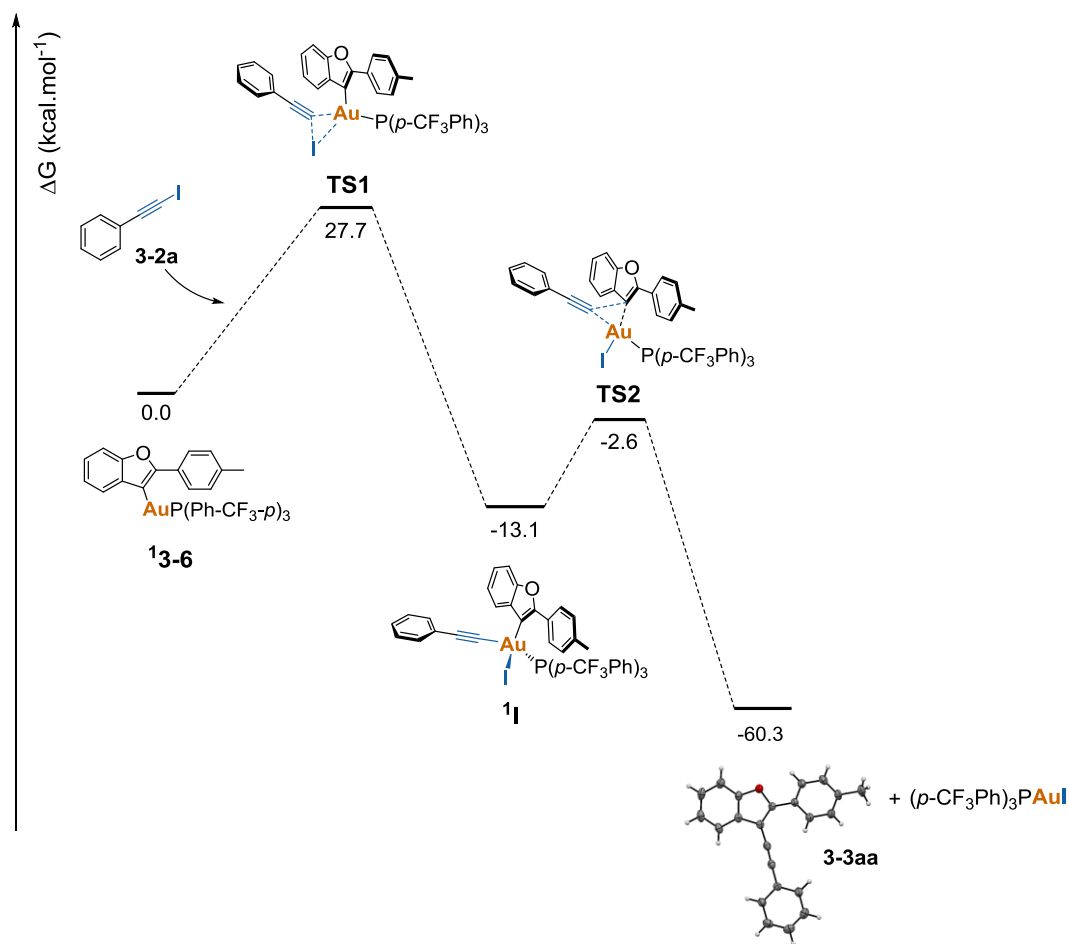


Figure 3-5. Potential energy surface of the reaction of **13-6** with **3-2a**. Gibbs free energies (CH₃CN) are given relatively to the starting products and are in kcal/mol. This work was done by Dr. Yves Gimbert and Dr. Héloïse Dossmann.

On the contrary, the reaction on the triplet potential energy surface appears more sinuous but much more favorable thermodynamically. The approach of **3-2a** to **3³⁻⁶** (along the Au-C (bearing the iodine) bond reaction coordinate) is leading to the formation of an intermediate complex **3^{II}**, lying down 18.5 kcal/mol below the reagents (Figure 3-6). Interestingly, the geometry adopted by **3-2a** in this complex is bent (I-C-C angle of 115 °) and reminiscent of that of **3-2a** (**3^{T1}**) (I-C-C angle of 129 ° vs 180° for **3-2a** in its ground state, see Experiment Part). This feature suggests that the **3³⁻⁶** complex may transfer energy to **3-2a** when these reactants are approaching each other. Checking the spin density along the Au-C (bearing the iodine) bond reaction coordinate confirms indeed that a transfer is occurring at a relatively long distance (from 3.6 Å, see Experiment Part). This feature suggests that **3³⁻⁶** could act as a relay for transferring energy to **3-2a** which would provide access to a reactive bent structure of the acetylenic compound. Starting then from complex **3^{II}** and by approaching the iodine

atom to gold, intermediate **3III** is localized on which Au(I) is changed to Au(III) and organic precursors are in *trans* position. The step occurs with low activation energy of 2.2 kcal/mol via **TS3**. By reducing the C-Au-C angle on **3III** (to bring together the two C's involved in the forthcoming new C-C bond), it was possible to localize a transition structure **TS4** requiring a formation barrier of 18.8 kcal/mol. **TS4** connects to the Au(III) complex intermediate **3IV** on which the formation of the key C-C bond between **3-6** and **3-2a** is observed but with the iodine still interacting with the slightly elongated triple bond ($d(\text{I-C}) = 2.29 \text{ \AA}$). Finally, from **3IV**, two pathway variants can be envisaged. First, the **3IV** complex may further rearrange to lead to a **3V** complex (-27 kcal/mol below **3IV**, Figure 3-6) via an inexpensive **TS5** transition structure (+0.001 kcal/mol compared to **3IV**). Then **3V** easily dissociates to lead to **3-3aa** + (*p*-CF₃Ph)₃PAuI (barrier **TS6** of 6 kcal/mol). An electronic decay of **3-3aa** can then be envisaged to lead to the final coupling product **3-3aa** + (*p*-CF₃Ph)₃PAuI. Another possible pathway would imply a direct S₀←T₁ electronic decay of **3IV**, leading to a complex which appears to be dissociative. It would thus give directly the cited above final coupling products (Figure 3-6).

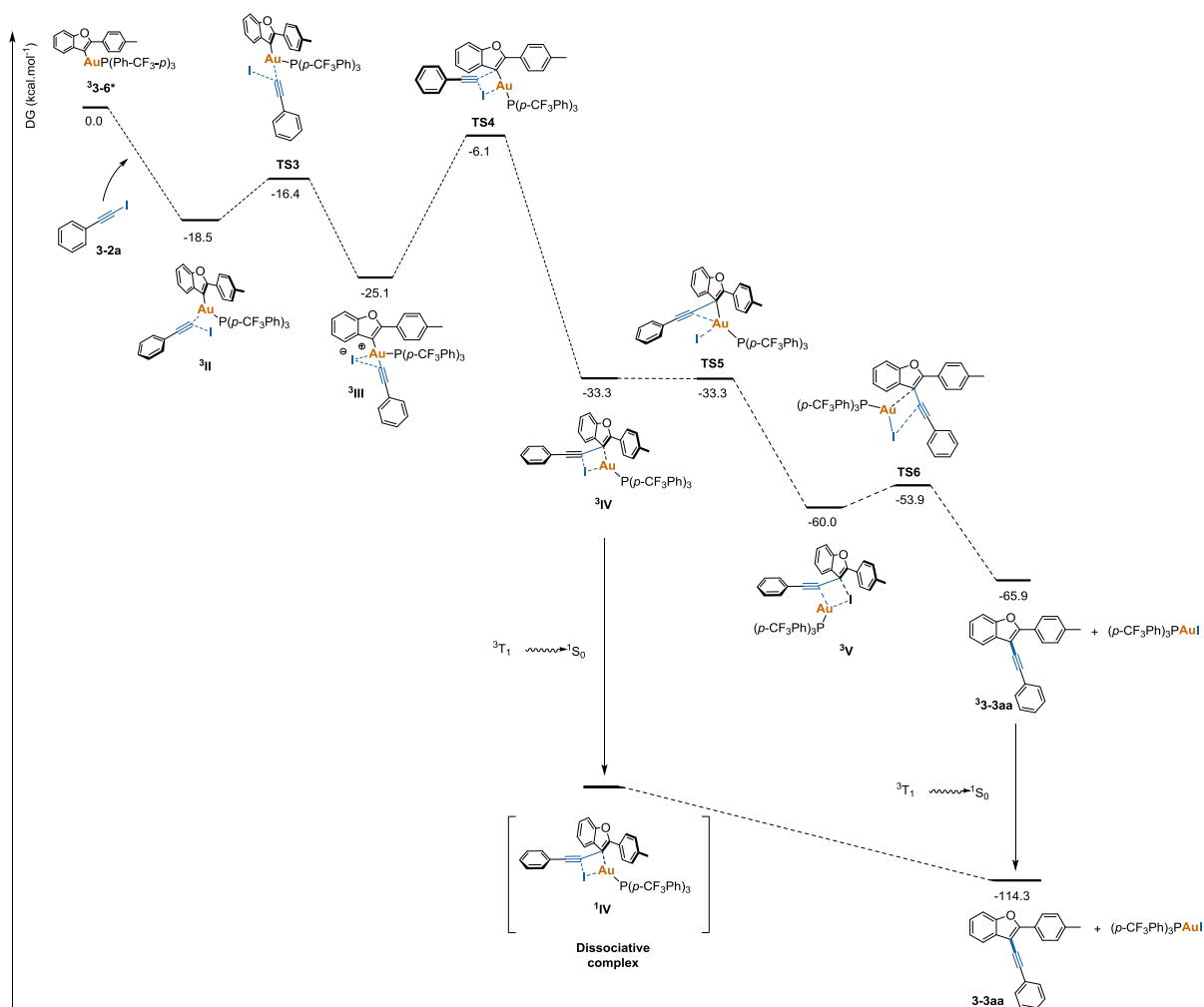


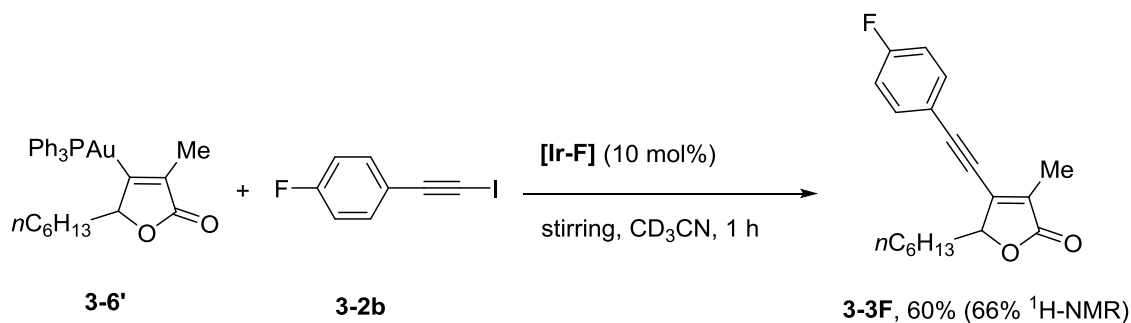
Figure 3-6. Potential energy surface of the reaction of **3-6** with **3-2a**. Gibbs free energies (CH₃CN) are given relatively to the starting products and are in kcal/mol. This work was done by Dr. Yves Gimbert and Dr. Héloïse Dossmann.

The proposed reaction pathway using **3-6** as a starting product appears thus extremely favorable from a thermodynamic point of view. All intermediate complexes and transition structures have indeed lower energies than the starting products. This would be highly coherent with the great efficiency of the reaction observed.

In addition to the use of [Ir-F], two additional factors appear to optimize this process. First, the substitution of Ph₃PAuCl by [Au-CF₃] appeared highly beneficial (Table 3-2, entry 3 vs 4), maybe because of the higher electrophilicity of [Au-CF₃] (Glorius).^{12a} Second, the adjunction of 1,10-phenanthroline allowed to observe a significant yield increase whatever the followed pathway. Compare for instance entry 4 vs 5 of Table 3-2 or entry 8 vs 9 of Table 3-2. The reason for this is not clearly established and several hypotheses are standing. For instance, some halogen bonding between phenanthroline and the alkynyl iodides **3-2** which are known halogen bonding donors¹⁴⁹ might be at the origin of the increased reactivity of the system.

4.3.4 Testing Other Vinyl Gold(I)

In addition to the vinylgold(I) **3-6**, we also did another alkylation of vinylgold(I) **3-6'** with **3-2b** under blue LEDs irradiation in the presence of iridium photocatalyst. The yield is good.



¹⁴⁹ (a) Cavallo, G.; Metrangolo, P.; Milani, R.; Pilati, T.; Priimagi, A.; Resnati, G.; Terraneo, G. The halogen bond. *Chem. Rev.* **2016**, *116*, 2478. (b) Dumele, O.; Wu, D.; Trapp, N.; Goroff, N.; Diederich, F. Halogen Bonding of (Iodoethynyl)benzene Derivatives in Solution. *Org. Lett.* **2014**, *16*, 4722.

4.4 Proposed Mechanism and Conclusion

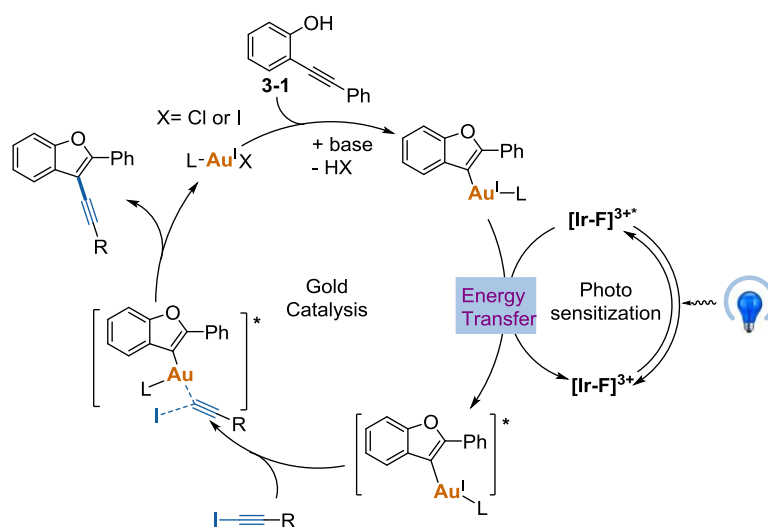


Figure 3-7. Photosensitized gold catalysis via energy transfer.

Finally, we proposed a mechanism of photosensitized gold catalysis via energy transfer. Firstly, the gold complex can react with phenol to form the vinylgold(I) intermediate. At the same time, when using blue LEDs light to irradiate this reaction, the ground state Ir photocatalyst is transformed to excited state. The latter will transfer the energy to the vinylgold(I) to excited state, the excited state vinylgold(I) will react with iodoalkyne **3-2**, undergo some lower energy intermediate, it form the final benzofuran compound and Au complex.

In conclusion, this study brings in light a new type of dual catalysis type of transformation involving electrophilic gold catalysis and iridium photosensitization which allows a Csp^2 - Csp cross coupling reaction useful for the alkylation of benzofurans. Novel mechanistic pathways have been uncovered. While a blue LEDs promoted oxidative addition of an alkynyl iodide partner on a gold(I) precatalyst would generate in a minor pathway, a catalytic gold(III) electrophilic species possibly competent for the benzofuran formation, the major pathway would rely on the presence of a photocatalyst. Excited $Ir[dF(CF_3)ppy]_2(dtbbpy)PF_6$ indeed interacts with a vinylgold(I) intermediate stemming from a gold(I) promoted 5-endo-dig *O*-cyclization via energy transfer to trigger oxidative addition at gold(I). In other words, the triplet excited state of the vinylgold(I) intermediate and the alkynyl iodide partner readily engages in a oxidative addition –trans/cis isomerization sequence which forges the desired Csp^2 - Csp bond after desexciting reductive elimination. This completely undescribed process in gold catalysis tunnels the difficult oxidative addition – reductive elimination sequence and opens new avenues in the field of excited state gold catalysis.

5 Experimental Section

5.1 General Informations

All reactions involving air sensitive reagents or intermediates were carried out in pre-heated glassware under an argon atmosphere using standard *Schlenk* techniques. All solvents and chemicals were used as received from suppliers (*Alfa Aesar*, *Sigma Aldrich*, *TCI*). Acetonitrile and methanol were purified by distillation over calcium hydride under dry argon atmosphere.

Photocatalysts $[\text{Ru}(\text{bpy})_3]_2(\text{PF}_6)_2$ and $\text{Ir}[\text{dF}(\text{CF}_3)\text{ppy}]_2(\text{dtbbpy})\text{PF}_6$ were prepared according to the procedures of Yoon¹⁵⁰ and Weaver¹⁵¹ respectively. The photocatalyst $[\text{Au}_2(\mu\text{-dppm})_2]\text{Cl}_2$ was obtained according to the literature.¹⁵² All other gold complexes were commercially available and used as received.

Chromatographic purifications of products were accomplished using force-flow chromatography (FC) on Davisil (LC60A) SI 60 Å (40 – 63 μm) silica gel. Thin layer chromatography (TLC) was performed on Merck 60 F254 silica gel plates. Filtrations through Celite[®] were performed using Hyflo Super Cel from Fluka.

¹H NMR spectra were recorded on a Bruker 400 AVANCE or 300 AVANCE (400 and 300 MHz respectively) and are calibrated with residual CDCl₃ protons signals at δ 7.26 ppm. ¹³C NMR spectra were recorded on a Bruker 400 AVANCE or 300 AVANCE (100 and 75 MHz respectively) and are calibrated with CDCl₃ signal at δ 77.00 ppm. ³¹P and ¹⁹F spectra were recorded on a Bruker 400 AVANCE. Data are reported as follows: chemical shift (δ ppm), multiplicity (s = singlet, d = doublet, t = triplet, q = quartet, qt = quintuplet, m = multiplet, bs = broad signal), coupling constant (Hz) and integration. IR spectra were recorded on a Bruker Tensor 27 (ATR diamond) and are reported in terms of frequency of absorption (cm⁻¹). High resolution mass spectrometry (HRMS) analyses were performed on a microTOF-ESI (Bruker) or LTQ-orbitrap-ESI or LTQ-orbitrap-APCI (Thermo scientific).

¹⁵⁰ Ishay, M. A.; Lu, Z.; Yoon, T. P. *J. Am. Chem. Soc.* **2010**, *132*, 8572.

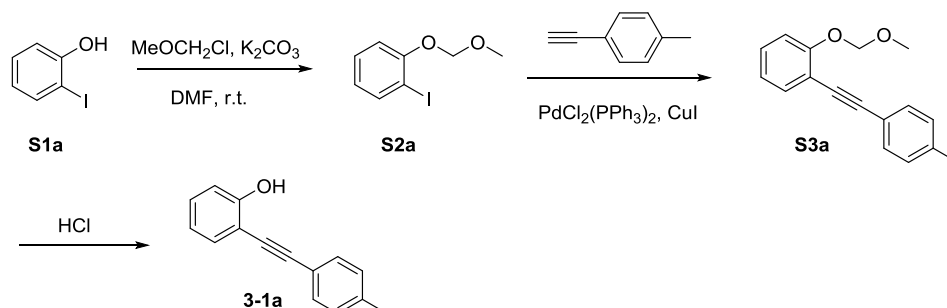
¹⁵¹ Singh, A.; Teegardin, K.; Kelly, M.; Prasad, K. S.; Krishnan, S.; Weaver, J. D. *J. Organomet. Chem.* **2015**, *776*, 51.

¹⁵² Revol, G.; McCallum, T.; Morin, M.; Gagosz, F.; Barriault, L. *Angew. Chem. Int. Ed.* **2013**, *52*, 13342.

5.2 Substrate Synthesis

5.2.1 Synthesis of 2-(Phenylethynyl)phenol Derivatives 3-1

General Procedure 1 (GP1): *Synthesis of 2-(Phenylethynyl)phenol 3-1a.*¹⁵³



MOMCl (1.1 g, 13.6 mmol, 1.5 equiv.) was added to a mixture of 2-iodo phenol **S1a** (2 g, 9.1 mmol, 1 equiv.) and K₂CO₃ (5.0 g, 36.36 mmol, 4 equiv.) in DMF (8 mL). The mixture was stirred at room temperature for 2 hours. The completion of the reaction was monitored by TLC (Pent/Et₂O: 9/1). The solution was diluted with diethyl ether (100 mL) and 60 mL of water were added. The layers were separated and the aqueous phase was extracted with diethyl ether (3 × 30 mL). The combined organic layers were washed with brine, dried over MgSO₄, filtered and concentrated under reduced pressure to afford the iodide **S2a** (2.4 g, quant). The latter was engaged without further purification in the next step. To a stirred solution of 1-ethynyl-4-methylbenzene (1.2 g, 10.0 mmol, 1.1 equiv.) and **S2a** (2.4 g, 9.1 mmol, 1.0 equiv.) in triethylamine (90 mL) were added PdCl₂(PPh₃)₂ (126.3 mg, 0.18 mmol, 2 mol%) and CuI (34.3 mg, 0.18 mmol, 2 mol%). The mixture was stirred at 65°C until complete consumption of **S2a** was observed by TLC (Pent/Et₂O: 9/1). The reaction mixture was cooled to room temperature, diethyl ether was added (50 mL) and the mixture was filtered through a plug of cotton wool. After removal of the solvent, the residue was purified by silica gel chromatography (Pent/Et₂O: 9/1) to afford **S3a** (2.07 g, 90%). The deprotection of MOM was conducted by addition of aqueous HCl (0.85 mL, 9.0 mmol, 6N) to a solution of **S3a** (2.07 g, 8.2 mmol) in MeOH (15 mL). The reaction mixture was stirred until the deprotection was completed. The mixture was diluted with water (50 mL) and diethyl ether (30 mL). The layers were separated and the aqueous phase was extracted with diethyl ether (3 × 30 mL). The combined organic layers were washed with brine, dried over MgSO₄, filtered

¹⁵³ Hashmi, A. S. K.; Ramamurthi, T. D.; Rominger, F. *Adv. Synth. Catal.* **2010**, 352, 971.

and concentrated under reduced pressure. The residue was purified by flash chromatography (Pent/Et₂O: 9/1) to afford **3-1a** (1.45 g, 85%) as a yellow solid.

5.2.2 Synthesis of (Iodoethynyl)benzene Derivatives 3-2

General Procedure 2 (GP2): Synthesis of (Iodoethynyl)benzene **3-2a**.¹⁵⁴

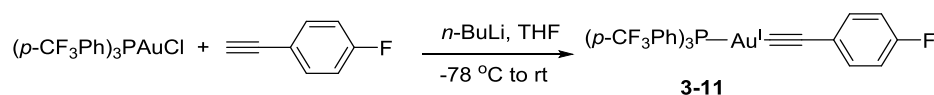
Iodine (1.1 g, 4.3 mmol) and morpholine (1.0 g, 1 ml, 11.7 mmol) were dissolved in benzene (5 ml) and the solution was stirred at RT for 30 min. Phenylacetylene (400 mg, 3.96 mmol) in benzene (5 ml) was added dropwise and the mixture was stirred at 45 °C for 24 h. The suspension was filtered and the residue was washed with Et₂O (2 × 20 ml). The combined organic layers were washed with saturated aqueous solutions of NH₄Cl (20 ml) and NaHCO₃ (20 ml) and H₂O (20 ml). The organic layer was dried over MgSO₄ and filtered. The solvent was removed under reduced pressure and the crude product was purified by column chromatography (silica gel, petroleum ether or *n*-pentane as eluent) to afford (iodoethynyl)benzene **3-2a** (0.82 g, 3.6 mmol, 92%) as colorless oil.

General Procedure 3 (GP3): Synthesis of Iodoalkynes **3-2f**.¹⁵⁵

To a stirred solution of 1-ethynyl-4-methylbenzene (232.3 mg, 2.0 mmol) in MeCN (4.0 mL) was added NIS (495 mg, 2.2 mmol) and DBU (0.318 mL, 2.2 mmol). The mixture was stirred at room temperature for 5 min. The reaction mixture was poured into water and then extracted with Et₂O (3 × 20 mL). The combined organic phase was washed with saturated brine (10 mL), dried over MgSO₄ and filtered. The solvent was removed under reduced pressure and the crude product was purified by flash chromatography (silica gel, petroleum ether or *n*-pentane as eluent) to give **3-2f** (411 mg, 85%) as a light red liquid.

5.2.3 Synthesis of Gold(I) Acetylide 3-11

Gold(I) acetylide was synthesized according a described procedure.¹⁵⁶



¹⁵⁴ Hashmi, A. S. K.; Döpp, R.; Lothschütz, C.; Rudolph, M.; Riedel, D.; Rominger, F. *Adv. Synth. Catal.* **2010**, 352, 1307.

¹⁵⁵ (a) Gao, Y.; Yin, M.; Wu, W.; Huang H.; Jiang, H. *Adv. Synth. Catal.* **2013**, 355, 2263. (b) Li, M.; Li, Y.; Zhao, B.; Liang F.; Jin, L.-Y. *RSC Adv.* **2014**, 4, 30046.

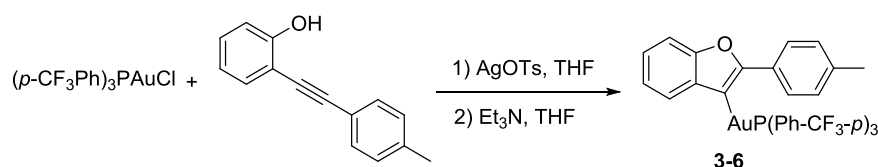
¹⁵⁶ Leyva-Pérez, A.; Doménech-Carbó, A.; Corma, A. *Nat. Commun.* **2015**, 6703.

A solution of *n*-BuLi (2.5 M in *n*-hexane, 0.1 ml, 0.25 mmol) was added over a solution of the 1-ethynyl-4-fluorobenzene (0.25 mmol) in dry THF (1 ml) at -78 °C. The mixture was magnetically stirred at -78 °C for 10 min and then added over a dispersion of the corresponding Au(I) salt (*p*-CF₃Ph)₃PAuCl (140 mg, 0.2 mmol) in dry THF (0.5 ml) at -78 °C. After stirring for 5 min, the mixture was left to warm up to room temperature and then magnetically stirred for 2 h. Then wet DCM (25 ml) was added, the mixture was stirred for 5 minutes and passed through a pad of Celite[®] under vacuum. If the resulting filtrates were still turbid a second filtration was performed. The DCM clear solution was concentrated under vacuum at room temperature and then *n*-hexane (25 ml) was added. The phosphine Au(I) acetylide precipitated and then the *n*-hexane was decanted. The solid was washed with two additional portions of *n*-hexane (25 ml) and finally dried under vacuum.

White solid, 93.9 mg, 60%. ¹H NMR (400 MHz, CD₃CN) δ 7.84-7.76 (m, 12H), 7.34 (q, *J* = 7.2, 3.2 Hz, 2H), 7.02 (t, *J* = 8.8 Hz, 2H); ¹³C NMR (101 MHz, CD₃CN) δ 136.1 (d, *J*_{C-P} = 14.6 Hz), 134.6 (d, *J*_{C-P} = 8 Hz), 134.3, 134.0, 133.7 (d, *J*_{C-P} = 10.4 Hz), 127.3 (m), 126.8 (m), 126.1, 123.4, 116.0 (q, *J*_{C-F} = 20.3 Hz); ¹⁹F NMR (376 MHz, CD₃CN) δ -63.77 (CF₃), -115.08 (F); ³¹P NMR (162 MHz, CD₃CN) δ 42.19; HRMS (ESI) calc. for C₂₉H₁₆AuF₁₀NaP⁺ [M+Na]⁺: 805.0388, found 805.0402.

5.2.4 Synthesis of the Vinylgold(I) Complexes 3-6

Vinylgold(I) compound was synthesized according a described procedure.¹⁵⁷



In a 25-mL *Schlenk* tube 112 mg (161 μmol) (*p*-CF₃Ph)₃PAuCl and 45 mg (161 μmol) AgOTs were dissolved in 6 mL of dry THF and stirred for 1 h. Then, 150 μL (1076 μmol) triethylamine and 31.9 mg (153 μmol) alkyne-phenol **3-1a** were added. The reaction mixture was stirred for 16 h at room temperature, filtered over a small column of basic aluminium oxide and washed with 50 mL of dry THF. The solvent was removed on the rotary evaporator without heating.

White solid, 115 mg, 82%. ¹H NMR (400 MHz, CD₃CN) δ 8.34 (d, *J* = 8.4 Hz, 2H), 8.06-8.01 (m, 12 H), 7.76-7.74 (m, 1H), 7.45 (d, *J* = 8.0 Hz, 1H), 7.17-7.07 (m, 4H), 2.39 (s,

¹⁵⁷ Hashmi, A. S. K.; Ramamurthi, T. D.; Rominger, F. *Adv. Synth. Catal.* **2010**, 352, 971.

3H); ^{13}C NMR (101 MHz, CD_3CN) δ 156.0, 140.0, 137.6, 136.1 (d, $J_{\text{C-P}} = 8.4$ Hz), 135.7, 135.2, 134.5, 132.5, 129.5, 127.2 (q, $J_{\text{C-F}} = 4.4$ Hz), 126.1, 125.1, 123.7, 123.4, 122.0, 110.8, 21.3; ^{19}F NMR (376 MHz, CD_3CN) δ -63.98; ^{31}P NMR (162 MHz, CD_3CN) δ 46.04; HRMS (ESI) calc. for $\text{C}_{36}\text{H}_{23}\text{AuF}_9\text{NaOP}^+ [\text{M}+\text{Na}]^+$: 893.0901, found 893.0904.

5.3 General Procedure for the Alkylative Cyclization

General Procedure for Optimization Studies

The photocatalyst (1 mol%), the gold(I) complex (5 mol %), K_2CO_3 , iodoalkynes **3-2a** and *o*-alkynylphenol **3-1a** (0.1 mmol) were introduced in a *Schlenk* tube equipped with a magnetic stirring bar in which MeCN (2 mL) was added. The mixture was degassed using three freeze pump-thaw cycles and purged with Ar, then irradiated with blue LEDs light for 16 h (unless mentioned). The stirring speed is equal to or more than 1200 rpm. The reaction was quenched with Et_2O (3 mL) and a 2 M HCl solution (3 mL) and the solution was extracted by Et_2O (3×5 mL). The combined organic layer was dried over MgSO_4 , filtered and concentrated under reduced pressure to give the crude product. Yields are determined by ^1H NMR using 1,3,5-trimethoxybenzene as an internal standard.

General Procedure 4 (GP4): Alkylative Cyclization of *o*-Alkynylphenols with Iodoalkynes.

The photocatalyst $\text{Ir}[d\text{F}(\text{CF}_3)\text{ppy}]_2(\text{dtbbpy})\text{PF}_6$ (1 mol%), the gold(I) complex (*p*- CF_3Ph) $_3\text{PAuCl}$ (5 mol %), K_2CO_3 (2.5 equiv), appropriate iodoalkyne **3-2** (0.15 mmol) and the *o*-alkynylphenol derivative **3-1** (0.1 mmol) were introduced in a *Schlenk* tube equipped with a magnetic stirring bar in which MeCN (2 mL) was added. The mixture was degassed using three freeze pump-thaw cycles and purged with Ar, then irradiated with blue LEDs light (a very simple irradiating setup used as depicted in pictures below) for 16 h (unless mentioned). The stirring speed is equal to or more than 1200 rpm. The reaction was quenched with Et_2O (3 mL) and a 2 M HCl solution (3 mL) and the solution was extracted by Et_2O (3×5 mL). The combined organic layer was dried over MgSO_4 , filtered and concentrated under reduced pressure to give the crude product. The residue was purified by FC on silica gel to afford the desired product.

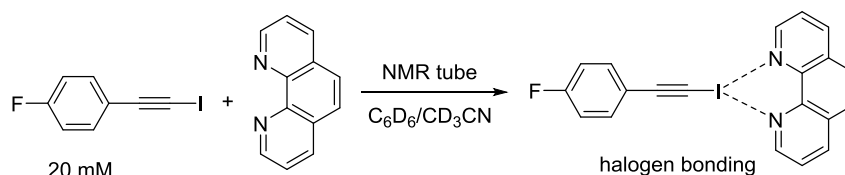


The simple photoreactor which is equipped with LED stripes ($\lambda_{\max} = 470 \text{ nm}$) on a beaker (the diameter is 7.5 cm, the height is 9.5 cm). An aluminum paper is put between the stirring plate and the beaker to reflect the light.

5.4 Investigation of Mechanism

5.4.1 Investigation of Halogen Bonding

a) NMR Titration Experiments of Iodoalkyne and Phen in C_6D_6 and CD_3CN



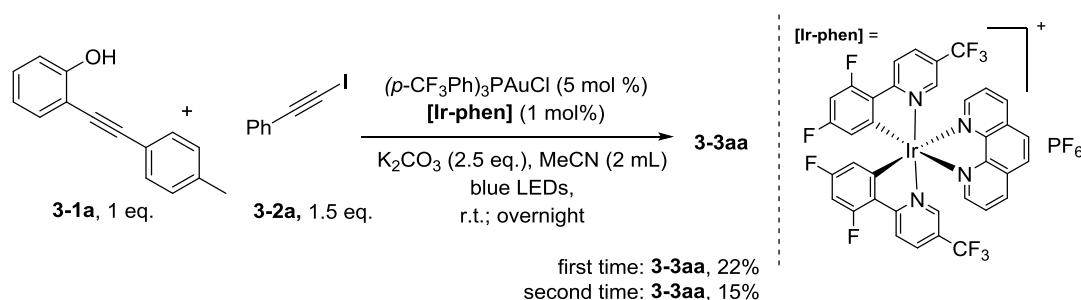
Entry	c (Phen) (mM)	$\Delta\delta$ ^{19}F shift (ppm) in C_6D_6	$\Delta\delta$ ^{19}F shift (ppm) in CD_3CN
1	0	0	0
2	10	0.02	0
3	20	0.03	0
4	50	0.15	0
5	100	0.32	0.01
6	150	0.35	0.04

Adding 17.7 mg of iodoacetylene into 3.6 mL C_6D_6 , get a $c_0 = 20 \text{ mM}$ 1-fluoro-4-(iodoethynyl)benzene host solution, divided in 6 small vials. Each vial was added by certain quantity 1,10-phenanthroline, to get the desired concentration of 1-fluoro-4-(iodoethynyl)benzene/1,10-phenanthroline pair solutions. Choosing the 1-fluoro-4-

(iodoethynyl)benzene as the halogen donor compound as the *para*-F group can increase the halogen donor property of iodoacetylene, moreover the chemical shift will be easily observed in ^{19}F NMR because of the F lable. The 1-fluoro-4-(iodoethynyl)benzene concentration was maintained constant as 20 mM. ^{19}F NMR chemical shifts are reported relative to fluorobenzene, which was added in traces as reference ($\delta = -113.1$ ppm). After that, NMR titration experiments in CD_3CN were performed and the chemical shifts were compared (Table 3-5).

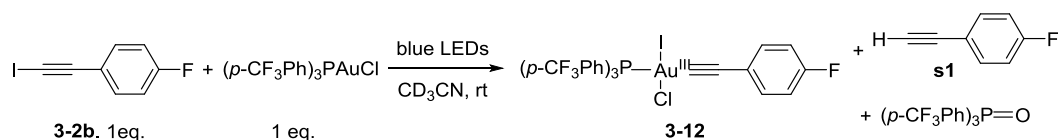
b) Synthesize of the [Ir-phen] Photocatalyst

Moreover, the [Ir-phen] photocatalyst was synthesized according to the procedure reported by Weaver.¹⁵⁸ The spectroscopic data match those previously reported in Weaver's literature. ^1H NMR (400 MHz, Acetone) δ 9.00 (dd, 2H, $J = 8.0, 1.2$ Hz), 8.67 (dd, 2H, $J = 5.2, 1.2$ Hz), 8.61 (dd, 2H, $J = 8.4, 2.4$ Hz), 8.44 (s, 2H), 8.33 (dd, 2H, $J = 8.8, 2.0$ Hz), 8.14 (dd, 2H, $J = 8.4, 5.2$ Hz), 7.85-7.84 (m, 2H), 6.90 (ddd, 2H, $J = 12.2, 9.6, 2.4$ Hz), 6.06 (dd, 2H, $J = 8.4, 2.4$ Hz); ^{19}F NMR (376 MHz, Acetone- d_6) δ -63.69 (s, 6F), -72.66 (d, 6F, $J = 703.1$ Hz), -104.88 (q, 2F, $J = 10.0, 9.0$ Hz), -108.12 (td, 2F, $J = 12.4, 2.6$ Hz).



5.4.2 Study on Gold(III) Acetylide Intermediate 12 of Type B

a) NMR Monitoring Experiment of 3-2b and Au(I) Complex

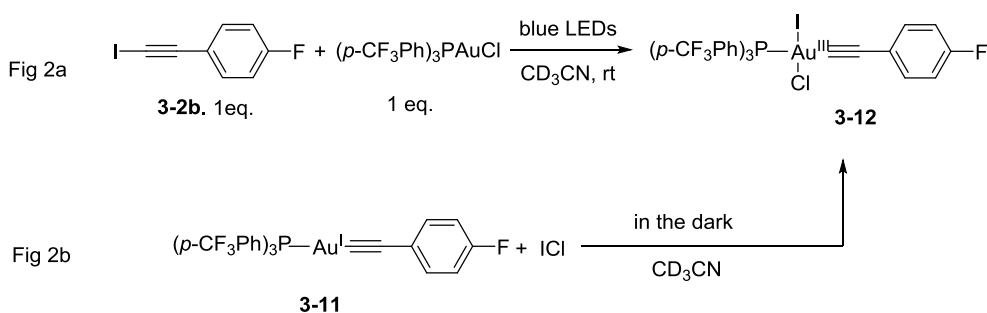


Iodoalkyne **3-2b** (0.055 mmol, 1.0 equiv.) was treated with a stoichiometric amount of (*p*- CF_3Ph) $_3\text{PAuCl}$ (38.7 mg, 0.055 mmol, 1.0 equiv.) in 0.6 mL of CD_3CN in a screw-cap NMR tube, protected by aluminium paper in advance. The CD_3CN solution of 85% phosphoric acid

¹⁵⁸ Singh, A.; Teegardin, K.; Kelly, M.; Prasad, K. S.; Krishnan, S.; Weaver, J. D. *J. Organomet. Chem.* **2015**, 776, 51.

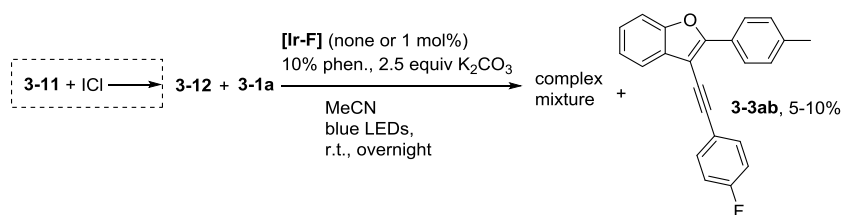
in a sealed melting point tube was used as the standard for ^{31}P -NMR ($\delta = 2.3$ ppm). The NMR tube capped with a fluoropolymer septum was evacuated and refilled with argon three times. No reaction was observed after addition of **3-2b** and $(p\text{-CF}_3\text{Ph})_3\text{PAuCl}$, still no reaction was observed after 60 min in the dark. After that, the tube with the reaction mixture was irradiated with blue LEDs for 0 to 40 min. The corresponding reaction mixtures were monitored by ^1H -NMR, ^{19}F NMR and ^{31}P -NMR analysis.

b) Cross Checking of the Gold(III) Acetylide Structure 3-12



To support the plausible formation of gold(III) acetylide intermediate **3-12**, gold(I) acetylide **3-11** (18.8 mg, 0.024 mmol) and ICl (1.0 M solution in DCM, 0.024 mL) were added in 0.6 mL of CD_3CN in a screw-cap NMR tube, protected by aluminium paper in advance. The NMR tube was capped with a fluoropolymer septum. After that, the tube with the reaction mixture was in the dark. The corresponding reaction mixtures were monitored by ^{19}F -NMR and ^{31}P -NMR analysis.

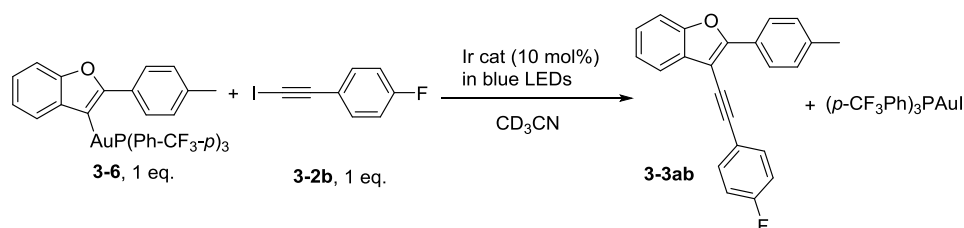
c) Generation of the Possible Gold(III) acetylide Intermediate 3-12 under Standard Condition



Gold(I) acetylide **3-11** (52 mg, 0.067 mmol, 0.67 eq.) and ICl (1.0 M solution in DCM, 0.067 mmol, 0.67 eq.) were introduced in a *Schlenk* tube equipped with a magnetic stirring bar in which MeCN (2 mL) was added, the tube with the reaction mixture was stirred in the dark for 30 min (if using pure ICl, the stirring time will be very short), then photocatalyst $\text{Ir}[d\text{F}(\text{CF}_3)\text{ppy}]_2(\text{dtbbpy})\text{PF}_6$ (1.2 mg, 1.0 mol% or none), K_2CO_3 (34.6 mg, 0.25 mmol, 2.5 equiv), and *o*-alkynylphenol **3-1a** (20.8 mg, 0.1 mmol, 1 eq.) were added into the *Schlenk*

tube. The mixture was degassed using three freeze pump-thaw cycles then was irradiated with blue LEDs light for 16 h. The stirring speed is equal or more than 1200 rpm. The reaction was quenched with Et₂O (3 mL) and a 2 M HCl solution (3 mL) and the solution was extracted by Et₂O (3 × 5 mL). The combined organic layer was dried over MgSO₄, filtered and concentrated under reduced pressure to give the crude product. The residue was purified by FC on silica gel to afford the desired product, 8% (5% without **[Ir-F]**) of final product can be obtained.

5.4.3 NMR Monitoring Experiment of the Reaction Between Vinylgold(I) **3-6** and **3-2b**



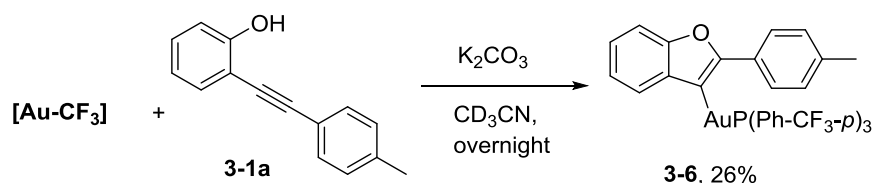
Tube A: The vinylgold(I) compound **3-6** (10 mg, 0.012 mmol, 1.0 equiv.) was treated with a stoichiometric amount of iodoalkyne **3-2b** (2.9 mg, 0.012 mmol, 1.0 equiv.) in 0.6 mL of CD₃CN in an NMR tube, protected by aluminium paper in advance. Add a small stirring bar into the NMR tube, stirring in blue LEDs light for 30 min. Add trimethoxybenzene (2.0 mg, 0.012 mmol) as internal standard into Tube A, do ¹H-NMR, ¹⁹F-NMR and ³¹P-NMR analysis. After that, Tube A with the reaction mixture was irradiated with blue LEDs for 2.5 h and 3.5 h, do ¹H-NMR, ¹⁹F-NMR and ³¹P-NMR analysis, again. The yields are the averages of two times.

Tube B: The vinylgold(I) compound **3-6** (10 mg, 0.012 mmol, 1.0 equiv.) and photocatalyst Ir[dF(CF₃)ppy]₂(dtbbpy)PF₆ (1.3 mg, 10 mol%) was treated with a stoichiometric amount of iodoalkyne **3-2b** (2.9 mg, 0.012 mmol, 1.0 equiv.) in 0.6 mL of CD₃CN in a NMR tube, protected by aluminium paper in advance. Add a small stirring bar into the NMR tube, stirring in blue LEDs light for 30 min. Add trimethoxybenzene (2.0 mg, 0.012 mmol) as internal standard into Tube B, do ¹H-NMR, ¹⁹F-NMR and ³¹P-NMR analysis. After that, Tube B with the reaction mixture was irradiated with blue LEDs for 2.5 h and 3.5 h, do ¹H-NMR, ¹⁹F-NMR and ³¹P-NMR analysis, again.

Tube C: The vinylgold(I) compound **3-6** (10 mg, 0.012 mmol, 1.0 equiv.) was treated with a stoichiometric amount of iodoalkyne **3-2b** (2.9 mg, 0.012 mmol, 1.0 equiv.) in 0.6 mL of CD₃CN in a NMR tube, protected by aluminium paper in advance. Add a small stirring bar into the NMR tube, stirring in blue LEDs light for overnight. Add trimethoxybenzene (2.0

mg, 0.012 mmol) as internal standard into Tube C, do $^1\text{H-NMR}$, $^{19}\text{F-NMR}$ and $^{31}\text{P-NMR}$ analysis. After comparing the pure $^1\text{H-NMR}$ spectrum of **3-3ab**, **3-4a** and **3-7**, it shows that the generated **3-3ab** is 33% yield, accompanied by 20% of **3-4a** and 35% of protodeauration product **3-7**.

5.4.4 Formation of Vinylgold(I) **3-6** under Standard Conditions



Tube D: Phenol **1a** (4 mg, 0.019 mmol, 1.0 equiv.) and K_2CO_3 (6.6 mg, 2.5 equiv.) were treated with a stoichiometric amount of $(p\text{-CF}_3\text{Ph})_3\text{PAuCl}$ (13.4 mg, 0.019 mmol, 1.0 equiv.) in 0.6 mL of CD_3CN in a NMR tube, protected by aluminium paper in advance. Add a small stirring bar into the NMR tube, stirring it for overnight in the dark. Add 1,3,5-trimethoxybenzene (0.019 mmol) as internal standard into Tube D, do $^1\text{H-NMR}$, $^{19}\text{F-NMR}$ and $^{31}\text{P-NMR}$ analysis, the formation of vinylgold(I) **6** was observed by NMR in 26% yield.

5.4.5 Fluorescence Quenching Study

Emission intensities were recorded on a Jasco FP-6200 spectrofluorometer. Dry acetonitrile was degassed by argon bubbling for 30 minutes before using. The complex $\text{Ir}[(\text{dF}(\text{CF}_3)\text{ppy})_2(\text{dtbbpy})](\text{PF}_6)$ was excited at 370 nm and the emission spectra were recorded between 400 and 600 nm. In a typical experiment, 3 μM solutions of $\text{Ir}[(\text{dF}(\text{CF}_3)\text{ppy})_2(\text{bpy})](\text{PF}_6)$ in acetonitrile were prepared with the appropriate concentration of quencher **6** in a 1.0 cm quartz cuvette and covered. After degassing with a stream of argon for 10 minutes, the emission spectrum of the sample was recorded.

The Stern-Volmer plot was done according the following equation: $\frac{I_f^0}{I_f} = 1 + k_q t_0 \cdot [Q]$.

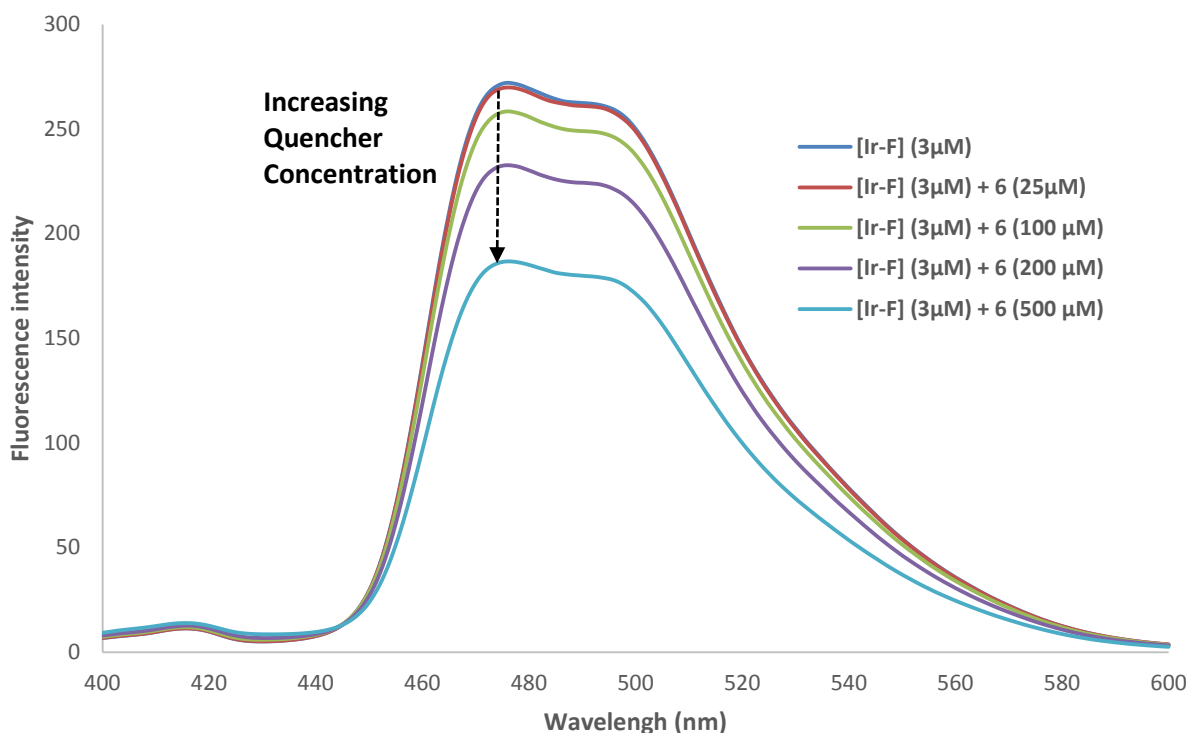


Figure 3-2. Fluorescence spectra, fluorescence quenching studies of **[Ir-F]** by vinylgold(I) **3-6** which exhibited a significant decrease of fluorescence intensity upon gradual addition of **3-6**. This work was done by Dr. Vincent Corcé.

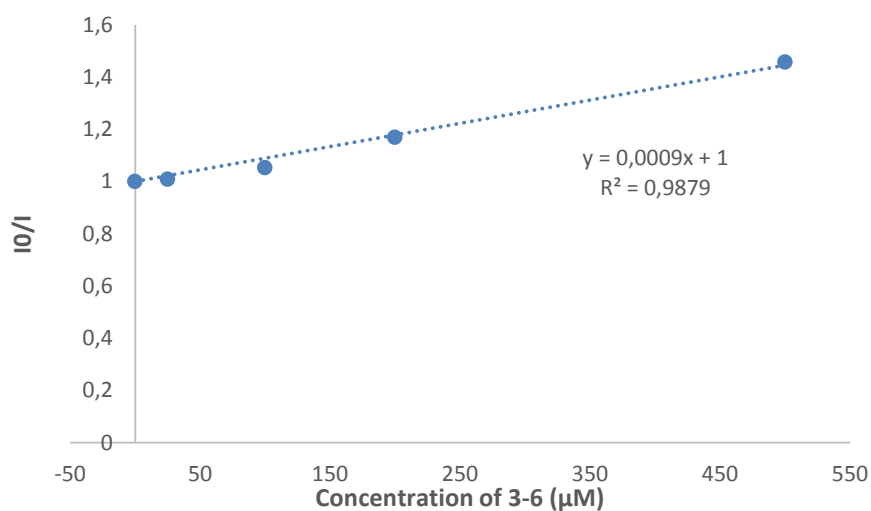


Figure 3-3. Stern-Volmer plot, A plot of the intensity ratio I^0/I versus the concentration of **3-6** showed a linear relation, following the Stern–Volmer law which allowed to determine a bimolecular quenching constants $k_q = 3.8 \cdot 10^8 \text{ l.mol}^{-1} \cdot \text{s}^{-1}$. This work was done by Dr. Vincent Corcé.

5.4.6 Cyclic Voltammetry

The voltammetric measurements of **3-2a** and **3-2a-Br** were recorded with a three electrodes apparatus (Glassy carbon, platinum plate, and saturated calomel were used as working, counter, and reference electrodes, respectively) in degassed CH₃CN with Bu₄NPF₆ (100 mM) as support electrolyte. Measurements were monitored on an AutoLab PSTAT10 electrochemical workstation. Cyclic voltammetry (CV) was used to estimate the redox potentials. The CVs were obtained with a step potential of 0.002 V at a scan rate of 0.1 V s⁻¹.

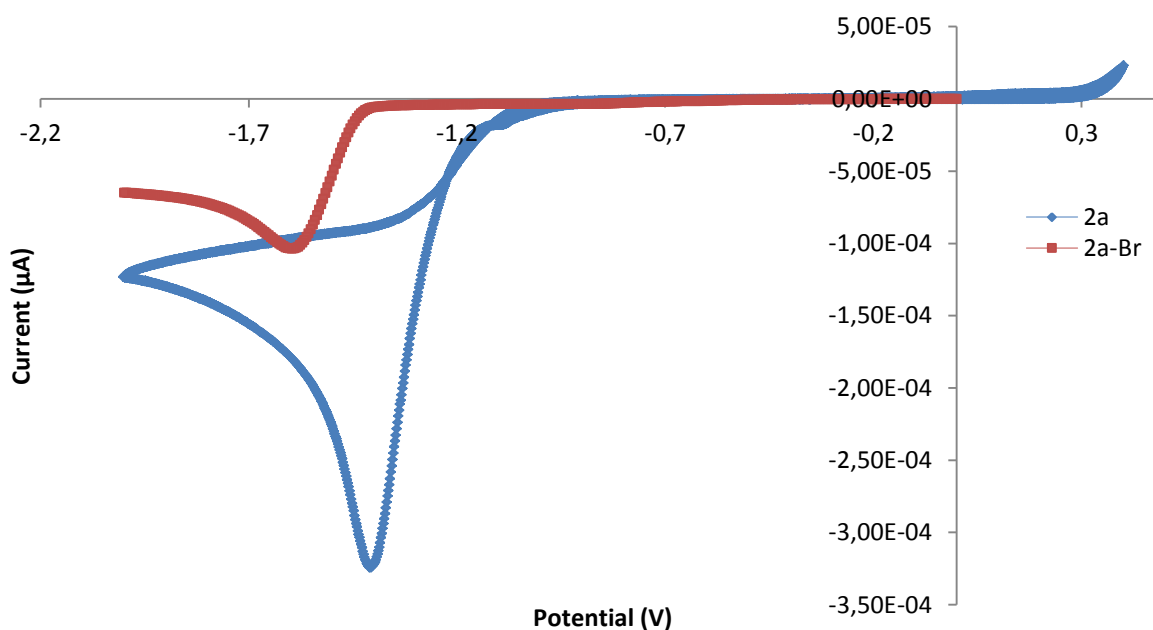


Figure S11. Cyclic Voltammetry of iodoethynyl benzene ($E_{1/2}(\mathbf{3-2a}) = -1.39$ V vs SCE) and bromoethynyl benzene ($E_{1/2}(\mathbf{3-2a-Br}) = -1.60$ V vs SCE).

5.4.7 Fluorescence Properties of Benzofuran 3-3aa

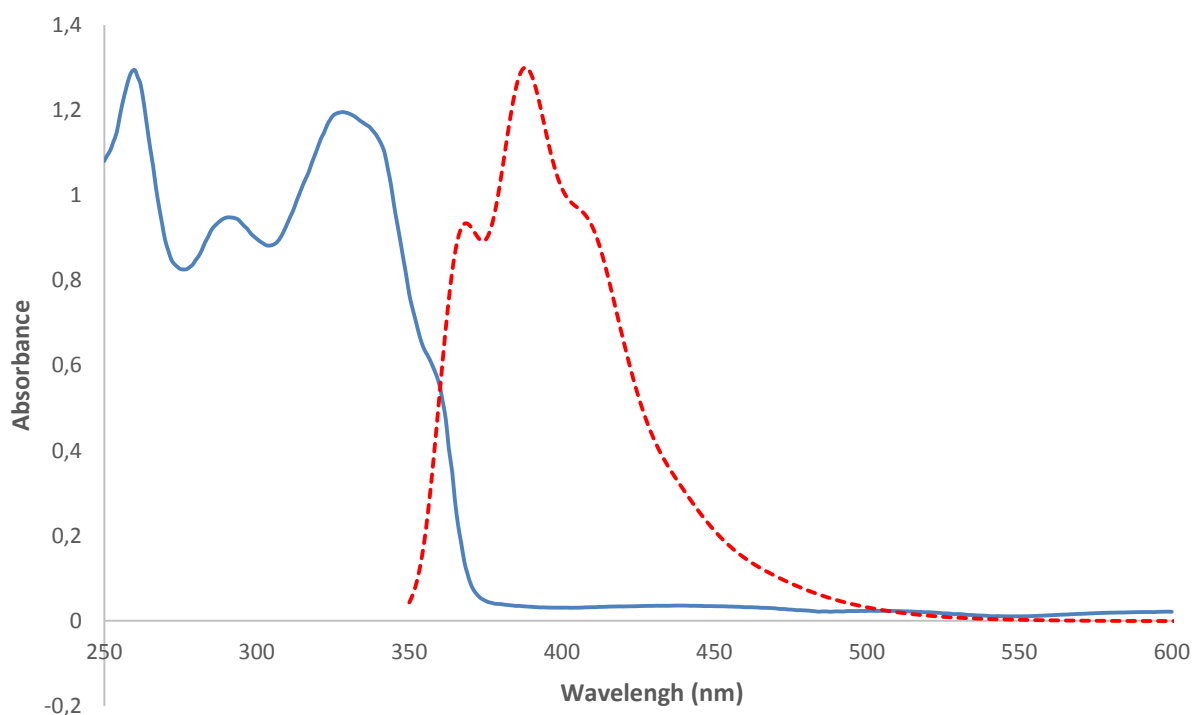
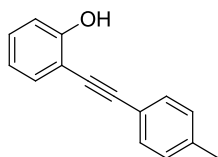


Figure SI4. UV-Vis absorption spectra of **3-3aa** (blue curve) and emission spectra (red curve).

Excitation at 330 nm, the maximum absorption shift is about 330 nm, and the maximum emission shift is about 390 nm, so the Stokes Shift is about 60 nm.

5.5 Compound Characterizations

2-(*p*-Tolylethynyl)phenol (**3-1a**)

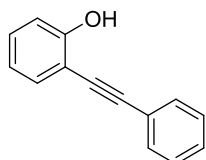


Following general procedure GP1 with 2-iodophenol (2 g, 9.25 mmol) and 4-ethynyltoluene (1.18 g, 10.2 mmol) to afford **3-1a** (1.2 g, 77% over three steps). The spectroscopic data match those previously reported in the literature.¹⁵⁹ ¹H NMR (300 MHz, CDCl₃) δ 7.45-7.40

¹⁵⁹ Martínez, C.; Álvarez, R.; Aurrecoechea, J. M. *Org. Lett.* **2009**, *11*, 1083.

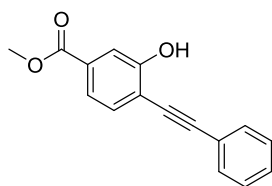
(m, 3H), 7.28-7.24 (m, 1H), 7.19-7.17 (m, 2H), 6.98 (bdd, $J = 8.4, 1.2$ Hz, 1H), 6.90 (td, $J = 7.5, 1.2$ Hz, 1H), 5.83 (s, 1H), 2.39 (s, 3H).

2-(Phenylethynyl)phenol (**3-1b**)



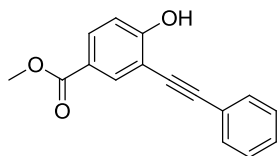
Following general procedure GP1 with 2-iodophenol (440 mg, 2 mmol) and phenylacetylene (225 mg, 2.2 mmol) to afford **3-1b** (287 mg, 74% over three steps). The spectroscopic data match those previously reported in the literature.¹⁶⁰ ¹H NMR (300 MHz, CDCl₃) δ 7.57-7.54 (m, 2H), 7.44 (dd, $J = 7.8, 1.8$ Hz, 1H), 7.40-7.37 (m, 3H), 7.31-7.26 (m, 1H), 7.01 (dd, $J = 8.1, 0.9$ Hz, 1H), 6.92 (td, $J = 7.5, 1.2$ Hz, 1H), 5.85 (s, 1H).

Methyl 3-hydroxy-4-(phenylethynyl)benzoate (**3-1c**)



Following general procedure GP1 with methyl 3-hydroxy-4-iodobenzoate (556 mg, 2 mmol) and phenylacetylene (224.7 mg, 2.2 mmol) to afford **3-1c** (454 mg, 90% over three steps). The spectroscopic data match those previously reported in the literature.¹⁶¹ ¹H NMR (300 MHz, CDCl₃) δ 7.65 (d, $J = 1.5$ Hz, 1H), 7.61-7.54 (m, 3H), 7.48 (d, $J = 8.1$ Hz, 1H), 7.40-7.38 (m, 3H), 5.95 (s, 1H), 3.92 (s, 3H);

Methyl 4-hydroxy-3-(phenylethynyl)benzoate (**3-1d**)



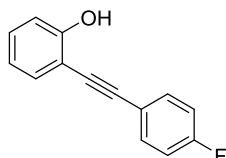
Following general procedure GP1 with methyl 4-hydroxy-3-iodobenzoate (556 mg, 2 mmol) and phenylacetylene (224.7 mg, 2.2 mmol) to afford **3-1d** (413.7 mg, 82% over three steps).

¹⁶⁰ Hashmi, A. S. K.; Ramamurthi, T. D.; Rominger, F. *Adv. Synth. Catal.* **2010**, 352, 971.

¹⁶¹ Xia, Z.; Khaled, O.; Mouriès-Mansuy, V.; Ollivier, C.; Fensterbank, L. *J. Org. Chem.* **2016**, 81, 7182.

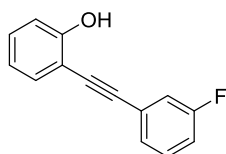
The spectroscopic data match those previously reported in the literature.¹⁶¹ ¹H NMR (300 MHz, CDCl₃) δ 8.15 (d, *J* = 2.1 Hz, 1H), 7.96 (dd, *J* = 8.7, 2.1 Hz, 1H), 7.57-7.53 (m, 2H), 7.40-7.38 (m, 3H), 7.02 (d, *J* = 8.7 Hz, 1H), 6.26 (s, 1H), 3.90 (s, 3H).

2-((4-Fluorophenyl)ethynyl)phenol (**3-1e**)



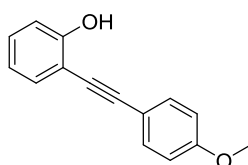
Following general procedure GP1 with 2-iodophenol (440 mg, 2 mmol) and 1-ethynyl-4-fluorobenzene (264 mg, 2.2 mmol) to afford **3-1e** (318 mg, 75% over three steps). The spectroscopic data match those previously reported in the literature.¹⁶² ¹H NMR (300 MHz, CDCl₃) δ 7.55-7.51 (m, 2H), 7.41 (dd, *J* = 5.7, 1.2 Hz, 1H), 7.29-7.26 (m, 1H), 7.08 (t, *J* = 6.6 Hz, 1H), 6.99-6.97 (m, 1H), 6.91 (td, *J* = 5.7, 0.6 Hz, 1H), 5.78 (s, 1H).

2-((3-Fluorophenyl)ethynyl)phenol (**3-1f**)



Following general procedure GP1 with 2-iodophenol (440 mg, 2 mmol) and 1-ethynyl-3-fluorobenzene (264 mg, 2.2 mmol) to afford **3-1f** (340 mg, 80% over three steps). The spectroscopic data match those previously reported in the literature.¹⁶² ¹H NMR (300 MHz, CDCl₃) δ 7.42 (dd, *J* = 5.7, 1.2 Hz, 1H), 7.37-7.23 (m, 4H), 7.11-7.06 (m, 1H), 7.00 (dd, *J* = 6.3, 0.6 Hz, 1H), 6.92 (td, *J* = 5.7, 0.9 Hz, 1H), 5.76 (s, 1H).

2-((4-Methoxyphenyl)ethynyl)phenol (**3-1g**)

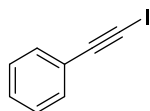


Following general procedure GP1 with 2-iodophenol (440 mg, 2 mmol) and 1-ethynyl-4-methoxybenzene (291mg, 2.2 mmol) to afford **3-1g** (292 mg, 65% over three steps). The

¹⁶² Sun, S.-X.; Wang, J.-J.; Xu, Z.-J.; Cao, L.-Y.; Shi, Z.-F.; Zhang, H.-L. *Tetrahedron* **2014**, *70*, 3798.

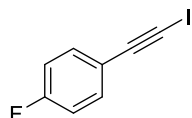
spectroscopic data match those previously reported in the literature.¹⁶³ ¹H NMR (400 MHz, CDCl₃) δ 7.82–7.79 (d, *J* = 8.8 Hz, 2H), 7.57–7.49 (m, 2H), 7.27–7.20 (m, 2H), 7.00–6.97 (d, *J* = 8.8 Hz, 2H), 6.89 (s, 1H), 3.87 (s, 3H).

(Iodoethynyl)benzene (**3-2a**)



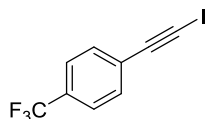
Following general procedure GP2 with phenylacetylene (400 mg, 3.96 mmol) to afford **3-2a** (0.82 g, 3.6 mmol, 92%). The spectroscopic data match those previously reported in the literature.¹⁶⁴ ¹H NMR (400 MHz, CDCl₃) δ 7.43–7.40 (m, 2H), 7.34–7.28 (m, 3H).

1-Fluoro-4-(iodoethynyl)benzene (**3-2b**)



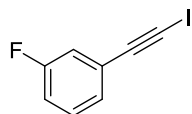
Following general procedure GP3 with 1-ethynyl-4-fluorobenzene (481 mg, 4.0 mmol) to afford **3-2b** (925 mg, 3.76 mmol, 94%). The spectroscopic data match those previously reported in the literature.¹⁶⁴ ¹H NMR (400 MHz, CDCl₃) δ 7.43–7.40 (m, 2H), 7.03–6.98 (m, 2H).

1-(Iodoethynyl)-4-(trifluoromethyl)benzene (**3-2c**)



Following general procedure GP3 with 1-ethynyl-4-(trifluoromethyl)benzene (681 mg, 4.0 mmol) to afford **3-2c** (1.07 g, 3.2 mmol, 90%). The spectroscopic data match those previously reported in the literature.¹⁶⁴ ¹H NMR (300 MHz, CDCl₃) δ 7.64–7.52 (m, 4H).

1-Fluoro-3-(iodoethynyl)benzene (**3-2d**)

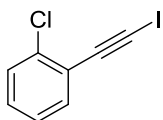


¹⁶³ Fischer, J.; Savage, G. P.; Coster, M. J. *Org. Lett.* **2011**, *13*, 3376.

¹⁶⁴ Xie, J.; Shi, S.; Zhang, T.; Mehrkens, N.; Rudolph, M.; Hashmi, A. S. K. *Angew. Chem. Int. Ed.* **2015**, *54*, 6046.

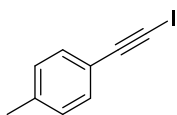
Following general procedure GP3 with 1-ethynyl-3-fluorobenzene (264 mg, 2.2 mmol) to afford **3-2d** (492 mg, 2 mmol, 90%). The spectroscopic data match those previously reported in the literature.¹⁶⁴ ¹H NMR (400 MHz, CDCl₃) δ 7.30–7.25 (m, 1H), 7.22–7.13 (m, 1H), 7.14–7.11 (m, 1H), 7.06–7.01 (m, 1H).

1-Chloro-2-(iodoethynyl)benzene (**3-2e**)



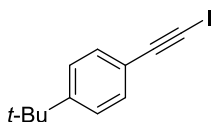
Following general procedure GP3 with 1-ethynyl-3-fluorobenzene (273 mg, 2.0 mmol) to afford **3-2e** (483 mg, 1.84 mmol, 92%). The spectroscopic data match those previously reported in the literature.¹⁶⁴ ¹H NMR (400 MHz, CDCl₃) δ 7.48–7.46 (m, 1H), 7.40–7.38 (m, 1H), 7.28–7.18 (m, 2H).

1-(Iodoethynyl)-4-methylbenzene (**3-2f**)



Following general procedure GP3 with 1-ethynyl-4-methylbenzene (232 mg, 2.0 mmol) to afford **3-2f** (445 mg, 1.84 mmol, 92%). The spectroscopic data match those previously reported in the literature.¹⁶⁴ ¹H NMR (400 MHz, CDCl₃) δ 7.38–7.36 (m, 2H), 7.34–7.32 (m, 2H), 1.30 (s, 9H).

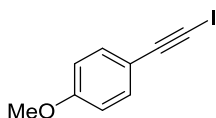
1-(*tert*-Butyl)-4-(iodoethynyl)benzene (**3-2g**)



Following general procedure GP3 with 1-(*tert*-butyl)-4-ethynylbenzene (316 mg, 2.0 mmol) to afford **3-2g** (517 mg, 1.82 mmol, 91%). The spectroscopic data match those previously reported in the literature.¹⁶⁵ ¹H NMR (400 MHz, CDCl₃) δ 7.38–7.36 (m, 2H), 7.34–7.32 (m, 2H), 1.30 (s, 9H).

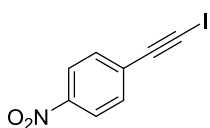
¹⁶⁵ Kilah, N. L.; Wise, M. D.; Serpell, C. J.; Thompson, A. L.; White, N. G.; Christensen, K. E.; Beer, P. D. *J. Am. Chem. Soc.* **2010**, *132*, 11893.

1-(Iodoethynyl)-4-methylbenzene (**3-2h**)



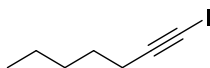
Following general procedure GP3 with 1-ethynyl-4-nitrobenzene (294 mg, 2.0 mmol) to afford **3-2h** (413 mg, 1.6 mmol, 80%). The spectroscopic data match those previously reported in the literature.¹⁶⁶ ¹H NMR (400 MHz, CDCl₃) δ 7.37 (d, *J* = 9.0 Hz, 2H), 6.83 (d, *J* = 9.0 Hz, 2H), 3.81 (s, 3H).

1-(Iodoethynyl)-4-nitrobenzene (**3-2i**)



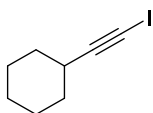
Following general procedure GP3 with 1-ethynyl-4-nitrobenzene (294 mg, 2.0 mmol) to afford **3-2i** (464 mg, 1.7 mmol, 85%). The spectroscopic data match those previously reported in the literature.¹⁶⁶ ¹H NMR (400 MHz, CDCl₃) δ 8.19 (d, *J* = 9.0 Hz, 2H), 7.57 (d, *J* = 9.0 Hz, 2H).

1-Iodohept-1-yne (**3-2j**)



Following general procedure GP3 with hept-1-yne (192 mg, 2.0 mmol) to afford **3-2j** (378 mg, 1.7 mmol, 85%). The spectroscopic data match those previously reported in the literature.¹⁶⁷ ¹H NMR (400 MHz, CDCl₃) δ 2.35 (t, *J* = 6.8 Hz, 2H), 1.55-1.48 (m, 2H), 1.40-1.27 (m, 4H), 0.90 (t, *J* = 7.2 Hz, 3H).

(Iodoethynyl)cyclohexane (**3-2k**)



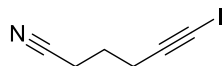
Following general procedure GP3 with ethynylcyclohexane (433 mg, 4.0 mmol) to afford **2k** (398 mg, 3.68 mmol, 92%). The spectroscopic data match those previously reported in the

¹⁶⁶ Dumele, O.; Wu, D.; Trapp, N.; Goroff, N.; Diederich F. *Org. Lett.* **2014**, *16*, 4722.

¹⁶⁷ Mader, S.; Molinari, L.; Rudolph, M.; Rominger, F.; Hashmi, A. S. K. *Chem. Eur. J.* **2015**, *21*, 3910.

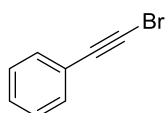
literature.¹⁶⁸ ¹H NMR (400 MHz, CDCl₃) δ 2.57-2.50 (m, 1H), 1.80-1.76 (m, 2H), 1.71-1.67 (m, 2H), 1.49-1.42 (m, 3H), 1.33-1.26 (m, 3H).

6-Iodohex-5-ynenitrile (**3-2l**)



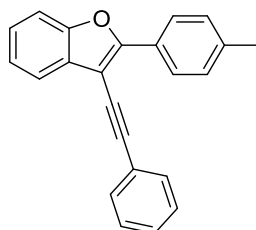
Following general procedure GP3 with hex-5-ynenitrile (186 mg, 2.0 mmol) to afford **3-2l** (368 mg, 1.68 mmol, 84%). The spectroscopic data match those previously reported in the literature.¹⁶⁹ ¹H NMR (400 MHz, CDCl₃) δ 2.57-2.54 (t, *J* = 6.8 Hz, 1H), 2.51-2.47 (t, *J* = 7.2 Hz, 1H), 1.91-1.84 (m, 2H).

(Bromoethynyl)benzene (**3-2a-Br**)



Following general procedure GP3 with ethynylbenzene (204 mg, 2.0 mmol) to afford **3-2a-Br** (340 mg, 1.88 mmol, 94%). The spectroscopic data match those previously reported in the literature.¹⁷⁰ ¹H NMR (300 MHz, CDCl₃) δ 7.47-7.44 (m, 2H), 7.35-7.28 (m, 3H).

3-(Phenylethynyl)-2-(*p*-tolyl)benzofuran (**3-3aa**)



Following general procedure GP4 with 2-(*p*-tolylethynyl)phenol **3-1a** (20.8 mg, 0.1 mmol) and (iodoethynyl)benzene **3-2a** (34.2 mg, 0.15 mmol). The crude product was purified by flash column chromatography (100:0 Pent:Et₂O) to afford **3-3aa** as a white solid (22 mg, 71%). Mp 117 °C. ¹H NMR (400 MHz, CDCl₃) δ 8.25 (d, *J* = 8.4 Hz 2H), 7.76-7.74 (m, 1H), 7.65-7.62 (m, 2H), 7.53-7.51 (m, 1H), 7.44-7.38 (3H), 7.37-7.30 (m, 4H), 2.44 (s, 3H); ¹³C NMR (101 MHz, CDCl₃) δ 156.7, 153.4, 139.4, 131.5, 130.0, 129.4, 128.5, 128.3, 127.5, 126.0, 125.1, 123.5, 123.3, 120.2, 111.1, 98.4, 96.5, 81.4, 21.5; IR (ATR) 2920, 2852, 2210,

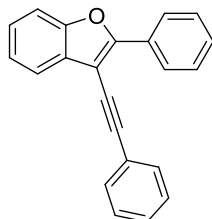
¹⁶⁸ Chen, S.-N.; Hung, T.-T.; Lin, T.-C.; Tsai, F.-Y. *Jnl Chinese Chemical Soc.* **2009**, *56*, 1078.

¹⁶⁹ Xie, L.-G.; Shaaban, S.; Chen, X.; Maulide, N. *Angew. Chem. Int. Ed.* **2016**, *55*, 12864.

¹⁷⁰ Li, M.; Li, Y.; Zhao, B.; Liang, F.; Jin, L.-Y. *RSC Adv.* **2014**, *4*, 30046.

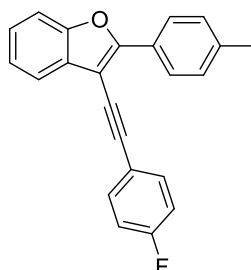
1739, 1453, 1378, 1243, 1192, 1097, 820, 810, 739, 880 cm^{-1} ; HRMS (APCI) calc. for $\text{C}_{23}\text{H}_{17}\text{O}^+$ $[\text{M}+\text{H}]^+$: 309.1274, found 309.1278.

2-Phenyl-3-(phenylethynyl)benzofuran (**3-3ba**)



Following general procedure GP4 with 2-(phenylethynyl)phenol **3-1b** (19.4 mg, 0.1 mmol) and (iodoethynyl)benzene **3-2a** (34.2 mg, 0.15 mmol). The crude product was purified by flash column chromatography (100:0 Pent:Et₂O) to afford **3-3ba** as a yellow solid (19.7 mg, 67%). The spectroscopic data match those previously reported in the literature.¹⁷¹ ¹H NMR (400 MHz, CDCl₃) δ 8.32 (dd, $J = 8.8, 1.2$ Hz, 2H), 7.76-7.71 (m, 3H), 7.68-7.65 (m, 2H), 7.56-7.50 (m, 3H), 7.46-7.33 (m, 3H); ¹³C NMR (101 MHz, CDCl₃) δ 157.02, 153.53, 131.67, 129.97, 129.63, 129.46, 128.74, 128.47, 126.14, 125.54, 125.44, 125.41, 123.56, 120.25, 111.32, 98.59, 95.23, 83.80.

3-((4-Fluorophenyl)ethynyl)-2-(*p*-tolyl)benzofuran (**3-3ab**)

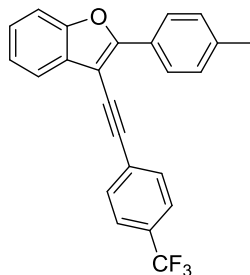


Following general procedure GP4 with 2-(*p*-tolylethynyl)phenol **3-1a** (20.8 mg, 0.1 mmol) and 1-fluoro-4-(iodoethynyl)benzene **3-2b** (36.9 mg, 0.15 mmol). The crude product was purified by flash column chromatography (100:0 Pent:Et₂O) to afford **3-3ab** as a colourless solid (22.8 mg, 70%). Mp 108 °C. ¹H NMR (400 MHz, CDCl₃) δ 8.22 (d, $J = 8.4$ Hz 2H), 7.73-7.71 (m, 1H), 7.61-7.58 (m, 2H), 7.53-7.50 (m, 1H), 7.35-7.29 (m, 4H), 7.10 (t, $J = 8.8$ Hz, 2H), 2.43 (s, 3H); ¹³C NMR (101 MHz, CDCl₃) δ 162.6 (d, $J_{\text{C-F}} = 251$ Hz), 156.7, 153.4, 139.5, 133.3 (d, $J_{\text{C-F}} = 8.5$ Hz), 129.9, 129.4, 127.4, 126.0, 125.1, 123.3, 120.2, 119.6 (d, $J_{\text{C-F}} = 3.5$ Hz), 115.8 (d, $J_{\text{C-F}} = 22.1$ Hz), 111.1, 98.3, 95.4, 81.1, 21.5; ¹⁹F NMR (282 MHz, CDCl₃) δ -110.7; IR (ATR) 2960, 2920, 2852, 1740, 1502, 1456, 1374, 1289, 1214, 1195,

¹⁷¹ Mandali, P. K.; Chand, D. K. *Synthesis*, **2015**, 47, 1661.

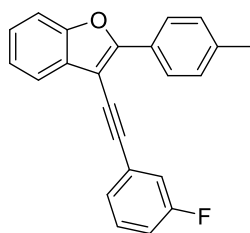
1153, 1087, 1010, 826, 819, 728 cm^{-1} ; HRMS (APCI) calc. for $\text{C}_{23}\text{H}_{16}\text{FO}^+$ $[\text{M}+\text{H}]^+$: 327.1180, found 327.1176.

2-(*p*-Tolyl)-3-((4-(trifluoromethyl)phenyl)ethynyl)benzofuran (**3-3ac**)



Following general procedure GP4 with 2-(*p*-tolylethynyl)phenol **3-1a** (20.8 mg, 0.1 mmol) and 1-(iodoethynyl)-4-(trifluoromethyl)benzene **3-2c** (44.4 mg, 0.15 mmol). The crude product was purified by flash column chromatography (100:0 Pent:Et₂O) to afford **3-3ac** as a yellow solid (28 mg, 75%). Mp 101 °C. ¹H NMR (400 MHz, CDCl₃) δ 8.21 (d, $J = 8.0$ Hz 2H), 7.74-7.65 (m, 5H), 7.54-7.52 (m, 1H), 7.38-7.32 (m, 4H), 2.44 (s, 3H); ¹³C NMR (101 MHz, CDCl₃) δ 157.4, 153.4, 139.8, 131.6, 130.1, 129.7, 129.5, 128.0, 127.2, 126.1, 125.4 (q, $J_{\text{C-F}} = 4.0$ Hz), 125.3, 124.9, 123.5, 120.1, 111.2, 97.8, 95.0, 84.1, 21.5; ¹⁹F NMR (282 MHz, CDCl₃) δ -62.8; IR (ATR) 2960, 2820, 2851, 1735, 1617, 1453, 1323, 1252, 1160, 1110, 1062, 1014, 959, 852, 832, 744, 605 cm^{-1} ; HRMS (APCI) calc. for $\text{C}_{24}\text{H}_{16}\text{F}_3\text{O}^+$ $[\text{M}+\text{H}]^+$: 377.1148, found 377.1142.

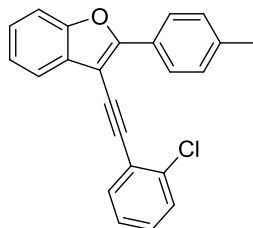
3-((3-Fluorophenyl)ethynyl)-2-(*p*-tolyl)benzofuran (**3-3ad**)



Following general procedure GP4 with 2-(*p*-tolylethynyl)phenol **3-1a** (20.8 mg, 0.1 mmol) and 1-fluoro-3-(iodoethynyl)benzene **3-2d** (36.9 mg, 0.15 mmol). The crude product was purified by flash column chromatography (100:0 Pent:Et₂O) to afford **3-3ad** as a white solid (25.5 mg, 78%). Mp 105 °C. ¹H NMR (400 MHz, CDCl₃) δ 8.21 (d, $J = 8.0$ Hz 2H), 7.74-7.71 (m, 1H), 7.53-7.51 (m, 1H), 7.41-7.29 (m, 7H), 7.11-7.06 (m, 1H), 2.44 (s, 3H); ¹³C NMR (75 MHz, CDCl₃) δ 162.5 (d, $J_{\text{C-F}} = 245.3$ Hz), 157.1, 153.4, 139.6, 130.0 (d, $J_{\text{C-F}} = 8.3$ Hz), 129.8, 129.4, 127.4, 127.3, 126.0, 125.2, 123.4, 120.1, 118.3, 118.0, 115.7 (d, $J_{\text{C-F}} = 21.2$ Hz), 111.2, 98.0, 95.2, 82.4, 21.5; ¹⁹F NMR (282 MHz, CDCl₃) δ -112.7; IR (ATR) 2960, 2920,

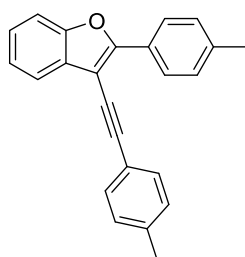
2853, 2208, 1739, 1574, 1456, 1375, 1253, 1184, 1166, 1144, 1089, 819, 781, 740, 672 cm^{-1} ;
HRMS (APCI) calc. for $\text{C}_{23}\text{H}_{16}\text{FO}^+$ $[\text{M}+\text{H}]^+$: 327.1180, found 327.1178.

3-((2-Chlorophenyl)ethynyl)-2-(*p*-tolyl)benzofuran (**3-3ae**)



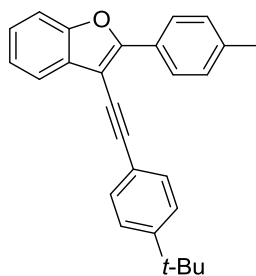
Following general procedure GP4 with 2-(*p*-tolylethynyl)phenol **3-1a** (20.8 mg, 0.1 mmol) and 1-chloro-2-(iodoethynyl)benzene **3-2e** (39.4 mg, 0.15 mmol). The crude product was purified by flash column chromatography (100:0 Pent:Et₂O) to afford **3-3ae** as a white solid (21.6 mg, 63%). Mp 110 °C. ¹H NMR (400 MHz, CDCl₃) δ 8.32 (d, J = 8.0 Hz 2H), 7.80-7.77 (m, 1H), 7.67-7.64 (m, 1H), 7.53-7.48 (m, 2H), 7.37-7.28 (m, 6H), 2.43 (s, 3H); ¹³C NMR (101 MHz, CDCl₃) δ 157.1, 153.4, 139.6, 135.5, 133.2, 130.0, 129.4, 129.4, 129.2, 127.2, 126.6, 126.1, 125.2, 123.5, 123.4, 120.3, 111.1, 98.1, 93.6, 86.7, 21.5; IR (ATR) 2916, 2855, 1460, 1442, 1259, 1195, 1097, 892, 818, 739, 654 cm^{-1} ; HRMS (APCI) calc. for $\text{C}_{23}\text{H}_{16}\text{ClO}^+$ $[\text{M}+\text{H}]^+$: 343.0884, found 343.0883.

2-(*p*-Tolyl)-3-(*p*-tolylethynyl)benzofuran (**3-3af**)



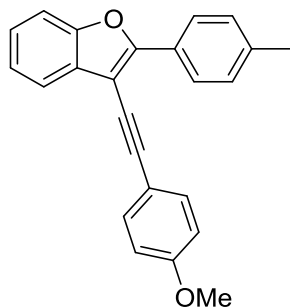
Following general procedure GP4 with 2-(*p*-tolylethynyl)phenol **3-1a** (20.8 mg, 0.1 mmol) and 1-(iodoethynyl)-4-methylbenzene **3-2f** (36.3 mg, 0.15 mmol). The crude product was purified by flash column chromatography (100:0 Pent:Et₂O) to afford **3-3af** as a white solid (20.3 mg, 63%). Mp 115 °C. ¹H NMR (400 MHz, CDCl₃) δ 8.24 (d, J = 8.4 Hz, 2H), 7.75-7.73 (m, 1H), 7.53-7.50 (m, 3H), 7.36-7.29 (m, 4H), 7.22 (dd, J = 8.8, 0.8 Hz, 2H), 2.43 (s, 3H), 2.41 (s, 3H); ¹³C NMR (101 MHz, CDCl₃) δ 156.5, 153.4, 139.3, 138.5, 131.4, 130.0, 129.4, 129.2, 127.5, 126.0, 125.0, 123.3, 120.4, 120.2, 111.1, 98.6, 96.7, 80.6, 21.6, 21.5; IR (ATR) 3029, 2960, 2920, 1502, 1448, 1243, 1193, 1193, 1093, 811, 839 cm^{-1} ; HRMS (APCI) calc. for $\text{C}_{24}\text{H}_{19}\text{O}^+$ $[\text{M}+\text{H}]^+$: 323.1430, found 323.1424.

3-((4-(*tert*-Butyl)phenyl)ethynyl)-2-(*p*-tolyl)benzofuran (**3-3ag**)



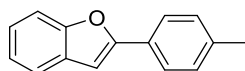
Following general procedure GP4 with 2-(*p*-tolylethynyl)phenol **3-1a** (20.8 mg, 0.1 mmol) and 1-chloro-2-(iodoethynyl)benzene **3-2g** (42.6 mg, 0.15 mmol). The crude product was purified by flash column chromatography (100:0 Pent:Et₂O) to afford **3-3ag** as a white solid (16.0 mg, 44%). Mp 114 C. ¹H NMR (400 MHz, CDCl₃) δ 8.24 (d, *J* = 8.0 Hz 2H), 7.74-7.72 (m, 1H), 7.57-7.55 (m, 2H), 7.52-7.50 (m, 1H), 7.44-7.42 (m, 2H), 7.35-7.30 (m, 4H), 2.43 (s, 3H), 1.36 (s, 9H); ¹³C NMR (101 MHz, CDCl₃) δ 156.5, 153.4, 151.7, 139.3, 131.3, 130.1, 129.4, 127.5, 126.0, 125.5, 125.0, 123.3, 120.5, 120.2, 111.1, 98.6, 96.7, 80.6, 34.9, 31.2, 21.5; IR (ATR) 2959, 2920, 2854, 2364, 1911, 1789, 1657, 1502, 1454, 1374, 1251, 1189, 1086, 1013, 936, 889, 824, 747, 701, 648, 604 cm⁻¹; HRMS (APCI) calc. for C₂₇H₂₅O⁺ [M+H]⁺: 365.1900, found 365.1903.

3-((4-Methoxyphenyl)ethynyl)-2-(*p*-tolyl)benzofuran (**3-3ah**)



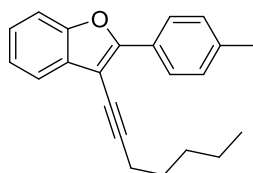
Following general procedure GP4 with 2-(*p*-tolylethynyl)phenol **3-1a** (20.8 mg, 0.1 mmol) and 1-(iodoethynyl)-4-methoxybenzene **3-2h** (38.7 mg, 0.15 mmol). The crude product was purified by flash column chromatography (100:0 Pent:Et₂O) to afford **3-3ah** as a yellow solid (11.9 mg, 35%). Mp 107 °C. ¹H NMR (400 MHz, CDCl₃) δ 8.24 (d, *J* = 8.4 Hz, 2H), 7.74-7.73 (m, 1H), 7.58-7.54 (m, 2H), 7.52-7.49 (m, 1H), 7.35-7.28 (m, 4H), 6.95-6.92 (m, 2H), 3.86 (s, 3H), 2.43 (s, 3H); ¹³C NMR (75 MHz, CDCl₃) δ 159.7, 156.3, 153.4, 139.2, 133.0, 130.1, 129.4, 127.6, 125.9, 125.0, 123.2, 120.2, 115.6, 114.1, 111.1, 98.7, 96.5, 79.9, 55.4, 21.5; HRMS (APCI) calc. for C₂₄H₁₉O₂⁺ [M+H]⁺: 339.1380, found 339.1377.

2-(*p*-Tolyl)benzofuran (**3-7**)



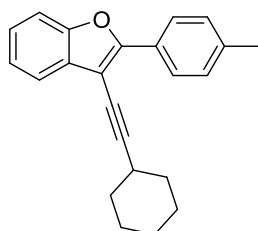
Following general procedure GP4 with 2-(*p*-tolylethynyl)phenol **3-1a** (20.8 mg, 0.1 mmol) and 1-(iodoethynyl)-4-nitrobenzene **3-7** (41.0 mg, 0.15 mmol). The crude product was purified by flash column chromatography (100:0 Pent:Et₂O) to afford **3-7** as a yellow solid (16.5 mg, 79%). The spectroscopic data match those previously reported in the literature.¹⁷² ¹H NMR (400 MHz, CDCl₃) δ 8.77 (d, *J* = 8.4 Hz, 2H), 7.59-7.56 (m, 1H), 7.53-7.51 (m, 1H), 7.29-7.20 (m, 4H), 6.9 (d, *J* = 1.2 Hz, 1H), 2.41 (s, 3H); ¹³C NMR (101 MHz, CDCl₃) δ 156.2, 154.8, 138.6, 129.5, 129.3, 127.8, 124.9, 123.9, 122.8, 120.7, 111.1, 100.5, 21.4.

3-(Hept-1-yn-1-yl)-2-(*p*-tolyl)benzofuran (**3-3aj**)



Following general procedure GP4 with 2-(*p*-tolylethynyl)phenol **3-1a** (20.8 mg, 0.1 mmol) and 1-iodohept-1-yne **3-2j** (33.3 mg, 0.15 mmol). The crude product was purified by flash column chromatography (100:0 Pent:Et₂O) to afford **3-3aj** as a yellow oil (12.7 mg, 42%). ¹H NMR (400 MHz, CDCl₃) δ 8.19 (d, *J* = 8.0 Hz, 2H), 7.65-7.63 (m, 1H), 7.48-7.46 (m, 1H), 7.32-7.25 (m, 4H), 2.59 (t, *J* = 7.2 Hz, 2H), 2.42 (s, 3H), 1.73-1.71 (m, 2H), 1.57-1.53 (m, 2H), 1.45-1.41 (m, 2H), 0.96 (t, *J* = 7.2 Hz, 3H); ¹³C NMR (101 MHz, CDCl₃) δ 155.9, 153.3, 138.9, 130.6, 129.2, 127.7, 125.7, 124.8, 123.0, 120.1, 110.9, 99.1, 98.0, 72.1, 31.2, 28.5, 22.3, 21.5, 20.0, 14.0; IR (ATR) 2960, 2920, 2851, 1740, 1457, 1373, 1195, 1156, 1078, 965, 814, 731, 717 cm⁻¹; HRMS (APCI) calc. for C₂₂H₂₃O⁺ [M+H]⁺: 303.1743, found 303.1732.

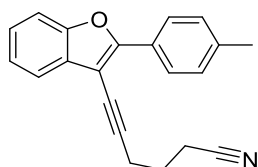
3-(Cyclohexylethynyl)-2-(*p*-tolyl)benzofuran (**3-3ak**)



¹⁷² Liao, L.-Y.; Shen, G.; Zhang, X.; Duan, X.-F. *Green Chem.*, **2012**, *14*, 695.

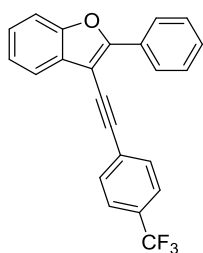
Following general procedure GP4 with 2-(*p*-tolylethynyl)phenol **3-1a** (20.8 mg, 0.1 mmol) and (iodoethynyl)cyclohexane **3-2k** (35.1 mg, 0.15 mmol). The crude product was purified by flash column chromatography (100:0 Pent:Et₂O) to afford **3-3ak** as a yellow oil (12.9 mg, 41%). ¹H NMR (300 MHz, CDCl₃) δ 8.20 (d, *J* = 8.4 Hz, 2H), 7.65-7.62 (m, 1H), 7.48-7.45 (m, 1H), 7.30-7.26 (m, 4H), 2.84-2.76 (m, 1H), 2.42 (s, 3H), 2.01-1.95 (m, 2H), 1.88-1.80 (m, 2H), 1.73-1.65 (m, 2H), 1.62-1.60 (m, 1H), 1.47-1.40 (m, 3H); ¹³C NMR (101 MHz, CDCl₃) δ 155.8, 153.3, 138.9, 130.5, 129.2, 127.7, 125.7, 124.8, 123.0, 120.1, 110.9, 102.02, 99.1, 72.1, 32.7, 30.2, 25.9, 24.8, 21.5; IR (ATR) 2960, 2919, 2851, 1738, 1457, 1373, 1243, 1175, 1075, 966, 822, 744, 716 cm⁻¹; HRMS (APCI) calc. for C₂₃H₂₃O⁺ [M+H]⁺: 315.1743, found 315.1734.

6-(2-(*p*-Tolyl)benzofuran-3-yl)hex-5-ynenitrile (**3-3al**)



Following general procedure GP4 with 2-(*p*-tolylethynyl)phenol **3-1a** (20.8 mg, 0.1 mmol) and 6-iodohex-5-ynenitrile **3-2l** (32.9 mg, 0.15 mmol). The crude product was purified by flash column chromatography (100:0 Pent:Et₂O) to afford **3-3al** as a yellow oil (7.5 mg, 25%). ¹H NMR (400 MHz, CDCl₃) δ 8.13 (d, *J* = 8.0 Hz, 2H), 7.62-7.60 (m, 1H), 7.50-7.47 (m, 1H), 7.32-7.28 (m, 4H), 2.81 (t, *J* = 6.8 Hz, 2H), 2.64 (t, *J* = 7.2 Hz, 2H), 2.42 (s, 3H), 2.11-2.03 (m, 2H); ¹³C NMR (101 MHz, CDCl₃) δ 156.6, 153.3, 139.4, 130.2, 129.4, 127.4, 125.8, 125.0, 123.2, 119.9, 119.0, 111.1, 98.2, 94.2, 74.3, 29.7, 24.7, 21.5, 19.1; IR (ATR) 2960, 2919, 2852, 2366, 1739, 1690, 1457, 1374, 1197, 1156, 1077, 965, 818, 747, 737, 717 cm⁻¹; HRMS (APCI) calc. for C₂₁H₁₈NO⁺ [M+H]⁺: 300.1383, found 300.1372.

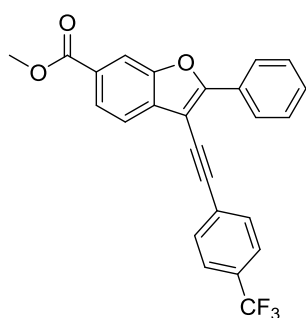
2-Phenyl-3-((4-(trifluoromethyl)phenyl)ethynyl)benzofuran (**3-3bb**)



Following general procedure GP4 with 2-(phenylethynyl)phenol **3-1b** (19.4 mg, 0.1 mmol) and 1-(iodoethynyl)-4-(trifluoromethyl)benzene **3-2b** (44.4 mg, 0.15 mmol). The crude

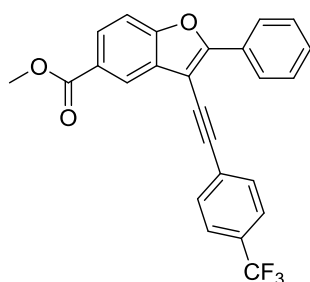
product was purified by flash column chromatography (100:0 Pent:Et₂O) to afford **3-3bb** as a yellow solid (26.1 mg, 72%). Mp 95 °C. ¹H NMR (400 MHz, CDCl₃) δ 8.33-8.31 (d, 2H), 7.76-7.65 (m, 5H), 7.56-7.50 (m, 3H), 7.46-7.42 (m, 1H), 7.40-7.32 (m, 2H); ¹³C NMR (101 MHz, CDCl₃) δ 157.0, 153.5, 131.7, 129.9, 129.6, 129.5, 128.7, 127.1, 126.1, 125.5, 125.4 (q, *J*_{C-F} = 3.9 Hz), 125.0, 123.6, 120.2, 111.3, 98.6, 95.2, 83.8; ¹⁹F NMR (376 MHz, CDCl₃) δ -62.7; IR (ATR) 3062, 2961, 2921, 2852, 1483, 1444, 1240, 1196, 1102, 1082, 1018, 899, 817, 741, 678, 619 cm⁻¹; HRMS (APCI) calc. for C₂₃H₁₄F₃O⁺ [M+H]⁺: 363.0991, found 363.0990.

Methyl 2-phenyl-3-((4-(trifluoromethyl)phenyl)ethynyl)benzofuran-6-carboxylate (**3-3cb**)



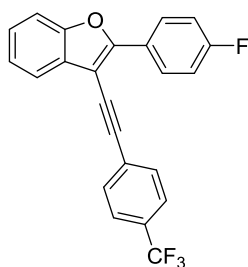
Following general procedure GP4 with methyl 3-hydroxy-4-(phenylethynyl)benzoate **3-1c** (25.2 mg, 0.1 mmol) and 1-(iodoethynyl)-4-(trifluoromethyl)benzene **3-2b** (44.4 mg, 0.15 mmol). The crude product was purified by flash column chromatography (100:0 Pent:Et₂O) to afford a mixture of **3-3cb** (22.3 mg, 53%) and methyl 2-phenylbenzofuran-6-carboxylate **3-3cb'** (5.0 mg, 19%), the ratio of **3-3cb:3-3cb'** = 1.00:0.37. ¹H NMR (400 MHz, CDCl₃) δ 8.35-8.33 (m, 2H), 8.24 (q, *J* = 0.8 Hz, 1H), 8.05 (dd, *J* = 8.0, 1.2 Hz, 1H), 7.78 (dd, *J* = 8.0, 0.8 Hz, 1H), 7.74-7.66 (m, 4H), 7.56-7.52 (m, 2H), 7.50-7.48 (m, 1H), 3.98 (s, 3H); ¹³C NMR (101 MHz, CDCl₃) δ 166.9, 159.6, 152.9, 133.9, 131.8, 130.2, 129.4, 129.3, 128.9, 127.5, 126.5, 125.5 (q, *J* = 3.7 Hz), 125.3, 125.0, 124.5, 119.9, 113.0, 101.3, 98.8, 83.0, 52.3; ¹⁹F NMR (376 MHz, CDCl₃) δ -62.8; IR (ATR) 2960, 2920, 2852, 1735, 1457, 1373, 1161, 1078, 967, 851, 726, 688 cm⁻¹; HRMS (APCI) calc. for C₂₅H₁₆F₃O₃⁺ [M+H]⁺: 421.1046, found 421.1049.

Methyl 2-phenyl-3-((4-(trifluoromethyl)phenyl)ethynyl)benzofuran-5-carboxylate (**3-3db**)



Following general procedure GP4 with methyl 4-hydroxy-3-(phenylethynyl)benzoate **3-1d** (25.2 mg, 0.1 mmol) and 1-(iodoethynyl)-4-(trifluoromethyl)benzene **3-2b** (44.4 mg, 0.15 mmol). The crude product was purified by flash column chromatography (100:0 Pent:Et₂O) to afford **3-3db** as a white solid (34.9 mg, 83%). Mp 109 °C. ¹H NMR (400 MHz, CDCl₃) δ 8.45 (dd, *J* = 2.0, 0.8 Hz, 1H), 8.33-8.30 (m, 2H), 8.10 (dd, *J* = 8.4, 1.6 Hz, 1H), 7.76-7.67 (m, 4H), 7.58-7.51 (m, 3H), 7.48-7.44 (m, 1H), 3.98 (s, 3H); ¹³C NMR (101 MHz, CDCl₃) δ 166.98, 158.20, 155.94, 131.78, 129.89, 129.70, 129.42, 128.81, 127.25, 126.78, 126.19, 125.94, 125.4 (q, *J* = 3.7 Hz), 122.60, 111.21, 98.94, 95.81, 82.87, 65.85, 52.27; ¹⁹F NMR (376 MHz, CDCl₃) δ -62.78; IR (ATR) 2960, 2920, 2852, 2209, 1714, 1605, 1554, 1443, 1326, 1291, 1251, 1233, 1156, 1099, 1058, 974, 837, 769, 733, 684 cm⁻¹; HRMS (APCI) calc. for C₂₅H₁₆F₃O₃⁺ [M+H]⁺: 421.1046, found 421.1048.

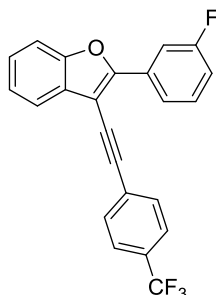
2-(4-Fluorophenyl)-3-((4-(trifluoromethyl)phenyl)ethynyl)benzofuran (**3-3eb**)



Following general procedure GP4 with 2-((4-fluorophenyl)ethynyl)phenol **3-1e** (21.2 mg, 0.1 mmol) and 1-(iodoethynyl)-4-(trifluoromethyl)benzene **3-2b** (44.4 mg, 0.15 mmol). The crude product was purified by flash column chromatography (100:0 Pent:Et₂O) to afford **3-3eb** as a yellow solid (19.4 mg, 51%). Mp 103 °C. ¹H NMR (400 MHz, CDCl₃) δ 8.32-8.29 (m, 2H), 7.75-7.66 (m, 5H), 7.55-7.52 (m, 1H), 7.39-7.33 (m, 2H), 7.23-7.19 (m, 2H); ¹³C NMR (101 MHz, CDCl₃) δ 163.2 (d, *J* = 251.5 Hz), 156.09, 153.46, 131.67, 129.54, 128.1 (d, *J* = 8.3 Hz), 126.98, 126.3 (d, *J* = 3.3 Hz), 125.57, 125.4 (q, *J* = 3.8 Hz) 123.65, 120.25, 116.02, 115.80, 111.27, 98.27, 95.17, 83.57; ¹⁹F NMR (376 MHz, CDCl₃) δ -62.8, -110.2; IR

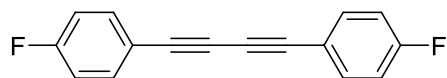
(ATR) 2960, 2920, 2852, 1739, 1603, 1503, 1456, 1375, 1323, 1230, 1159, 1104, 1060, 1008, 833, 795, 739 cm^{-1} ; HRMS (APCI) calc. for $\text{C}_{23}\text{H}_{13}\text{F}_4\text{O}^+$ $[\text{M}+\text{H}]^+$: 381.0897, found 381.0899.

2-(3-Fluorophenyl)-3-((4-(trifluoromethyl)phenyl)ethynyl)benzofuran (**3-3fb**)



Following general procedure GP4 with 2-((3-fluorophenyl)ethynyl)phenol **3-1f** (21.2 mg, 0.1 mmol) and 1-(iodoethynyl)-4-(trifluoromethyl)benzene **3-2b** (44.4 mg, 0.15 mmol). The crude product was purified by flash column chromatography (100:0 Pent:Et₂O) to afford **3-3fb** as a colourless solid (23.6 mg, 62%). Mp 105 °C. ¹H NMR (400 MHz, CDCl₃) δ 8.11-8.09 (m, 1H), 8.07-8.04 (m, 1H), 7.77-7.66 (m, 5H), 7.56-7.54 (m, 1H), 7.51-7.46 (m, 1H), 7.42-7.33 (m, 2H), 7.16-7.11 (m, 1H); ¹³C NMR (101 MHz, CDCl₃) δ 162.9 (d, $J = 246.5$ Hz), 155.49, 153.57, 131.9 (d, $J = 8.7$ Hz), 131.69, 130.4 (d, $J = 8.5$ Hz), 129.40, 126.86, 125.98, 125.5 (q, $J = 3.8$ Hz) 123.75, 121 (d, $J = 2.9$ Hz), 120.44, 116.39, 116.18, 113.05, 112.81, 111.41, 99.64, 95.96, 83.29; ¹⁹F NMR (376 MHz, CDCl₃) δ -62.8, -112.0; IR (ATR) 2960, 2920, 2852, 1740, 1457, 1373, 1319, 1177, 1136, 850, 719 cm^{-1} ; HRMS (APCI) calc. for $\text{C}_{23}\text{H}_{13}\text{F}_4\text{O}^+$ $[\text{M}+\text{H}]^+$: 381.0897, found 381.0900.

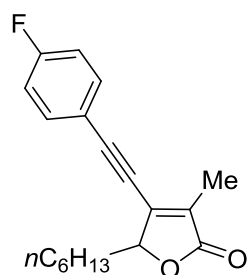
1,4-bis(4-fluorophenyl)buta-1,3-diyne (**s4**)



Following general procedure GP4 to afford **s4** (17 mg, 0.072 mmol, 36%). The spectroscopic data match those previously reported in the literature.¹⁷³ ¹H NMR (400 MHz, CDCl₃) δ 7.51 (m, 4H), 7.34-7.04 (m, 4H); ¹⁹F NMR (376 MHz, CDCl₃) δ -108.487, -108.501, -108.509, -108.515, -108.523, -108.531, -108.537, -108.546, -108.560.

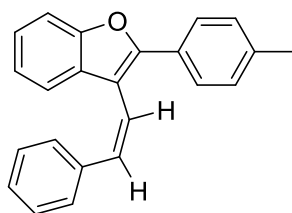
¹⁷³ Yin, K.; Li, C.; Li, J.; Jia, X. *Appl. Organometal. Chem.* **2011**, 25, 16.

4-((4-fluorophenyl)ethynyl)-5-hexyl-3-methylfuran-2(5H)-one (**3-3F**)



Following procedure of NMR monitoring experiments. Yellow oil, 7.1 mg, 60%. ^1H NMR (400 MHz, CD_3CN) δ 7.63-7.59 (m, 2H), 7.22-7.17 (m, 2H), 4.98-4.95 (m, 1H), 2.13 (s, 3H), 1.98-1.97 (m, 3H), 1.69-1.63 (m, 1H), 1.44-1.39 (m, 2H), 1.32-1.30 (m, 4H), 0.90-0.86 (m, 3H); ^{13}C NMR (101 MHz, CD_3CN) δ 174.2, 164.37 (d, $J_{\text{C-F}} = 251.5$ Hz), 143.9, 135.2 (d, $J_{\text{C-F}} = 9.1$ Hz), 133.0, 117.2, 116.9, 105.1, 83.0, 80.4, 33.5, 32.3, 29.6, 25.1, 23.2, 14.3, 10.5; ^{19}F NMR (376 MHz, CD_3CN) δ -110.10; HRMS (ESI) calc. for $\text{C}_{19}\text{H}_{22}\text{FO}_2^+$ $[\text{M}+\text{H}]^+$: 301,1598, found 301,1598.

(Z)-3-Styryl-2-(p-tolyl)benzofuran (**3-8**)

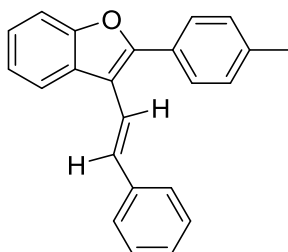


Following the reported literature.¹⁷⁴ An oven-dried *Schlenk* tube containing a Teflon-coated stir bar was charged with $\text{Pd}_2(\text{dba})_3$ (1.8 mg, 1 mol%), dppb (3.4 mg, 4 mol%) and alkyne **3-3aa** (0.2 mmol). The *Schlenk* tube was sealed and then evacuated and backfilled with argon (3 cycles). 0.2 mL of dioxane was subsequently injected. After stirring the mixture at room temperature for 15 min, 16 μL of HCO_2H was injected and the reaction was heated to 80 $^\circ\text{C}$ for 15 h. After removal of the solvent under vacuo, the residues were passed through a short silica chromatography (particle size 40-50 μm , hexane or hexane/ethyl acetate as eluent) to afford alkene **3-8** as a yellow solid (52.8 mg, 85%). Mp 101 $^\circ\text{C}$. ^1H NMR (400 MHz, CDCl_3) δ 7.87 (d, $J = 8.0$ Hz, 2H), 7.48 (d, $J = 8.0$ Hz, 1H), 7.31-7.27 (m, 4H), 7.22-7.18 (m, 1H), 7.14-7.12 (m, 2H), 6.96 (td, $J = 7.6, 0.8$ Hz, 2H), 6.91-6.86 (m, 2H), 6.69 (d, $J = 12$ Hz, 1H), 2.42 (s, 3H); ^{13}C NMR (101 MHz, CDCl_3) δ 154.1, 152.2, 138.5, 137.2, 132.9, 129.4, 128.8,

¹⁷⁴ Shen, R.; Chen, T.; Zhao, Y.; Qiu, R.; Zhou, Y.; Yin, S.; Wang, X.; Goto, M.; Han, L.-B. *J. Am. Chem. Soc.* **2011**, *133*, 17037.

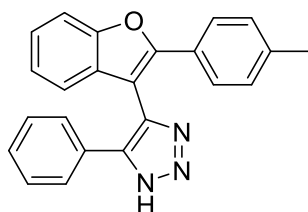
128.3, 128.1, 127.7, 127.4, 126.8, 124.1, 122.3, 121.6, 120.2, 113.1, 110.8, 21.4; HRMS (APCI) calc. for $C_{23}H_{19}O^+$ $[M+H]^+$: 311.1430, found 311.1429.

(*E*)-3-Styryl-2-(*p*-tolyl)benzofuran (**3-9**)



Following the reported literature.¹⁷⁵ An oven-dried *Schlenk* tube containing a Teflon-coated stir bar was charged with $Pd_2(dab)_3$ (1.8 mg, 1 mol%), dppb (1.7mg, 2 mol %) and alkyne **3-3aa** (0.2 mmol). The *Schlenk* tube was sealed and then evacuated and backfilled with argon (3 cycles). 0.4 mL of dioxane was subsequently injected. After stirring the mixture at room temperature for 15 min, 48 μ L of aqueous HCO_2H (25%) was added. The reaction was heated to 80 °C for 2 h, and another 48 μ L of aqueous HCO_2H (25%) was added. The reaction was heated at 80 °C for another 8 h. After removal of the solvent under vacuo, the residues were passed through a short silica chromatography (particle size 40-50 μ m, hexane or hexane/ethyl acetate as eluent) to afford alkene **3-9** as a yellow solid (53.4 mg, 86%). The spectroscopic data match those previously reported in the literature.¹⁷⁶ 1H NMR (400 MHz, $CDCl_3$) δ 7.99-7.96 (m, 1H), 7.73 (d, $J = 8.0$ Hz, 2H), 7.56-7.54 (m, 3H), 7.41-7.29 (m, 9H), 2.45 (s, 3H); ^{13}C NMR (101 MHz, $CDCl_3$) δ 154.4, 153.7, 138.9, 137.9, 130.7, 129.5, 128.7, 128.0, 127.9, 127.9, 127.5, 126.2, 124.6, 123.1, 120.9, 120.1, 114.0, 111.3, 21.4.

5-Phenyl-4-(2-(*p*-tolyl)benzofuran-3-yl)-1H-1,2,3-triazole (**3-10**)



¹⁷⁵ Shen, R.; Chen, T.; Zhao, Y.; Qiu, R.; Zhou, Y.; Yin, S.; Wang, X.; Goto, M.; Han, L.-B. *J. Am. Chem. Soc.* **2011**, *133*, 17037.

¹⁷⁶ Álvarez, R.; Martínez, C.; Madich, Y.; Denis, J. G.; Aurrecochea, J. M.; de Lera, Á. R. *Chem. Eur. J.* **2010**, *16*, 12746.

Following the reported literature.¹⁷⁷ A mixture of **3-3aa** (0.2 mmol), NaN₃ (52 mg, 0.8 mmol), and DMF (10 mL) was stirred at 180 °C for 36 h. The mixture was concentrated in vacuo, added to water, and extracted with EtOAc (3×50 mL). Organic layers were combined, dried over MgSO₄, filtered, concentrated, and purified by flash column chromatography to afford triazole **3-10** (43.6 mg, 62%) as a yellow solid. Mp 100 °C. ¹H NMR (400 MHz, CDCl₃) δ 7.62-7.59 (m, 2H), 7.57 (d, *J* = 8.4 Hz, 1H), 7.47 (d, *J* = 8.0 Hz, 2H), 7.33-7.29 (m, 1H), 7.22-7.19 (m, 5H), 7.07 (d, *J* = 8.4 Hz, 2H), 2.29 (s, 3H); ¹³C NMR (75 MHz, CDCl₃) δ 153.9, 153.9, 139.3, 129.3, 129.0, 128.8, 128.7, 128.6, 127.8, 126.9, 126.7, 126.5, 124.9, 124.1, 123.3, 120.0, 111.2, 104.2, 21.3; HRMS (ESI) calc. for C₂₃H₁₇N₃NaO⁺ [M+Na]⁺: 374.1264, found 374.1272.

5.6 Crystallographic Data

A single crystal of each compound was selected, mounted onto a cryoloop, and transferred in a cold nitrogen gas stream. Intensity data were collected with a BRUKER Kappa-APEXII diffractometer with graphite-monochromated Mo-K α radiation. Data collections were performed with APEX2 suite (BRUKER). Unit-cell parameters refinement, integration and data reduction were carried out with SAINT program (BRUKER). SADABS (BRUKER) was used for scaling and multi-scan absorption corrections. In the WinGX suite of programs,¹⁷⁸ the structure were solved with different programs (cf cif files) and refined by full-matrix least-squares methods using SHELXL-14.¹⁷⁹

The following table contains crystal data collection and structure refinement information for **3-6** and **3aa**. CCDC 1850902-1850903 contain the supplementary crystallographic data for this paper. These data can be obtained free of charge from The Cambridge Crystallographic Data Centre via www.ccdc.cam.ac.uk/data_request/cif.

Identification code	6	3aa
Empirical formula	C36 H23 Au F9 O P	C23 H16 O
Formula weight	870.48	308.36
Temperature	200(2) K	200(2) K
Wavelength	0.71073 Å	0.71073 Å
Crystal system	Monoclinic	Orthorhombic
Space group	P 1 21/n 1	P b c a
Unit cell dimensions		
a (Å)	18.5154(6)	11.0356(4)
b (Å)	9.8647(4)	12.8018(5)
c (Å)	19.4489(6)	23.3379(9)

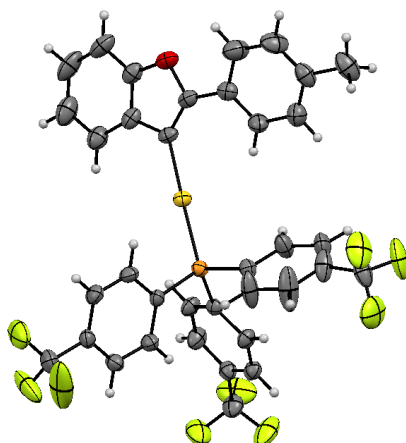
¹⁷⁷ Guo, H.-M.; Tanaka, F. *J. Org. Chem.* **2009**, *74*, 2417.

¹⁷⁸ Farrugia, L. J. *J. Appl. Crystallogr.* **1999**, *32*, 837.

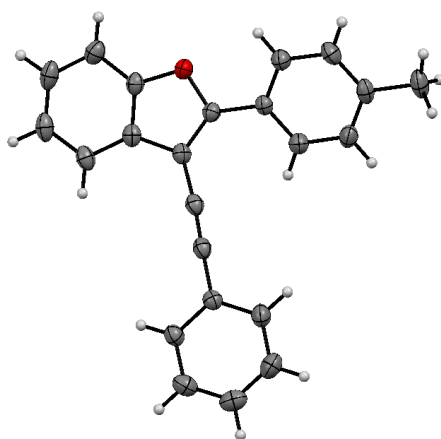
¹⁷⁹ Sheldrick, G. M. *Acta Crystallogr. Sect. C Struct. Chem.* **2015**, *71*, 3.

α (°)	90	90
β (°)	113.180(2)	90
γ (°)	90	90
Volume (Å ³)	3265.5(2)	3297.1(2)
Z	4	8
Density (calculated Mg/m ³)	1.771	1.242
Absorption coefficient (mm ⁻¹)	4.634	0.074
F(000)	1688	1296
Theta range for data collection	2.36 to 25.93°	2.59 to 30.22°
Index ranges	-26<=h<=19, -14<=k<=13, -27<=l<=27	-15<=h<=15, -10<=k<=10, -32<=l<=33
Reflections collected	43036	27964
Independent reflections	10005 [R(int) = 0.0589]	5060 [R(int) = 0.0383]
Data / restraints / parameters	10005 / 0 / 461	5060 / 0 / 218
Goodness-of-fit on F ²	0.989	1.124
Final R indices [I>2sigma(I)]	R1 = 0.0343, wR2 = 0.0682	R1 = 0.0595, wR2 = 0.1367
R indices (all data)	R1 = 0.0635, wR2 = 0.0760	R1 = 0.0868, wR2 = 0.1547
Absolute structure parameter	n/a	n/a
Extinction coefficient	n/a	n/a
Largest diff. peak and hole	2.629 and -0.480 e.Å ⁻³	0.316 and -0.233 e.Å ⁻³
CCDC number	1850903	1850902

X-ray structure of **3-6**.



X-ray structure of **3-3aa**.



5.7 Theoretical Studies

5.7.1 Choice of the Method

All calculations were performed using the Gaussian 09 software package.¹⁸⁰ Optimization of geometries, frequency and single point energy calculations were done using the PBE0 functional¹⁸¹ with the following basis set: SDD¹⁸² for Au, 6-311G*¹⁸³ I and 6-31G**¹⁸⁴ for others atoms. The effect of solvation (in MeCN) was modeled using the ‘SMD’ model.¹⁸⁵ The nature of all stationary points was confirmed by analyzing the harmonic vibrational frequencies.

The effect of dispersion was probed by comparing the calculated structural parameters with the PBE0 functional with or without the D3BJ dispersion term. For **3-6**, X-ray data were available (this work) and served as a reference (Figure SI5).

¹⁸⁰ Gaussian 09, Revision **D.01**, M. J. Frisch, G. W. Trucks, H. B. Schlegel, G. E. Scuseria, M. A. Robb, J. R. Cheeseman, G. Scalmani, V. Barone, B. Mennucci, G. A. Petersson, H. Nakatsuji, M. Caricato, X. Li, H. P. Hratchian, A. F. Izmaylov, J. Bloino, G. Zheng, J. L. Sonnenberg, M. Hada, M. Ehara, K. Toyota, R. Fukuda, J. Hasegawa, M. Ishida, T. Nakajima, Y. Honda, O. Kitao, H. Nakai, T. Vreven, J. A. Montgomery, Jr., J. E. Peralta, F. Ogliaro, M. Bearpark, J. J. Heyd, E. Brothers, K. N. Kudin, V. N. Staroverov, R. Kobayashi, J. Normand, K. Raghavachari, A. Rendell, J. C. Burant, S. S. Iyengar, J. Tomasi, M. Cossi, N. Rega, J. M. Millam, M. Klene, J. E. Knox, J. B. Cross, V. Bakken, C. Adamo, J. Jaramillo, R. Gomperts, R. E. Stratmann, O. Yazyev, A. J. Austin, R. Cammi, C. Pomelli, J. W. Ochterski, R. L. Martin, K. Morokuma, V. G. Zakrzewski, G. A. Voth, P. Salvador, J. J. Dannenberg, S. Dapprich, A. D. Daniels, Ö. Farkas, J. B. Foresman, J. V. Ortiz, J. Cioslowski, and D. J. Fox, Gaussian, Inc., Wallingford CT, 2009.

¹⁸¹ (a) Perdew, J. P.; Burke, K.; Ernzerhof, M. *Phys. Rev. Lett.* **1996**, *77*, 3865. (b) Adamo, C.; Barone, V. *J. Chem. Phys.* **1999**, *110*, 6158.

¹⁸² (a) Dunning Jr. T. H.; Hay, P. J. in *Modern Theoretical Chemistry*, Ed. H. F. Schaefer III, Vol. 3 (Plenum, New York, 1977) 1-28; (b) Wedig, U.; Dolg, M.; Stoll, H.; Preuss, H. in *Quantum Chemistry: The Challenge of Transition Metals and Coordination Chemistry*, Ed. A. Veillard, Reidel, and Dordrecht (1986) 79.

¹⁸³ Glukhovstev, M. N.; Pross, A.; McGrath, M. P.; Radom, L. *J. Chem. Phys.* **1995**, *103*, 1878.

¹⁸⁴ Hehre, W.J.; Ditchfield, R.; Pople, J. A. *J. Chem. Phys.* **1972**, *56*, 2257.

¹⁸⁵ Marenich, A. V.; Cramer, C. J.; Truhlar, D. G. *J. Phys. Chem. B* **2009**, *113*, 6378.

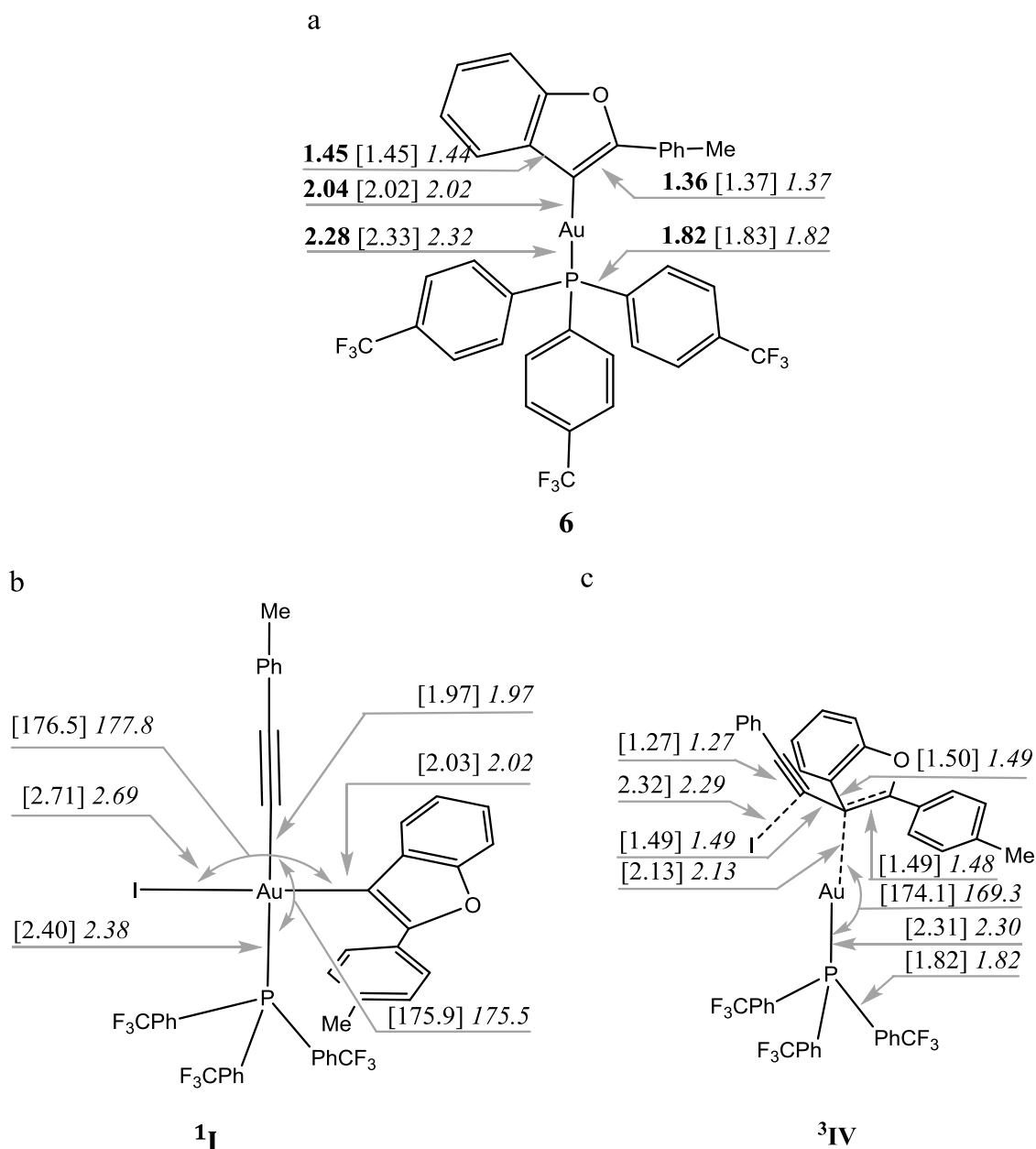


Figure SI5: Selected bond lengths (Å) for **3-6**, **1_I** and **3_{IV}**; X-ray data (for **3-6**) [PBE0] and PBE0-D3BJ levels of theory.

Both of the methods used (PBE0 and PBE0-D3BJ) give globally values in very good agreement with X-ray data. They slightly overestimate the P-Au bond distance (deviation of ca. 0.04 Å) and underestimate the Au-C(cycle) bond distance (deviation of 0.02 Å). Concerning the differences between selected main bond lengths around gold in **1_I** structure by using BPE0 or PBE0-D3BJ functionals, the deviation is ca. 0.01 Å except for the bond P-Au and I-Au (0.02 Å). For **3_{IV}**, the deviation for all bonds is about 0.01 Å except for the C-I distance (0.03 Å). As these results do not show a clear effect by including a dispersion factor within the PBE0 functional, geometry optimizations have been performed without this term.

5.7.2 Singlet potential energy surface exploration

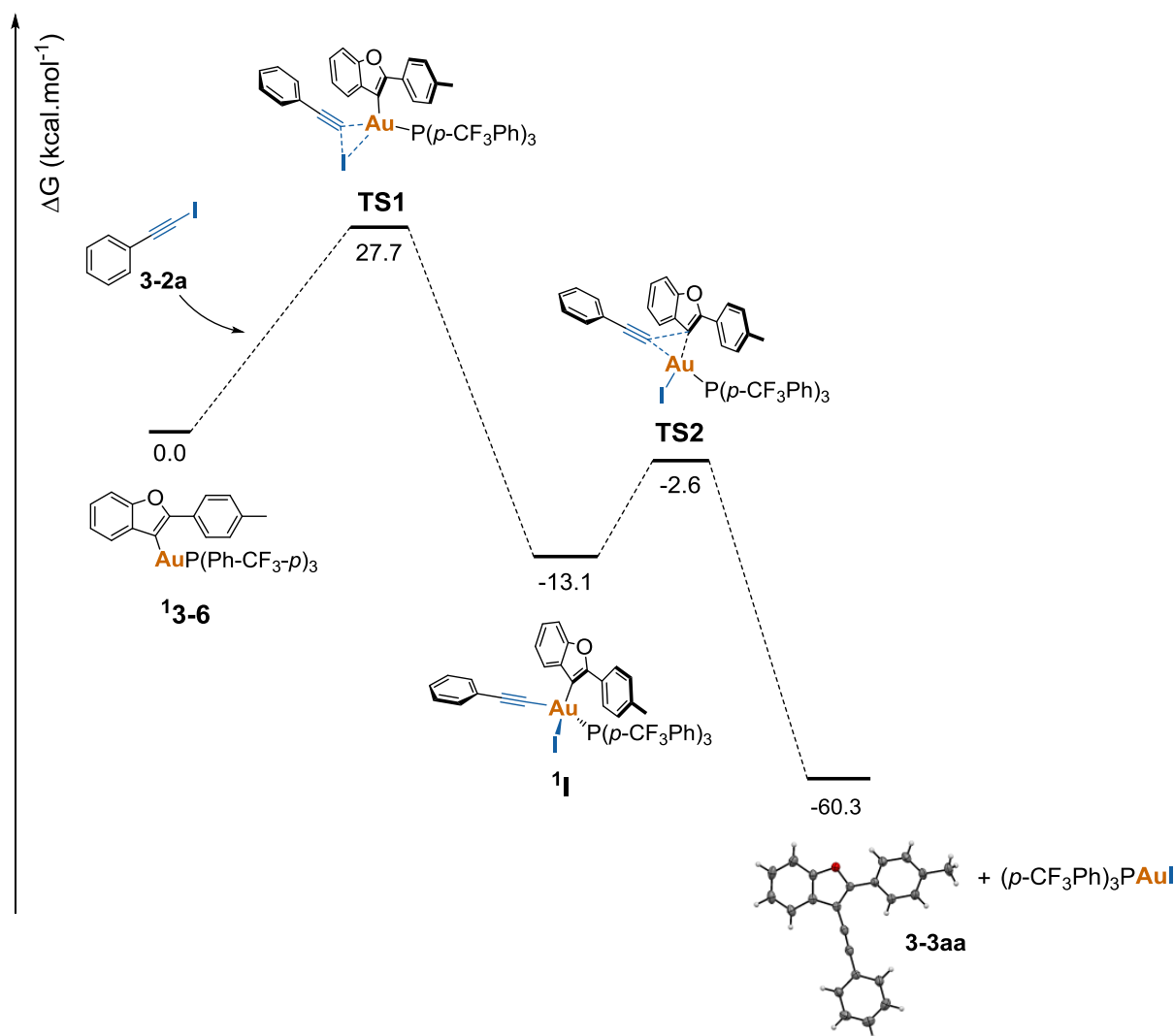


Figure SI6. Potential energy surface of the reaction of **13-6** with **3-2a**. Gibbs free energies (CH_3CN) are given relatively to the starting products and are in kcal/mol.

5.7.3 Energy Transfer from the Photosensitizer

The spin density of $^3[\text{Ir-F}]$ (3T_1) was determined with the complex either isolated or in the vicinity of **3-6** at the B3LYP/Def2-SV(P) level of theory including GD3 dispersion. Results show that part of the $[\text{Ir-F}]^*$ spin density is transferred to the furan moiety of the gold complex **3-6**, indicating thus that an energy transfer is taking place (Figure 2g and h in the article), which is coherent with the quenching studies performed on $[\text{Ir-F}]$ with **6** (Figure SI2 and Figure SI3). This feature thus leads to the formation of **3-6** in an excited electronic state which may further reacts with (iodoethynyl)benzene **3-2a**.

Similarly, the approach of **2a** to $^3[\text{Ir-F}] (^3T_1)$ was probed. In this case, no energy transfer is observed (Figure SI7).

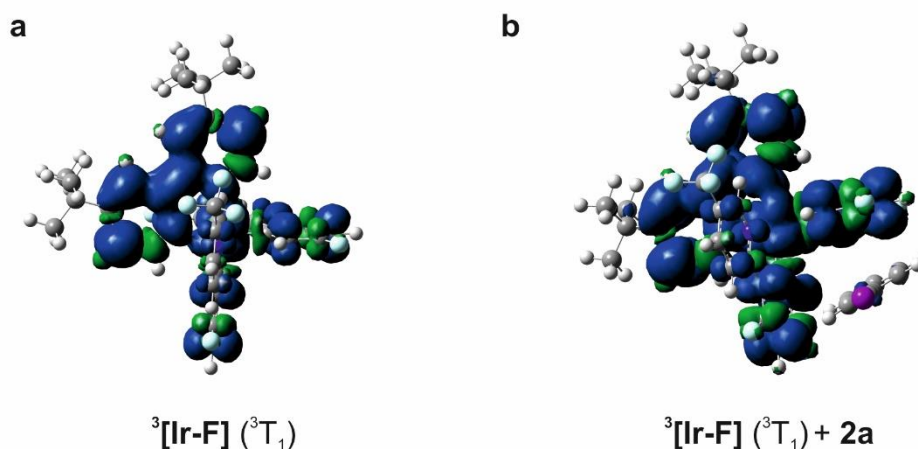


Figure SI7. Spin density isosurface (isovalue 0.0006 a.u.) of **a-** isolated $^3[\text{Ir-F}]$ complex and **b-** $[\text{Ir-F}] (^3T_1)$ in the vicinity of **3-2a**.

5.7.4 TD-DFT Calculations

Time-dependent-DFT (TD-DFT) calculations were carried out on the gas-phase optimized geometry of **3-6** using the same level of theory as described above (PBE0/SDD(Au),6-311G*(I),6-31G**(other atoms)). The simulated UV-vis spectrum of **3-6** is shown in Fig. SI8. Within the blue-LEDs energy range (470 nm), only one excited electronic state of **3-6** is accessible (3T_1 , 504 nm), all others are located at higher energy (Table SI1).

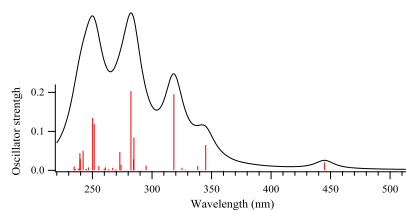


Figure SI8: Simulated gas-phase absorption spectrum (solid black line, a.u.) and TD-DFT calculated oscillators of the first 80 excited states of **3-6** (S_0) (red bars).

Table SI1. TD-DFT calculated transitions 1-80 for **3-6** (S_0).

Excited	λ (nm)	f	$\langle S^{*2} \rangle$	Excited	λ (nm)	f	$\langle S^{*2} \rangle$
---------	----------------	---	--------------------------	---------	----------------	---	--------------------------

State			State				
1	503.71	0.0000	2	41	277.1	0.0000	2
2	447.12	0.0000	2	42	276.13	0.0000	2
3	446.36	0.0006	0	43	274.02	0.0144	0
4	444.96	0.0206	0	44	273.61	0.0000	2
5	439.26	0.0000	2	45	273.43	0.0000	2
6	385.03	0.0000	2	46	273.01	0.0469	0
7	383.06	0.0005	0	47	272.02	0.0000	2
8	360.36	0.0000	2	48	270.55	0.0000	2
9	360.15	0.0011	0	49	270.19	0.0003	0
10	357.93	0.0000	2	50	269.75	0.0000	2
11	357.58	0.0000	2	51	269.67	0.0028	0
12	355.81	0.0000	2	52	269.21	0.0000	2
13	352.22	0.0000	2	53	268.89	0.0007	0
14	345.11	0.0652	0	54	268.09	0.0000	2
15	341.98	0.0000	2	55	266.96	0.0065	0
16	340.43	0.0000	2	56	264.93	0.0000	2
17	338.37	0.0117	0	57	263.91	0.0000	2
18	327.88	0.0000	2	58	263.72	0.0032	0
19	327.76	0.0018	0	59	263.22	0.0000	2
20	325.84	0.0000	2	60	261.44	0.0000	2
21	325.2	0.0063	0	61	260.84	0.0080	0
22	318.33	0.1953	0	62	259.88	0.0043	0
23	316.49	0.0000	2	63	258.71	0.0000	2
24	309.64	0.0000	2	64	255.33	0.0116	0
25	300.78	0.0000	2	65	253.91	0.0000	2
26	295.07	0.0126	0	66	251.49	0.1190	0
27	291.8	0.0000	2	67	250.16	0.1343	0
28	291.53	0.0000	2	68	246.6	0.0076	0
29	291.37	0.0005	0	69	245.07	0.0022	0
30	289.31	0.0000	2	70	244.53	0.0037	0
31	288.75	0.0000	2	71	242.15	0.0506	0
32	284.78	0.0844	0	72	240.39	0.0003	0
33	284.56	0.0000	2	73	239.75	0.0295	0
34	284.5	0.0280	0	74	239.48	0.0441	0
35	283.53	0.0000	2	75	239.36	0.0056	0

36	282.9	0.0000	2	76	238.01	0.0042	0
37	282.3	0.2035	0	77	236.25	0.0006	0
38	282.27	0.0000	2	78	235.76	0.0028	0
39	278.24	0.0000	2	79	234.79	0.0023	0
40	278.22	0.0011	0	80	234.63	0.0100	0

A natural transition orbital (NTO) analysis was undertaken to get deeper insight into the nature of the ${}^3T_1 \leftarrow {}^1S_0$ transition involved. The difference observed in the density map suggests that the transition has predominantly a ligand-to-metal charge transfer (LMCT) character (Figure SI9).

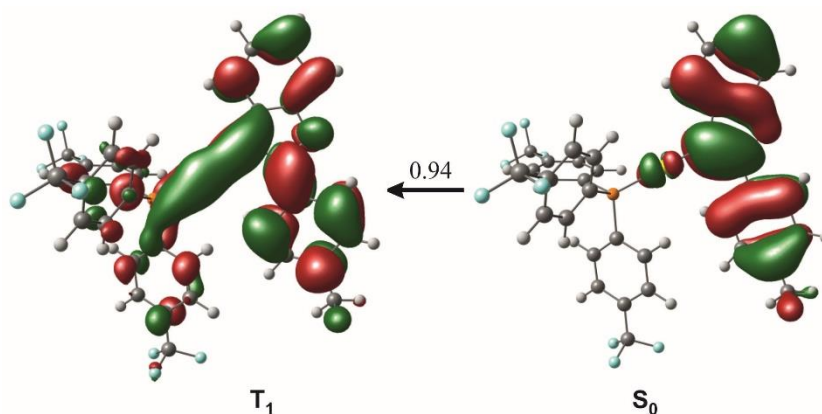


Figure SI9. Natural transition orbitals of the ${}^3T_1 \leftarrow {}^1S_0$ transition in **3-6** (isovalue 0.017 a.u.). The associated weight is indicated on the arrow.

5.7.5 Structural and Energetics Data

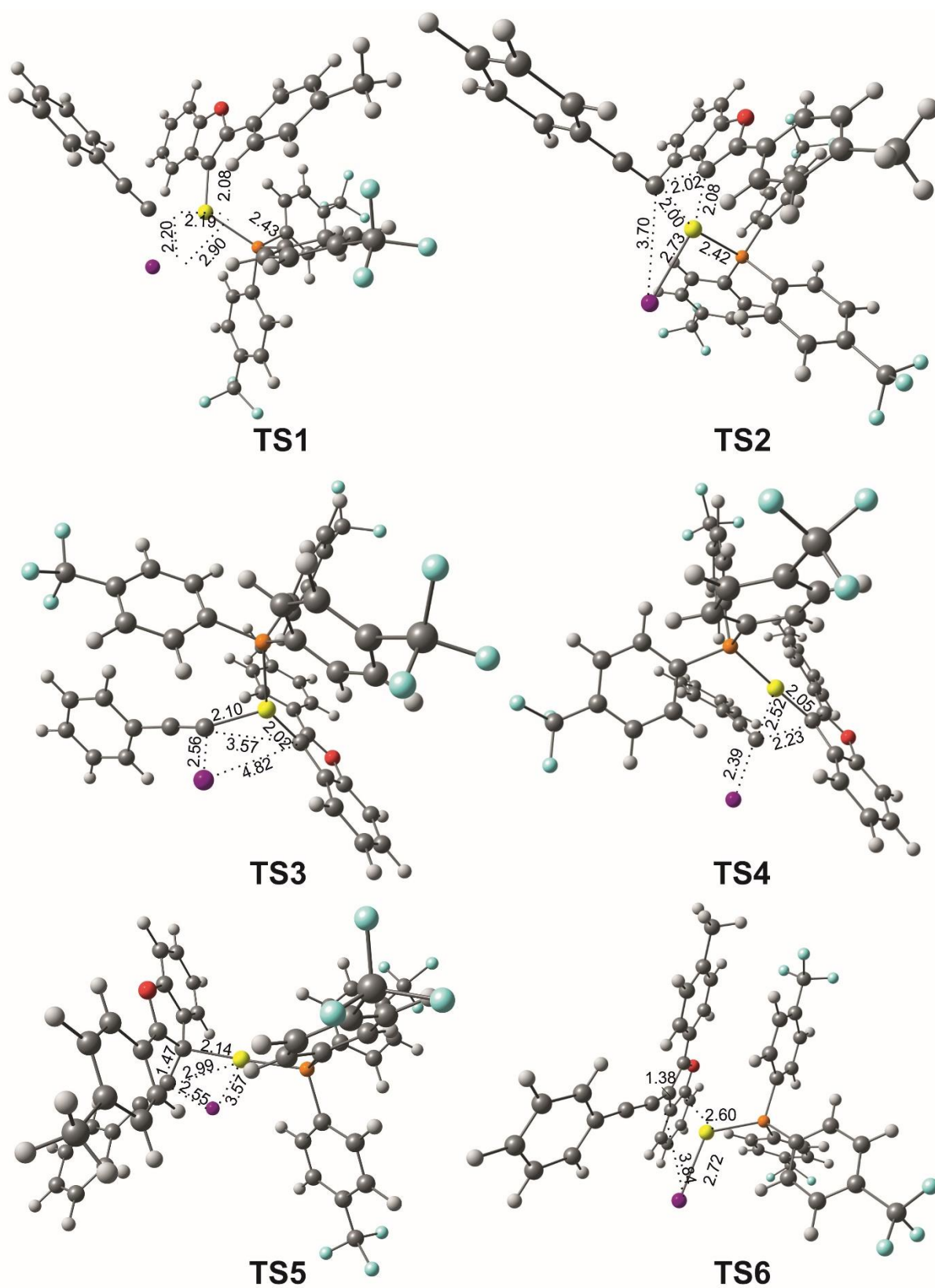


Figure SI10. Transition structures implied complexes implied in this work (singlet and potential energy surfaces). Selected bond lengths are in Å.

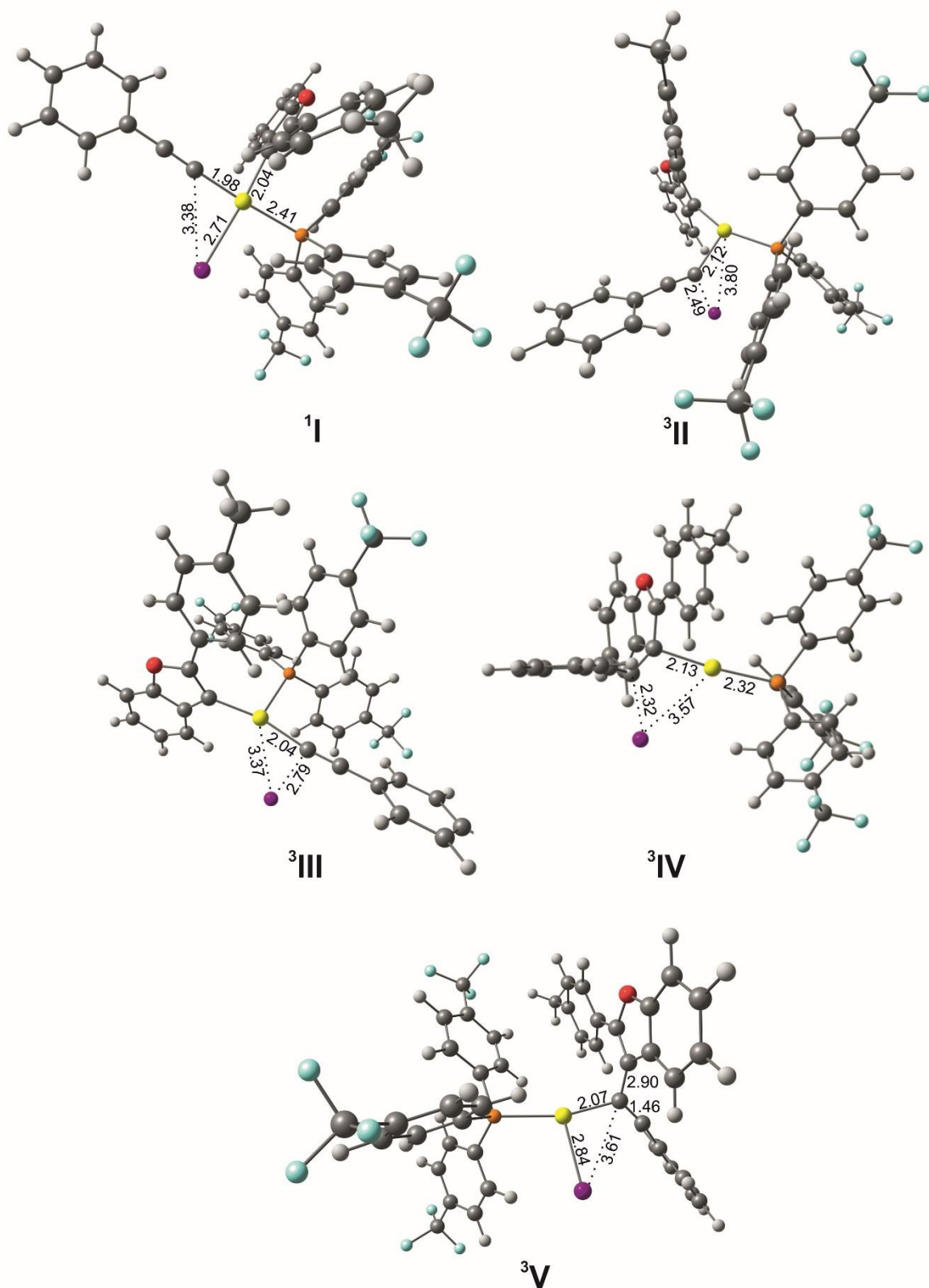


Figure SII1. Structures of all intermediate complexes implied in this work (singlet and potential energy surfaces). Selected bond lengths are in Å.

Table SI2. Energetics data (kcal/mol) obtained at the PBE0/SDD(Au)-6-311G*(I)-6-31G** (other atoms) level of theory.

	ΔE	$\Delta E+ZPE$	ΔG	ΔG_{MeCN}	ΔG_{MeCN}^C	
¹6+2a	0.0	0.0	0.0	0.0	0.0	
<i>Singlet potential energy surface^a</i>	TS1	28.6	28.1	30.8	27.7	26.8
	¹I	-7.2	-6.0	-1.8	-13.1	-18.0
	TS2	1.9	2.0	4.3	-2.6	-4.6
	¹3aa + L₃PAuI	-59.3	-57.6	-55.8	-60.3	-60.8
³6+2a	0.0	0.0	0.0	0.0	0.0	
<i>Triplet potential energy surface^b</i>	³II	-15.4	-13.7	-12.8	-18.5	-17.8
	TS3	-14.7	-13.2	-10.3	-16.4	-15.3
	³III	-23.4	-21.3	-18.6	-24.9	-28.3
	TS4	-3.8	-2.9	-0.8	-6.1	-7.8
	³IV	-34.1	-32.5	-31.0	-33.3	-31.7
	TS5	-33.6	-32.1	-30.3	-33.2	-31.4
	³V	-57.8	-55.2	-52.8	-60.0	-59.7
	TS6	-52.1	-51.1	-47.5	-54.0	-57.4
³(3aa + L₃PAuI)	-65.7	-64.2	-61.2	-66.6	-66.6	

^a Energies given relatively to ¹6+2a using the following values: electronic energy = -10060.5370657 H, zero-point energy = 0.6109347 H, thermal correction to Gibbs free energy = 0.5053327 H and solvation free energies = -10060.5843242.

^b Energies given relatively to ³6+2a using the following values: electronic energy = -10060.4519073 H, zero-point energy = 0.6069063 H, thermal correction to Gibbs free energy = 0.4991023H and solvation free energies = -10060.4982052.

^c Value including dispersion by a Single Point calculation (PBE0-D3BJ)

5.7.6 Activation of Iodo-ethynylbenzene 3-2a

The bent structure of **3-2a** found in the association complex ³II appears to be one of the key points that explain that the reaction of **3-2a** and **3-6** requires photoactivation to proceed. On the singlet potential energy surface (PES), the approach of **3-2a** to **3-6** does not lead to a bending of the I-C-C angle whereas it happens on the triplet PES (Fig SI12a). This bent structure is similar to the geometry adopted by **3-2a** in a triplet state (**3-2a**(³T₁), Fig SI12c). Indeed, in such a state, the C-I bond length increases from 1.98 Å (singlet state **3-2a**(¹S₀)) up to 2.19 Å and the I-C-C angle changes from 180 to 128 degrees with a triple bond that stretches to 0.07 Å (compared with **3-2a** (¹S₀), Fig SI12b). In the ³II complex, the C-I distance is 2.49 Å and the C-C-I angle, 115 degrees. It seems thus that an energy transfer is

occurring while $^3\mathbf{3-6}$ approaches to $\mathbf{3-2a}$, enabling to promote $\mathbf{3-2a}$ in a triplet excited state (that is not possible between $[\text{Ir-F}] (^3T_1)$ and $\mathbf{2a}$, see above), thus causing a change of geometry and making it reactive.

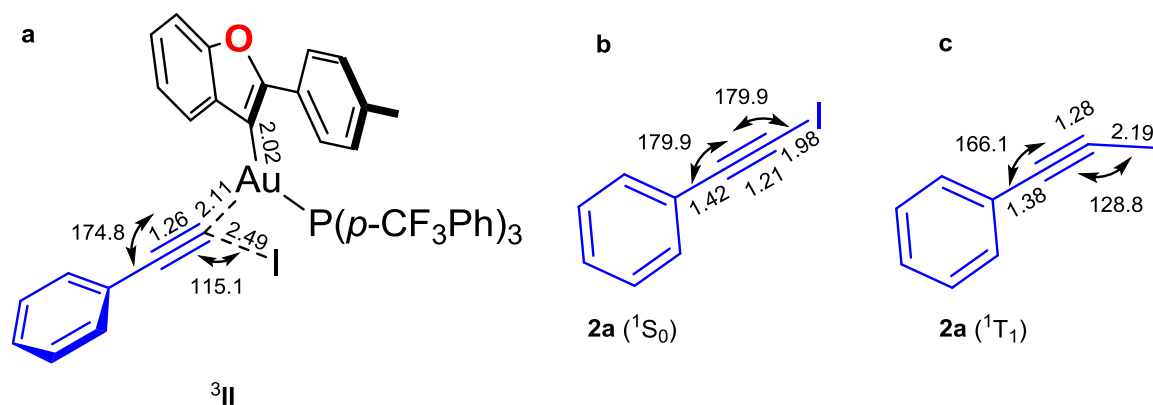


Fig. SI12. Structures and selected bond lengths (Å) and angles (degrees) of $^3\mathbf{II}$ and $\mathbf{3-2a}$ (1S_0 and 3T_1).

This feature was confirmed by checking the evolution of the spin density of the $^3\mathbf{II}$ complex when approaching $^3\mathbf{3-6}$ to $\mathbf{3-2a}$ (Fig. SI13). Thus, starting from the long-distance reactive species and following the $\text{C}_I\text{-Au}$ coordinate until the formation of $^3\mathbf{II}$ ($d(\text{C}_I\text{-Au}) = 2.11$ Å), an energy transfer starts to be observed between $^3\mathbf{3-6}$ and $\mathbf{3-2a}$ at distance of 3.6 Å. It becomes very strong at 2.8 Å. This process leads therefore to an activation of $\mathbf{3-2a}$ within the $^3\mathbf{II}$ complex.

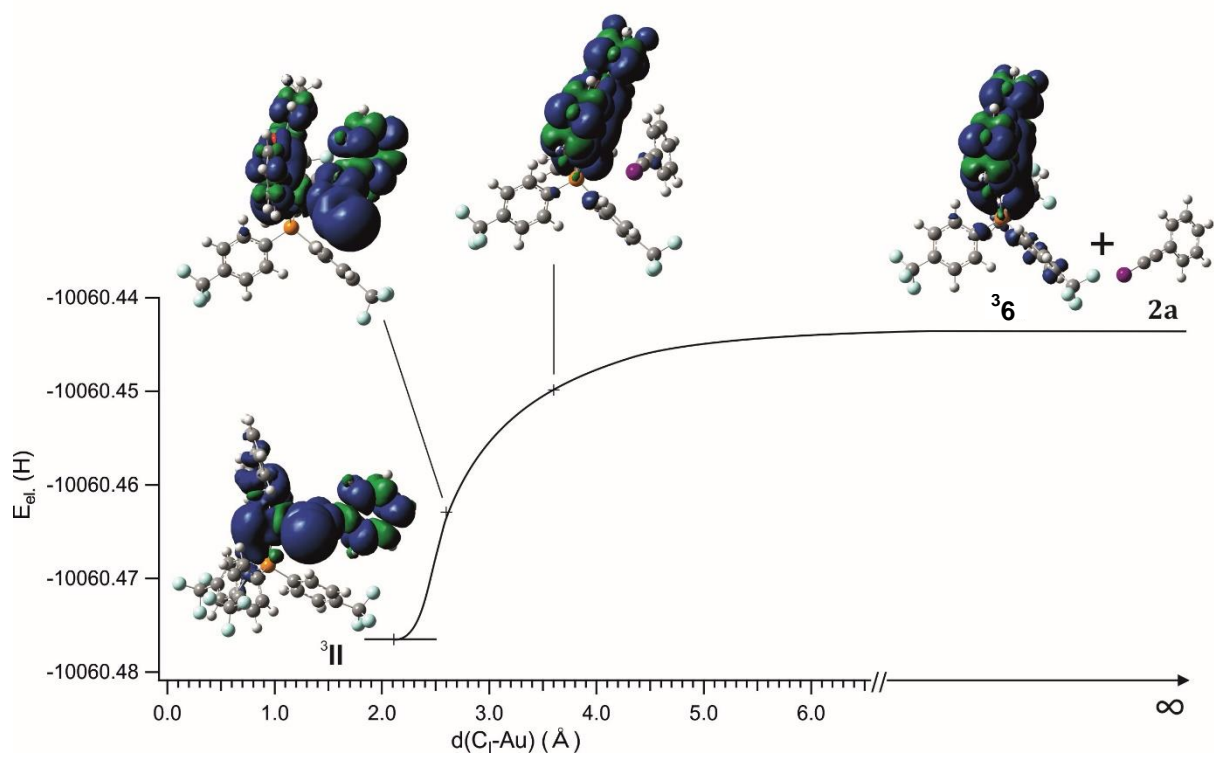
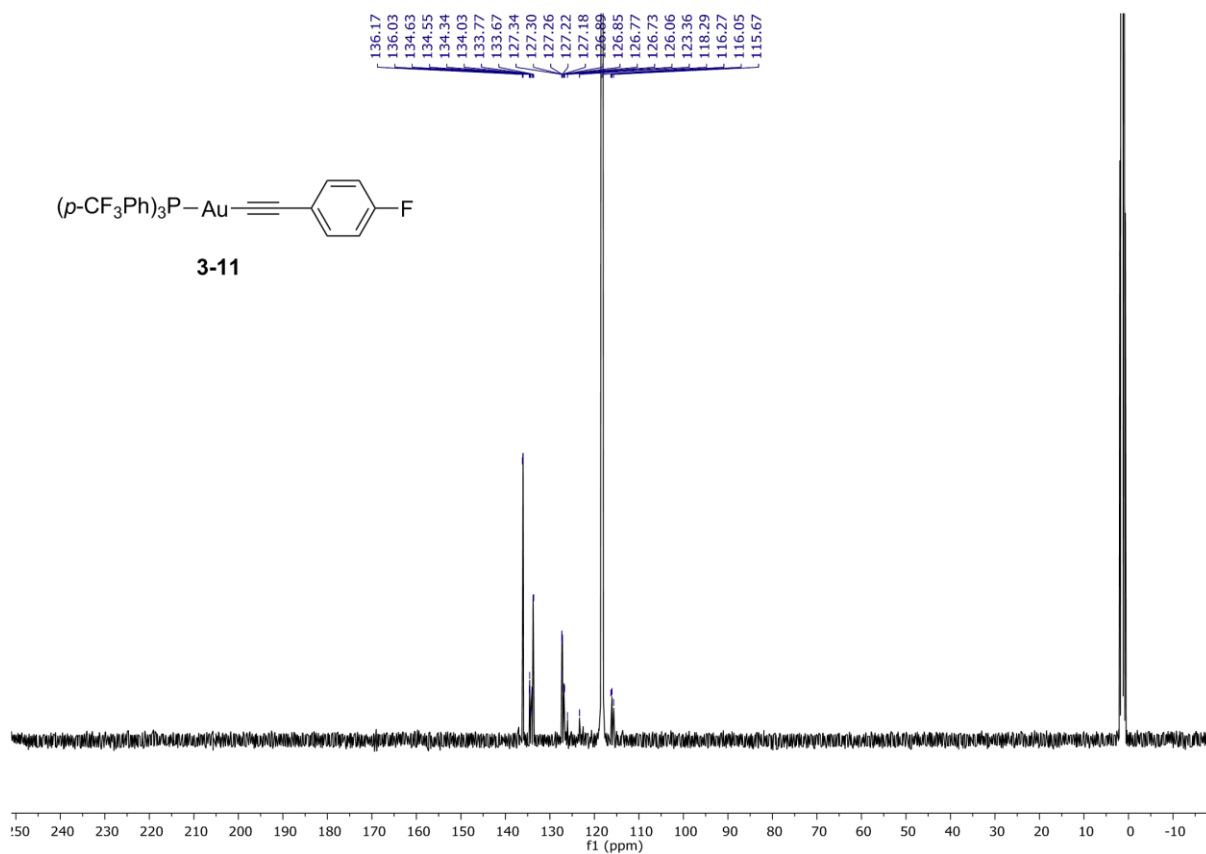
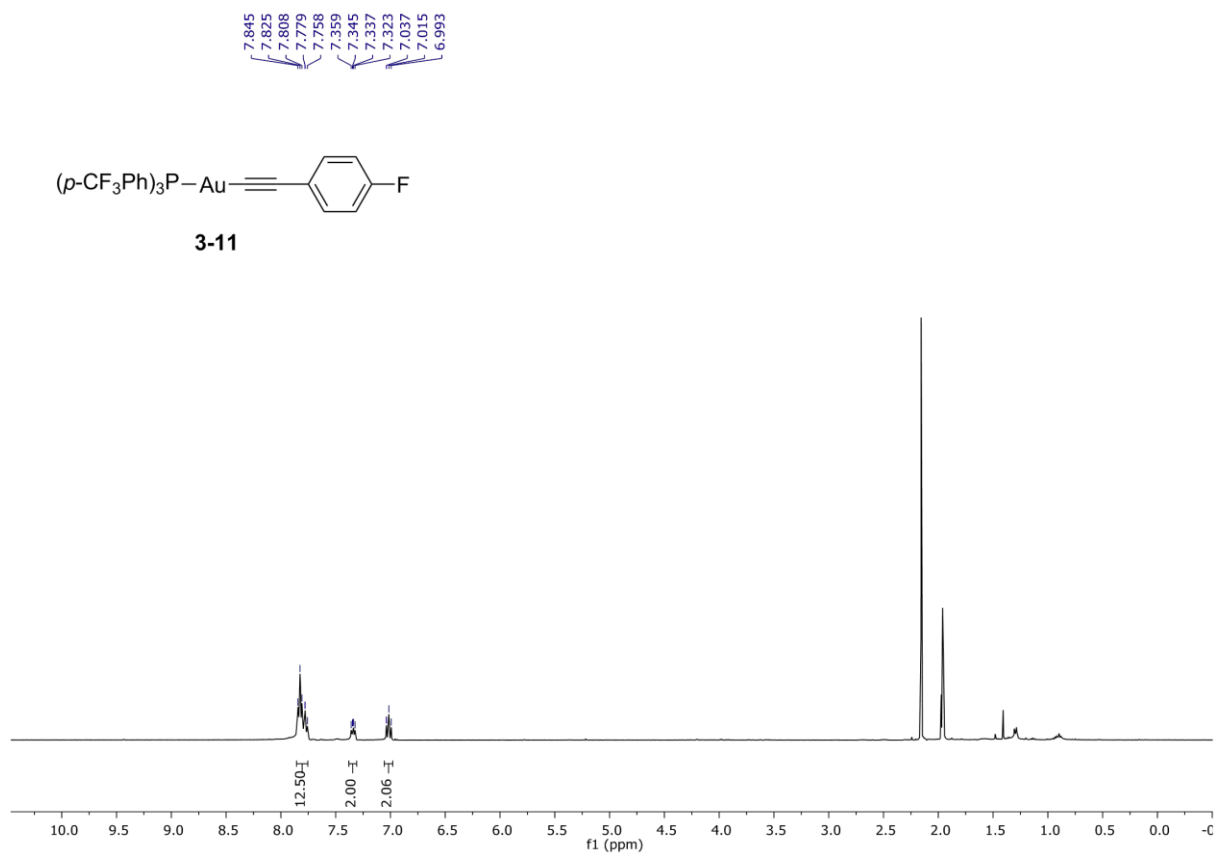
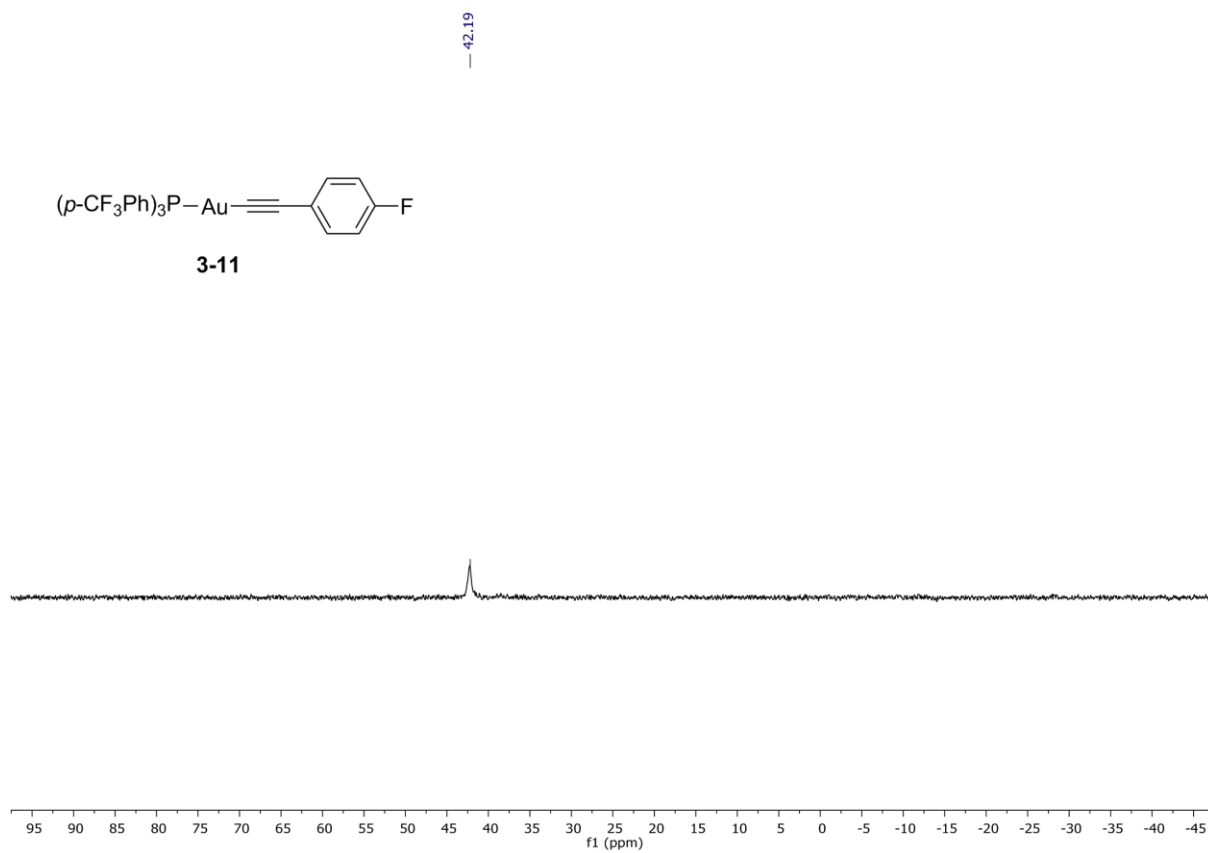
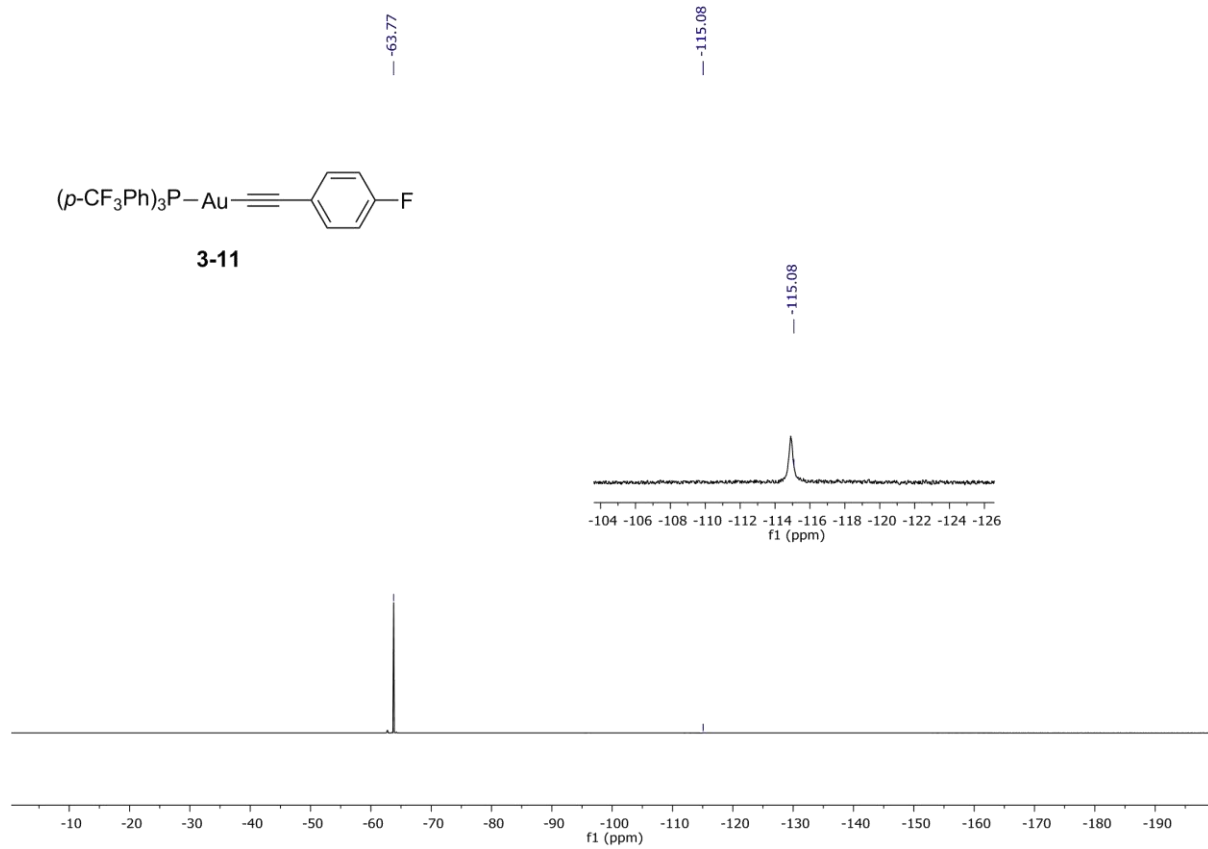
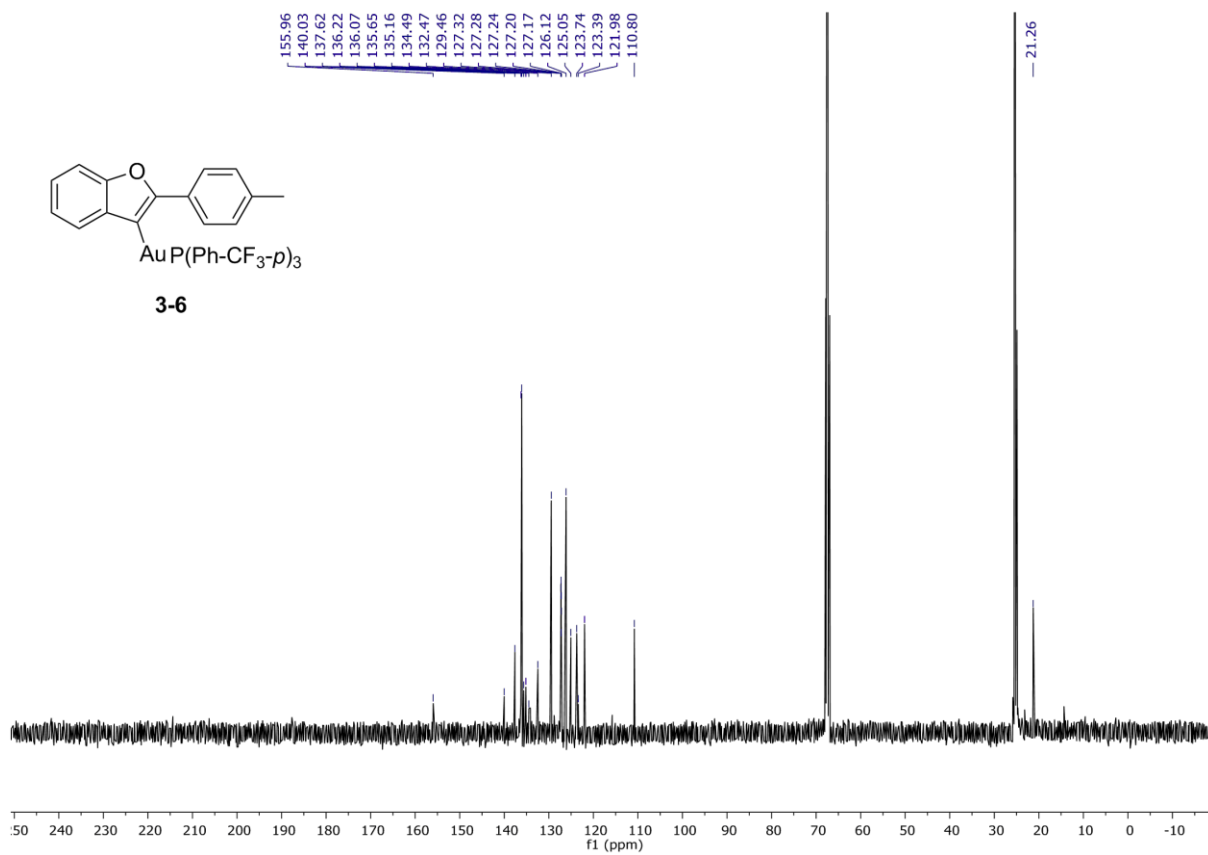
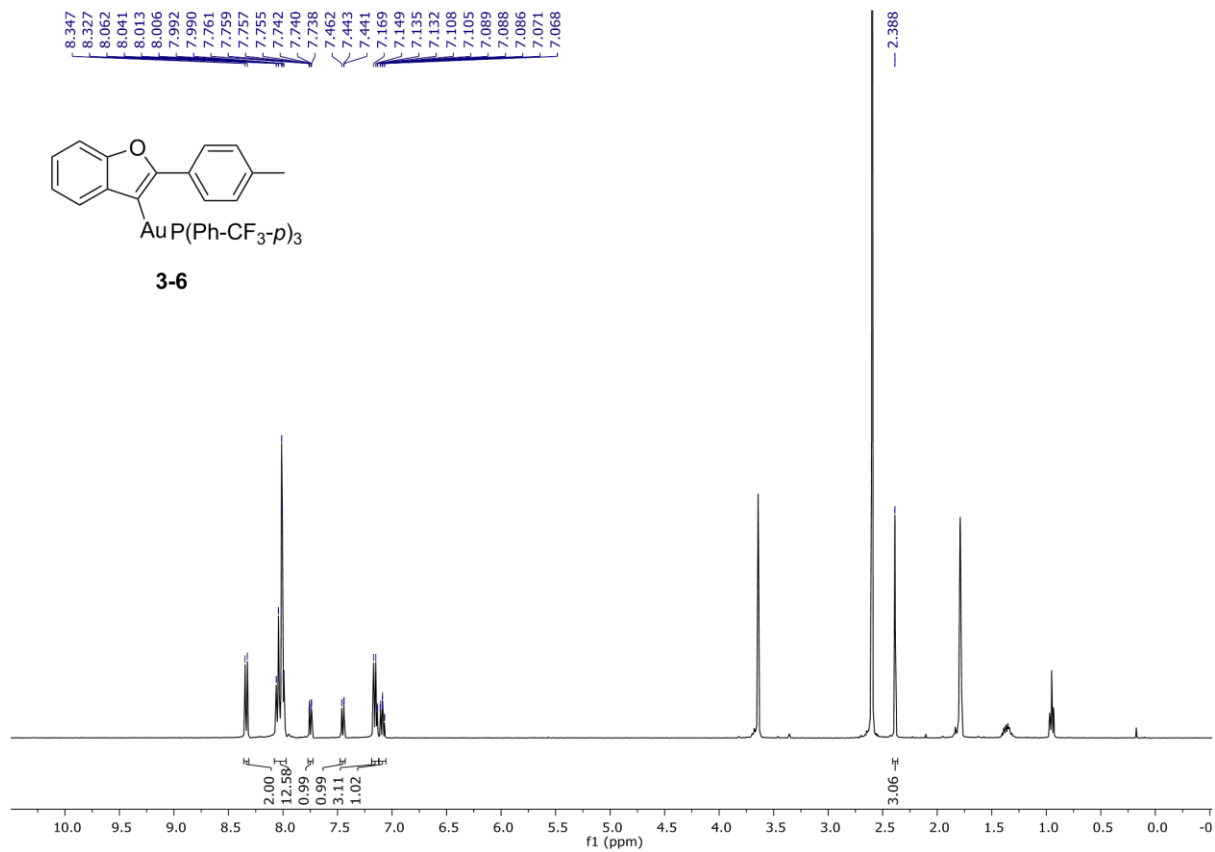


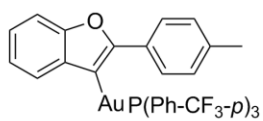
Fig SI13. Evolution of the spin density isosurface (isovalue 0.0006 a.u.) of 3II in the vicinity of **3-2a** along the C_I -Au coordinate (C_I is the carbon atom in **3-2a** bearing the iodine atom).

5.8 NMR Spectral Data

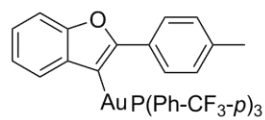
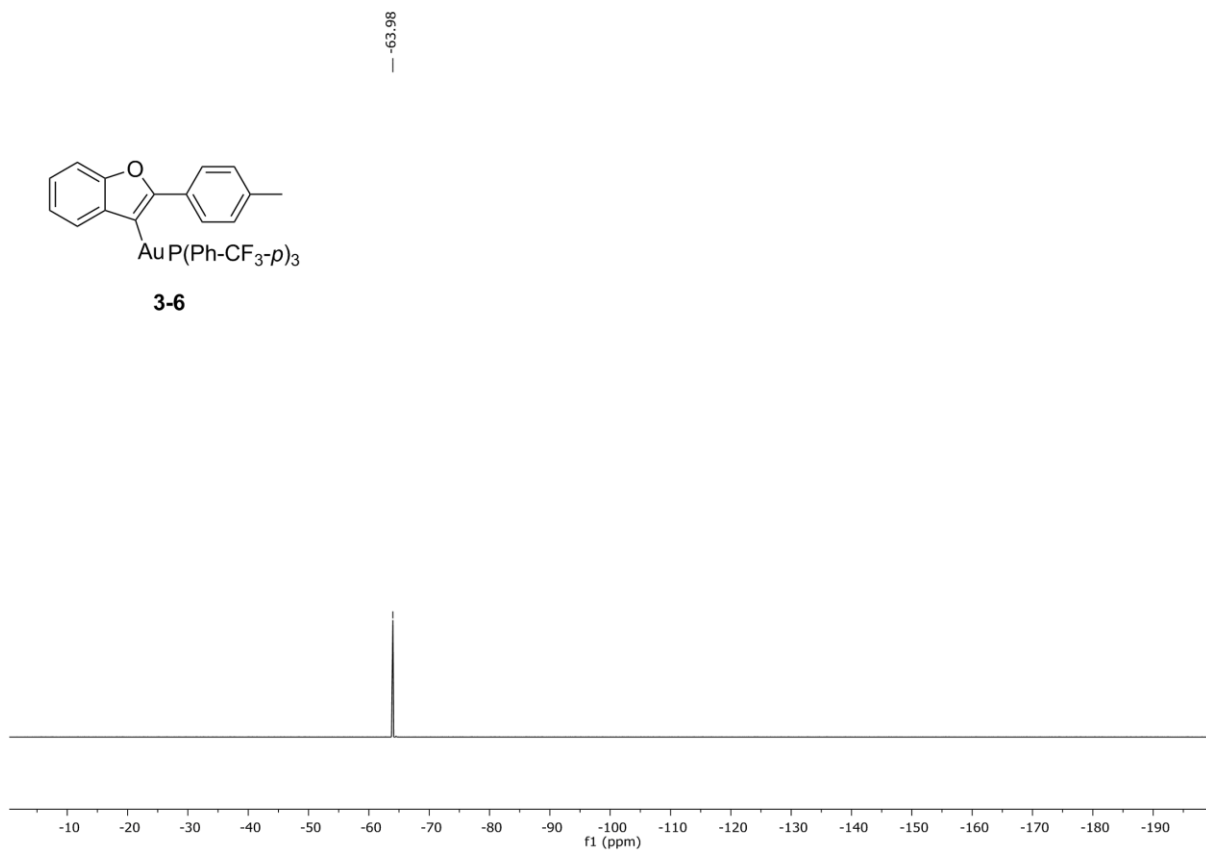




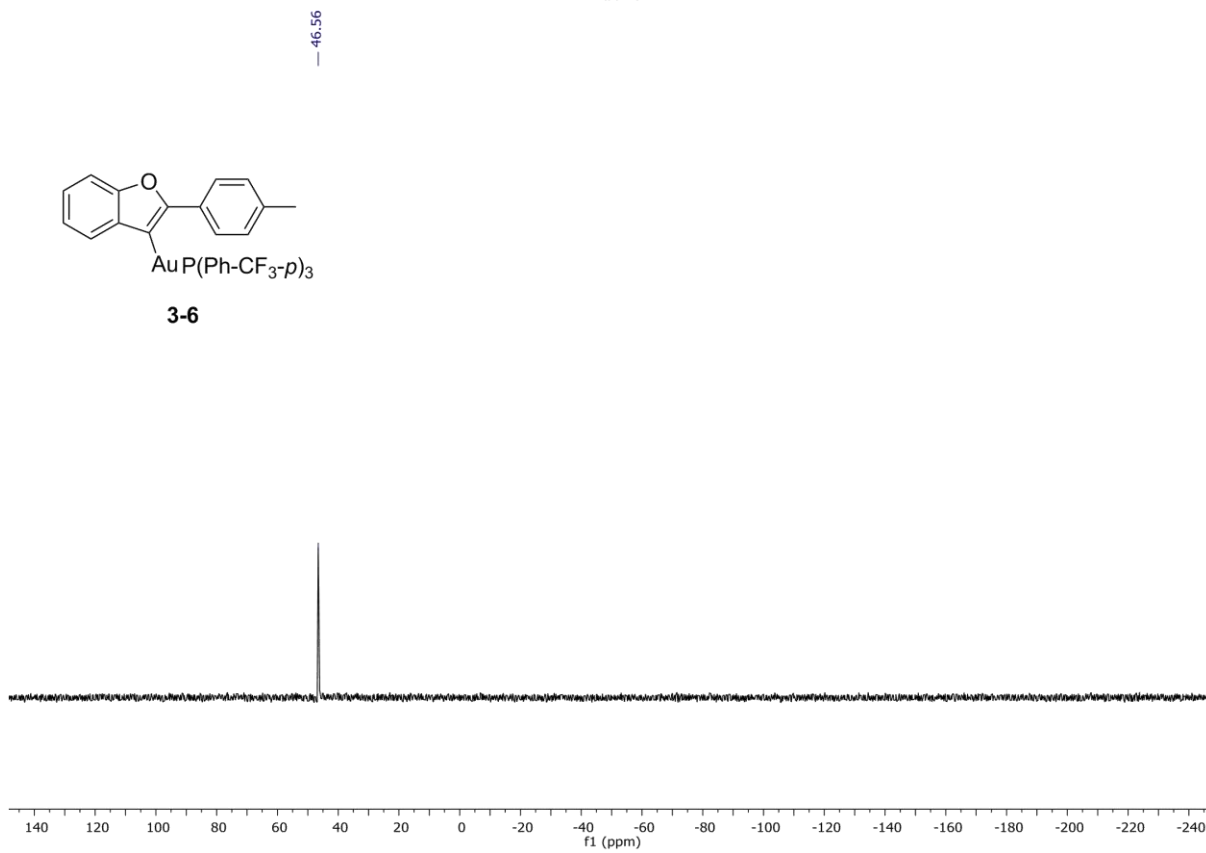




3-6



3-6



General Conclusion

This Ph.D. work has been aimed to study of gold catalysis under visible light irradiation. We aimed to synthesize benzofuran derivatives from *o*-alkynylphenols and aryl diazonium salts or iodoalkynes in the presence of a catalytic mixture of a gold(I) complex and a photocatalyst under visible light irradiation. Two successful transformations involving gold(I) catalysis under visible light are summarized in Figure GC.

Based on our previous works on gold catalysis and photocatalysis, firstly, we present a novel dual photoredox/gold catalysis process by arylation cyclization of *o*-alkynylphenols with aryl diazonium salts. This reaction occurs smoothly at room temperature in the absence of base and/or additives and offers an efficient approach to heterocyclic scaffolds. The scope of the transformation is wide, and the limitations are discussed. The reaction is proposed to proceed through a photoredox-promoted generation of a vinylgold(III) intermediate, formed by addition of the aryl radical to the gold catalyst and modulation of the oxidation state by the photocatalyst, following undergo reductive elimination to provide the heterocyclic coupling adduct.

Utilizing this transformation to iodoalkynes leads to new mode of activation of gold(I) complexes. Later, we developed a new method for the synthesis of valuable alkynyl benzofuran derivatives devised from *o*-alkynylphenols and iodoalkynes in the presence of a catalytic mixture of Au(I) and Ir(III) under blue LED irradiation. With a significantly high redox potential of the Au(I)/Au(III) couple, gold (I) complexes typically exhibit some unwillingness to undergo an oxidized state of the shuttle unless special ligands, reagents or reaction conditions on gold (I) are used, while it's easy to occur with many transition metals. A new protocol has been designed for C-C bond formation to overcome this obstacle.

Under visible light irradiation, the triplet excited state of the vinylgold(I) intermediate and the alkynyl iodide partner readily engages in a oxidative addition–*trans/cis* isomerization sequence, following deliver Csp²-Csp cross-coupling products after reductive elimination. An energy transfer event rather than a redox pathway was demonstrated by the mechanistic and modeling studies. This dual gold/photocatalytic process provides a novel mode of activation in gold homogenous catalysis. Thus, a new method for the synthesis of valuable alkynyl benzofuran derivatives has been devised from *o*-alkynylphenols and iodoalkynes in the presence of a catalytic mixture of Au(I) and Ir(III) under blue LED irradiation.

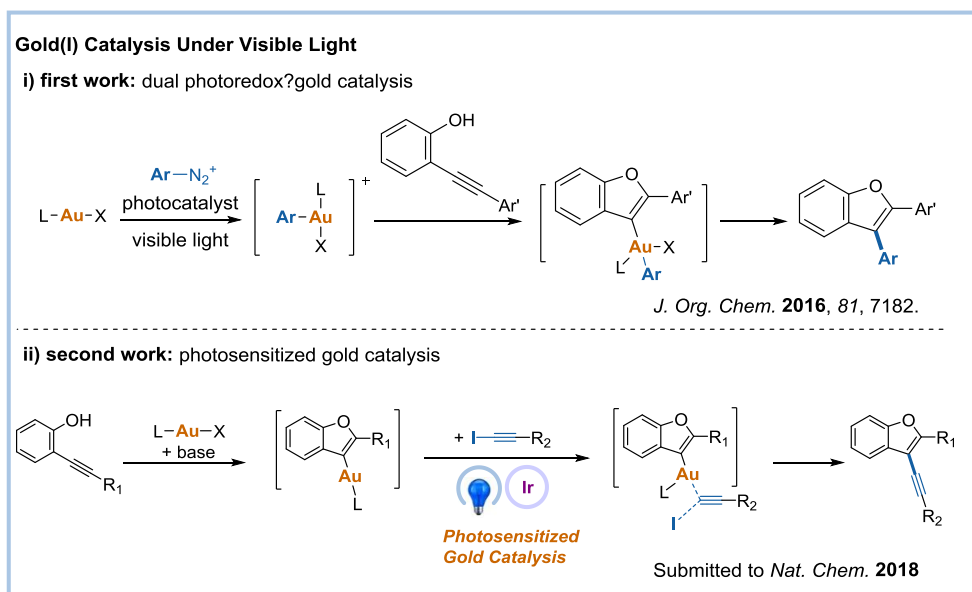


Figure GC. Gold catalysis under visible light.

A summary of the results presented in the manuscript is shown in the Figure GC. These studies bring in light of dual gold and photocatalysis process.



Panda, Zhonghua Xia, 2018

Zhonghua XIA, MACO, IPCM, UMR 8232, Sorbonne Université

Gold(I) Catalysis Under Visible Light

Abstract: This thesis has focused on the study of a dual catalytic process involving gold catalysis and photocatalysis. We aimed to synthesize benzofuran derivatives from *o*-alkynylphenols and aryl diazonium salts or iodoalkynes in the presence of a catalytic mixture of a gold(I) complex and a photocatalyst under visible light irradiation. Firstly, we present a novel dual photoredox/gold catalysis process by arylative cyclization of *o*-alkynylphenols with aryldiazonium salts. This reaction occurs smoothly at room temperature in the absence of base and/or additives and offers an efficient approach to heterocyclic scaffolds. The reaction is proposed to proceed through a photoredox-promoted generation of a vinylgold(III) intermediate, formed by addition of the aryl radical to the gold catalyst and modulation of the oxidation state by the photocatalyst, which undergo reductive elimination to provide the heterocyclic coupling adduct. Later, we developed a new method for the synthesis of valuable alkynyl benzofuran derivatives devised from *o*-alkynylphenols and iodoalkynes in the presence of a catalytic mixture of Au(I) and Ir(III) under blue LED irradiation. Under visible light irradiation, the triplet excited state of the vinylgold(I) intermediate and the alkynyl iodide partner readily engaged in a oxidative addition–*trans/cis* isomerization sequence, deliver Csp²-Csp cross coupling products after reductive elimination. An energy transfer event rather than a redox pathway was demonstrated by the mechanistic and modeling studies. This dual gold/photo catalytic process provides a novel mode of activation in gold homogenous catalysis.

Keywords: Goldcatalysis, Visible Light, *o*-Alkynylphenols, Aryl Diazonium Salts, Iodoalkynes.

Gold(I) Catalysis Sous Lumière Visible

Résumé: Cette thèse s'intéresse à l'étude d'un double processus catalytique, la catalyse à l'or et la photocatalyse. Nous avons cherché à synthétiser des dérivés benzofuranique à partir d'*o*-alkynylphénols et de sels d'aryle diazonium ou d'iodoalcynes en présence d'un mélange catalytique d'un complexe d'or (I) et d'un photocatalyseur sous irradiation à la lumière visible. Dans un premier temps, nous présentons un nouveau procédé de catalyse duale photoredox/or par cyclisation arylative d'*o*-alkynylphénols avec des sels d'aryle diazonium. Cette réaction s'effectue dans des conditions douces à température ambiante en l'absence de base et/ou d'additifs et offre une approche efficace pour la formation de squelettes hétérocycliques. La réaction proposée fait intervenir un intermédiaire vinyl or(III) formé par addition du radical aryle sur le catalyseur d'or et par modulation de l'état d'oxydation du complexe par le photocatalyseur. Après élimination réductrice le produit de couplage hétérocyclique est obtenu. Dans un deuxième temps, nous avons mis au point une nouvelle méthode pour la synthèse de dérivés alcynylbenzofuraniques élaborés à partir d'*o*-alkynylphénols et d'iodoalkynes en présence d'un mélange catalytique d'Or (I) et d'Ir (III) sous irradiation de LEDs bleues. Sous irradiation à la lumière visible, le triplet excité de l'intermédiaire vinyl-or(I) et de l'iodure d'alcyne partenaire s'engage facilement dans une séquence d'isomérisation par addition *trans-cis*-oxydante, enfin l'élimination réductrice permet la formation des produits de couplage croisé Csp²-Csp. Les études mécanistiques et de modélisation ont mis en évidence un phénomène de transfert d'énergie plutôt qu'un processus redox. Ce double procédé catalytique or/photoredox fournit un nouveau mode d'activation dans la catalyse homogène à l'or.

Mots Clés: Catalyse à l'or, lumière visible, *o*-alkynylphénols, Sels d'Aryle Diazonium, Iodoalkynes.